Universitat Politècnica de València
Departamento de Máquinas y Motores Térmicos

Analysis of combustion concepts in a poppet valve two-stroke downsized compression ignition engine designed for passenger car applications

Doctoral Thesis
Presented by:
Daniela de Lima Moradell
Directed by:
Dr. Jesús Benajes Calvo
Dr. Ricardo Novella Rosa

Valencia, June 2016

Doctoral Thesis

Analysis of combustion concepts in a poppet-valve two-stroke downsized compression ignition engine designed for passenger car applications

Presented by: Daniela de Lima Moradell
Directed by: Dr. Jesús Benajes Calvo
Dr. Ricardo Novella Rosa

Tribunal:

President: Dr. José María Desantes Fernández
Secretary: Dr. Francisco Tinaut Fluixá
Vocal: Dra. Bianca Vaglieco

Examining Board:

Dra. Bianca Vaglieco
Dr. Louis LeMoine
Dr. José Rodríguez Fernández

Valencia, June 2016

Resumen. El trabajo de investigación presentado en esta tesis doctoral está enmarcado en el desarrollo y optimización del sistema de combustión de un novedoso motor de dos tiempos de encendido por compresión, que presenta una arquitectura de barrido por válvulas en culata, y que ha sido diseñado para aplicaciones de automoción dentro de la gama de coches compactos. El objetivo principal de esta investigación ha consistido en mejorar el conocimiento existente sobre los motores dos tiempos con arquitectura de barrido por válvulas, y a la vez identificar los principales vínculos entre los procesos de renovación de la carga y de combustión, con el fin de cuantificar su impacto sobre la formación de emisiones contaminantes y el rendimiento térmico del motor. Adicionalmente, se desea optimizar las prestaciones de este motor de dos tiempos operando con el proceso de combustión diésel convencional controlada por mezcla, así como evaluar el potencial de distintos conceptos avanzados de combustión de baja temperatura con fase de premezcla extendida, con el fin de reducir los niveles de emisiones contaminantes y mejorar el consumo específico de combustible del motor.

La metodología utilizada en esta tesis ha sido concebida combinando un enfoque teórico-experimental, que permite maximizar la información que se puede obtener acerca de los fenómenos físicos involucrados en los diferentes procesos objeto de estudio, y a la vez conservar un enfoque de optimización eficiente reduciendo en la medida de lo posible el número de ensayos experimentales requeridos. Con la finalidad de analizar en detalle la relación que existe entre las condiciones en el cilindro (como lo es la concentración de oxígeno, la temperatura de combustión y el dosado local) y el proceso de formación de emisiones contaminantes, especialmente de NO_x y hollín, se desarrollaron y utilizaron distintas herramientas teóricas para complementar y sustentar los comportamientos y tendencias observadas mediante los ensayos experimentales, tanto para el modo de combustión diésel convencional como para los conceptos avanzados de combustión.

Para la consecución de dichos objetivos se ha seguido una estructura secuencial en la cual el trabajo de investigación ha sido desarrollado en dos grandes bloques: primero, se analizó y optimizó el proceso de combustión diésel convencional, mediante la combinación adecuada de parámetros de operación del motor que modifican apreciablemente las características del proceso de combustión controlada por mezcla; y segundo, se logró implementar y evaluar el desempeño de dos conceptos avanzados de combustión, específicamente el modo combustión altamente premezclado de tipo HPC utilizando diésel como combustible (acrónimo de "Highly-Premixed Combustion") y el modo de combustión parcialmente premezclada de tipo PPC ("Partially Premixed Combustion") utilizando un combustible con mayor resistencia a la auto-ignición (en este caso se utilizó gasolina de octanaje 95). En esta segunda fase, se hizo énfasis en el análisis del concepto de combustión PPC con gasolina, ya que este arrojó los resultados más prometedores durante la fase inicial de implementación. Consecuentemente, la última etapa de la investigación se centró en el estudio detallado del efecto de distintos parámetros de inyección sobre las características del proceso de combustión de tipo PPC. Finalmente, se ha comparado críticamente dicha operación en modo PPC con los resultados obtenidos operando con el modo de combustión diésel convencional, en cuanto al nivel final de emisiones contaminantes, al consumo de combustible y rendimiento indicado y al desempeño general del motor.

Resum. El treball d'investigació presentat en esta tesi està emmarcat en el desenvolupament i optimització del sistema de combustió d'un nou motor dos temps d'encesa per compressió, amb configuració d'escombratge per vàlvules, i que ha estat dissenyat per a aplicacions d'automoció dins de la gamma de cotxes compactes. L'objectiu principal d'esta investigació ha consistit a millorar el coneixement existent sobre els motors dos temps amb configuració d'escombratge per vàlvules, així com també identificar els principals vincles entre els processos de renovació de la càrrega i de combustió, a fi de quantificar el seu impacte sobre la formació d'emissions contaminants i el rendiment tèrmic del motor. Addicionalment, es desitja optimitzar les prestacions d'este nou motor operant amb el mode convencional de combustió dièsel per difusió, així com avaluar el potencial de noves maneres de combustió de baixa temperatura amb fase de premescla extesa, per a controlar el nivell d'emissions i el consum de combustible.

La metodologia utilitzada en esta tesi s'ha plantejat des d'un punt de vista teóric experimental, que permet maximitzar la informació que es pot obtindre sobre els fenòmens basics involucrats en els diferents processos objecte d'estudi, i al mateix temps conservar un enfocament d'optimització eficient reduïnt en la mesura del possible el nombre d'proves experimentals requerit. Amb la finalitat d'analitzar en detall la relació que existeix entre les condicions en el cilindre (com ho és la concentració d'oxigen, la temperatura de combustió i el dosatge local) i el procés de formació d'emissions contaminants, especialment de NO_x i sutge, es van desenvolupar i van utilitzar distintes eines teòriques per a complementar i sustentar els comportaments i tendències observades per mitjà dels assajos experimentals, tant per al mode de combustió dièsel convencional com per als conceptes avançats de combustió.

Per a abordar eixe objectiu, s'ha seguit una estructura seqüencial, en la qual el treball d'investigació s'ha desenvolupat en en dos grans blocs: en primer lloc, es va analitzar i va optimitzar el procés de combustió dièsel convencional, per mitjà de la combinació adequada de paràmetres d'operació del motor que modifiquen apreciablement les característiques del procés de combustió controlada per difusió; i en segon lloc, es va aconseguir implementar i avaluar les prestacions de dos conceptes avançats de combustió de baixa temperatura premesclats, específicament el mode combustió altament premesclat HPC (acrònim de "Highly-Premixed Combustion") utilitzant dièsel com a combustible i el mode de combustió parcialment premesclat PPC ("Partially Premixed Combustion") utilitzant un combustible amb major resistència a l'autoignició (en aquest cas s'ha utilitzat gasolina d'octanatge 95). En esta segona etapa, es va fer èmfasi en l'anàlisi del concepte de combustió PPC amb gasolina, ja que aquest va presentar els resultats més prometedors durant la fase inicial d'implementació. Conseqüentment, l'última etapa de la investigació es va centrar en l'estudi detallat de l'efecte de distints paràmetres d'injecció sobre les característiques del mode de combustió PPC. Finalment, s'ha comparat críticament la dita operació en mode PPC amb els resultats obtinguts operant amb el mode de combustió dièsel convencional, quant al nivell final d'emissions contaminants, al consum de combustible i rendiment indicat, i a les prestacions generals del motor.

Abstract. The research work presented on this thesis has been performed in the framework of the development and optimization of the combustion system of a novel two-stroke CI engine, with a scavenging configuration through poppet-valves, which has been specifically designed for a light-duty vehicle application. The main objective of this investigation is to improve the existing understanding about two-stroke poppet-valves engines, and assess the main relationships between the gas exchange and combustion processes in this type of architecture, with the aim of evaluating their impact on the exhaust emissions formation processes and on final engine efficiency. Then, the performance of this two-stroke engine is going to be optimized while operating in conventional diesel mixing-controlled controlled combustion; and in a second step, two advanced premixed combustion concepts will be evaluated to identify their potential for decreasing NO_x and soot emissions compared to CDC as well as its main technological limitations.

The methodology proposed on this thesis combines both a theoretical and experimental approach, that allows maximizing the available information about the basic phenomena involved in the various processes under study, while also keeping an efficient optimization approach to reduce as much as possible the number of necessary experimental tests. Additionally, to analyze in detail the physical relationships between the local cylinder gas conditions (such as the oxygen concentration, the combustion temperature and the equivalence ratio) and the formation of exhaust emissions, particularly NO_x and soot, it was necessary to develop and setup different theoretical tools to complement and support the experimentally measured trends.

To achieve these objectives, the research work has been divided in two sequential stages: first, the conventional diesel combustion is studied and optimized, based on a proper combination of engine settings that have a strong influence over the characteristics of the mixing-controlled combustion; and in a second step, two advanced combustion concepts are implemented and analyzed, the highly-premixed combustion (HPC) of diesel and the partially premixed combustion (PPC) using a fuel with higher resistance to autoignition (in this case it has been used a RON95 gasoline). In this phase of the research, special emphasis has been made to the gasoline PPC concept, since this combustion mode showed the highest potential and most promising results during the initial implementation studies. Accordingly, the last stage of the research was mainly focused on the detailed study of the effect of different injection settings over the characteristics of the gasoline PPC concept. Finally, the main results obtained with the gasoline PPC concept have been compared against the optimized points found in CDC, in regards to the final exhaust emissions levels, specific fuel consumption and indicated efficiency.

"Coming together is a beginning;
keeping together is progress;
working together is success"
Henry Ford

a mi familia y a Manuel

Agradecimientos

Cuando hago un recuento de estos últimos años, ni yo misma logro creer las experiencias que he vivido y todo lo que he aprendido de esta travesía que ha estado llena de retos y logros tanto a nivel personal como profesional. Sin duda, mi historia no sería igual si no hubiese tenido a mi lado a todas esas personas que han compartido este camino conmigo, que me han inspirado y me han enseñado a ser humilde, a disfrutar de las cosas más simples del día a día, y a siempre sentirme orgullosa de lo que hago. A esas personas que han visto potencial en mí y me han brindado la oportunidad y los medios para desarrollarlo, así como a aquellas que siempre me han brindado su apoyo y cariño incondicional. Todo lo que pueda expresar en estas páginas de agradecimientos no representa ni el 1% de mi gratitud hacia cada uno de ustedes.

Primero quisiera darle las gracias de forma muy especial a mi tutor y mentor, Ricardo Novella, y de igual manera incluir en este agradecimiento a Gabriel Alcantarilla, quien ha sido el responsable de la instalación experimental y me brindó su invaluable apoyo y experiencia durante la ejecución de los ensayos. Ambos han sido para mí un claro ejemplo de profesionalismo, compromiso e integridad, y han jugado un rol fundamental en mi formación doctoral y profesional. Sin su aporte y ayuda tanto técnica como humana no hubiese sido posible la realización de esta tesis, que ha sido el fruto de un arduo trabajo en equipo, y que representa un logro tanto de ellos como mío. Quiero que sepan que aún en los días de trabajo más duros e intensos, siempre me sentí infinitamente agradecida y afortunada de poder contar con ustedes. Gracias por todo nuevamente.

Adicionalmente quisiera extender estos agradecimientos a Jesús Benajes, por la confianza que depositó en mí, así como por su aportación científica a esta Tesis, ya que siempre estuvo involucrado de cerca en el seguimiento de este trabajo de investigación. Así mismo, quiero expresar mi más profundo agradecimiento al Departamento de Máquinas y Motores Térmicos, y en particular a sus dos directores, Francisco Payri y José María Desantes, por permitirme realizar mi formación doctoral en este centro de investigación, el cual se convirtió en mi segundo hogar durante casi 5 años. De igual manera, quisiera agradecer a todo el personal de secretaría e informática, así como a los técnicos del laboratorio, por todo el apoyo y ayuda que siempre me brindaron.

No puedo dejar a un lado a mi familia, a mis padres y a mi hermana, quienes son el pilar más importante en mi vida. Sin ustedes no sería quien soy hoy. Gracias por su amor infinito, por la paciencia y fortaleza que tienen, por darme el mejor ejemplo de cómo ser feliz y por enseñarme qué es lo verdaderamente importante en este mundo. Separarme de ustedes y asumir que íbamos a vivir a 7256 km de distancia, ha sido la decisión más dura que he tomado en mi vida. Sin embargo, hoy estoy convencida de que cuando llegue el día en que volvamos a estar juntos, podré ofrecerles todo lo que se merecen y más, y lograremos recuperar todos esos momentos que nos hemos perdido estos últimos años. La familia es lo más importante, de eso no me queda duda. Quiero que nuestro futuro esté lleno de celebraciones de cumpleaños, de días del padre y de la madre, aniversarios, y sobre todo, de oportunidades para ver crecer a Andrés y que él pueda conocer a su tía Dany en persona y no sólo por Skype.

Mi segundo gran pilar ha sido y seguirá siendo Manuel Rivas, quien es mi mejor amigo, mi compañero de vida, mi confidente, mi cómplice y mi protector; quien ha vivido conmigo esta gran aventura, y quien ha estado a mi lado siempre apoyándome y transmitiéndome su fuerza y su valor. Él me ha enseñado que no hay montañas lo suficientemente altas para que sean imposibles de escalar, que sólo tenemos que tener paciencia, entrenar lo suficiente y trabajar juntos para alcanzar la cima y poder disfrutar de las vistas una vez arriba. No existen palabras para agradecerte todo lo que haces por mí, y nunca dejas de sorprenderme, por eso te amo, te admiro, y doy gracias por tenerte a mi lado. También quisiera agradecer especialmente a Ana Margarita Perea, Nicasio Rivas y Miguel Rivas, por hacerme sentir parte de la familia; y así mismo, incluir en este agradecimiento a todos los *Rivas-Perea*, por el cariño y apoyo que me han brindado durante los años, y por ser siempre tan especiales conmigo.

I would like to express my most sincere gratitude to Renault RSA and the European Commission in the framework of the FP7-Transport Grant Agreement for funding this research work, and give my especial thanks to Pascal Tribotté, who was the technical leader responsible for the POWERFUL project, and also the brain behind the conception and design of this novel two-stroke engine concept. Pascal merci beaucoup pour vos conseils, l'aide technique apportée, vos idées originales et innovantes et toutes vos suggestions. J'ai appris beaucoup de la technologie des moteurs grâce à vous, et j'espère voir à l'avenir une voiture Renault équipée d'un moteur à deux temps. Ce serait génial. In addition, I would also like to acknowledge all the other members of the two-stroke POWERFUL team, who were also involved in the development of this engine: Nicolas Quechon, Philipppe Obernesser and Vincent Dugue, from Renault RSA; and Gaetano De Paola and Cyprien Ternel, from IFP Energie Nouveles. It was an honour for me to participate in this big collaborative project, and I really enjoyed going back to IFP (my alma mater) and being able to see (and drive) the final outcome of this challenging project.

I would also like to thank the Division of Combustion Engines of Lund University, especially to professors Bength Johannson, Per Tunestål, Öivind Andersson and Martin Tuner, for offering me the opportunity to learn about their expertise in advanced combustion concepts and optical techniques in IC engines. Many thanks also to the people (staff and Phd students) integrating this research group for giving me such a warm welcoming during my stay in Sweden, I hope we will meet again someday along our careers in the automotive industry.

Quisiera hacer una mención especial a los distintos alumnos que estuvieron involucrados en la realización de esta tesis, especialmente a Josep Gómez Soriano y Antonio Revert por el apoyo y ayuda prestada durante la realización del modelo y los cálculos CFD; así como a Kevin Thein, David Olivera, José David Conejero, y Juan Pedro Martínez; con quienes compartí muchas horas delante del motor y además me brindaron su ayuda en el procesado de datos experimentales. Así mismo, me gustaría expresar mi más sincero agradecimiento a toda la gente de la línea de combustión con la cual he convivido durante estos años: incluyendo a los profesores Xemary, José Manuel, Antonio, José Vicente y Jaime por ofrecerme siempre sus sabios consejos; así como a mis compañeros Edu, Walter, Carlos, Johanness y Vicent por hacer que el día a día en el primer piso fuese mucho más ameno y divertido. Especialmente quisiera

agradecer a Eduardo Belarte por su paciencia y por aguantarme hasta en mis días de locura, no hubiese podido pedir un mejor compañero de despacho. ¡Gracias por todo Edu!

Por último, aunque no menos importante, quisiera darle las gracias a mis grandes amigos con quienes he compartido tanto mis dichas como mis penas estos últimos años. Gracias a ellos me llevo conmigo un baúl lleno de valiosos recuerdos y momentos inolvidables de esta etapa que compartimos juntos en Valencia, incluyendo las tradicionales salidas de los jueves, los viernes de vóley, muchas tardes de verano en la playa, barbacoas, paellas, fallas, noches de Nintendo 64 y demás... Dentro este grupo inigualable de personas quisiera recordar con mucho cariño a los CMTeros originales: Gaby, Mariany, Juanma, Simón, JeanGui, Chris, Dany; al combo latino: Sebas, Alberto, Leo y Jesús junto con las niñas del grupo Jeanik, Ilse y Mary; a los chicos del equipo de Formula Student UPV: Lucas, Arturo, Antón, Marco, Kevin, Javi; y a mis mejores amigos, "roomates" en algún momento y hermanos de cariño por siempre: Juan Pablo Viera, Alejandro Veloz, Luis García y Juan Carlos Álvarez, con quienes espero poder seguir compartiendo nuevas aventuras y desafíos en un futuro.

Finally, I would also like to thank Kotaro Maeda and François Lafossas from Toyota Motor Europe, as well as Nick Allaert from Alten Belgium, for all their support and understanding during the last months of preparation of this manuscript.

Table of Contents

Index of Figures

Index of Tables

Nomenclature

Latin

AFR	Air/fuel ratio
CH_4	Methane concentration
CO	Carbon monoxide emissions
CO_2	Carbon dioxide emissions
Cp	Specific heat capacity at constant pressure
Cv	Specific heat capacity at constant pressure
dP/da_{max}	Maximum pressure gradient
h	Specific enthalpy per unit of mass
H	Absolute enthalpy
$\overline{h}$	Specific enthalpy per mol
HC	Unburnt hydrocarbon emissions
K_1	Constant term of the mixing time equation depending on engine configuration
m	Mass
$\dot{M}$	Momentum flux
MC	Mixing capacity
MF	Merit function
n	Mole number of a species involved in a reaction
NO_x	Nitrogen oxides (NO y NO_2)
$Olap$	Overlap period between the IVO and the EVC (in crankangle)
OV_i	Objective/target value for each output considered in a merit function
P	Pressure
PM	Particulate matter emissions
PN	Particulate number

Pw	Power
Q	Mass flow rate
Q_w	Heat transfer between the cylinder gas and the walls
r	Radial coordinate of the spray
R	Universal gas constant
R^2	Coefficient of determination
RV_i	Response value for each output considered in a merit function
$S(t)$	Spray penetration as function of time
t	Time
T	Temperature
THC	Total hydrocarbon emissions
u	Axial velocity of the injected fuel
V	Volume
x	Axial coordinate of the spray
X	Molar fraction / volumetric
Y	Mixture fraction
$\%fuel$	Fuel split or distribution between the injections

Greek

α_i, β_i	Coefficients to control the weight of each response inside a merit function
Δ	Variation/Increment
ΔP	Difference between intake and exhaust average manifold pressures
η	Efficiency
θ	Spray angle
ε	Referred to the k-ε turbulent flow model
μ	Average value of a sample data
ϕ	Injector nozzle hole diameter
Φ	Equivalence ratio
φ	Referred to a solved quantity in the CFD model
ρ	Density
σ	Standard deviation

Superscripts

o	Standard conditions

Subscripts

ad	Relative to adiabatic conditions
air	Relative to fresh intake air conditions
atm	Relative to atmospheric conditions
bb	Relative to the blow-by flow
$char$	Relative to the charging of the cylinder
cl	Relative to the center line of the spray
$comb$	Referred to combustion efficiency
$corr$	Corrected
cyl	Relative to the conditions in the interior of the cylinder
del	Referred to the delivered mass of incoming intake air (fresh + EGR)
eff	Effective
$evap$	Relative to evaporative conditions
exh	Relative to the exhaust manifold conditions
$fresh$	Relative to the fresh intake air flow
$form$	Formation
$fuel$	Relative to the fuel
g	Relative to the gas
ind	Referred to indicated efficiency
inj	Relative to the fuel injection
int	Relative to the intake manifold conditions
i, j	Relative to the species in the reactants, products
IVC	Relative to the conditions at the intake valve closing timing
max	Maximum
$main$	Referred to the main injection
mix	Referred to mixing time
$O2$	Relative to the species oxygen
o	Relative to the conditions at the outlet of the injector nozzle
$prod$	Relative to the products involved in a chemical transformation
$rail$	Relative to the fuel conditions on the injection common rail system
$reac$	Relative to the reactants involved in a chemical transformation
res	Referred to the residual burnt gas that remains trapped in the combustion chamber after the exhaust phase
ret	Referred to the retained mass of incoming intake air
$scav$	Relative to the scavenging of the cylinder
SC	Supercharger

short	Referred to the short-circuited gas that goes from the intake to the exhaust without being trapped in the cylinder
stoich	Relative to stoichiometric conditions
theor	Referred to the theoretical trapped mass at reference conditions
unburnt	Relative to the conditions of the unburnt mixture
$80\%MBF$	Relative to the conditions at the time where 80 % of the fuel has been burnt
1	Referred to the first early injection (pilot injection)
2	Referred to the second injection (main)
3	Referred to the third injection (post-injection)

Acronyms

aEoI	Crankangle after the end of injection
aSoI	Crankangle after the start of injection
aTDC	Crankangle after Top-dead-center
bTDC	Crankangle before Top-dead-center
BMEP	Brake Mean Effective Pressure
BSFC	Brake Specific Fuel Consumption
CA10, CA50, CA90	Referred to the crankangle where 10 %, 50 % and 90 % of the fuel injected mass has been burnt
CAFE	Clean Air For Europe Program
CDC	Conventional diesel combustion
CFD	Computational Fluid Dynamics
CI	Compression ignition
CR	Compression ratio
DOC	Diesel oxidation catalyst
DoE	Design of experiments
DPF	Diesel Particulate Filter
EGR	Exhaust Gas Recirculation
EoC	End of combustion
EoI	End of injection
ER	Expansion ratio
EVC	Exhaust valve closing
EVO	Exhaust valve opening
EU5,EU6	Referred to the Euro 5 and Euro 6 emissions regulations
FMEP	Friction Mean Effective Pressure

GDI	Gasoline direct injection
GHG	Green-house gases
GPF	Gasoline particulate filter
HCCI	Homogeneous charge compression ignition
HSDI	High speed direct injection
HTR	High temperature reaction stage
ICE	Internal combustion engine
ID	Ignition delay
IEA	International Energy Agency
IGR	Internal Gas Recirculation
IMEP	Indicated Mean Effective Pressure
IVC	Intake valve closing
IVO	Intake valve opening
ISFC	Indicated specific fuel consumption
KHP	Ketohydroperoxide
LDV	Light-duty vehicles
LPG	Referred to liquefied petroleum gas engines
LNT	Lean NO_x trap aftertreatment system
LOL	Lift-off length
LTC	Low temperature combustion
LTHC	Low thermal homogeneous combustion
LTR	Low temperature reaction stage
NEDC	New European Driving Cycle
NG	Referred to natural gas engines
NTC	Negative Temperature Coefficient
NVO	Negative valve overlap
Olap	Overlap duration
PAH	Poly-aromatic hydrocarbon
PCCI	Premixed charge compression ignition
PEMS	Portable emissions monitoring systems
PFI	Port fuel injection
PLIF	Planar Laser Induced Fluorescence
PPC	Partially premixed combustion
PPCI	Partially premixed compression ignition

PRESS	Predicted error sum of squares
R&D	Research and development
RCCI	Reactivity controlled compression ignition
RMSE	Root mean squared error
RoHR	Rate of heat release
RSM	Response surface methods
SCR	Selective catalytic reduction aftertreatment system
SI	Spark ignition
SoI	Start of injection
SoE	Start of energizing
SoC	Start of combustion
TDC	Top-dead-center
TR	Trapping ratio
VVA	Variable valve actuation systems
VVT	Variable valve timing
WLTP	Worldwide Harmonized Light Vehicles Test Procedure

Chapter 1

Introduction

Contents

1.1 Introduction

The studies presented on this investigation are focused in the development of a new engine concept for a small passenger car: A two-stroke poppet-valves HSDI CI engine. As an introduction to this document, this chapter approaches the global context and restrictions driving the current and future trends in engine research and development. First, an overview of different aspects such as energy demand and projected trends in global CO_2 emissions, European emission standards for light duty vehicles, and main technology trends in R&D of modern powertrains for passenger cars is presented in Section 1.2. Second, the investigation is contextualized making special emphasis in the interests and

challenges that supposes the development of a two-stroke engine concept for automotive applications. Accordingly, the objectives of this thesis are defined in Section 1.4, and finally, an outline of the structure of the manuscript is given in Section 1.5 so that the reader can get an overview of the thesis contents.

1.2 Background and motivation

1.2.1 The Global Energy Outlook

Our world runs on energy. It is essential to our way of life and to support human development and global economic growth. An input of energy is required for everything we do on a daily basis, from fueling our cars, to heating our homes, to powering the electric appliances we depend on. Consequently, as consumer demand for more goods and services grow, energy demand is accordingly increased. Furthermore, future energy supply and demand, as well as the related environmental and social contexts are conditioned by a group of uncertainties that are very difficult to predict, such as the global economic and geopolitical situations and new technical innovations and resources.

Global total primary energy supply (TPES) more than doubled between 1973 and 2012, mainly relying on fossil fuels. Despite the growth of non-fossil energy (such as nuclear and hydropower), the share of fossil fuels within the world energy supply was only slightly reduced over the past 40 years, from 86.7 % to 81.7 % [1]. The total final energy consumption nearly doubled in this period, and if current trends continue unaltered, it could rise another 70 % by 2050. Continuing to supply energy without adopting strong energy efficiency measures will become unsustainable.

The International Energy Agency (IEA) in its report "CO_2 emissions from fuel combustion" states that the use of energy represents the largest source of greenhouse gases, with 69 % of share of the global anthropogenic GHG, where 90 % corresponds to carbon dioxide (CO_2) emissions. The energy sector includes emissions from fuel combustion (which dominates the total GHG emissions) and fugitive emissions, which are intentional or unintentional releases of gases resulting from production, processes, transmission, storage and use of fuels. According to the data presented by the IEA for year 2012, global CO_2 emissions derived from fuel combustion reached a maximum of 31.7 Gt (billion metric tons) of CO_2, which translate into a 1.2 % year-on-year increase in emissions since 2000. According to the IEA 2014 report, two sectors combined produced nearly two-thirds of global CO_2 emissions in 2012: power generation which accounted for 42 % and transport which accounted

for 23 %. In the later case, data from 2011 showed that consumption in transport increased by 25 % compared to 2000 levels, with road transport taking the largest share (approximately 75 %). Passenger light-duty vehicles (LDV) consumed slightly more than 40 % of total transport energy demand.

Countries around the world are increasingly aware of the urgent need to transform and improve the way they use energy. At the United Nations climate negotiations in Cancun (2010) and in Copenhagen (2009), governments agreed that the increase in global average temperature must be held below 2 °C, compared to pre-industrial levels. In order to reach this climate goal, 42 industrialized countries submitted quantified economy-wide emission reduction targets for 2020, and 45 developing countries submitted nationally appropriate mitigation actions. However, none of these commitments will be implemented before 2020. Therefore, urgent action is required before 2020 in order to keep a realistic opportunity for an efficient and effective international agreement from that date, and also to limit the "emission gap" between expected emission levels and those needed for reaching the 2 °C target [2].

The 2 °C Scenario projected by the IEA, estimates that the energy-related CO_2 emissions has to be cut by more than half [3] for year 2050, with the highest contribution (51 %) in the CO_2 reduction coming from the power generation sector, while the second largest contribution (20 %) is given by improvements in the transport sector. In the case of transport sector, oil still remains as the predominant fuel source for freight and road transportation, while conventional Internal Combustion Engine (ICE) vehicles is very likely to continue dominating the market at least in the mid-term (until 2030). To achieve the vision of a sustainable energy system, low-carbon and energy-efficient technologies must be deployed together rather than in isolation across all end-use sectors.

1.2.2 Emission standards for light duty vehicles

Diesel engines are an increasingly popular choice amongst consumers in Europe, with over half now opting for this type of powertrain. Penetration of diesel engines in the European market of LDV grew rapidly since 1990, reaching 55 % of market share in 2013. In the rest of the world, the share of diesel engines in the transportation sector still remains confined in its majority to heavy-duty applications for freight transport. Despite the strong regional differences in the automotive markets across the world, and even when the energy and fuel supply is expected to diversify in the future, the ICE will continue to play a major role for both light- and heavy-duty

applications. The massive use of ICE's added to the continuous increase in demand for road transportation, started to raise governments awareness about air quality, specially in dense populated regions, since the late 70's in the United States, and later, in the early 90's in the case of Europe. Gaseous pollutants such as carbon monoxide (CO), particulate matter (PM), oxides of nitrogen (NO_x=NO+NO_2) and unburned hydrocarbons (HC) have serious environmental and health implications. Consequently, most governments in developed countries and more recently in some developing countries, have imposed stringent vehicle emissions regulations that are continuously being tightened further.

In March 2001 the European Commission launched the Clean Air For Europe (CAFE) Programme. This led to the adoption of a thematic strategy on air pollution, presented in a communication of 21 September 2005, where it was stated that further reductions in emissions from the transport sector (air, maritime and land transport), from households and from the energy, agricultural and industrial sectors are needed to achieve EU air quality objectives. In this context, the task of reducing vehicle emissions should be approached as part of an overall strategy. Later, in 2007 the European Commission agreed on a package of proposals that followed the European Council's commitments to fight climate change.

The Euro 5 and Euro 6 standards are one of the measures designed to reduce emissions of particulate matter and ozone precursors such as nitrogen oxides and hydrocarbons. In particular, a considerable reduction in NO_x emissions from diesel vehicles is necessary to improve air quality and comply with limit values for pollution. The Euro 5 standard came into force on 1 September 2009 for the approval of vehicles, and from 1 January 2011 for the registration and sale of new cars; while the Euro 6 standard came into force on 1 September 2014 for the approval of vehicles, and from 1 January 2015 for the registration and sale of new types of cars [4].

Table 1.1 shows an overview of the limits established by the EU standards in terms of regulated pollutants for compression ignition (diesel) and positive ignition (gasoline, NG, LPG, ethanol,...) vehicles. In the case of diesel vehicles, a 80 % reduction in particulates plus a 28 % decrease in NO_x emissions were established in the Euro 5, compared to the Euro 4 standards. For petrol vehicles, a 25 % reduction in NO_x emissions in addition to a new limit in PM that did not exist in the Euro 4 standard (solely for direct-injection (DI) petrol engines) were introduced in the Euro 5. As soon as the Euro 6 standard entered into force, a further reduction in NO_x emissions (more than 50 %) is applied to diesel vehicles, while combined emissions of hydrocarbons

Stage	CO [g/km]	THC [g/km]	NO_x [g/km]	$THC+NO_x$ [g/km]	PM [g/km]	PN [1/km]
Compression Ignition (Diesel)						
Euro 4	0.5	-	0.25	0.30	0.025	-
Euro 5	0.5	-	0.18	0.23	0.005	6.0×10^{11}
Euro 6	0.5	-	0.08	0.17	0.005	6.0×10^{11}
Positive Ignition (Gasoline, NG, LPG, ethanol,...)						
Euro 4	1	0.1	0.08	-	-	-
Euro 5	1	0.1	0.06	-	0.005	-
Euro 6	1	0.1	0.06	-	0.005	6.0×10^{11}

Table 1.1. *EU emission standards for passenger cars (category M_1).*

and NO_x is also reduced. Finally, in order to ensure that emissions of ultra fine particulate matter (with diameter of 0.1 μm and below) are controlled, the Commission introduced a particle number (PN) based approach to emissions of PM in addition to the mass-based approach which was conventionally used. The number based approach to emissions of PM as well as the measurement method should draw on the results of the UN/ECE's Particulate Measurement Programme (PMP). A PN limit of 6.0×10^{11} 1/km is established in the Euro 5.b for diesel vehicles and Euro 6 for petrol vehicles. It is applicable only to gasoline cars using a DI engine, while a limit of 6.0×10^{12} 1/km can be applied within the first three years from the Euro 6 effective dates, to allow manufacturers an additional time period to develop alternatives to meeting the regulations besides gasoline particulate filters (GPF), acknowledged to perform well and be cost effective [5].

Following the strategy adopted in 2007, the EU put in place a comprehensive legal framework to reduce CO_2 emissions from new light duty vehicles as part of efforts to ensure it meets its GHG emissions reduction targets under the Kyoto Protocol and beyond. The CO_2 cars proposal issued in 2009 is the most important element of the EU's strategy to improve the fuel economy of cars, which accounts for about 12 % of the EU's carbon emissions [6].

For passenger cars, manufacturers are obliged to ensure that their new car fleet does not emit more than an average of 130 g/km by 2015 -with the target phased in from 2012- and 95 g/km by 2021, phased in from 2020. Moreover,

each car manufacturer separately must meet an average specific CO_2 limit that depends on the mass of vehicles it produces. The 2015 and 2021 targets represent reductions of 18 % and 40 %, respectively, compared with the 2007 fleet average of 158.7 g/km. In terms of fuel consumption, the 2015 target is approximately equivalent to 5.6 L/100 km for gasoline and 4.9 L/100 km for diesel cars; while the 2021 target equates to approximately 4.1 L/100 km for gasoline cars and 3.6 L/100 km for diesel cars.

Legislation adopted in 2014 laying down the modalities of the 2020/2021 targets asks the European Commission to come forward with post-2020 targets by the end of 2015. The intention is to ensure that CO_2 emissions from light-duty vehicles continue to be reduced, providing certainty and security to the automotive industry to carry out long-term investments and develop innovative technologies. However, the current status of CO_2 emissions from cars are still very far away from the European Council's proposed target. Furthermore, it also exist a gap between the performance of emissions control measures during type approval tests and their effectiveness under real operating conditions, mainly because of the difference between the current conventional test of New European Driving Cycle (NEDC) and the real world driving conditions. Particularly, the NEDC cycle concentrates on low load and low speed operation, and includes a number of tolerances and flexibilities, which does not accurately reflects state-of-the-art technologies or the highly dynamic engine behavior for the wide range of operation typically covered in real driving conditions.

Recently a lot of interest is given to the Worldwide Harmonized Light Vehicles Test Procedure (WLTP), which was developed at the United Nations level through UNECE and is planned to replace the NEDC cycle in 2017 [7]. The WLTP has been designed on the basis of the in-use driving databases provided by Europe, India, Japan, Korea and USA. Urban, extra-urban, highway, and autobahn cycles are tested in series and each individual countries would arithmetically adjust the weighting of these cycles to best-match their regional driving behavior. Europe is also looking at using these cycles or portable emissions monitoring systems (PEMS) to reduce in-use emissions relative to vehicle certification value. Depending on the details, still in development, the in-use emissions program could drive the design of emissions systems and dictate different approaches.

Looking at the context presented so far, it seems evident that the automotive industry is facing an era of unprecedented challenges. A combination of severe emission legislations regulations, demanding targets in terms of CO_2 levels, new dynamic and more realistic test vehicle procedures,

and complex and rapidly changing regional and global markets, is pushing the boundaries of engine research and development (R&D) like it has never been seen. There is a real need to develop clean combustion engines with minimum environmental impact. The future generation of powertrain concepts must reach incredibly high efficiency levels, and make the best use of cost-effective technologies to decrease exhaust emissions both through advanced combustion strategies and complex after-treatment systems. Furthermore, it has to meet all of these requirements while also satisfying customer expectations in terms of engine performance, fun-to-drive, noise and acoustic comfort.

1.2.3 Main technology trends in R&D of modern powertrains for passenger cars

The large majority of passenger cars, which have to meet the already mentioned highly demanding targets, are powered either by a spark ignition (SI) gasoline engine or a compression ignition (CI) diesel engine. Although projections for 2050 seems quite far in the future, if we consider the time required to bring new engine concepts into production, together with the years needed to bring beneficial new technologies to the market and therefore into everyday use; we can realize that major efforts and investments in engine R&D are needed today, to develop sustainable propulsion systems that can really be competitive and permeate the global vehicle fleet in the next decades.

The main technological challenge for the CI diesel engine is to maintain its competitive advantage in terms of efficiency, and therefore, fuel consumption, compared to the SI gasoline engine. The diesel engine has to meet the Euro 6 standards, which are particularly severe in terms of NO_x and PM emissions, while keeping or even decreasing its current CO_2 levels, in a wide range of driving and environmental conditions that will be established in new testing procedures for complying with future Real Driving Emissions (RDE) standards. A relevant progress has been made specially on common-rail high speed direct injection (HSDI) systems, advanced turbo-charging, cooled exhaust gas recirculation (EGR), optimized combustion chamber and nozzle design, as well as sophisticated control algorithms [8]. However, the conventional mixing-controlled combustion taking place in a DI diesel engine, where injection, evaporation, mixture preparation and combustion occur nearly at the same time, leads to very different local condition in terms of temperature and air/fuel ratio, promoting the formation of both NO_x and PM emissions. The PM and NO_x emissions can be individually suppressed, but it exist a clear trade-off when trying to reduce both emissions simultaneously.

Different approaches have been explored in the past decade to resolve this natural disadvantage of the conventional diesel combustion (CDC) concept. From one side, exploring advanced combustion strategies which aim to decrease in-cylinder pollutant formation; and on the other side, the use of external or passive after-treatment systems to destroy or reduce engine-out emissions in the exhaust line before being expelled into the atmosphere. Many of these advanced combustion strategies can be classified as low temperature combustion (LTC) concepts which strive for a low combustion temperature or/and increased degree of premixing prior to combustion, to reduce NO_x and PM formation. A few examples of the numerous explored premixed LTC concepts are: "homogeneous charge compression ignition" (HCCI), "premixed charge compression ignition" (PCCI), "reactivity controlled compression ignition" (RCCI), "partially premixed compression ignition (PPCI)" and "partially premixed combustion" (PPC) [9–11]. However, even when the potential for simultaneous reduction of NO_x and PM has been already confirmed; there are still many issues to be resolved before adopting these technologies widespread, specially in terms of limited load/speed operating range. The strengths and limitations of these new combustion concepts will be described in detail in Chapter 2.

In the case of the SI gasoline engine, the main challenge is to reduce drastically fuel consumption and CO_2, while maintaining its intrinsic characteristics of comfort, simpler after-treatment systems and lower cost compared to the new generation of diesel engines. Downsizing and turbocharging in combination with electronic variable valve actuation (VVA) and gasoline direct injection (GDI) are nowadays key technologies for SI engines to cope with the challenges of improving fuel consumption and driveability [12, 13]. Moreover, the interest of SI engines is particularly important for the small class vehicle, where provides the best compromise in terms of cost/benefit ratio. Regarding unique emissions control requirements, GDI engines also have high PN emissions and need specific technologies to meet the emerging Euro 6 PN regulations. PN emissions generally come from cold start and from accelerations, but can be also emitted throughout the test cycle. Remediation approaches generally revolve around keeping the flame out of the rich, high-temperature PM-formation zone using improved air-fuel mixing, reduced wall impingement of the fuel, increased fuel injection pressure and cooled EGR. Finally, technologies like stratified and lean burn combustion, or further extending the operational range of EGR, could continue to improve the current efficiency and performance levels of GDI engines [13, 14]. Controlled auto-ignition (CAI) at low load conditions combined with spark ignition at high load conditions, is also a promising option to reduce CO_2 while

significantly reducing pollutant emissions. However, further advancements in advanced strategies for engine control are still needed to better control the auto-ignition mode and the transition between both regimes.

To comply with emissions limits, both SI and CI engines need to use dedicated after-treatment systems [12]. The three-way catalyst was develop more than 30 years ago for SI engines running in stoichiometric conditions. Diesel oxidation catalysts (DOC) have been introduced in 1989 for light-duty CI engines and later in 2000 the diesel particulate filter (DPF). The NO_x reduction is one of the foremost development challenges to maintain the diesel engine as the combustion engine with higher fuel efficiency for the future. From current point of view, only the lean NO_x trap (LNT) as well as selective catalytic reduction (SCR) technology, or a combination of both (LNT+SCR), present promising solutions in order to achieve the demanded high NO_x conversion efficiencies. The unavoidable increased complexity, and associated cost, of the after-treatment systems of a modern Euro 6 diesel engines could risk its competitiveness against the gasoline SI engine, especially in the small and compact vehicle classes. However, the introduction of PM and PN regulation in GDI engines for Euro 6, could require the use of dedicated particulate filter (GPF) in addition to the traditional TWC, or even the use of dedicated NO_x after-treatment systems in the cases of lean burn gasoline engines; which would also increase the complexity and costs of gasoline emissions control.

Figure 1.1 shows the main technology trends for the light-duty powertrain presented by the European Road Transport Research Advisory Council (ERTRAC) in the European Roadmap with projections up to 2030 [15]. In this future scenario, the use of alternative fuels in ICE starts to play an important role. In the case of SI engines, the modern platform based on downsizing/turbocharging/VVA enables a wide flexibility in adapting the combustion process to the specific characteristics of each fuel, which represents the ideal way to exploit the benefit of using compressed natural gas (CNC) from both fossil and renewable sources (biomethane). For CI engines, the development of process technologies for synthetic diesel by Fischer-Tropsch (FT) and hydrogenated vegetable oils (HVO) enables a wider panel of combustion approaches thanks to the specific fuel properties, specially higher cetane number and lower aromatics composition.

In terms of propulsion technology, the projections for alternative powertrain technologies up to 2050 suggest that more than a half of new light-duty vehicles will still be powered by an ICE equipped with advanced concepts and technologies. Even when a substantial fraction of these can be

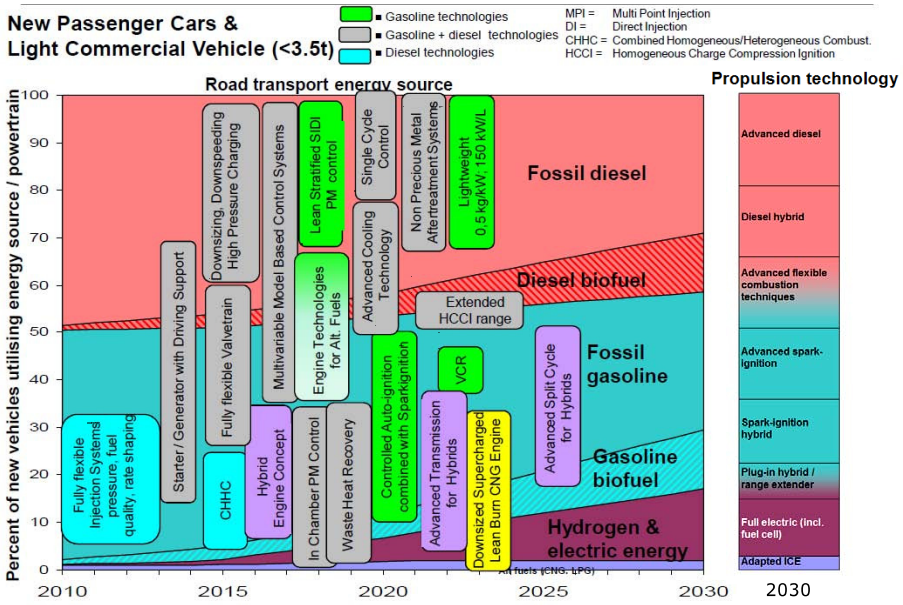

Figure 1.1. *Main technology trends and research needs for light-duty ICE powertrains to 2030. Source: ERTRAC Roadmap 2011 [15].*

expected to be vehicles with an ICE as the sole source of propulsion, the market penetration of hybrid technologies is expected to increase its share by 2030, therefore, ICE's will increasingly be integrated with electric motors and batteries in a wider range of hybrid powertrains. In this frame, there is a real potential in engine R&D for developing a clean, light and compact ICE's to cope with the hybrid powertrain increased complexity. Furthermore, reducing the costs of the complete drivetrain by keeping the ICE and after-treatment system costs to a minimum, could play a major role in increasing the competitiveness and market share of hybrid vehicles in the mid- and long-term.

1.3 Context of the research

The present study has been conceived in the frame of the development of a new engine concept for a small-size passenger car: a two-stroke CI engine with scavenge loop through poppet-valves in the cylinder head. The advantages of two-stroke engines over four-stroke engines are widely known. A two-stroke engine is capable of producing greater specific power due to its doubled firing

frequency compared to conventional four-stroke engine. Moreover, it offers a compact size and a lower weight with respect to engine output, and potentially lower mechanical losses [16].

However, the natural disadvantages and challenges of conventional two-stroke engines have restricted its use to very particular applications. For instance, gasoline SI two-stroke engines are particularly useful in lightweight (portable) applications such as motorcycles and small-engined devices, like chainsaws and outboard motors; whereas, CI diesel two-stroke engines are traditionally used in large applications, such as ships, locomotives and electricity generation. Even when the concept of a two-stroke diesel engine prototype was explored by several automotive companies in the 90's, including Yamaha Motor Co. [17], Toyota [18], AVL [19–21] and Daihatsu [22], none of them achieved to successfully place it into production.

The combination of two-stroke cycle and poppet intake and exhaust valves is unusual [16]. Two-stroke engines typically have either intake and exhaust ports in the cylinder wall or an intake port and exhaust poppet valve [23]. Conventional ported two-stroke engine while providing a compact and cheap power plant, have several disadvantages in terms of controlling the gas exchange by the piston movement, which can lead to compromised engine efficiency and power output due to the symmetric/fixed timing operation, in addition to high hydrocarbon emissions from lubricating oil, excessive oil consumption, unstable part-load combustion, and lower engine durability from asymmetric heating by the flow in the ports, as well as increased piston ring wear [16, 23–25]. A good compromise can be achieved if a poppet-valves design is adopted, maintaining the benefits of high specific power of the two-stroke cycle and the big advantage of sharing most of the components and mechanical design with mass production four-stroke engines, so the initial investment and production costs can be kept relatively low. Nevertheless, the scavenging is intrinsically inefficient in the poppet-valves architecture, producing some trapping difficulties that have to be managed [25].

In addition, one of the major drawbacks of the two-stroke architecture that have limited its application in the automotive field in the past, was the direct short-circuiting of the fresh intake flow and extremely complex scavenging process, which is also dependent on the intake and exhaust acoustics, and therefore, on the engine speed [16, 23–25]. Despite these well-known shortcomings, a renewed interest in the two-stroke engine as an automotive powertrain has come about with the availability of direct injection systems, advanced boosting technologies, variable valve actuation mechanisms, faster modeling and control tools, and the possibility of implementing advanced

combustion concepts [26–35]. On one hand, the use of DI systems can facilitate both SI and CI operation with flexible control of the in-cylinder air/fuel ratio without the risk of fuel short-circuiting; while on the other hand, the use of valves for intake and/or exhaust (either in poppet-valves or uniflow architecture) coupled with VVA to modify the opening and closing timings, can help optimizing the scavenging efficiency in a wider range of operation. Additionally, an external compressor or pump can be used to assist and improve the scavenging and charging processes.

Even when the first applications of the HCCI and CAI combustion were originally developed to improve combustion stability of gasoline two-stroke engines during the decades comprised between the 80's and 90's [36, 37], there has been only few modern studies that have attempted to evaluate the potential of the two-stroke engine as a suitable platform for implementing advanced combustion concepts [28, 31, 33, 38–41].

In this context, the idea of a two-stroke engine with poppet valves architecture for an automotive application was recently revived in the framework of a large-scale collaborative project called "Powertrain for future light-duty vehicles (POWERFUL)" funded by the European Union, as part of the Seventh Framework Programme Consortium Agreement (FP7) related to Sustainable Surface Transport. The concept of the POWERFUL project is to develop SI and CI powertrains for LDV, based on integrated technology sub-systems considering all main aspects -engine, after-treatment and fuels- to be able to answer to the challenges posed by real-world CO_2 and pollutant emissions expected beyond 2015.

The two-stroke engine could represent a cost-effective solution to modern engines for the small class vehicles, that can meet the pollutants legislation and keep competitive efficiency levels [42]. It offers two potential solutions which are of great interest to be explored:

- Potential for extreme engine downsizing, by reducing the volume either by decreasing cylinder unitary displacement or the number of cylinders, while keeping equivalent torque and power output.
- Potential for implementing advanced combustion concepts, overcoming the low power density and noise limitation observed when operating with HCCI and PCCI combustion modes, by doubling the firing frequency of four-stroke engines, producing almost twice torque and power output at the same engine displacement.

Within the POWERFUL Project, the sub-project V3 "Two-stroke diesel application for small vehicle" leaded by Renault, was dedicated to the

development of a 0.73 L two-stroke two-cylinder research diesel engine, which is essentially half of Renault's 1.5 L dCI base. This two-stroke engine concept integrates a common-rail HSDI system, a VVA mechanism to have flexibility for controlling both intake and exhaust timings, plus an advanced air charging system that combines a turbocharger with a mechanically driven supercharger to attain the boost requirements.

Considering the limitations and restrictions given by the context of this research work, it appears clear that the development a two-stroke CI engine for light-duty vehicles represents an important challenge from the conception, design and optimization point of view. It not only requires advanced calculation, modeling and experimental tools; but also a close cooperation and interaction between the engine manufacturer, the vehicle integration designers, the parts supplier, and the research institutions involved in such large-scale project. Further research and development performed at the institute CMT-Motores Térmicos of this new engine concept have been continued to be supported and funded within the frame of different private contracts accorded with Renault.

Accordingly, some of the questions that arise during the development phase of this engine concept, and that this research work aims at answering, are:

- How to optimize the scavenging characteristics of the poppet-valves architecture without compromising the combustion chamber design?
- How to properly burn the fuel in conventional diffusive diesel combustion with an internal aerodynamic governed by scavenge?
- Is it possible to reach and improve the performance and emission levels of the current four-stroke diesel engine?
- Which is the real potential of the two-stroke engine for controlling and extending the operating range of advanced combustion concepts?
- Is the concept viable for a production automotive engine?

1.4 Objectives of the research

The research work presented in this thesis focuses in the analysis of the air management and combustion processes in the two-stroke poppet-valves architecture under study, with special attention on pollutants emissions formation/oxidation processes, as well as the factors influencing the engine

thermal efficiency. Three main aspects have strong relevance, and will be studied in detail throughout this investigation:

- The influence of the main air management control levers over the in-cylinder conditions. For instance, this refers to how a given intake or exhaust pressure, valves timing, or EGR ratio affects the scavenging and trapping characteristics, and determines the gas composition and temperature at the beginning of the close cycle.
- The relationship between the in-cylinder conditions and local mixture air/fuel ratio, with the development of the combustion process, and additionally, their impact on final emissions levels.
- The major influential factors that play important roles in determining the indicated efficiency in this two-stroke configuration.

Based on these fundamental points, the main objective defined for this investigation is to: **Improve the existing understanding and assess the main relationships between the gas exchange and combustion processes in two-stroke poppet-valves engines, and evaluate their impact on exhaust emissions formation and final engine thermal efficiency.** To achieve this global objective, it is necessary to develop specific methodologies and tools for the efficient analysis and proper optimization of the air management and combustion processes in two-stroke engines.

In this regard, the other specific objectives of the research work that are pursued in this thesis are:

- Analysis and optimization of the performance and limits of the two-stroke poppet-valves engine concept when operating in conventional diesel mixing-controlled conditions; considering air management and combustion characteristics, pollutants emissions, fuel consumption and efficiency.
- Implementation of the low temperature highly premixed combustion (HPC) concept in the two-stroke engine with diesel fuel, to identify its potential for emissions reduction as well as its technological limitations.
- Implementation and optimization of the partially premixed combustion (PPC) concept in the two-stroke engine using gasoline fuel. It also includes evaluating its potential for emissions reduction and efficiency improvement, and study the use of different injection strategies for extending its operating range and improving its performance.

1.5 Outline of the thesis

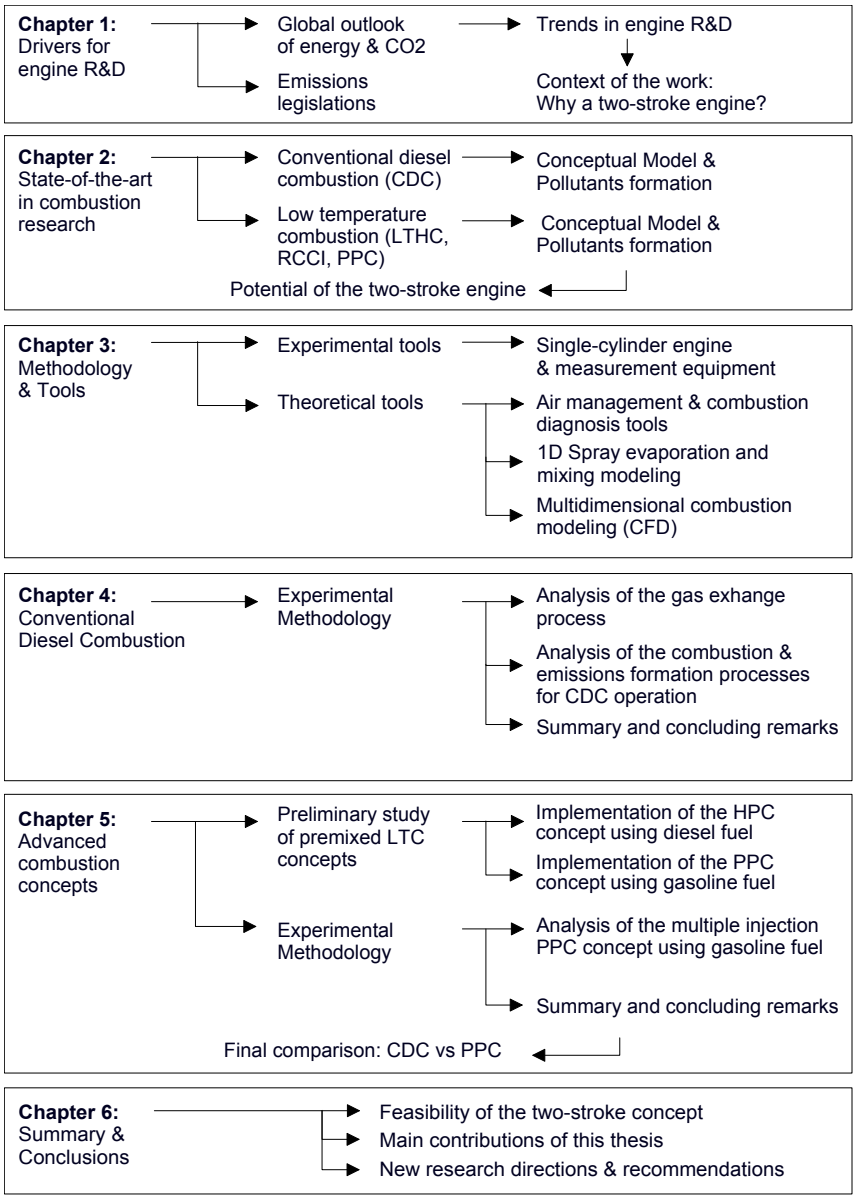

Figure 1.2. *Outline of the thesis.*

This thesis is organized in six chapters including the present introduction (Chapter 1). The outline of this document is presented in 1.2. In a first step, a thorough literature review is performed in Chapter 2, focused on the most relevant research works in the fields of formation and control of pollutants emissions in CI engines to assess the state-of-the-art.

In a second step, the correct definition of an appropriate methodology is essential to reach the objectives defined for this thesis. Furthermore, specific experimental and theoretical tools are required for the proper analysis of the results, specially when considering the added complexity from the two-stroke operation. In this regard, Chapter 3 is dedicated to an overview of the experimental installation and measurement equipment used in the study, the definition of the general testing methodology proposed along the thesis, and finally, the most relevant experimental and theoretical tools used during the analysis of results.

Chapter 4 and Chapter 5, are mainly based in the experimental results obtained with the single-cylinder research version of the two-stroke poppet-valves engine; but also include relevant information extracted from a 3D CFD model of the engine, to further illustrate the governing phenomena affecting the mixture preparation, combustion development and emissions formation processes.

The first stage of the research work, shown in Chapter 4, comprises the studies related to the analysis and optimization of conventional diesel combustion in the single-cylinder two-stroke research engine. A dedicated Design of Experiments (DoE) methodology is explained along Chapter 4, for easily identifying cause/effect relations of the main air management parameters on the cylinder conditions, and consequently on combustion process and exhaust emissions. The final objective is to optimize engine performance in terms of emissions and efficiency at different load/speed operating conditions, in order to fulfill a predefined set of optimization targets, and to obtain a reference base point to compare CDC against advanced combustion concepts.

Chapter 5 focuses on the implementation and evaluation of advanced combustion concepts with the aim of improving the conventional NO_x-PM trade-off inherent to the CDC concept. As an introduction to this chapter, the highly premixed combustion (HPC) concept using diesel fuel has been implemented through a set of parametric studies, to identify the main limitations and drawbacks of the homogeneous combustion concept when combined with high reactivity fuels. Departing from this background, a new line of research is defined, where switching to a lower reactivity fuel

(gasoline) and adopting a partially premixed combustion (PPC) strategy is well justified on the base of new parametric studies performed on the single-cylinder two-stroke engine while keeping a single-injection strategy. The next stage of the research, is dedicated to the analysis and optimization of the gasoline PPC concept using a multiple injection strategy. First, a detailed description of the main aspects controlling the PPC mode is performed, with support from specific experimental tests as well as multidimensional CFD calculations. Then, the effect of the most important injection settings is evaluated at different load conditions, to quantify their impact over the combustion characteristics, local cylinder conditions, exhaust emissions and final efficiency levels. Finally, the engine performance results are compared against optimized diesel operation, to fully assess the potential and related challenges of the gasoline PPC concept.

The last chapter (Chapter 6) outlines the main conclusions of this research work, and highlights the most relevant results obtained in this study to propose optimization paths to further improve the performance and emissions level of the engine concept under development. Finally, new possible research directions are formulated together with the recommendation of future tasks and studies.

Bibliography

[1] *Key World Energy Statistics 2014.* International Energy Agency IEA Publications, 2014.

[2] Elzen Michel den, Roelfsema Mark, Hof Andries, Botcher Hannes and Grassi Giacomo. *Analysing the emission gap between pledged emission reductions under the Cancun Agreements and the 2C climate target.* PBL Netherlands Environmental Assessment Agency. European Comission Joint Research Centre, 2012.

[3] *Energy Technology Perspectives 2014. Harnessing Electricity Potential.* International Energy Agency IEA Publications, 2014.

[4] *Regulation 715/2007 of the European Parliament and of the Council of 20 June 2007 on type approval of motor vehicles with respect to emissions from light passenger and commercial vehicles (Euro 5 and Euro 6) and on access to vehicle repair and maintenance information.* Official Journal of the European Union, 2007.

[5] *Comission Regulation 459/2012 of 29 May 2012 amending Regulation 715/2007 of the European Parliament and of the Council and Commission Regulation No 692/2008 as regards emissioos from light passenger and commercial vehicles (Euro 6).* Official Journal of the European Union, 2012.

[6] *Regulation 443/2009 of the European Parliament and of the Council of 23 April 2009 setting emission performance standards for new passenger cars as part of the Community's integrated approach to reduce CO2 emissions from light-duty vehicles.* Official Journal of the European Union, 2009.

[7] Tutuianu Monica, Marotta Alessandro, Steven Heinz, Eva Ericsson, Haniu Takahiro, Ichikawa Noriyuki and Ishii Hajime. *Development of a World-wide Worldwide harmonized Light duty driving Test Cycle (WLTC). Technical Report.* UNECE DHC subgroup, 2013.

[8] Knecht Walter. "Diesel engine development in view of reduced emission standards". *Energy*, Vol. 33 n^o 2, pp. 264–271, 2008.

[9] Yao Mingfa, Zheng Zhaolei and Liu Haifeng. "Progress and recent trends in homogeneous charge compression ignition (HCCI) engines". *Progress in Energy and Combustion Science*, Vol. 35 n^o 5, pp. 398–437, 2009.

[10] Saxena Samveg and Bedoya Ivan D. "Fundamental phenomena affecting low temperature combustion and HCCI engines, high load limits and strategies for extending these limits". *Progress in Energy and Combustion Science*, Vol. 39 n^o 5, pp. 457–488, 2013.

[11] Reitz Rolf D. and Duraisamy Ganesh. "Review of high efficiency and clean reactivity controlled compression ignition (RCCI) combustion in internal combustion engines". *Progress in Energy and Combustion Science*, Vol. 46 n^o 0, pp. 12–71, 2015.

[12] Johnson Timothy V. "Vehicular Emissions in Review". *SAE International Journal of Engines*, Vol. 5 n^o 2, pp. 216–234, 2012.

[13] Alkidas Alex C. "Combustion advancements in gasoline engines". *Energy Conversion and Management*, Vol. 48 n^o 11, pp. 2751–2761, 2007.

[14] Galloni E., Fontana G. and Palmaccio R. "Effects of exhaust gas recycle in a downsized gasoline engine". *Applied Energy*, Vol. 105 n^o 0, pp. 99–107, 2013.

[15] *European Roadmap. Future Light-Duty Powertrain Technologies and Fuels.* ERTRAC Working Group on Energy and Environment, 2011.

[16] Heywood J.B., Sher E. and Engineers Society of Automotive. *The Two-stroke Cycle Engine: Its Development, Operation, and Design.* Taylor and Francis, 1999.

[17] Masuda Tatsuyuki, Itoh Hideaki and Ichihara Yasusi. "Research on the Practical Application of 1 liter, Semi-DI, 2-Stroke Diesel Engine to Compact Cars". In *SAE Technical Paper*, volume 1999-01-1249, 1999.

[18] Nomura K and Nakamura N. *Development of a New Two-Stroke Engine with Poppet-Valves: Toyota S-2 Engine.* A New Generation of Two-Stroke Engines for the Future? Proceedings of the International Seminar, Rueil-Malmaison, France, Editions Technip, Pairs, 1993.

[19] Knoll R and Gutmann P. "The two-stroke engine professional List diesel engine for future small comfort cars.". In *In proceedings of the SIA International Congress, April 1996, Paris, France.*, 1996.

[20] Knoll R. "The two-stroke List diesel -a new approach to motorize small comfort cars.". In *In proceedings of the FISITA Congress, June 1996, Prague, Czech Republic.*, 1996.

[21] Knoll Reinhard. "AVL Two-Stroke Diesel Engine". In *SAE Technical Paper*, volume 981038, 1998.

[22] Co. Daihatsu Motor. "Ltd, Press Information.". In *The 61st International Motor Show (IAA), Frankfurt 2005.*, 2005.

[23] Blair G.P. *Design and Simulation of Two-stroke Engines.* Society of Automotive Engineers, 1996.

[24] Jante Alfred. "Scavenging and Other Problems of Two-Stroke Cycle Spark-Ignition Engines". In *SAE Technical Paper*, volume 680468, 1968.

[25] Enrico Mattarelli, Giuseppe Cantore and Carlo Alberto Rinaldini. *Advances in The Design of Two-Stroke, High Speed, Compression Ignition Engines*, volume Chapter 5. InTech, 2013.

[26] Duret Pierre. *A new generation of two-stroke engines for the future?* Editions Technip, Pairs, 1993.

[27] Abthoff J., Duvinage F., Hardt T., Kramer M. and Paule M. "The 2-Stroke DI-Diesel Engine with Common Rail Injection for Passenger Car Application". In *SAE Technical Paper*, volume 981032. SAE International, 1998.

[28] Osborne R. J., Stokes J., Lake T. H., Carden P. J., Mullineux J. D., Helle-Lorentzen R., Evans J. C., Heikal M. R., Zhu Y., Zhao Hua and Ma T. "Development of a Two-Stroke/Four-Stroke Switching Gasoline Engine - The 2/4SIGHT Concept". In *SAE Technical Paper*, volume 2005-01-1137, 2005.

[29] Hooper P. R., Al-Shemmeri T. and Goodwin M. J. "Advanced modern low-emission two-stroke cycle engines". *Proceedings of the Institution of Mechanical Engineers, Part D: Journal of Automobile Engineering*, Vol. 225 n^o 11, pp. 1531–1543, 2011.

[30] Turner J. W. G., Blundell D. W., Pearson R. J., Patel R., Larkman D. B., Burke P., Richardson S., Green N. M., Brewster S., Kenny R. G. and Kee R. J. "Project Omnivore: A Variable Compression Ratio ATAC 2-Stroke Engine for Ultra-Wide-Range HCCI Operation on a Variety of Fuels". *SAE Int. J. Engines*, Vol. 3 n^o 1, pp. 938–955, 2010.

[31] Dahl Daniel and Denbratt Ingemar. "Valve Profile Adaptation, Stratification, Boosting and 2-Stroke Strategies for Raising Loads of Gasoline HCCI Engines". *SAE International Journal of Engines*, Vol. 5 n^o 3, pp. 1033–1045, 2012.

[32] Vashishtha Ashish, Rathinam Balamurugan, Delahaye Laurent, Ravet Frederic and Justet Frederic. "Study of Intake Ports Design for Ultra Low Cost (ULC) Gasoline Engine Using STAR-CD". In *SAE Technical Paper*, volume 2012-01-0407, 2012.

[33] Zhang Yan, Ojapah Mohammed, Cairns Alasdair and Zhao Hua. "2-Stroke CAI Combustion Operation in a GDI Engine with Poppet Valves". In *SAE Technical Paper*, volume 2012-01-1118, 2012.

[34] Pohorelsky Ludek, Brynych Pavel, Macek Jan, Vallaude Pierre-Yves, Ricaud Jean-Charles, Obernesser Philippe and Tribotte Pascal. "Air System Conception for a Downsized Two-Stroke Diesel Engine". In *SAE Technical Paper*, volume 2012-01-0831, 2012.

[35] Laget O, Ternel C, Thiriot J, Charmasson S, Tribotte P and Vidal F. "Preliminary Design of a Two-Stroke Uniflow Diesel Engine for Passenger Car". In *SAE Technical Paper*, volume 2013-01-1719, 2013.

[36] Onishi Shigeru, Jo Souk Hong, Shoda Katsuji, Jo Pan Do and Kato Satoshi. "Active Thermo-Atmosphere Combustion (ATAC) - A New Combustion Process for Internal Combustion Engines". In *SAE Technical Paper*, volume 790501. SAE International, 1979.

[37] Duret Pierre and Moreau Jean-Francois. "Reduction of Pollutant Emissions of the IAPAC Two-Stroke Engine with Compressed Air Assisted Fuel Injection". In *SAE Technical Paper*, volume 900801, 1990.

[38] Iijima Akira, Watanabe Takashi, Yoshida Koji and Shoji Hideo. "A Study of HCCI Combustion Using a Two-Stroke Gasoline Engine with a High Compression Ratio". In *SAE Technical Paper*, volume 2006-32-0043, 2006.

[39] Zhao H. *HCCI and CAI engines for the automotive industry*. Woodhead Publishing in mechanical engineering. Woodhead Pub., 2007.

[40] Zhang Yan, Zhao Hua, Ojapah Mohammed and Cairns Alasdair. "CAI combustion of gasoline and its mixture with ethanol in a 2-stroke poppet valve DI gasoline engine". *Fuel*, Vol. 109 n^o 0, pp. 661–668, 2013.

[41] Zhang Y. and Zhao H. "Investigation of combustion, performance and emission characteristics of 2-stroke and 4-stroke spark ignition and CAI/HCCI operations in a DI gasoline". *Applied Energy*, Vol. 130 n^o 0, pp. 244–255, 2014.

[42] Tribotte Pascal, Ravet Frederic, Dugue Vincent, Obernesser Philippe, Quechon Nicolas, Benajes Jesus, Novella Ricardo and De Lima Daniela. "Two Strokes Diesel Engine - Promising Solution to Reduce CO2 Emissions". *Procedia - Social and Behavioral Sciences*, Vol. 48, pp. 2295–2314, 2012.

Chapter 2

Literature review

Contents

2.1 Introduction

Historically, the emissions targets (prior to Euro 5) in diesel engines were achieved for the most part without exhaust-gas after-treatment. In-cylinder strategies combining higher fuel injection pressure, higher boost and lower intake temperatures, adjustments to fuel injection timing, low to moderate levels of exhaust gas recirculation (EGR), and improved combustion chamber design were sufficient. The later targets (from Euro 5), however, have been achieved or are expected to be achieved through a combination of both in-cylinder strategies and after-treatment devices. After years of development, viable after-treatment technologies are now available, but their widespread adoption usually supposes higher economic costs, fuel economy penalties, great space requirements and increased complexity for engine calibration. Therefore, continuous improvements of in-cylinder strategies to further reduce engine-out emissions and thereby lessen the after-treatment requirements are still of great interest.

This chapter is structured in two main sections. The first section focuses in the conventional diesel combustion (CDC) concept, and aims to provide the reader with a fast overview of the phenomenological description of the different phases observed in a mixing-controlled combustion process, including a review of the traditional conceptual models that describes temporal and spatial formation of pollutants emissions in a diesel combustion, and finishing with the representation of the CDC process in the Kamimoto & Bae "ϕ-T" diagram to contextualize the definition of different LTC combustion modes.

In the second section, the state-of-the-art and most recent advancements in LTC combustion concepts are briefly summarized, focusing in the mixture preparation process and main combustion characteristics of each concept, its technological potential for emission reduction and efficiency improvements and challenges to be addressed. For the purposes of the discussion presented in this thesis, the literature review makes special emphasis in the strategies which present high or moderate degree of premixing prior to combustion, excluding the mixing-controlled LTC strategies.

2.2 Overview of the Conventional Diesel Combustion concept

Significant progress has been made in the last years in furthering our understanding of the nature of the diesel combustion process. In this regard,

this section intents to provide an updated summary of the main physical and chemical processes occurring inside the combustion chamber of a direct injection diesel engine. The approach is rather conceptual, intending to describe such processes in a qualitative way, and it calls upon conceptual models which researchers of the engine community have develop on behalf of the experiments they performed and the phenomena they observed.

2.2.1 Phenomenological description of the mixing-controlled combustion process

The most appropriate way to start with the review of diesel combustion is probably to keep a simplistic view when describing the main processes occurring inside the cylinder, starting at the moment when the fuel leaves the injector nozzle and is injected into the combustion chamber, where it exist a high density and high temperature environment that promotes mixing, evaporation, and ignition of the fuel-air mixture. Assuming a single injection strategy timed relatively close to TDC with a sufficiently long duration, the analysis of the injection rate and the rate of heat release (RoHR) allow identifying the different phases of the combustion process following a chronological order, as presented in Figure 2.1. The RoHR is obtained from the analysis of the cylinder pressure using a 0-dimensional model based on the application of the first law of thermodynamics. This parameter accounts for the intensity with which the chemical energy contained within the fuel is released. The main phases of diesel combustion are conventionally defined as follows:

1. Ignition delay: This first stage covers the period between the start of injection (SoI) and the start of combustion (SoC); or more explicitly between the time at which the first fuel droplet enters the combustion chamber environment and the time where the energy release starts to grow significantly. During this phase the fuel is injected with no apparent or very little increase in the RoHR, as shown in Figure 2.1. Fuel injection begins slightly before top-dead-center (TDC), where the in-cylinder gases are hot and dense. The liquid-fuel spray mixes with the ambient gases, which provide the thermal energy to vaporize the fuel. The forming hot mixture of vaporized fuel and ambient gas is very unstable and chemical pre-reactions of low intensity start to develop. These small reactions will lead to the spontaneous self-ignition of the mixture, unleashing highly exothermic reactions until the chemical rate of the heat release eventually exceeds the vaporization energy rate. This point marks the start of

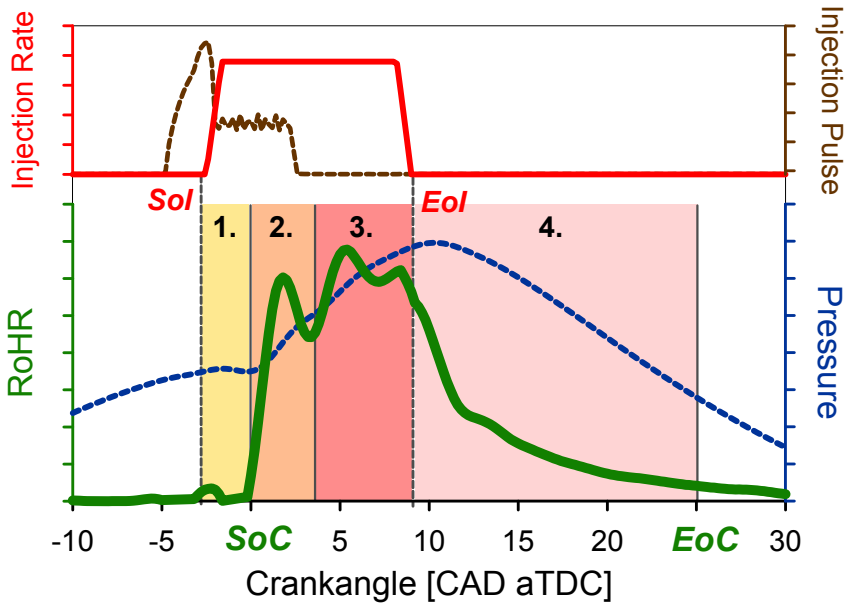

Figure 2.1. *Definition of the diesel combustion phases by comparison of the fuel injection rate with the RoHR trace.*

the high temperature phase of the RoHR, which is distinguished by a measurable pressure increase, that defines the end of the ignition delay and the start of combustion.

2. Premixed combustion: During the premixed burn that follows, the ignition reactions rapidly accelerate propagating to all the vaporized fuel injected during the delay that was premixed during the time lag before ignition, consuming the available oxygen in the overall fuel-rich mixtures. The burning of this premixed mixture is primarily controlled by chemical kinetics so the energy is released at a fairly high rate, producing the first characteristic peak on the RoHR trace. After the premixed burn, the RoHR typically decreases to a lower level until reaching a relative minimum (time derivative of RoHR equal to 0), which indicates the end of the premixed combustion phase and the transition towards the mixing-controlled stage.

3. Fast mixing-controlled combustion: During this phase, the injection and combustion processes continue to develop simultaneously, so the mixing process of the injected fuel continue to be sustained mainly by

the momentum flux induced by the spray. The heat is assumed to be released at the same rate as the fuel mixes with air, and a diffusion flame is established. The reaction zone is located where the fuel-air mixture reaches stoichiometric conditions. If the injection duration is long enough, the flame structure stabilizes reaching quasi-steady conditions, which are kept until the end of the injection (EoI).

4. Slow mixing-controlled combustion: When the injector needle starts to close a transitory state in the injection rate begin, until the holes are finally closed, and the introduction of mass and momentum disappears. The amount of mixture remaining in the chamber continue to burns but a slower rate, which is distinguished in the RoHR by the progressive decay in the energy released, shown in Figure 2.1. Combustion looses intensity and the flame loses its quasi-stationary structure, adopting more random configurations, until the flame finally quenches and puts an end to the whole combustion process (EoC).

Recent research within optically accessible engines and constant volume vessels, added to the further development of laser sheet imaging diagnostics, has provided a means for making detailed measurements of the diesel combustion process and define the structure of diesel flames. Although a more accurate description of the temporal sequence is obtained compared to what was previously introduced with the traditional evolution of the RoHR, most of the new contribution actually concerns the spatial resolution of the related physical and chemical processes.

In 1997, Dec [1] proposed a conceptual model for conventional diesel combustion, which was subsequently extended by Flynn et al. [2] in 1999, and became widely accepted by the scientific community as an important foundation for the understanding and modeling of the in-cylinder processes responsible for diesel engine performance and pollutant emissions characteristics. The original conceptual model applies to conventional diesel conditions, having a single-injection phased shortly before TDC, without EGR, and long enough to achieve a significant "quasi-steady" period so the majority of the fuel burns during mixing-controlled conditions. In this conditions, there is a negative ignition dwell meaning that the injection and combustion events are overlapped during a given fraction of the time. A few additional contributions, provided by subsequent studies relevant to the original Dec's conceptual model, are also included in the following description. Finally, the late-cycle processes occurring after the end of injection, which are not described in Dec's conceptual model but are supported by later investigations, are also addressed in the last section of this description.

2.2.1.1 Pre-combustion jet dynamics, ignition and stabilization period

Prior to the onset of ignition, the processes involved in spray formation are entirely driven by physical phenomena, until the oxygen content of the mixture triggers the first chemical reactions, and modifies both its physical and chemical environment. To isolate the physical aspects from the chemical aspects, different type of experiments and studies related to the injection and spray characterization are performed under non-reactive atmospheres. For instance, the internal flow characterization of the injector, which has been widely studied by Gimeno [3, 4] and Hermens [5], focuses on the study of the associated fuel pressure drops and efficiency losses, starting from the rail and arriving to the nozzle orifice outlet, which are credited for the major part to liquid friction but also to complex phenomena like cavitation, which is extensively detailed in the works of Salvador [6]. The understanding of the phenomena occurring between the orifice extremities, before the fuel is finally released in the combustion chamber, is essential for engine design as it fixes both the fuel mass flow rate and its momentum flux.

Once injected within the chamber, the liquid fuel atomizes into small droplets which possibly reform by coalescence before their vaporization. Fuel mixes with air at a rate controlled by the momentum flux created by the pressure drop between the injector nozzle and the chamber, then, a spray forms and goes through a succession of purely physical processes which breaks down into liquid fuel atomization, air entrainment and fuel vaporization. First, the liquid phase atomizes and then each spray penetrates into the combustion chamber, expanding into a roughly conical jet, as the in-cylinder gases (typically air or a mixture of air with EGR) entrained into the jet increases with downstream distance from the injector. Such processes are also very similar to those when injecting the same spray into an atmosphere of inert gases. The works of Correas [7], Arrègle [8], Ruiz [9] and López [10] provide in-depth discussions about the physical processes leading to liquid jet atomization and their modeling.

Entrainment correlations predict that the increasing entrainment downstream causes the equivalent ratio to vary along the jet axis approximately inversely with the downstream distance [11–13], and direct fuel vapor measurements confirm this prediction [14]. The equivalence ratio is defined as the ratio of local fuel-ambient charge mass ratio to the stoichiometric fuel-ambient mass ratio. During this process, enough energy is entrained to heat up and evaporate the liquid fuel. At some distance downstream of the injector nozzle, all of the fuel enters the vapor phase establishing the

location of the termed "liquid length" [11, 15, 16]. The liquid length can be reliably predicted to find the location where the fuel-ambient ratio is such that the thermal energy added to the jet by the entrained gas is sufficient to fully-vaporize the fuel [15, 17]. This predictions implies that for high-pressure diesel injection, vaporization is limited by mixing (i.e., entrainment), not by droplet atomization and vaporization processes. Based on this statement, the behavior of a diesel spray can be assimilated as an analogous gaseous jet, since the local conditions inside the spray depend on the global mixing rate of the fuel and the ambient charge, rather than on the local phenomena occurring at the droplets. Further implementation of these hypothesis were included in the 1D-models of García [18], Pastor [19] and Musculus [20, 21], while adding time-resolution and a more elaborated radial distribution of the fuel mass. These 1D models, although with strong hypotheses, can reasonably predict spray morphology and give a quantitative assessment of the spray mixture fraction field, especially at high density levels, while keeping a low computational time and cost compared to multidimensional 3D-CFD models.

Figure 2.2 shows a sequence of idealized schematics of the early stages of the diesel combustion event originally presented by Dec and Flynn et al., which has been slightly modified by Musculus to include contributions from later investigations [1, 22–26]. The sequence begins immediately after the start of fuel injection and show the development of a liquid jet, continuing through the premixed burn and up to the start of quasi-steady combustion. Some of the changes that were made compared to the original model of Dec, is that the new representation includes formaldehyde (representative of the first-stage ignition), and soot and its precursors (PAHs) are presented in a single color (red). The crank angle instants selected for the sequence are also marked in the apparent RoHR profile shown on top of the figure.

For the first three crank angle degrees (0.5 ms) of the fuel injection, the liquid fuel (dark brown) and vapor fuel (light brown) penetrate together, until the fuel is fully vaporized stabilizing the liquid length at around 25 mm, from where the vapor fuel continues to penetrate beyond the liquid forming a sheath of vaporized fuel-air mixture around the jet's periphery and at the leading edge of the jet. Fuel heating and vaporization causes a local cooling effect in the spray region, inhibiting temporally the ignition chemistry and consuming energy. As additional hot air is entrained into the jet, temperatures within the jet increases up to a level from which the first stage of ignition begins, and from that point, the mixture switches to an unstable state and chemical reactions of hydrocarbon oxidation propagate to the surrounding. The onset of this chain reaction technically marks the end of what is called the "physical induction phase" of ignition.

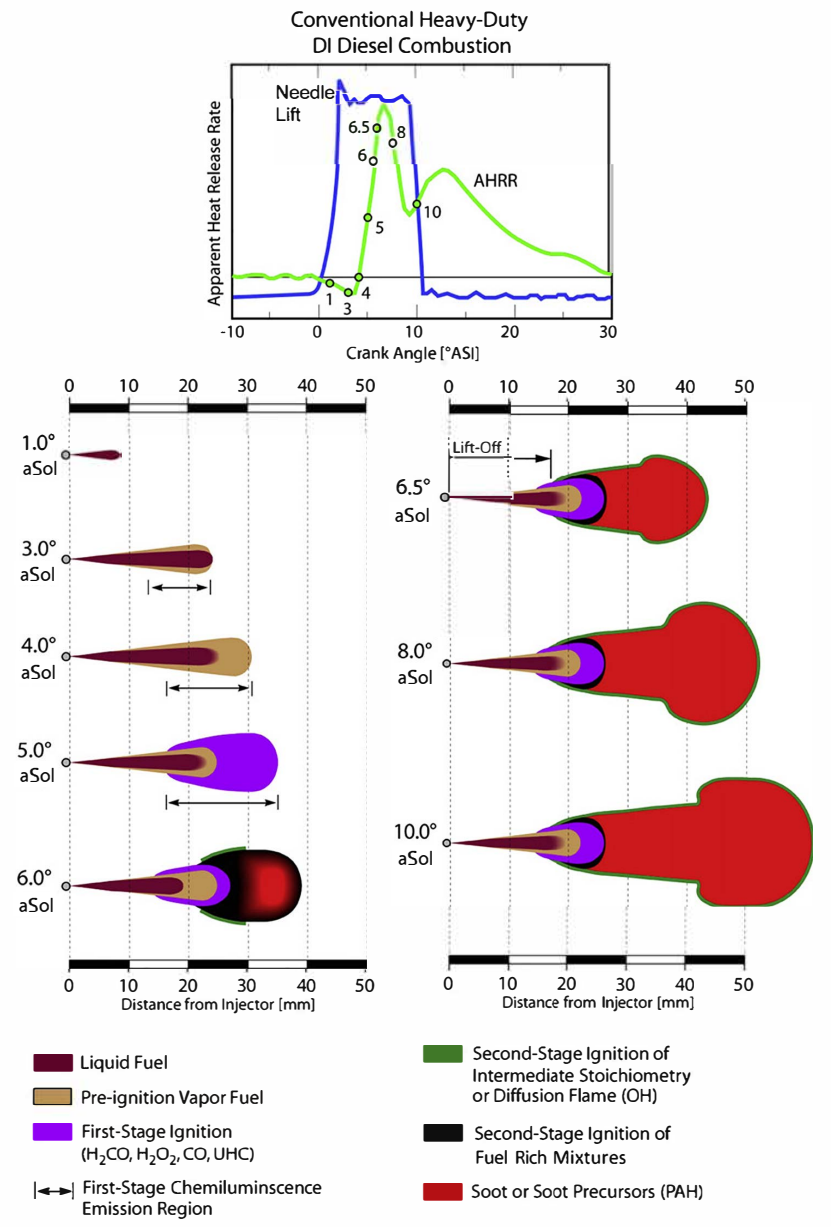

Figure 2.2. *Schematics of early flame images from laser measurements. The notation aSoI refers to a given crankangle value after the* SoI. *Source: Flynn et al [2].*

At this point of the discussion, it is important to remark that the detailed chemical kinetics of ignition itself is controlled by fuel molecule structure, oxygen content and temperature. Furthermore, typical diesel fuels are composed by a mixture of thousands of chemical species, including single- and multiple-ring aromatics, olefins, and branched- and straight-chain alkanes. The large fraction of long, straight-chain alkane species are responsible for much of the two-stage ignition chemistry characteristic of diesel fuels.

The first-stage ignition period begins with the first detectable chemical activity in terms of chemiluminescence or rise in pressure, and progresses until the rapid increase in the rate of heat release, which defines the start of the premixed burn and second-stage of ignition. Dec and Espey [25, 27] studied in detail the phasing of the flame development respect to the cylinder pressure signal in an optically accessible engine. From this investigation it was possible to observe the appearance of low-intensity chemiluminescence in the rich vapor region of the spray prior to the main heat release. Some isolated spots were first detected until developing uniformly in the rich leading portion of the jet. This later instant appeared to match the very first heat release, before it could even recover from the heat absorption due to fuel evaporation. Further spectroscopic analysis revealed that such chemiluminescence observed in this first-stage ignition is due mainly to the formation of formaldehyde (H_2CO) and CH radical. Then, Higgins et al. [28] confirmed that the first-stage ignition chemistry grows broadly in the region of the spray comprised between the liquid length and the penetrating tip of the spray, in agreement with Dec and Espey's observations [25]. It is worth to note that the duration of the first-stage ignition period can vary depending on the resolution of the hardware employed for the measurement, and on the selected criteria used to consider the RoHR as "significant" to mark the beginning of the premixed burn. This period is usually referred to in the literature as "low-temperature ignition" or "cool flames" [2, 23, 25, 29].

Chemiluminescence emission from first-stage pre-ignition reactions starts to appear early in the downstream part of the jet, indicated by double-ended arrows in the schematics shown in Figure 2.2 from 3.0 ° aSoI. Formaldehyde, which is important because it can be conveniently accessed by laser-induced fluorescence forms during first-stage ignition [22, 24, 25], in agreement with results obtained with chemical kinetics modeling for stoichiometric, and fuel-rich and fuel-lean reactions [30]. The temperature increase during the first-stage ignition is estimated to be between 200 K to 300 K, reaching temperatures around 825 K to 900 K at the core of the spray; although only two-thirds are attributed to the cool-flame heat release, while the rest is caused by hot air entrainment, so the mixing process still plays an important role in

the heating of the mixture. A short time (1 CAD to 2 CAD or 100 μs to 200 μs) after chemiluminescence from the initial ignition reactions is first detected, the reactions evolve into a highly exothermic second-stage of ignition, leading to the "premixed burn" phase of diesel combustion.

The region of the jet that first ignite is fuel-rich and as temperature rapidly increases, poly-aromatic hydrocarbon (PAH) which are soot-precursor species quickly form in the hot (1600 K to 2000 K), fuel-rich combustion products of the premixed burn. Soot formation follows shortly after, filling the entire downstream jet cross section. For conventional diesel conditions, the timescales of second-stage ignition, traced by OH formation, and soot precursor formation are very short because of the rapid temperature increase. Note that in this case, the high ambient temperature, rich ignition mixtures, and low dilution levels accelerate the transition between phases, so that the individual ignition stages are not easily distinguished in the apparent rate of heat release profile. OH (marked in green) appears in isolated spots at the periphery of the jet [27] close to the same timing as soot precursor formation (see schematic at 6.0 ° aSoI), indicating nearly simultaneous combustion of fuel-rich and intermediate stoichiometry regions of the jet.

Short time after ignition, near the peak RoHR of the premixed burn, the OH layer grows and forms a diffusion flame on the periphery of the fuel-rich, high-temperature downstream region of the jet [24, 27]. The flame front moves, on one side downstream of the spray towards the jet tip, and on the other, towards the nozzle until the balance between the flame front speed and the velocities within the spray is found and "quasi-steady conditions" are reached. The upstream edge of the diffusion flame does not extend fully to the injector nozzle, but rather it remains some distance downstream, termed the "lift-off length" (LOL) due to reasons not yet well understood. A zone of first-stage combustion products (formaldehyde) still persist upstream of the lifted diffusion flame [23, 24].

Finally, it is worth to note that during the processes of second-stage ignition, the liquid length decreases somewhat, likely due to local temperature rise at the start of combustion, including a temperature increase because of compression heating from the premixed burn. Several different interpretations can be found in the literature about this transition from premixed- to diffusive-phase, if the reader wants to have a more thorough description it is referred to the research carried out by Dec and Coy [27]), and more recently by Bruneaux [24] and Higgins [28].

2.2.1.2 Quasi-steady period

After the initial transient of the jet penetration and ignition processes, but before the end of injection, the flame front establishes and progresses until reaching its natural maximum length and the jet enters in "quasi-steady" period -during which the characteristic description of the combusting jet does not change-, while being sustained by the convective and diffusive contribution of fuel and oxygen. For the operating conditions depicted in the schematics shown in Figure 2.2, quasi-steady conditions are established around 10 crank angle degrees after the start of injection. A more detailed schematics of Dec's conceptual model during the "quasi-steady" period is introduced in Figure 2.3. As discussed by Dec, this schematic shows some hypothesized features in addition to those actually determined from laser sheet imaging [1, 2].

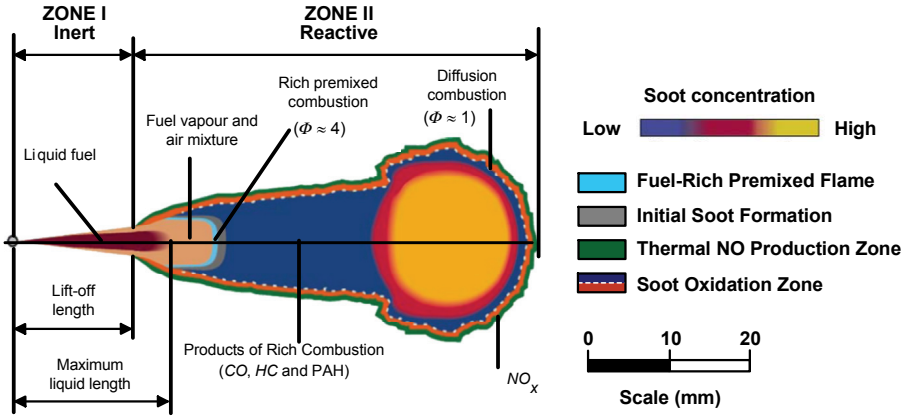

Figure 2.3. *Schematics of Dec's conceptual model during the quasi-steady period of diesel combustion. Source: Dec [1, 2].*

According to the schematics presented in Figure 2.3, a first zone can be distinguished (zone I), in the region located between the nozzle exit and the lift-off length. All the physical processes related to atomization, air entrainment and mixture vaporization, which were previously described, basically take place in this first zone. This region behave like a non-reactive and evaporative spray although the physical mixing process can be altered by the presence of the diffusive flame downstream this zone.

Downstream the lift-off length, the flame adopts the typical structure of a diffusion flame, denoted as zone II, where the internal structure of the jet is occupied by combustion products partially oxidized in a premixed rich zone,

surrounded by the stoichiometric diffusive reaction surface which impedes the oxygen to flow towards the core of the jet.

Because the flame is lifted, fuel and air are premixed upstream of the diffusion flame, and Dec hypothesized that a standing premixed reaction zone would form near the lift-off length, as depicted in Figure 2.3, where the rich combustion reactions would consume all the oxygen entrained in the first non-reactive region. Later studies performed by Idicheria and Pickett [23] and also by Bruneaux [24] showed formaldehyde formation upstream of the lift-off length in the jet cross section that is consumed downstream the lift-off length, indicating the existence of autoignition reactions, which is consistent with such a standing premixed reaction zone.

The degree of premixing of fuel with ambient gases upstream of the lift-off length is critical for soot formation in the jet [31]. The amount of entrainment upstream of the premixed combustion zone increases with increasing lift-off length, so that the equivalence ratio of the mixture entering the standing reaction zone decreases with increasing lift-off length. Soot formation decreases as the equivalence ratio at the lift-off is reduced, until reaching a threshold of equivalence ratio near to 2, from which no soot formation appears in the jet [14, 32]. The magnitude of the lift-off length and the equivalence ratio at the lift-off are affected by many factors, including ambient gas temperature, density, oxygen concentration, injection pressure, orifice diameter, and also fuel properties [32, 33]. Under typical diesel conditions, the equivalence ratio at the lift-off length is well above the threshold for soot formation, so that the jet is typically filled with soot, as shown in Figure 2.3.

Flynn et al. [2] estimate that in the quasi-steady jet, the temperature of the liquid fuel jet rises by mixing with hot air from its injection temperature of approximately 350 K to a temperature of 650 K to 700 K before it enters the region surrounded by the diffusion flame sheath. Inside the diffusion flame the recirculated products of partial combustion can be entrained into the jet, causing a rapid increase to about 825 K where oxidation reactions can be completed rapidly. The energy released by the initial low temperature fuel oxidation reactions are sufficient, given the local rich conditions of the mixture, to cause the local temperature to rise well above 1150 K. This is the temperature threshold where reaction rates increase sharply leading to the complete consumption of all available oxygen and driving local temperatures up to 1600 K.

Only 10 % to 15 % of the fuel energy is released in this rich premixed reaction zone, and the resulting combustion products (typically a mixture of

CO, partially burned fragments of hydrocarbons and PAH's) are transported through the interior of the plume toward the boundary of the stoichiometric diffusion flame, increasing their temperature through radiative and convective heat transfer from the flame front. Dec and Flynn also speculate the detailed formation processes of soot particles within the jet as: pyrolisis of the fuel into simple straight-chain hydrocarbons, followed by cyclization of these straight-chain hydrocarbons into PAH's and graphitic sheets of PAH, coagulation of the graphitic sheets into small primary particles, and agglomeration of these small primary particles into soot aggregates. When moving downstream along the axis of the reacting diesel jet, the soot concentration increases with longer residence time at these locally fuel-rich and high temperature conditions.

As the fuel fragments and partially oxidized products approach the diffusion flame, they become hotter as they arrive to a very thin reaction zone, with a thickness inferior to 120 μm [27], where the remaining 90 % to 85 % of the heat of combustion is released and local temperatures reach levels close to the adiabatic flame temperature at stoichiometric conditions. More precisely, the intermediate combustion products including hydrocarbons and soot, complete their oxidation into carbon dioxide and water when finding the adequate amount of oxygen by diffusion into the burning flame from the exterior of the flame sheath.

Laser imaging performed by Dec and Tree [34] and also by Kosaka [35] confirm how the soot particles are observed within the inner area of the flame, surrounded by the reaction surface, traced by the existence of the OH radical fluorescence. Moreover, Dec and Tree also confirm that soot particles almost disappears in the outside region of the flame, indicating the complete oxidation of soot which is dominated by the OH radical at stoichiometric conditions, as they travel across the flame front [34]. Dec represents the shape of the reactive surface including a head vortex on the leading side of the flame, as depicted in Figure 2.3. This vortex is created during the transient development before the flame reaches its natural length. In this region, soot concentration peaks as its formation and growth are favored by the high temperature and the long residence time required by the rich combustion products to reach the flame surface. In Dec's LIF measurements, nitrogen oxides formation is observed initially in a relatively thin surface surrounding the exterior of the diffusion-burning interface, consistent with the ideal conditions of high temperature (around 2700 K) and oxygen excess that are required for the appearance of this species [36]. NO formation is rapid in zones of high OH concentration and in magnitude it mirrors the OH behavior, therefore, OH can provide an indirect and qualitative indication of likely NO distributions and regions of formation, which is useful due to the diagnostic difficulties associated with

direct optical detection of NO. Once NO_x has been formed, it can diffuse both into and away from the diffusion flame sheath. It is worth to comment that even when approximately two thirds of the tail pipe NO_x is created during the vigorous portion of heat release, since the NO thermal formation path is a relatively slow chemical process, around 33 % of the NO_x is formed during the late-stage of combustion happening in the expansion process.

The original Dec's conceptual model for conventional diesel combustion was applied only through the quasi-steady period, prior to the end of injection, so it did not describe late-cycle processes occurring after the end of injection. However, the end of the injection event is associated with relevant processes both from mixing and combustion point of view, which also affect the formation and destruction of pollutants, and therefore, the final emissions level.

2.2.1.3 Late-cycle mixing and ignition transient period

This final phase of combustion comprises the time period after the fuel injection ends (EoI) until the remaining fuel burns and the combustion process is completely extinguished (EoC). This period was previously identified in the RoHR by the progressive decay in the energy release, which corresponded to the slow mixing-controlled stage of combustion.

When the injector needle starts to close a transitory state begins, which is marked by the ramp-down in the injection rate that finishes when the holes are completely closed, and the introduction of mass flow rate and momentum that previously sustained the diffusive flame finally stops. Arregle et al. [37] state that even when the spray momentum is not introduced any longer, the amount of mixture remaining in the chamber continue to mix with air, partly due to the existing turbulence in the combustion chamber given by swirl and piston displacement, but primarily by the residual energy coming from the injection process.

For diesel sprays at typical engine conditions, the mixtures produced after the transient ramp-down near EoI have not been investigated in great detail as in the case of the quasi-steady conditions. Two early studies done by Kim et al. and also by Bruneaux at constant-volume spray chambers, that primarily investigated downstream jet mixing at non reactive evaporating conditions through in-cylinder vapor-phase fuel imaging, showed that the equivalence ratio in the near-injector region appears to rapidly decrease after the EoI [38, 39]. Moreover, fuel concentrations within the transient jet were apparently lower than the observed during the period sustained by

the injection. Even when the importance of the transient after EoI for conventional diesel combustion is still not well established; in the case of low temperature combustion (LTC) where the injection usually takes place in a lower density and oxygen environment, this transient ramp-down processes might gain higher relevance. Recent observations lead to the questions of whether or not this mixing behavior at EoI, observed under non-combusting conditions, could contribute to HC emissions under combusting conditions; and how it affects the combustion of the remaining unburned mass in the chamber after the EoI.

In this regard, Musculus et al. further investigated this hypothesis in an optical engine to study conditions with spray-to-spray interactions, also at inert and evaporating conditions [40]. The objective of the study was to directly measure in-cylinder fuel-vapor concentrations near EoI and to estimate the potential contribution of incomplete combustion of these mixtures to engine HC emissions. Quantitative fuel-vapor concentration measurements were performed using a fuel-tracer (toluene) planar laser-induced fluorescence (PLIF) diagnostics, while operating the optical engine under non-combusting conditions (pure nitrogen intake stream). Figure 2.4 shows a time-sequence of local equivalence ratio contour plots, derived from the ensemble-average of 50 images measured by toluene fluorescence. Although the vapor fuel concentration data were acquired with pure nitrogen in the intake, an effective equivalence ratio was calculated, assuming an intake oxygen concentration of 12.7 % by volume, which is typical of a high EGR condition [40] similar to the levels used to attain LTC conditions [41–43].

Figure 2.4 shows how shortly after the EoI, the post-injection jet quickly shifts to a distribution with centerline equivalence ratio clearly increasing with downstream distance, contrary to that for a steady jet, where the equivalence ratio monotonically decreases with downstream distance. Further data from single-shot instantaneous Raleigh-scattering measurements in a constant-volume combustion chamber under similar conditions, also showed lean mixtures near the injector after the EoI, confirming the fuel tracer measurements done in the optical engine [40]. Comparisons of equivalence ratio contours at similar downstream positions before and after the EoI are consistent with an increased mixing rate after the EoI. If vaporization is similarly limited by entrainment and mixing after the EoI, as in the case of the quasi-steady jet, then upstream vaporization of liquid fuel implies that the fuel-specific entrainment must increase after the EoI.

To explore the theoretical entrainment behavior after the EoI, a series of one-dimensional numerical jet model calculations were performed by Musculus

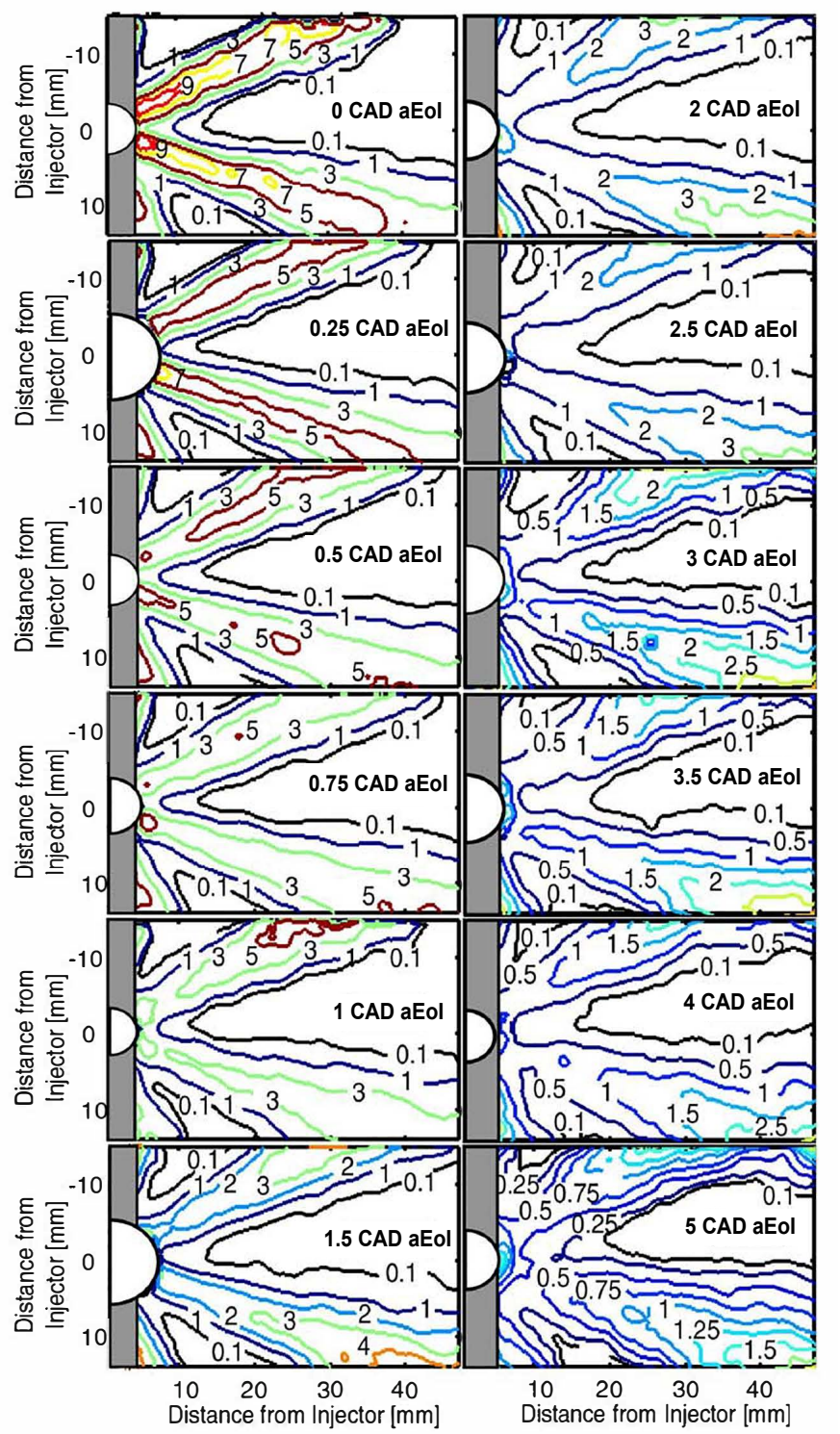

Figure 2.4. *Ensemble-averaged equivalence ratio contours measured using toluene-PLIF after the end of injection. The notation aEoI refers to a given crankangle value after the* EoI. *Source: Musculus et al. [40].*

et al. [20], adding a spatial and temporal discretization to allow the study of non-steady injection rates. The model predicts that when the fuel flow from the injector stops, an axial mass flux deficit arises near the injector, which comes from the assumption that the jet spreading angle remains constant, even as injection ends. Hence, continuity requires that the ambient gas entrainment must increase to compensate for the reduced mass flux at the nozzle. After this initial increase in entrainment, momentum exchange between the jet fluid and the low-momentum ambient gases further reduces the axial velocities in the jet, which reinforces the mass flux deficit, driving yet more entrainment. This process builds and propagates downstream as a wave of increased entrainment, commonly referred as an "entrainment wave" [20]. Finally, although the experimental observations of liquid fuel vaporization and mixing after injection, as well as computer modeling [44, 45], are consistent with the entrainment wave hypothesis, there is no definitive experimental velocity measurements to confirm the increased entrainment flows predicted by the models.

Focusing on the combustion characteristics during this late-stage, Musculus studied the regions of the fuel jet that undergo second-stage combustion after the EoI, through high-speed chemiluminescence imaging in a reacting environment with 12% of oxygen concentration at the constant-volume chamber, simulating the conditions of the experiments previously performed at the optical engine reported also in [40]. Figure 2.5 shows a time-sequence from a single injection event at high EGR rate, with similar conditions to those shown in Figure 2.4. The start of second-stage combustion begins at approximately 0.6 ms before EoI, yielding a negative ignition dwell. An approximate boundary for the reaction zone is indicated by the white contour line overlaid on the image. For the conditions used in this study, the sequence shows that the head of the jet continues to penetrate across the chamber, but there is little change in the near-injector second-stage combustion reaction zone during the time of injection. Thus, the near-injector reaction zone remains approximately the same until about 0.8 ms after EoI and the reaction zone does not recede back toward the injector. Instead, the reaction zone begins to thin at the edges of the jet by 0.8 ms and then moves downstream by 1.1 ms after EoI. The fact that the second-stage combustion reaction does not recede back to the injector means that upstream fuel-lean mixtures located near the nozzle do not burn to completion. Then, the formation of fuel-lean mixtures near the injector after EoI may therefore play a significant role in inhibiting their complete combustion, acting as a source of HC emissions, particularly in high EGR or highly diluted conditions, as the ones used in Musculus studies [40].

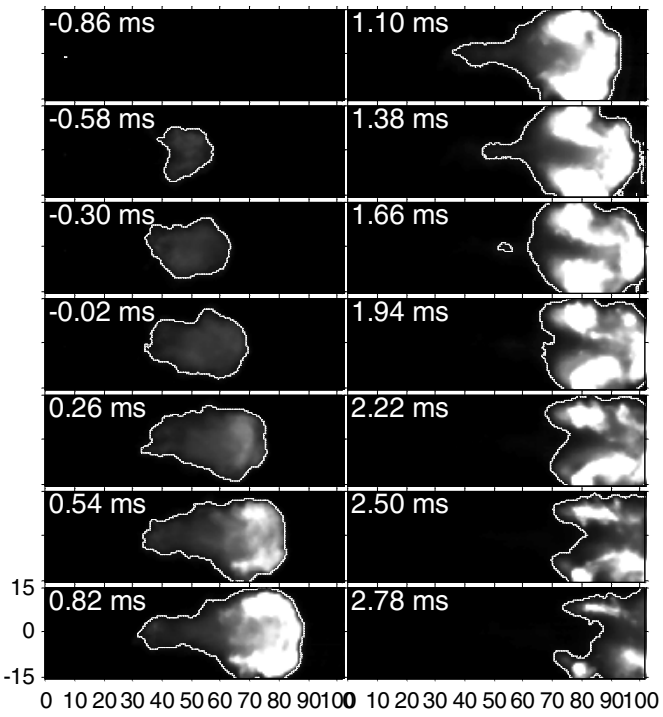

Figure 2.5. *Second-stage chemiluminescence time sequence at times relative to the end of injection in a low oxygen (12%) environment. Source: Musculus et al. [40].*

From these experimental observations, Musculus suggests that the evolution of the reactive zone after the EOI is strongly dependent on the speed of the end-of-injection transient, which will later affect late-cycle HC emissions. For instance, injectors with faster end of injection transients may maintain high axial velocities until very near EOI, that would more effectively stabilize the downstream reaction zone so that it could not recede back upstream. Then, when the jet velocities near the reaction zone decrease, the upstream mixture might be too lean for ignition to occur, as in the case observed in Figure 2.5. On the contrary case, injectors with slower end of injection transients may not maintain high jet velocities near the EOI, so that the reaction zone can propagate upstream before the mixture becomes too lean to support the reactions.

Even though there are not many reported studies specifically focused on the conditions that affects combustion recession, several researchers have observed the behavior of soot recession back towards the injector nozzle during

the transition from high to low-temperature combustion conditions. In this regard, Dec and Kelly-Zion [46] had previously observed that in the case of high-reactivity typical diesel operation conditions, the reaction zone usually recedes back towards the injector after the EoI, and some soot can still be formed in this upstream region as well. Accordingly, the flame standoff and premixed reaction zone disappear, and the reacting jet looses its quasi-steady configuration evolving into a structure formed by combustion products completely surrounded by a diffusion flame. Then, the jet-like nature of the soot-filled combusting region gradually disappears as the upstream portion is carried downstream, by its remaining momentum, to the leading portion of the jet which is spreading out along the piston bowl wall. Oxidation continues to reduce the size of the soot-filled combusting region, breaking it into separate, smaller "pockets" of combustion, until combustion eventually stops either by the complete oxidation of the remaining fuel pockets or because of the extinction of the combustion reactions due to the decrease in local temperatures. Dec suggest that incomplete burnout in the bulk gases, that result in engine-out soot emissions, can be derived from two causes: the first, could be the insufficient time to complete combustion and oxidation before the exhaust valve opening; and the second, is the extinction of the combustion reactions at the periphery of the remaining soot pockets, which becomes predominant with increased dilution due to lower combustion and product gas temperatures [46].

More recently, Knox et al. [47] studied the role of the ambient and injection conditions in either promoting or suppressing the "combustion recession" phenomena. They focused on analyzing the effect of ambient temperature, oxygen concentration, injection pressure and fuel type over the likelihood of combustion recession, in a large range of test conditions obtained at a constant-volume spray facility, using high-speed chemiluminescence and Schlieren imaging during the EoI transient.

Knox found that the time required for mixtures near the injector nozzle to reach second-stage ignition is increased as the conditions became less reactive by decreasing ambient temperature, up to a point where combustion recession became progressively weaker until it was no longer observed [47]. During the transition between high and low ambient temperatures (or its analogous case when decreasing oxygen concentration), the behavior of combustion recession changes from spatially sequential ignition to separated, or isolated, ignition sites that eventually merge. Regarding injection conditions, increasing the injection pressure lead to a faster entrainment wave and thus leaner (but also hotter) mixtures at comparable instances after EoI. These lean mixtures have slower kinetics compared to more fuel-rich (but colder) mixtures at lower

injection pressures, consequently increasing the time required for combustion recession [47].

It is worth to note how the likelihood of combustion recession also appears to be fuel dependent, specially for non-diesel-like fuels with little or no cool-flame behavior. Furthermore, combustion recession studies performed both by Musculus [40] and Knox [47] focused on negative ignition dwell conditions, where a quasi-steady lift-off length is established prior to the EOI. Therefore, combustion recession under positive ignition dwell conditions (typical of premixed LTC combustion strategies), where the entrainment wave passes through near-nozzle mixtures long before combustion begins in the main jet, can be expected to behave quite differently. Multiple injections, which further alter the transient near nozzle mixing field are also expected to induce different behaviors in combustion recession.

2.3 Fundamentals of advanced combustion concepts

In 1988, Kamimoto and Bae [48, 49] generated a conceptual model of soot particle formation in a conventional diesel diffusion flame based on a combination of optical visualization techniques and in-cylinder gas sampling methods. This early work demonstrated the conditions required for soot particle and NO formation, as well as for particle oxidation, that were going to be later supported by Dec's observations [1]. Kamimoto mapped the soot formation region in terms of local flame temperature and equivalence ratio (ϕ), using the results obtained in their experiments and the available published data at that time. NO formation region was determined by the Zeldovich equations and it was also plotted on the same diagram. Then, the time histories of ϕ and T of the flame which were obtained by a gas sampling study, were plotted on the diagram to form a trajectory. This representation of the in-cylinder conditions, along with the regions where pollutant formation occurs, first introduced by Kamimoto, became a widely used tool to link combustion and emission formation processes and to analyze qualitatively different trajectories followed during the combustion process.

2.3.1 Paths to achieve a clean in-cylinder combustion process

A schematic of the well-known ϕ-T diagram has been adapted from Potter and Durret [50] and is presented in Figure 2.6, to illustrate the trajectory of a fuel parcel undergoing a conventional diesel combustion event (upper plot) and two other possible paths that allow attaining a low NO_x-soot combustion

event (bottom plot). In conventional diesel combustion, injection of fuel into the combustion chamber initiates an adiabatic mixing process (represented by the green line) until the ignition temperature is reached (marked in gray). At point B, the fuel parcel undergoes a rich premixed reaction in which part of the fuel energy is rapidly released bringing the mixture close to the flame temperature (denoted as T_{flame} and plotted in red) at the current ϕ for the given ambient oxygen concentration. Some additional mixing will occur during this rapid temperature increase, though it is not shown in Figure 2.6. After the first premixed combustion, the remaining of the fuel energy is released as the rich products continue to mix with oxygen (C-D) following the diffusion flame temperature path. The maximum flame temperature is obtained at stoichiometric conditions (ϕ= 1). Beyond ϕ= 1, no significant chemical heat release occurs and mixing serves to lower the temperature of the fuel element. During its trajectory, the fuel parcel crosses the two peninsulas where the local conditions promotes first the production of soot and later the formation of NO_x. Then, it results evident from the above description that the formation of both soot and NO_x depends strongly on the path followed during the combustion process. Note that only the path of one fuel element is depicted in Figure 2.6 for ease of understanding; in real conditions, there exist a broader spectrum of local equivalence ratios inside the spray that leads to other fuel paths.

Several researchers have continued to use the ϕ-T representation as a tool to better understand various types of combustion concepts, combining numerical zero dimensional calculations with detailed chemical kinetic models to define pollutants formation regions, together with multidimensional CFD engine simulations to get the evolution of the in-cylinder conditions during combustion. In this regard, extensive research efforts have been focused in finding different approaches to decrease in-cylinder combustion temperatures, with the aim of avoiding the soot and NO_x formation peninsulas. Such strategies can be broadly classified as low-temperature combustion (LTC).

One option consist of operating the engine at very low oxygen concentrations (i.e. introducing extremely high EGR rates) to significantly decrease flame temperatures and avoid completely the soot formation region even when rich combustion still occurs, as it is presented schematically in the "blue path" shown in Figure 2.6. This strategy was initially explored by Akihama et al. [51], which referred to it as smokeless rich combustion. These first findings were important because they showed that engine-out PM emissions did not continue to follow the classic NO_x-PM trade-off when increasing the EGR rate beyond a critical level, from which the combustion

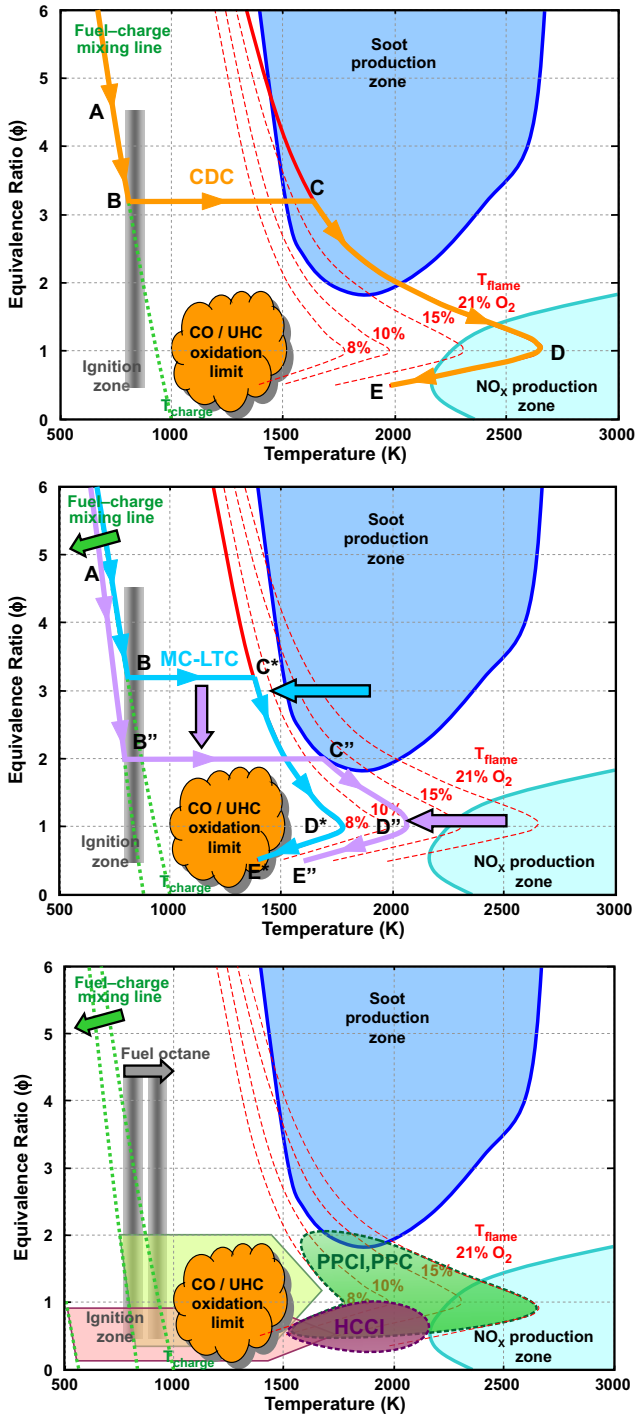

Figure 2.6. *ϕ-T diagram for CDC (top), mixing-controlled LTC (medium) and premixed LTC strategies (bottom). Adapted from Potter and Durrett [50].*

temperatures become low enough to sharply reduce or even inhibit in-cylinder particle formation, despite the worsened oxidation conditions.

Later, numerous investigations that can be categorized as mixing-controlled LTC strategies have been reported in the literature [51–55]; where the focal point among them is to keep the injection timing near to TDC to retain combustion control with the mixing process; while the flame temperature is decreased below a threshold of 2200 K to 2100 K by introducing high rates of EGR. In addition, this approach to LTC was usually combined with strategies that enhance the mixing rate, and/or increase the mixing times by extending the ignition delay, as is schematically depicted in the "purple path" in Figure 2.6. For example, using high injection pressures, high swirl ratios and small nozzle diameters help increasing air entrainment before the lift-off consequently decreasing the equivalence ratios by the time of ignition. Other strategies targeting to slightly extend the ignition delay, include lowering the charge temperature during the mixing process, by decreasing either the geometric compression ratio or the effective compression ratio if a variable valve actuation system is used. A common characteristic of the mixing-controlled LTC strategies is that the injection and combustion events are typically overlapped, maintaining a negative ignition dwell (time between EoI and SoC) as in CDC.

An important trade-off that must be balanced in these mixing-controlled LTC systems occurs between keeping combustion temperatures low enough to achieve ultra low NO_x and PM, but simultaneously high enough (over 1500 K) to assure high combustion efficiency. When temperatures are suppressed to levels in the range of 1500 K to 1800 K, oxidation chemistry slows down and CO-CO_2 conversion can become especially problematic. In fact, CO and unburned hydrocarbon (HC) usually exceed acceptable levels well before soot formation is substantially inhibited [54, 56], which have been demonstrated to be a common problem in many mixing-controlled LTC concepts. This concept remains outside the scope of this investigation, so it will not be further discussed along the review of the advanced LTC concepts. If the reader is interested in a more thorough description about the mixing-controlled LTC strategies, it can be referred to the works of Amorim [57] and Benajes et al. [58, 59].

Rather than using such extreme EGR rates, most LTC strategies address PM emissions by promoting pre-combustion mixing. As observed in the ϕ-T diagram, soot forms during and after combustion in regions that are more fuel-rich than stoichiometric, so increasing mixing times prior to combustion can reduce or eliminate the soot-forming, fuel-rich mixtures. If the ignition

delay is sufficiently extended to achieve a positive ignition dwell, meaning that injection and combustion events are no longer overlapped, the strategy can be categorized in the group of premixed LTC concepts. In the past two decades, numerous premixed LTC strategies with various names and acronyms have been proposed in investigations and reported in the literature. However, the defining characteristics of these strategies have become less distinct as they have broadened so that they overlap with each other.

Going back to the ϕ-T map, the location and slope of the mixing line is conditioned by the injection timing and the charge thermodynamic conditions, and accordingly, by the mixing process happening in the time comprised between the SoI and the SoC, defined as the ignition delay. In addition, another option to further extend the ignition delay and decrease local equivalence ratios at the time of ignition, is to shift the ignition temperature zone towards higher temperatures by using fuels with better resistance to autoignition as is the case of gasoline-like fuels. Therefore, the reactivity of the fuel (given by the cetane or octane number of the fuel) is one more lever that can effectively be used to control the combustion process in premixed LTC modes. Given the large variety of homogeneous and partially premixed strategies it results difficult to summarize all of them in only one path, so instead, they have been represented as desirable areas in the ϕ-T map, where most of the premixed LTC modes should be framed, to avoid both NO_x and soot formation zones and assure proper CO oxidation.

For the purposes of this investigation, the premixed LTC strategies can be broadly categorized into two groups, according to the desired degree of premixing. The first broad category comprises strategies that falls within the often termed "homogeneous-charge compression ignition" (HCCI), "low thermal homogeneous combustion" (LTHC) or "highly premixed combustion" (HPC), where vaporized fuel is well mixed with the charge gas in a basically homogeneous mixture prior to ignition, and is everywhere fuel-lean. Ignition timing is kinetically controlled, and is therefore decoupled from the timing of the fuel injection event. The second broad category include all strategies that have been termed as "partially premixed compression ignition" (PPCI) or "partially premixed combustion" (PPC); where direct injection is used along with more moderate mixing times. They can be distinguished from the first group by a more heterogeneous charge distribution at ignition compared to HCCI and HPC, that includes not only fuel-lean but also fuel-rich mixtures. Ignition is also more closely coupled to the fuel injection event than with HCCI, though chemical kinetics still play an important role.

As it was previously shown in Figure 2.6, the homogeneous or highly premixed combustion (HCCI and HPC) can be schematically represented in the ϕ-T map similar to a constant volume combustion typically in the fuel-lean region (well below ϕ= 1) at more or less constant equivalence ratio, since the mixing process occurs quite early in the compression stroke (or even before/during the intake phase) when local temperature and density are low. The fuel/air charge is reasonably uniform, and it can be assumed that the local ϕ has been mixed to a globally lean ϕ in the combustion chamber. When the fuel/air charge achieves the reactivity conditions required to autoignite, rapid bulk combustion occurs almost simultaneously in the chamber, without the formation of a high temperature flame front or diffusion flame. The bulk combustion of an overly lean and diluted mixture, added to a relatively low oxygen concentration typically used in HCCI, drastically decreases combustion temperature to avoid entering the NO_x formation peninsula; while soot formation is also hindered by the absence of zones with rich equivalence ratios. Although it seems that a wide range of equivalence ratio values is possible, in practice the suitable values are limited by two factors: for rich or near-stoichiometric mixtures, the probability of intense knock restricts the HCCI operating range to medium and low loads; while with too lean mixtures, the local burning temperatures can be so low that incomplete combustion occurs, leading to a sharp rise in CO and HC emissions.

To achieve this kind of "ideal" HCCI combustion, three major aspects should be addressed: first, how to create a homogeneous or relatively uniform mixture; second, how to ignite such a mixture; and third, how to control combustion so that engine performance and emissions can be optimized. In order to meet these demands, the parameters influencing the combustion process: mixture formation, composition and thermodynamic state of the cylinder charge, as well as fuel properties; must be carefully adjusted interdependently.

The approaches to achieve HCCI or HPC operation in diesel engines, vary greatly among the many strategies reported in the literature. The fuel can be either injected in the intake system [60, 61] or directly into the cylinder; very early during the compression stroke [62–66], or combining early pre-TDC injections and post-TDC injections [64, 67].

In general terms, the early-injection approach has been the most widely used strategy to assure obtaining a relatively uniform fuel-air mixture before the onset of ignition. However, due to the lower air temperature and density, preventing fuel impingement onto the bowl and liner walls is still a challenging task, specially when using low volatility fuels such as diesel. To minimize

the over-penetration and wall wetting that can occur when fuel is injected well before TDC, the simultaneous optimization of injector nozzle (such as a narrow angle injector, impinging nozzles), combustion chamber shape, injection strategy (multiple or modulated injections) and air management (swirl ratio and boost pressure) is of great importance for the performance of HCCI/HPC combustion modes [61–64, 67–75].

Finally, in most HCCI or HPC engines the autoignition delay is no longer governed by physical phenomena, but mainly by chemistry. This means that the start of combustion is not triggered by the injection event, but by the high temperature achieved near the end of the compression stroke. In such cases, the high tendency to autoignition of diesel fuels, characterized by a high cetane index and a two-stage chemistry, will tend to provoke a too early onset of ignition which will lead to early phasing of combustion during the compression stroke, and will ultimately restrict the operating range of this concept to low loads [60, 76]. In this regard, the strategies that aim to extend the ignition delay of diesel fuel, through decreased charge reactivity, either by lowering cylinder oxygen concentration (i.e. introducing EGR) or by affecting the time-temperature history of the charge (i.e. lowering compression ratio), are also beneficial to further provide additional mixing time allowing a higher degree of homogenization of the fuel/air mixture.

Besides the previously exposed difficulties linked to the poor volatility of diesel-like fuels, the high reactivity (low resistance to autoignition) inherently limits the available time for premixing the injected fuel, making it even more difficult to guarantee a proper homogenization of the fuel/air mixture before the onset of combustion. In this regard, Yao et al. [77] investigated the influence of the octane number of different PRF mixtures on combustion, performance and emissions characteristics of an HCCI engine. The test results showed that HCCI combustion could be controlled and the HCCI operating range was extended by burning different octane number fuels at different engine modes, i.e. burning low/high octane number fuel at low/high load mode respectively. So, this investigation confirms that it exists an optimum octane number that allows the highest indicated thermal efficiency depending on the engine load.

Following this approach, more recent investigations have focused on the fuel reactivity control, which is commonly referred to as reactivity controlled compression ignition (RCCI) or dual-fuel CI [78–85]. The RCCI concept relies on injecting two separate fuels, one which is highly reactive (a two-stage ignition fuel for instance) and another which is less reactive (single-stage ignition fuel) [86]. By varying the relative amounts or timings of

injection of the two fuels, combustion can be controlled [87]. For example, in a RCCI engine that combines gasoline and diesel fuel, combustion timing can be advanced with injection of more diesel fuel to take advantage of its higher reactivity. Alternatively, a small amount of diesel fuel can be directly injected in-cylinder just before the desired combustion timing to create a pilot ignition which ignites the rest of the mixture. Even when it provides a higher flexibility to control combustion timing and consequently a wider range of operation compared to single-fueled HCCI engines, it requires using two separate injection systems to supply the fuels, considerably increasing the complexity and cost of the engine. For the present investigation, only one fuel (either diesel or gasoline) will be supplied with a common rail direct injection system, so the dual-fuel or RCCI combustion modes will be excluded from this research work. To find a more thorough description about the RCCI concept, the reader is referred to the works of Belarte [88] and Benajes [87, 89].

A different approach consists on maintaining some level of inhomogeneity in fuel concentration and temperature in the charge, which is enough to produce a positive effect on the autoignition and combustion process [90–92]. Accordingly, intentionally creating some degree of stratification in the mixture to take advantage of the charge cooling effects of relatively late injection timings, and also the chemical kinetic effects of the presence of slightly richer regions, can be effectively used to control in some extend the onset of ignition and the combustion rate [93, 94]. From the previous discussion, it seems that the natural evolution of HCCI engines led to the investigation of different control strategies that moved away from a truly homogeneous charge, to switch instead to partially premixed (or stratified) charge that could provide some degree of stratification in the fuel-air mixture with the aim of recovering the control over the heat release rate. Keeping only one fuel supply, thereby excluding dual-fuel or RCCI approach, the second broad category of premixed LTC combustion concepts comprises all strategies that have been termed as "Premixed Compression Ignition" (PCI), "Partially Premixed Compression Ignition" (PPCI) or "Partially Premixed Combustion" (PPC), which will be further described in detail in the next section.

2.3.2 Phenomenological description of the partially premixed combustion process

As it was previously discussed, in HCCI engines a very long mixing period is required to form a lean and uniform mixture, so for early DI strategies it is necessary to inject fuel at a fairly early timing in the initial stages of the compression stroke. If the engine hardware is not carefully optimized for

such early timings, a large amount of the sprayed fuel adheres to the wall, causing problems of oil dilution and a decline in combustion efficiency. To solve this problem, PPCI or PPC combustion aims at achieving premixing by increasing ignition retardation while injecting fuel still at slightly early timings but closer to the top dead center compared to HCCI. Therefore, this approach allows operating diesel engines in between fully homogeneous combustion and fully diffusive combustion, where low emissions can be still attained, but while retaining some control over the combustion timing with the injection event.

A positive ignition dwell is typically achieved using high EGR rates, which helps retarding ignition, usually in combination with slightly lower compression ratio and relatively higher injection pressures and smaller nozzle hole diameter, providing enough time for some degree of premixing to occur for all of the injected fuel, including fuel from the very end of injection. Shorter injection durations as well as multiple injection strategies also help to achieve a positive ignition dwell and provide better control on the ϕ stratification.

As with the previous combustion modes (CDC and HCCI), to realize the full potential of PPCI or PPC strategies, the in-cylinder physical and chemical mechanisms leading to the emissions formation processes must be well understood. So, the following subsections intent to provide the reader with a brief summary of some relevant experimental observations, that helped improving the current understanding of in-cylinder mixing and ignition related phenomena occurring when operating with the partially premixed combustion mode using diesel-like fuels. These studies served as the basis for the development of the LTC conceptual model for low-load, single-injection, EGR-diluted, partially premixed DI diesel combustion. Finally, the effect of fuel ignition properties over the overall PPCI combustion process, as well as over the performance of the concept will be briefly discussed in the last subsection.

The PPCI or PPC diesel combustion process typically exhibits a two-stage heat release, as in the case of HCCI and HPC concepts, due to the characteristic two-stage ignition behavior of diesel-like fuels. Low temperature reactions (LTR) account for the first stage of the heat release, while the high temperature reactions (HTR) are responsible for the second stage. Approximately 7 to 10% of the energy is released during the first stage, and the remaining energy is released during the second stage. The main phases of diesel direct injection PPCI and PPC combustion can be distinguished as follows:

1. Ignition delay: As in CDC, this first stage is defined as the period between the start of injection (SoI) and the start of combustion (SoC);

which in the case of PPCI is marked by the start of the low temperature reaction (LTR) phase. During the ignition delay phase the fuel is injected early during the compression stroke with no increase in the pressure or RoHR, in an environment with low temperature and density conditions which do not favor the evaporation and mixing of low volatility diesel fuels. At some point after the EoI, pressure and temperature are increased enough to start the first-stage pre-ignition reactions that will lead to the measurable LTR regime observed in the RoHR.

2. Low temperature reaction (LTR) regime: The first stage of the heat release curve is associated with low temperature kinetic reactions, which are typically lower than the hydrogen peroxide (H_2O_2) breakdown temperature (above 1000 K) [95–97]. The rapid heat release observed in the low temperature zone (less than 850 K) is caused by the first-stage pre-ignition reactions. First, the oxidation of the fuel molecules builds a pool of ketohydroperoxide (KHP) species [30, 95, 96]. Then, the decomposition of KHP species during the LTR regime, results in a pool of radicals that oxidize hydrocarbon fragments from the fuel, raising the temperature in the course of the first stage of ignition. In addition to increasing temperature, three important species are also formed during the first stage of ignition: formaldehyde (H_2CO), CO, and H_2O_2, which is important because it is a key player in the second stage of ignition.

3. Negative temperature coefficient (NTC) regime: Following the LTR stage, a time delay exists prior to the HTR known as the "negative temperature coefficient (NTC) regime". The reaction of alkyl radicals with oxygen molecules is highly temperature and pressure dependent, so with increased temperatures, the equilibrium of this reaction shift toward the reactants, and by roughly 850 K the addition of O_2 to the alkyl radical is almost completely extinguished [98]. As a result, the rate of the heat release for the LTR is reduced [99, 100], during a period where overall reaction rate decreases though the in-cylinder temperature continues to increase. After the first stage of ignition, gradual oxidation of formaldehyde and other reactions continue to produce hydroperoxy radicals (HO_2), which continue to build up a relatively stable pool of H_2O_2. At the same time it is being formed, some H_2O_2 decomposes into OH radical species, but until temperature reaches 1000 K, the production reactions outweigh decomposition, and the pool of H_2O_2 continues to build.

4. High temperature reaction (HTR) regime: As the temperature rises above 1000 K, H_2O_2 decomposition exceeds production rates, releasing

a pool of OH radicals that accelerates the overall rate of oxidation of the fuel molecules, leading to rapid heat release [95–97, 100, 101]. The start of the HTR regime is marked by second-stage ignition, that increases the temperature to above 1200 K where hot ignition takes over through the branching reaction of H and O_2 to form O and OH radicals. During this HTR phase, most of the fuel chemical energy is released in a short period of time, and formaldehyde, CO and UHC are consumed while OH is formed in abundance.

The two-stage ignition chemistry and main reaction paths are quite similar between HCCI and PPCI, and note that they are also present for conventional diesel combustion. However, the local conditions in terms of temperature, equivalence ratio and dilution are the main factors that dictate the transition and "dwell" between the two phases of ignition, and also the fates of important species such as CO and HC after the second-stage of ignition. Consequently, the level of ϕ-stratification will directly affect both the ignition and the characteristics of the PPCI combustion process. But aside from the mixture stratification, the ignition chemistry can be affected by the charge thermodynamical conditions (i.e. oxygen concentration and temperature) and the fuel chemistry (i.e ignition quality of the fuel); as in the case of HCCI.

If the PPCI mode is represented in the ϕ-T map, shown in Figure 2.6, the location and slope of the mixing line is conditioned by both the injection timing and the mixing process happening during the ignition delay. Typically, the injection strategy and cylinder thermodynamic conditions used for early-injection PPCI, provides enough mixing time (due to extended ignition delay) to achieve a minimum level of pre-mixing in all the fuel parcels before the onset of ignition, to eliminate over-rich regions with ϕ greater than 2 where soot formation is promoted. Intentionally, at the start of combustion it has to exist some degree of stratification in the mixture (including fuel-rich and fuel-lean ϕ) to attain sequential autoignition, from the most reactive towards the less reactive fuel parcels, and also to allow keeping the control over the combustion phasing with the timing of the injection event. At the same time, to avoid the NO_x formation peninsula the combustion temperature has to be lowered below 2200 K, so introducing large amounts of EGR (over 40 %) is typically required.

The partially premixed LTC strategies may be further divided into two subcategories according to the fuel injection and combustion timing, which is earlier or later than for conventional diesel combustion. The majority of studies have investigated early-injection PPC, where the fuel is injected

in the middle to late compression stroke [102–113]. Other studies have explored late-injection PPC, which includes Nissan's "Modulated Kinetics" (MK) regime [114–116] and similar late-injection strategies [117], for which fuel is injected very near TDC or in the early expansion stroke. In either case, the gases into which the fuel is injected are either initially colder and less dense because of less compression (for early-injection PPC), or become cooler during and after injection because of expansion (late-injection PPC). This is combined with the effects of introducing large amounts of EGR, to slow down the pre-ignition chemistry providing greater mixing times compared to conventional diesel combustion. This review will primarily focus on the early-injection PPC strategies, excluding late-injection or MK concepts, since excessively late combustion timings typically lead to a dramatic increase in HC and CO emissions that substantially punishes combustion efficiency, but more importantly, causes an unacceptable loss in terms of engine thermal efficiency.

For early-injection PPC, the injection event is located during compression stroke but relatively closer to TDC, so the ignition delay phase and the mixing time period are shorter compared to early-injection DI HCCI. When injecting closer to TDC, the higher density and temperatures will enhance the evaporation and mixing of the fuel compared to HCCI, but they will also promote the start of LTR, which will increase the EGR requirements to further slow down ignition chemistry and avoid early onset of autoignition. Keeping relatively shorter mixing times are required to assure some level of mixture stratification in terms of equivalence ratio, retaining proper control over combustion phasing with the timing of the injection event. As in the case of HCCI, the main combustion stage denoted as HTR, is much faster and exhibits a higher peak in the RoHR compared to conventional diesel mixing-controlled combustion, since the majority of the fuel is still burnt in premixed conditions without the appearance of a diffusion flame, what typically leads to greater levels of combustion noise. After the main premixed combustion, the RoHR falls to nearly zero, with relatively minor or not evident mixing-controlled heat release.

2.3.2.1 Mixture preparation

For early-injection PPCI, the fuel is injected in a lower density environment compared to CDC (where the injection occurs near TDC) but still in relatively better conditions compared to early-injection HCCI. Typical injection timing reported in a large number of PPCI strategies can vary between -50 CAD aTDC to -20 CAD aTDC, where density (and pressure and

temperature) is increasing due to compression. So, the spray behavior can be largely affected depending on the ambient conditions given at the start of injection.

Okude et al. [118] reported one of the first detailed examinations of the basic requirements for premixed combustion operation, which he called "Premixed Compression Ignition", by performing spray observation experiments in a high-pressure vessel and combustion studies in a single-cylinder diesel engine. First, to verify the feasibility of the PPCI combustion, Okude recorded the spray evolution for one injection hole in the high-pressure vessel to study the necessary time for the spray to be diluted. The ambient condition was set equivalent to a typical density in the cylinder in the vicinity of −30 CAD aTDC. Distribution of local equivalence ratios in the spray was analyzed from the images using the transmission decay method. In addition, the frequency distribution $dm/d\phi$ of concentration of the mixture was calculated, which represents the cumulative mass dm of fuel contained in width $d\phi$ of the equivalence ratio [118].

Figure 2.7 shows how the equivalence ratios in the spray are widely distributed from lean to over-rich immediately after the EoI, but then rapidly shift to the lean side within a given lapse of time. The distribution in ϕ shows that little mixture of an equivalence ratio of 2 or greater remains immediately after the EoI, however, these results correspond to a condition without EGR. In PPCI combustion, however, as a large amount of EGR is introduced, the reduction in oxygen concentration in the ambient gas may cause the distribution of equivalence ratios to shift to the over-rich side.

This analysis was complemented with subsequent spray observation experiments, during which the fuel injection pressure and the nozzle hole diameter were changed. Considering an environment with 40 % of EGR, a period of time of approximately 3 ms would be necessary for mixtures of an equivalence ratio of 2 or greater to completely disappear (denoted as required mixing period). This period corresponds to approximately 15 CAD to 20 CAD at an engine speed of 1000 rpm. When the fuel injection pressure is changed with a conventional nozzle, the required mixing period decreases with an increase in the fuel injection pressure, but the range of variation is narrow, specially in the range of 80 MPa and higher pressures. On the other hand, when a nozzle with a smaller injection hole diameter is used, the required mixing period can be shortened by 50 % or more as compared with using a conventional nozzle. These results revealed that the mixture can be effectively diluted to such an extent that no soot is formed, even by placing fuel injection in the vicinity of the top dead center if the mixing conditions are properly

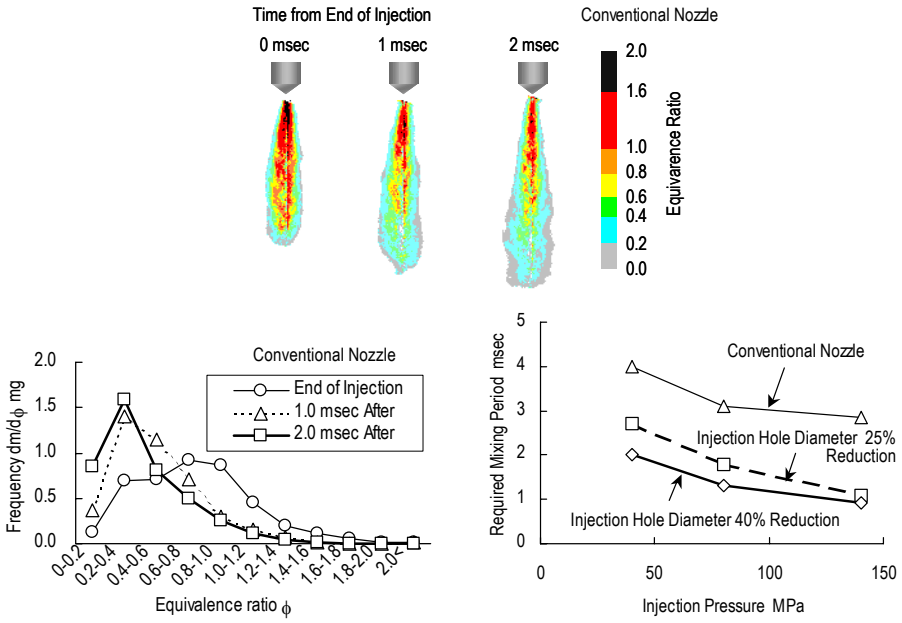

Figure 2.7. *Fuel distribution of spray (upper plot), frequency distribution of equivalence ratio (lower left side) and effect of fuel injection pressure and nozzle hole diameter on required mixing period (lower right side). Source: Adapted from Okude et al. [118].*

optimized, and the ignition-timing is sufficiently delayed in order to assure the required mixing period [118].

Similarly to early-DI HCCI conditions, the liquid length and the spray penetration for early-injection PPCI will extend much farther compared to the typical values reported with conventional diesel combustion. Figure 2.8 shows some simulation results reported by Liu et al. [119] regarding the in-cylinder fuel spray targeting regions for two different early-injection timings (-55 CAD aTDC and -35 CAD aTDC), when using a 150° included angle nozzle; as well as the effect of ambient density over the spray penetration. In the case of extremely low ambient density values, as the typically obtained at -55 CAD aTDC, the penetration can be large enough so that liquid film can impinge onto the cylinder surfaces forming liquid films. So in the case of small bore light-duty engines, featuring bowl rim radius of 20 mm to 25 mm, liquid fuel impingement onto the cylinder surfaces may easily occur, specially if a conventional wide angle nozzle is used, as it is confirmed by Figure 2.8.

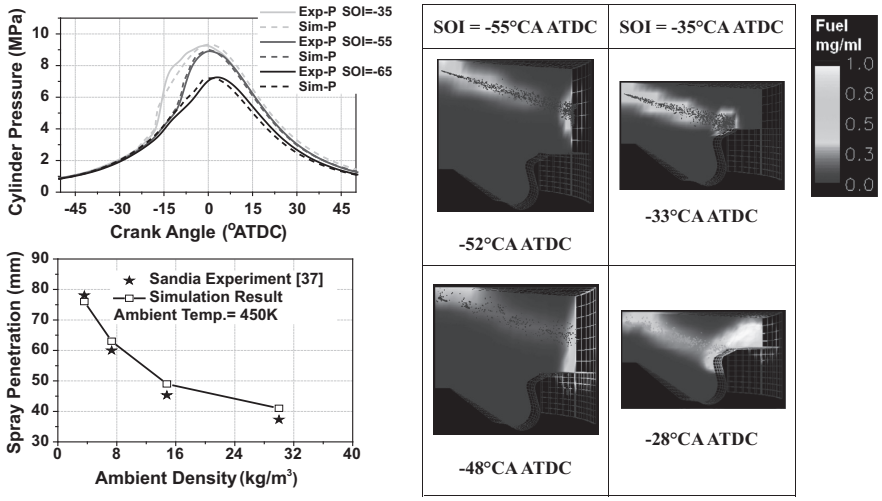

Figure 2.8. *Simulation of in-cylinder fuel spray targeting regions for early-injection PPCI strategy with* 150° *included angle nozzle. Source: Liu et al. [119].*

After the injection rate peaks, the deceleration of the liquid fuel exiting the nozzle increases local entrainment of ambient gases near the nozzle, as it was previously explained in section 2.2.1.3. For typical early-injection PPCI operating conditions where the injection takes place in much cooler and less-dense ambient gases, the liquid fuel behavior during and after the end-of-injection transient may behave quite differently compared to high temperature diesel sprays. In this regard, Kook et al. [120] performed liquid-fuel Mie-Scattering imaging at a relatively colder (600 K), lower ambient-density (5.22 kg/m^3) condition, from a single-hole injector in a constant-volume chamber. Figure 2.9 shows the Mie-scatter signal level in grayscale and the outer boundary of the liquid-fuel is showed with the contour line. For the test conditions, the injection duration is short enough that liquid fuel never reaches the quasi-steady liquid length, which is indicated for reference by a dashed line at the right of the images. With a relatively fast end-of-injection ramp-down, and the cooler, lower ambient density conditions, the maximum liquid-fuel penetration length does not retreat back to the injector during and after the end of injection, as it typically happens in the case of high-temperature conventional diesel sprays. Instead, after the EoI at 360 μs aSoI the liquid fuel detaches from the injector, and liquid fuel remains downstream until about 1000 μs aSoI.

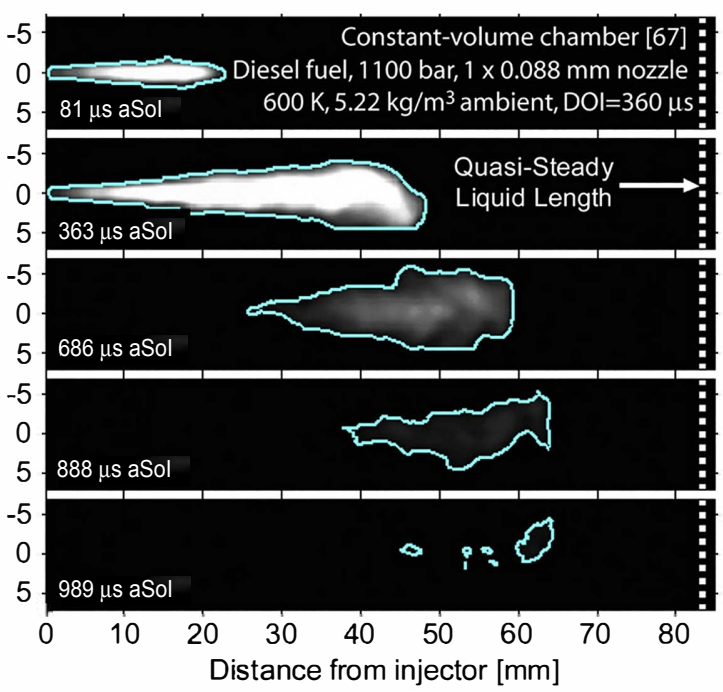

Figure 2.9. *Liquid diesel-fuel Mie-Scattering images at low ambient density in a constant-volume chamber. Source: Kook et al. [120].*

Intermediate conditions in terms of density and temperature may produce liquid fuel distributions that split after the EoI, with liquid fuel remaining for a short time both near the injector and far downstream, but with a liquid-free gap in the middle. An example of such a split liquid fuel distribution was reported by Musculus [121], in a light-duty engine operating with an early-injection (SoI at −23 CAD aTDC) PPCI combustion regime. Mie-scatter liquid-fuel image recorded at a timing shortly after the EoI is shown in Figure 2.10. The injector is the same as that used to obtain the images shown in Figure 2.9, but is fitted with a conventional multi-hole nozzle. Although the most intense light scattering is observed near the nozzle, distinct regions of liquid fuel are found both in the squish volume and in the piston bowl. Liquid in the squish volume may form films along the piston top and the head, that may correspond to a significant increase in soot and unburned hydrocarbons due to overly fuel-rich regions. The observed behavior on the liquid fuel distribution indicate that liquid-fuel vaporization may transition

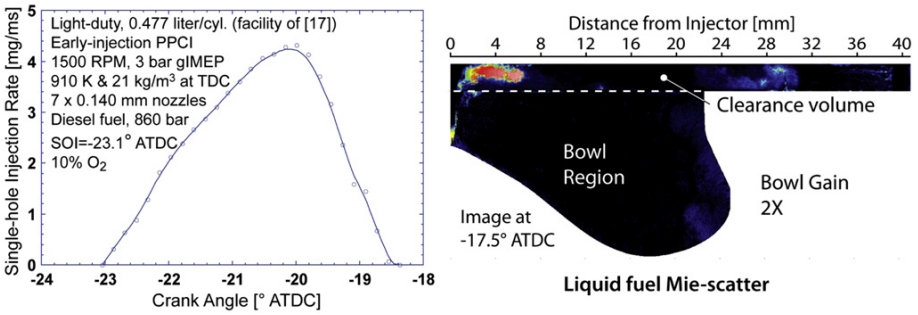

Figure 2.10. *Liquid diesel-fuel Mie-Scattering image in a light-duty optical engine for early injection PPCI conditions. Source: Musculus et al. [121].*

from retreating to splitting to detaching after the EoI, depending on the ambient conditions and the injector dynamics (ramp-down of the injector).

The theoretical entrainment behavior predicted by 1D jet model calculations during and after the EoI transient, similarly to what was previously discussed in section 2.2.1.3, is in agreement with the experimental observations of liquid-fuel vaporization at such low density conditions. For conditions with short liquid length, the entrainment wave reaches the liquid length quickly, increasing entrainment and completely vaporizing the fuel downstream first, causing the liquid length to retreat back to the injector. For conditions with a relatively long liquid length, the entrainment wave reaches the liquid length later, and therefore affects the upstream mixtures earlier, causing the upstream flow to completely vaporize first so that the liquid spray detaches from the injector. So, for early injection into cooler and less dense ambient gases, or injections with a more rapid EoI transient, the liquid spray may either detach from the injector or separate into individual segments, and may persist as liquid much later into the cycle. However, for all jets the penetration is reduced after the entrainment wave reaches the head of the jet, and mixing and vaporization are enhanced in the wake of the entrainment wave, so wall-wetting can be mitigated to some degree by shortening the injection duration.

Since the PPCI regime requires attaining a positive ignition dwell, between the EoI and the SoC, the typical quasi-steady spray structure observed in high-temperature mixing-controlled combustion will not appear in early-injection PPCI conditions. Instead, a fuel mixture distribution stretching from fuel-lean mixtures near the injector towards fuel-rich mixtures downstream

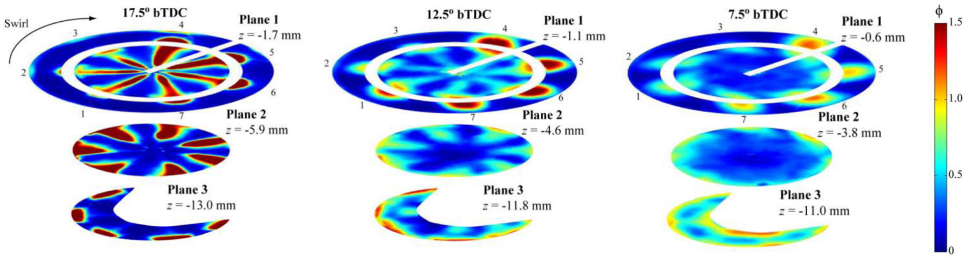

Figure 2.11. *Mean equivalence ratio distribution measured with toluene-PLIF in a light-duty optical engine for early injection PPCI conditions. Source: Petersen et al. [110].*

close to the bowl is expected to exist at the time of ignition. This fuel distribution would resemble more to the one showed in Figure 2.4 for the last frames of the PLIF sequence measured during the transient period after the EoI.

Petersen et al. [110] reported experimental tracer-based PLIF measurements of fuel distributions performed at Sandia National Laboratories in the same optical light-duty engine configuration as the one shown in Figure 2.10, to provide a two-dimensional view of the pre-combustion equivalence ratio distribution at low load, highly dilute, slightly boosted early-injection PPCI condition. Equivalence ratio distributions are presented at a single vertical plane and three different horizontal planes within the combustion chamber; where Plane 1 is located at the mid-plane of the squish volume for each crank angle, Plane 2 is located at the rim of the piston bowl, and Plane 3 is located where the radius of the piston bowl is a maximum, so these two last measurement planes also move upward as the engine cycle progresses. Figure 2.11 shows three different instants acquired during the ignition delay period, the LTR phase, and the onset of the high-temperature combustion, which occurs near 5 CAD aTDC.

For the selected operating condition, the injection timing is phased at −23.1 CAD aTDC and the fuel sprays are targeted at the rim of the piston bowl. At −17.5 CAD aTDC, the spray has already contacted the bowl rim, splitting the fuel mass between the squish and bowl regions. The fuel in Plane 1 has penetrated across the cylinder and the rich mixtures located in the head of the spray have entered the squish volume. The portion of the spray that enters the piston bowl (Plane 3) translates along the outer-edge of the bowl wall with a very small amount of radial spreading. Shortly after, the local equivalence ratios continue to decrease in all three planes and the

sprays begin to deflect in the direction of the swirl flow. At -12.5 CAD aTDC, the fuel in Plane 1 has penetrated across the squish region and approaches the cylinder bore wall. Throughout the early portion of the ignition delay period, the penetration of each individual spray is clearly different, causing the equivalence ratio distribution to be asymmetric about the cylinder axis. As the cycle progresses, the fuel/air mixture located in the center of Plane 1 and 2 continues to mix towards excessively lean equivalence ratios below 0.5, fuel-rich mixtures are found near the head of the jet, whether in the squish volume or in the bowl. The lean mixtures close to the nozzle are likely generated by the over-mixing of the tail-end of the spray. These overly-lean fuel/air mixtures located near the injector tip may have equivalence ratios well below the lean-limit for complete combustion, so they will likely become a significant source of HC and CO emissions at these conditions.

2.3.2.2 Ignition and combustion process

As it was already discussed in sections 2.2.1.1, the presence of formaldehyde (H_2CO) is first detected at the start of first-stage ignition, and persist until it is destroyed at the second stage of ignition. Formaldehyde exists during the dwell between the two stages of ignition, and the length of which depends on mixture stoichiometry.

As Musculus describes in [121], in the case of light-duty engines operating under early-injection PPCI conditions, the fuel jets may strike the piston walls even before the first stage of ignition starts, substantially altering their structure, as it was demonstrated by Figure 2.10. High levels of swirl may also cause additional distortion to the jet structure. Figure 2.12 shows a single cycle H_2CO PLIF image measured in the same light-duty engine at the same early-injection PPCI operating conditions as the liquid-fuel Mie-scatter images and the ϕ distribution shown in Figures 2.10 and 2.11. The schematic on the right of Figure 2.12 illustrates the location of the laser sheet against the various fuel-jet axes. Note that on the right-side the laser contains the jet axis, while on the left-side it bisects the angle between adjacent jets. The H_2CO PLIF image is taken at -12.5 CAD aTDC, which corresponds to an instant where the LTR phase has already started, and it is close to its maximum peak. At this time, the fuel jets have already impinged the bowl rim where they split and penetrate both into the squish and in into the bowl, as it was clearly seen in Figure 2.11. Note that the swirl has deflected the jet out of the plane of the laser sheet in the right-side (jet-axis plane), while the left-side (off-axis plane) contains significant amounts of fuel. Formaldehyde appears at the onset of first-stage ignition, and it is first visible in the upstream regions of the jet

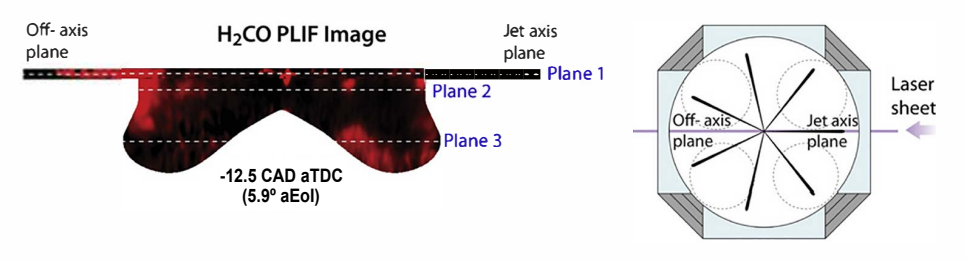

Figure 2.12. *Single-cycle H_2CO PLIF image measured in a light-duty optical engine for early injection PPCI conditions. Source: Musculus et al..*

where leaner mixtures are expected, but shortly after fills the entire jet cross section, including the richer regions near the head of the jet. The PLIF image in Figure 2.12 confirm the presence of H_2CO, throughout the split head of the jet, both in the squish region of the off-axis plane at the left, and at the bottom right of the bowl in the jet-axis plane. Note that the bottom left of the bowl is not well illuminated as the laser sheet enters from the right and is refracted by the quartz piston tip.

Simultaneous measurement of OH and H_2CO in this optical light-duty engine are not reported for the early-injection PPCI conditions showed above. However, other H_2CO LIF measurements reported in the literature showed that the formaldehyde formation rapidly grows filling the fuel jet cross section in PPCI operation with positive ignition dwell. In this regard, Hildinssong et al. [122] studied a split injection LTC condition (that he referred to as "pilot injection"), with a first early injection placed at -30 CAD aTDC and a second injection close to TDC at -3 CAD aTDC, where the mixture distribution resembles to a stratified PPCI condition. Figure 2.13 shows the sequence of simultaneous PLIF of H_2CO and OH at this light-duty engine, for the split early-injection case.

In the case shown Figure 2.13, the total combustion duration of this split early-injection PPCI concept is substantially longer compared to a typical HCCI combustion. The first injection placed at -30 CAD aTDC makes the formaldehyde formation to appear some CAD after the EoI, as it can be seen at -15 CAD aTDC to -5 CAD aTDC, in a pattern that resembles the shape of the fuel jets. Traces of the second injection of fuel can be seen at 4 CAD aTDC, that are probably caused by the scattering of the laser light from the fuel jets. The OH signal is first detected at the start of the HTR phase of the rate of heat-release, and shortly after, large structures of OH are seen in thorough the head of the jets. The maximum OH signal intensity

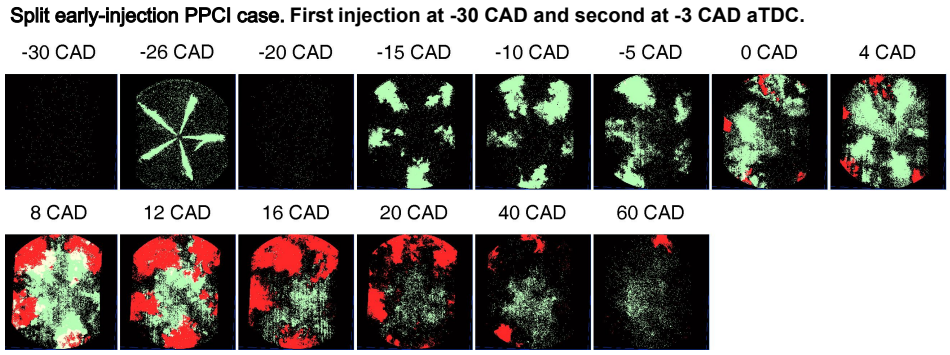

Figure 2.13. *Single-shot images of H_2CO and OH for split injection PPCI conditions in a light-duty engine. Source: Hildingsson et al. [122].*

matches pretty well the peak of the second-stage ignition (HTR) in the RoHR. As OH appears in the image for TDC and the second injection is seen at 4 CAD aTDC it is evident that the first injection ignites the charge. The appearance of significant OH downstream near the head of the jets therefore suggests that those mixtures are of intermediate stoichiometry, between ϕ= 0.5 and ϕ= 1.2 approximately.

In addition to the distinct separation of first- and second-stage ignition processes and the associated timing of H_2CO and OH appearance for PPCI LTC compared to conventional diesel combustion, the spatial distribution of OH is also broader. In the case of CDC, OH initially appears on the periphery of the jet, and it generally remains on the periphery in a thin diffusion flame throughout the quasi-steady period. However, for PPCI LTC conditions, OH first appears downstream and quickly fills much of the jet cross-section with broad distributions across the jet width.

In most cases, H_2CO and OH surfaces are not significantly overlapped, which is consistent with the consumption of H_2CO by OH at second-stage ignition. Nevertheless, a partial overlap of formaldehyde and OH can be seen at 8 CAD aTDC (clearly greater than it was for HCCI), due to the fact that formaldehyde is also being formed from the fuel from the second injection at places where the fuel from the first injection already has begun to generate OH. It can also be noted that in contrast to HCCI, there is very little, formation of OH in the center of the cylinder. The lack of OH in the central region near the nozzle could imply that the overly fuel-lean mixtures in this area does not reach second-stage ignition, however, the combustion would most likely have

been more complete for this case if there would have been a bowl-in-piston to promote the mixing and not letting the fuel spray all the way to the cylinder walls. Finally, the surface where formaldehyde is detected is much larger in the case of HCCI compared to the split early-injection case, as it was expected, since for HCCI the fuel had sufficiently long time to properly mix with the air, filling most of the cylinder. From these observations, it seems that the surface of formaldehyde, and the overlap with OH, might be fairly good qualitative indicators of the level of stratification in the cylinder charge.

Following the approach used by Dec and Flynn for CDC [1, 2], and based on the available experimental optical diagnostics observations, as well as homogeneous reactor simulations that serve to clarify the impact of finite-rate chemistry on the ignition and combustion process, Musculus proposed a new conceptual description for typical EGR-diluted low-load PPCI LTC conditions [121]. The proposed model does not intend to describe all LTC strategies, but rather a common subset with the following characteristics:

- LTC is achieved by EGR, with oxygen concentrations in the range of 10 % to 15 %, so soot may form in fuel-rich mixtures.
- Fuel injection timing may be either early- or late- injection PPCI. In either case, the ignition dwell is positive so that fuel is partially premixed before combustion, however, it has to be short enough so ignition is still somewhat coupled to the injection timing.
- The fuel injector uses conventional small-orifice diesel nozzles to produce typical diesel-like sprays.
- Fuel is delivered in a single-injection event.
- Fuel is a diesel-type, with two-stage ignition chemistry.

Figure 2.14 shows the proposed conceptual model for single early-injection, low load, EGR-diluted, PPCI LTC light-duty DI diesel combustion. The late-injection PPCI case is excluded from this literature review but the reader can refer to the works of Musculus et al. [121] for additional information.

Like the behavior observed in conventional diesel combustion, liquid and vapor fuel initially penetrate together, with little difference seen in the penetration of the two phases. However, the jet penetration rate is higher with early-injection PPCI, as it was already discussed, due to the lower ambient density at the time of injection. For the light load considered, the peak rate of injection occurs at 3 ° aSoI, so as the injection rate falls the entrainment wave

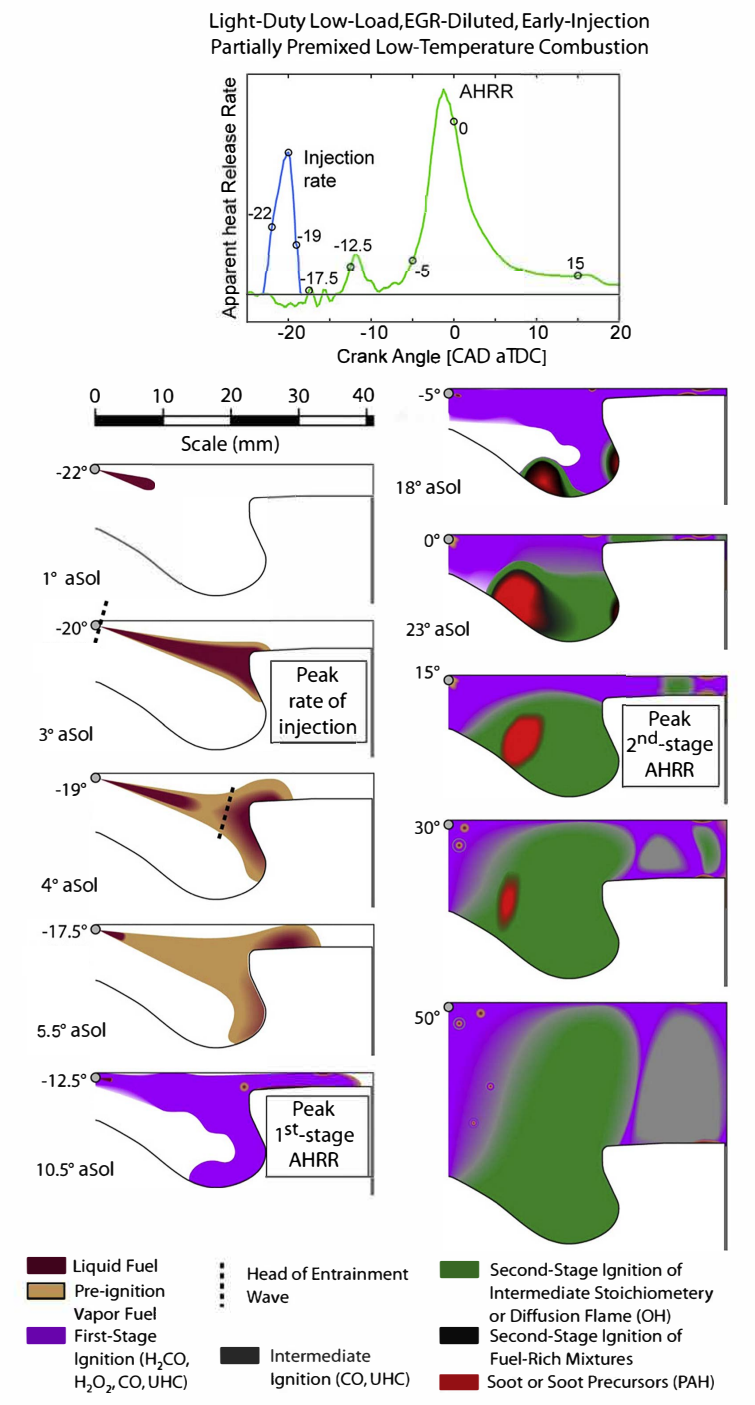

Figure 2.14. *Schematics of Musculus's conceptual model for single early-injection, low load, EGR-diluted, PPCI low-temperature light-duty DI diesel combustion. Source: Musculus et al. [121].*

(marked in dashed black line) is initiated at the injector, but at this CAD the liquid phase has already impacted the bowl rim. Right after the EoI at 4.5 ° aSoI, liquid fuel still remains near the bowl rim, at the head of the jet. The liquid near the bowl rim persists for a few more CAD, and penetrates farther into the squish volume and deeper into the bowl, as well as leaving a fuel film around the bowl rim. Generally, the maximum liquid penetration is similar to the maximum observed vapor penetration.

The LTR phase associated with the first-stage of ignition peaks near −12.5 CAD aTDC, and is delayed considerably from the injection event proving a positive ignition dwell, unlike the case of CDC. Formaldehyde fluorescence (in violet) is observed throughout much of the jet structure, from fuel-lean to fuel-rich mixtures, that now has penetrated deeper into the bowl and farther into the squish volume. Shortly after the first-stage of ignition, just as the heat release associated with the second-stage ignition is starting, a two-zone spatial distribution of fluorescence is regularly observed deep in the bowl. The two zones are often separated by a fluorescence-free zone. Although the mixture preparation processes leading to this two-zone structure are not well understood, toluene fuel-tracer PLIF measurements, such as those shown in 2.11, indicate that both zones are fuel-rich, as shown in the schematic at −5 CAD aTDC.

Just beyond the peak apparent heat release rate near TDC, second-stage ignition has been reached in much of the mixture deep in the bowl (0 CAD aTDC). At this time, PAH (soot) fluorescence from the head of the jet is now positioned in the inner portion of the bowl and is more pronounced, and fluorescence from the outer, re-entrant region of the bowl is considerably reduced. Second-stage ignition is also achieved within the squish volume at this time. Although fuel-rich mixture is measured within the squish volume at the start of second-stage heat release, equivalence ratios are sufficiently low that significant soot or PAH is not formed. While over-lean mixture between the fuel jets is undoubtedly present and leads to regions of unburned H_2CO and HC, strong fluorescence is only observed from regions near liquid films: along the head near the bowl rim and well within the squish volume, on both the head and piston surface.

At later crank angle after TDC, volume expansion due to heat release within the bowl and the reverse squish flow induced by piston motion push the lean mixture exhibiting continued H_2CO fluorescence into the squish volume, eventually forming a two-zone distribution of HC and CO. In the inner zone near the cylinder center, the HC and the CO distribution is dominated by lean mixture within which discrete fuel droplets are embedded. A second zone,

generally larger in extent, is found within the squish volume and is positioned closer to the piston top than to the head. With early-injection PPCI, the squish volume HC and CO are associated with at least four different sources: lean mixture from the edges of the fuel jets that penetrate directly into the squish volume; lean, bulk-gas mixtures from near the bowl rim and the central clearance volume that are forced/drawn into the squish volume; liquid films and associated rich mixtures on the piston top and surface of the head; and crevice HC which is trapped in the upper corner of the cylinder and along the cylinder wall. At the light-load operating condition considered for this conceptual model, lean bulk-gas mixtures within the squish volume and the central region of the cylinder are the typically the most dominant sources of engine out HC and CO emissions.

Different investigations have demonstrated the potential of diesel PPCI LTC concept for complying with stringent emissions limits in terms of NO_x and PM, however, as it is expected other emissions including CO and HC typically exceed regulated limits, so they still remain to be a common problem among these strategies [54, 102, 103, 106, 123–125]. Moreover, the required longer ignition dwell times can also lead to excessive pressure rise rates and higher noise level, specially when increasing fueling rate, so this can impose additional constraints on the required dilution level or injection timing, driving further increases in CO and HC, or it may ultimately restrict PPCI operation to the low-to-mid load range similar to the case of HCCI. So, the comparatively lower combustion efficiency, as well as non-optimal heat release phasing, will also bring penalties in fuel consumption for diesel PPCI operation compared to conventional mixing-controlled conditions.

As the load increases, it gets more difficult to retard the onset of ignition due to the intrinsically higher gas temperatures and global equivalence ratio approaching stoichiometric, so the fuel will tend to ignite shortly after the start of injection, shifting the possible range of SoI closer to TDC (as in CDC conditions) to avoid the onset of knocking-like combustion. As a result, high load PPCI operation will be typically restricted by the ignition dwell, and also by stoichiometric conditions, so the fuel introduced in the latter part of the injection event will typically be burnt in a quasi-steady jet diffusion flame (not in premixed mode), transitioning towards a mixing-controlled LTC combustion.

Noehre et al. [53] demonstrated high load diesel PPC operation, up to 15 bar IMEP in a heavy-duty single-cylinder engine, combining low compression ratio, extremely high EGR and intake pressure levels, high swirl, and engine operation close to stoichiometric conditions that allowed

simultaneous reduction of NO_x and soot emissions. At these high load conditions (12.5 and 15 bar IMEP) even when the ignition delay was comparatively longer than in typical CDC, combustion occurred while injection was still proceeding (negative ignition dwell), so the lower soot emissions seemed to be a result of partial premixing for the fuel injected prior the SoC, combined with substantially lower local peak combustion temperatures (below 1600 K) and enhanced mixing (high density and swirl), which are conditions that resembled more like a mixing-controlled LTC. However, as it was expected the simultaneous soot-NO_x reduction had to be paid with a decline in combustion efficiency due to a dramatic rise of HC and CO emissions.

2.3.3 Fuel effects in PPCI or PPC engines

The effect of fuel properties on the partially premixed combustion relates to their combined impact on the mixing preparation process and on the ignition delay. Accordingly, achieving long enough ignition delay to assure a positive ignition dwell, when using high cetane diesel fuel (CN$<$ 40) in PPCI conditions, requires higher dilution levels (very high EGR rates) and typically lower compression ratios, in addition to comparatively advanced or retarded timings than the typically used in CDC.

Pioneering research work performed by Kalghatgi et al. [126, 127] in a heavy-duty engine first demonstrated how a fuel in the gasoline autoignition range (RON$>$ 60) could be used in a CI engine for improving the performances and expand the range of the PPCI mode. The higher ignition delay of such fuels provided more time for the fuel and air to premix before the time of ignition, resulting in a larger fraction of premixed combustion. This advantage can be used to relax the requirements in terms of EGR, or injection pressure and nozzle hole diameter for a gasoline PPC engine. These preliminary studies confirmed the potential of using gasoline-like fuels in CI engines, where gasoline PPC operation made possible to attain very low NO_x (0.58 g/kW h) and smoke emissions (0.07 FSN) with promising indicated fuel consumption (179 g/kW h) levels at a load condition of 15.95 bar of IMEP. At the same operating conditions, to get such low level of smoke with Swedish MK1 diesel fuel, IMEP had to be below 6.5 bar.

Starting from 2008, PPC using gasoline-like fuels was extensively studied both in heavy-duty and in light-duty engines at the Combustion Engines Division from Lund University. For instance, Hildingsson et al. [128] studied the effect of fuel octane number of different gasoline-like fuels in a light-

duty single-cylinder engine, compared to diesel keeping a single-injection PPC strategy. To get the same combustion phasing (CA50) for gasoline-like fuels as with diesel, the fuel injection had to start earlier in the cycle; and this timing had to be advanced as RON was increased. The optimum fuel octane number for gasoline PPC operation appeared to be in the 75 RON to 85 RON range for the engine compression ratio (16) and operating conditions used. Lower octane fuels might start losing their advantage over diesel in terms of ignition delays while higher octane fuels will have ignition difficulties at lower loads and higher EGR levels.

Regarding the effect of fuel volatility, Hildingsson et al. also investigated if high volatility was also needed along with low cetane (high octane) to get more premixed combustion leading to low NO_x and smoke conditions [129]. The same light-duty engine as the used in [128] was run on four fuels in the diesel boiling range with different cetane numbers, and three fuels in the gasoline boiling range with different octane numbers. The results showed that a fuel in the diesel boiling range but with a high aromatics content (75%vol), thus yielding a very low cetane number that entered the gasoline autoignition range; behaved like a high octane gasoline providing low NO_x and low smoke levels even at high load and high speed conditions, as a consequence of its higher resistance to autoignition. This is explained by the fact that aromatic fuels become relatively more resistant to autoignition compared to paraffinic fuels as the pressure increases while the temperature is held constant, confirming that the true autoignition quality of gasoline-like fuels cannot be determined by just one number like CN or RON at all operating conditions. Another interesting remark is that for the conditions studied, if two fuels had the same ignition and combustion delay at a given operating condition, they exhibited comparable emissions and maximum pressure rise rates regardless of the differences in volatility or fuel composition [129, 130]. Thus, for PPC the autoignition quality of a given fuel appears to be far more important than its volatility or composition in this type of combustion.

Manente et al. [107–109, 131] studied the operable load range of the PPC concept as function of the fuel octane number, for different gasoline fuels with RON spanning from 69 to 99, together with PRF20 and diesel MK1, in a heavy-duty single-cylinder engine. The engine was run with 50 % of EGR and was boosted to maintain air excess ratio (lambda) around 1.5. For the selected test conditions, it was possible to operate in PPC mode up to an engine load of 25 bar IMEP using the high RON fuels, since the longer ignition delay allowed for additional mixing time as the load was increased [131]. However, it was not possible to run at low engine loads with high RON fuel due to misfire conditions. Figure 2.15 presents the operable load range as function of RON

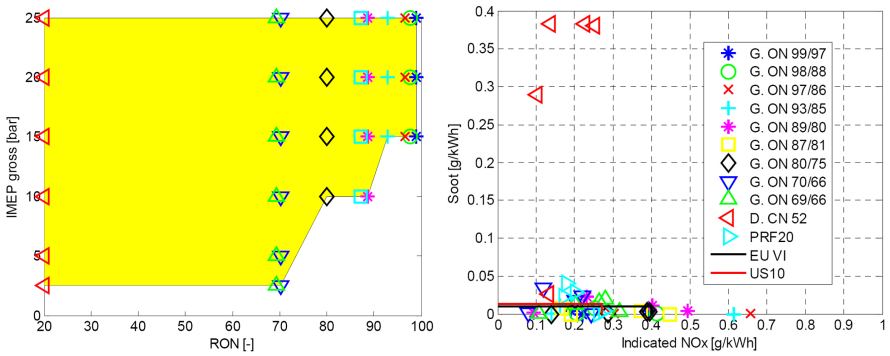

Figure 2.15. *Operating range of gasoline PPC as function of the fuel RON. Source: Manente et al. [131].*

for the studied fuels, as well as the soot-NO_x trade-off along with the EU VI and US10 emission requirements.

In the case of light-duty engines, Solaka et al. [132] studied the impact of ignition quality and chemical properties on engine performance and emissions during low load PPC operation. The objective of this work was to examine the low load limit for PPC at approximately 50 % of EGR and lambda equal to 1.5, since those levels had been suggested as optimal in the work done by Manente [109]. The low load limits with stable combustion were found between 5 bar to 7 bar of IMEP for the gasoline fuels, with higher limit for the highest RON (88.6 and 87.1) fuels, while diesel had the lowest low-load limit of 3 bar IMEP. By increasing lambda while keeping EGR ratio, with extended boosting, all the fuels could be operated down to 2 bar IMEP. However, combustion efficiency was low and the coefficient of variation of the IMEP was high as a consequence of the higher misfire trend. Using a variable valve train system is of practical interest because obtaining such a high boost pressure with a standard turbo-charging system at low engine speed and load is quite challenging. So, the approach reported by Borgqvist et al. [133, 134] consisted of using negative valve overlap (NVO) strategies to trap hot residuals in the cylinder, hence, increasing the temperature at IVC to promote autoignition at such low loads. These investigations showed the viability of the gasoline PPC concept for achieving very high efficiency and low emissions in a much wider load range compared to diesel PPC.

From the previous discussion, it appears that extending gasoline PPC operation to cover the full engine map is a feasible but still challenging task, that requires combining suitable injection strategy along with optimum

thermodynamic conditions; in addition to advanced air charging technologies, NVO or re-breathing strategies, or using a gasoline (or a fuel blend) in the autoignition range of 70 to 80 RON which is not commercially available in the market. If the RON of the fuel is too low, the ignition delay will be too short and comparable to conventional diesel fuel so achieving PPC combustion becomes difficult; on the contrary, if RON is too high, at some operating conditions such as starting and low load operation the ignition delay will be too high for stable combustion to occur [128]. Greater stratification of the mixture can be achieved through multiple injections of the fuel [126, 131, 135–137] so that heat release is distributed in time decreasing the noise level and the maximum pressure gradient.

More recently, many research groups from Lund University [138–142], University of Wisconsin Madison [135], University of Cambridge [143], Argonne National Laboratory [112, 113, 144–146], and Delphi Corporation [147–149] have performed additional experimental and numerical investigations operating with the gasoline PPC mode. Different injection strategies were explored with various levels of EGR, boost pressure, intake temperature and swirl ratios at different engine loads and speeds. In general, reported results confirmed how it is possible to implement PPC with very high efficiency, very low NO_x emissions and also lower soot levels, in a much wider range of load operation compared to diesel PPC. However, even when results are highly promising, many practical issues still remain under investigation before reaching a production-viable powertrain system; i.e. injection systems requirements (injector type and optimum injection pressures), piston and combustion chamber design, boost system requirements, control strategies, among others.

2.4 Summary and concluding remarks

This chapter focused on describing the fundamental aspects related to the physical and chemical mechanism occurring inside the combustion chamber of a direct injection CI diesel engine, in the frame of mixing-controlled CDC as well as advanced LTC concepts with high (HCCI and HPC) to moderate (PPCI and PPC) degree of premixing. Significant insight into the mixture preparation, autoignition and combustion process, leading to the formation of the main pollutants emissions (NO_x, PM, CO and HC), has been supported with a review of different experimental and numerical investigations that have become the foundation of well-established conceptual models for both CDC and LTC concepts.

From the phenomenological description of the mixing-controlled combustion process presented in section 2.2.1, it becomes clear that the CDC concept is characterized by high NO_x and PM emissions, since the fuel/air mixture spans a wide range of local equivalence rations and temperatures, as it was shown in the ϕ-T diagram. In CDC, the fuel injection occurs near TDC, where in-cylinder density and temperature are reaching its maximum values, so the ignition and combustion typically occur while the fuel is still being injected and mixed yielding a negative ignition dwell. Then, the combustion rate is controlled by the injection and air entrainment rate into the fuel spray. Accordingly, the regions with high temperature and relatively low ϕ in the periphery of the flame lead to NO_x formation, while PM formation is promoted in the high ϕ, intermediate temperature region found in the core of the spray.

Asides from the need of decreasing the current levels of harmful emissions derived from diesel combustion, research efforts are also directed towards further improving engine efficiency to reduce fuel consumption and CO_2 emissions. In this regard, engine downsizing by decreasing the number of cylinders plays a key role for CO_2 reduction, since it is directly associated to the improvement in overall efficiency due to the reduction of friction losses and by operating the engine at higher load levels where indicated efficiency is improved, as well as the reduction in the total vehicle weight. In this context, switching to a two-stroke cycle would allow increasing drastically the engine specific power by doubling the firing events per crankshaft revolution, making it possible to downsize total engine displacement by almost a factor of two while keeping similar torque and power output. Additionally, the potential of the two-stroke cycle for providing a compact and lighter powertrain with high power-to-weight ratio that could be used in small/economic diesel passenger cars or as range extender in hybrid applications, further encouraged the investigation of CDC operation on the current two-stroke engine under development.

From the review of advanced combustion concepts in CI engines presented in section 2.3, and excluding the mixing-controlled LTC concepts, the primary focus of most of strategies currently under investigation is to promote a sufficiently premixed low-temperature combustion; in order to slow down or even avoid the chemical reactions leading to thermal NO_x formation due to a drastic reduction in the local temperatures inside the combustion chamber, while PM formation is hindered by the absence of high local ϕ during the combustion process. From the general overview of homogeneous (HCCI) and highly premixed (HPC) combustion concepts presented in section 2.3.1, it has been confirmed how the combustion of a globally lean charge with ϕ well below

1 is effective for reducing simultaneously NO_x and PM emissions. However, the operating region of this strategy with high cetane fuels is restricted to low loads due to very early combustion phasing and a corresponding lack of power density and combustion control. Additionally, high levels of CO and HC emissions are often unavoidable due to extremely over-mixed mixtures that fail to reach second-stage ignition, as well as liquid fuel impingement onto the cylinder liner surfaces.

To overcome the problems of diesel HCCI operation; research efforts have been shifted towards partially premixed combustion concepts (PPCI and PPC), where slightly retarded injection timings compared to HCCI are used to enable partial mixing of the mixture, then eliminating over-rich regions with ϕ greater than 2 where soot is formed, while NO_x emissions are reduced by lowering combustion temperatures below 2200 K through the use of large amounts of EGR. Different strategies has been investigated in order to promote enough mixing time prior to ignition when high cetane fuels are used, the majority of those were focused on a combination of lower compression ratio and high fractions of cooled EGR to slow down the chemical reactions, high injection pressures and swirl level to speed up the mixing process, and/or the use of multiple or split injection strategies. Assuring some degree of stratification on the equivalence ratio is mandatory for allowing proper control over the combustion phasing with the injection timing. Even when the control over combustion phasing is regained when switching from HCCI to PPC mode operation, the range for simultaneous reduction of NO_x and PM by introducing high EGR rates is somehow limited, and a sharp decline in combustion efficiency is still unavoidable when using high cetane fuels.

An additional lever that allows extending the mixing time before the onset of ignition, is to decrease the reactivity of the cylinder charge by using fuels with higher resistance to auto-ignition (low cetane fuels) as is the case of gasoline-like fuels. In the case of gasoline PPC concept, the reported results in terms of emissions and engine indicated efficiencies are far better than those attainable operating with any other advanced combustion concept with diesel fuel. However, there is still an optimum zone in the engine map where the ignition characteristics of a given fuel are better matched to the engine operating condition, which may result in a limited load range for PPC operation depending on the octane number of the fuel. This supposes that the PPC concept typically requires different fuel reactivity and/or advanced valvetrain and boost/EGR systems to ensure proper ignition control, and optimize emissions and efficiency levels in the entire engine map.

In this regard, the two-stroke engine under study provides a high flexibility to control the internal gas recirculation (IGR) rates by means of the air management settings, to effectively change the cylinder gas temperature evolution in a much wider range compared to four-stroke engines. Thus, two-stroke operation has intrinsically much more potential to adjust the cylinder charge thermochemical conditions and consequently affect the combustion environment, which is a key action to control the combustion process and the final emission levels in the frame of both highly and partially premixed combustion concepts. Additionally, two-stroke operation has gained renewed interest in the frame of application of advanced combustion concepts, since it intrinsically provides equivalent torque response with only half the indicated mean effective pressure (IMEP) required in four-stroke operation for equal engine displacement. This may solve some of the intrinsic problems related HCCI/PPC operation at high loads, by restricting the operating range to low and medium loads where these concepts perform the best, while still keeping maintaining the expected engine performance.

In agreement with the previous discussion, an important research effort is still needed to be done to foreseen the real potential of the two-stroke engine architecture for improving the state-of-the-art four-stroke CI engines in terms of their respective pollutant emissions and efficiency levels, and also to identify the compatibility of the two-stroke engine in the frame of application of advanced combustion concepts.

Bibliography

[1] Dec John E. "A Conceptual Model of DI Diesel Combustion Based on Laser-Sheet Imaging". In *SAE Technical Paper*, volume 970873, 1997.

[2] Flynn P.F., Durrett R.P., Hunter G.L., Zur Loye A.O., Akinyemi O. C., Dec John E. and Westbrook Charles K. "Diesel combustion: An integrated view combining laser diagnostics, chemical kinetics, and empirical validation". In *SAE Technical Paper*, volume 1999-01-0509, 1999.

[3] Gimeno J. *Desarrollo y aplicacion de la medida del flujo de cantidad de movimiento de un chorro diesel.* PhD thesis. Universitat Politecnica de Valencia, Departamento de Maquinas y Motores Termicos, 2008.

[4] Payri R., Garcia J.M., Salvador F. and Gimeno J. "Using spray momentum flux measurements to understand the influence of diesel nozzle geometry on spray characteristics". *Fuel*, Vol. 84 n^o 5, pp. 551–561, 2005.

[5] Hermens S. *Influence of diesel injector nozzle geometry on the injection and combustion process.* PhD Thesis. Universitat Politecnica de Valencia, Departamento de Maquinas y Motores Termicos, 2008.

[6] Salvador F.J. *Estudio teorico experimental de la influencia de la geometria de la tobera de inyeccion sobre las caracteristicas del flujo interno y del chorro*. PhD thesis. Universitat Politecnica de Valencia, Departamento de Maquinas y Motores Termicos, 2003.

[7] Correas D. *Estudio Teorico-Experimental del chorro libre diesel isotermo*. PhD Thesis. Universitat Politecnica de Valencia, Departamento de Maquinas y Motores Termicos, 1998.

[8] Arregle J. *Analisis de la estructura y dinamica interna de chorros diesel*. PhD thesis. Universitat Politecnica de Valencia, Departamento de Maquinas y Motores Termicos, 1997.

[9] Ruiz S. *Estudio Teorico-Experimental de los procesos de atomizacion y de mezcla en los chorros diesel D.I.* PhD thesis. Universitat Politecnica de Valencia, Departamento de Maquinas y Motores Termicos, 2003.

[10] Lopez J.J. *Estudio Teorico-Experimental del chorro libre diesel no evaporativo y de su interaccion con el movimiento del aire*. PhD thesis. Universitat Politecnica de Valencia, Departamento de Maquinas y Motores Termicos, 2003.

[11] Naber Jeffrey D. and Siebers Dennis L. "Effects of Gas Density and Vaporization on Penetration and Dispersion of Diesel Sprays". In *SAE Technical Paper*, volume 960034, 1996.

[12] Ricou F. P. and Spalding D. B. "Measurements of entrainment by axisymmetrical turbulent jets". *Journal of Fluid Mechanics*, Vol. 11 n^o 01, pp. 21–32, 1961.

[13] Pope Stephen B. *Turbulent flows*. Cambridge university press, 2000.

[14] Pickett Lyle M., Manin Julien, Genzale Caroline L., Siebers Dennis L., Musculus Mark P. B. and Idicheria Cherian A. "Relationship Between Diesel Fuel Spray Vapor Penetration/Dispersion and Local Fuel Mixture Fraction". *SAE Int. J. Engines*, Vol. 4 n^o 1, pp. 764–799, 2011.

[15] Siebers Dennis L. "Scaling Liquid-Phase Fuel Penetration in Diesel Sprays Based on Mixing-Limited Vaporization". In *SAE Technical Paper*, volume 1999-01-0528. SAE International, 1999.

[16] Canaan R., Dec J., Green R. and Daly D. "The Influence of Fuel Volatility on the Liquid-Phase Fuel Penetration in a Heavy-Duty D.I. Diesel Engine". In *SAE Technical Paper*, volume 980510, 1998.

[17] Desantes Jose M., Lopez J. Javier, Garcia Jose M. and Pastor Jose M. "Evaporative Diesel Spray Modeling". *Atomization and Sprays*, Vol. 17 n^o 3, pp. 193–231, 2007.

[18] Garcia-Oliver J.M. *Aportaciones al estudio del proceso de combustion turbulenta de chorros en motores diesel de inyeccion directa*. PhD thesis. Universitat Politecnica de Valencia, Departamento de Maquinas y Motores Termicos, 2004.

[19] Pastor Jose V., Javier Lopez J., Garcia Jose M. and Pastor Jose M. "A 1D model for the description of mixing-controlled inert diesel sprays". *Fuel*, Vol. 87 n^o 13-14, pp. 2871–2885, 2008.

[20] Musculus Mark P. B. and Kattke Kyle. "Entrainment Waves in Diesel Jets". In *SAE Technical Paper*, volume 2009-01-1355, 2009.

[21] Musculus M. P. B. "Entrainment waves in decelerating transient turbulent jets". *Journal of Fluid Mechanics*, Vol. 638, pp. 117–140, 2009.

[22] Kosaka H, Aizawa T and Kamimoto T. "Two-dimensional imaging of ignition and soot formation processes in a diesel flame". *International Journal of Engine Research*, Vol. 6 n^o 1, pp. 21–42, 2005.

[23] Idicheria Cherian A. and Pickett Lyle M. "Formaldehyde Visualization Near Lift-off Location in a Diesel Jet". In *SAE Technical Paper*, volume 2006-01-3434. SAE International, 2006.

[24] Bruneaux G. "Combustion structure of free and wall-impinging diesel jets by simultaneous laser-induced fluorescence of formaldehyde, poly-aromatic hydrocarbons, and hydroxides". *International Journal of Engine Research*, Vol. 9 n^o 3, pp. 249–265, 2008.

[25] Dec John E. and Espey Christoph. "Chemiluminescence Imaging of Autoignition in a DI Diesel Engine". In *SAE Technical Paper*, volume 982685. SAE International, 1998.

[26] Dec John E. and Espey Christoph. "Ignition and Early Soot Formation in a DI Diesel Engine Using Multiple 2-D Imaging Diagnostics". In *SAE Technical Paper*, volume 950456. SAE International, 1995.

[27] Dec John E. and Coy Edward B. "OH Radical Imaging in a DI Diesel Engine and the Structure of the Early Diffusion Flame". In *SAE Technical Paper*, volume 960831. SAE International, 1996.

[28] Higgins B, Siebers D and Aradi A. "Diesel-Spray Ignition and Premixed-Burn Behavior". In *SAE Technical Paper*, volume 2000-01-0940, 2000.

[29] Idicheria C. A. and Pickett L. M. "Ignition, soot formation, and end-of-combustion transients in diesel combustion under high-EGR conditions". *International Journal of Engine Research*, Vol. 12 n^o 4, pp. 376–392, 2011.

[30] Curran H. J., Gaffuri P., Pitz W. J. and Westbrook C. K. "A Comprehensive Modeling Study of n-Heptane Oxidation". *Combustion and Flame*, Vol. 114 n^o 1-2, pp. 149–177, 1998.

[31] Chartier Clement, Aronsson Ulf, Andersson Oivind, Egnell Rolf, Collin Robert, Seyfried Hans, Richter Mattias and Alden Marcus. "Analysis of Smokeless Spray Combustion in a Heavy-Duty Diesel Engine by Combined Simultaneous Optical Diagnostics". In *SAE Technical Paper*, volume 2009-01-1353. SAE International, 2009.

[32] Siebers Dennis L. and Higgins B. "Flame Lift-Off on Direct-Injection Diesel Sprays Under Quiescent Conditions". In *SAE Technical Paper*, volume 2001-01-0530, 2001.

[33] Pickett L. M. and Siebers D. L. "Orifice diameter effects on diesel fuel jet flame structure". In *Proceedings of the Fall Technical Conference of the ASME Internat Combustion Engine Division*, pp. ICE 37–41, 2001.

[34] Dec John E. and Tree Dale R. "Diffusion-Flame / Wall Interactions in a Heavy-Duty DI Diesel Engine". In *SAE Technical Paper*, volume 2001-01-1295. SAE International, 2001.

[35] Kosaka Hidenori, Nishigaki Takahiro, Kamimoto Takeyuki, Sano Takashi, Matsutani Akira and Harada Shinichi. "Simultaneous 2-D Imaging of OH Radicals and Soot in a Diesel Flame by Laser Sheet Techniques". In *SAE Technical Paper*, volume 960834. SAE International, 1996.

[36] Dec John E. and Canaan Robert E. "PLIF Imaging of NO Formation in a DI Diesel Engine". In *SAE Technical Paper*, volume 980147, 1998.

[37] Arregle J., Lopez J. J., Garcia J. M. and Fenollosa C. "Development of a zero-dimensional Diesel combustion model: Part 2: Analysis of the transient initial and final diffusion combustion phases". *Applied Thermal Engineering*, Vol. 23 n^o 11, pp. 1319–1331, 2003.

[38] Kim T. and Ghandhi J. "Quantitative 2-D Fuel Vapor Concentration Measurements in an Evaporating Diesel Spray using the Exciplex Fluorescence Method". In *SAE Technical Paper*, volume 2001-01-3495, 2001.

[39] Bruneaux Gilles. "Mixing Process in High Pressure Diesel Jets by Normalized Laser Induced Exciplex Fluorescence Part I: Free Jet". In *SAE Technical Paper*, volume 2005-01-2100. SAE International, 2005.

[40] Musculus Mark P. B., Lachaux Thierry, Pickett Lyle M. and Idicheria Cherian A. "End-of-Injection Over-Mixing and Unburned Hydrocarbon Emissions in Low-Temperature-Combustion Diesel Engines". In *SAE Technical Paper*, volume 2007-01-0907. SAE International, 2007.

[41] Musculus Mark P. B. "Multiple Simultaneous Optical Diagnostic Imaging of Early-Injection Low-Temperature Combustion in a Heavy-Duty Diesel Engine". In *SAE Technical Paper*. SAE International, 2006.

[42] Lachaux Thierry and Musculus Mark P. B. "In-cylinder unburned hydrocarbon visualization during low-temperature compression-ignition engine combustion using formaldehyde PLIF". *Proceedings of the Combustion Institute*, Vol. 31 n^o 2, pp. 2921–2929, 2007.

[43] Singh S, Reitz R D, Musculus M P B and Lachaux T. "Validation of engine combustion models against detailed in-cylinder optical diagnostics data for a heavy-duty compression-ignition engine". *International Journal of Engine Research*, Vol. 8 n^o 1, pp. 97–126, 2007.

[44] Hu Bing, Musculus Mark P. B. and Oefelein Joseph C. "The influence of large-scale structures on entrainment in a decelerating transient turbulent jet revealed by large eddy simulation". *Physics of Fluids*, Vol. 24 n^o 4, pp. 045106, 2012.

[45] Singh Satbir and Musculus Mark P. B. "Numerical Modeling and Analysis of Entrainment in Turbulent Jets After the End of Injection". *Journal of Fluids Engineering*, Vol. 132 n^o 8, pp. 081203–081203, 2010.

[46] Dec John E. and Kelly-Zion Peter L. "The Effects of Injection Timing and Diluent Addition on Late-Combustion Soot Burnout in a DI Diesel Engine Based on Simultaneous 2-D Imaging of OH and Soot". In *SAE Technical Paper*, volume 2000-01-0238. SAE International, 2000.

[47] Knox Benjamin W, Genzale Caroline L., Pickett L., Garcia-Oliver Jose M. and Vera-Tudela Walter. "Combustion Recession after End of Injection in Diesel Sprays". In *SAE Technical Paper*, volume 2015-01-0797, 2015.

[48] Aoyagi Y., Kamimoto T., Matsui Y. and Matsuoka S. "A Gas Sampling Study on the Formation Processes of Soot and NO in a DI Diesel Engine". In *SAE Technical Paper*, volume 800254, 1980.

[49] Kamimoto Takeyuki and Bae Myurng Hoan. "High Combustion Temperature for the Reduction of Particulate in Diesel Engines". In *SAE Technical Paper*, volume 880423, 1988.

[50] Potter Mike and Durrett Russ. "High-Efficiency Clean Combustion Design for Compression Ignition Engines". In *2006 Diesel Engine-Efficiency and Emissions Research (DEER) Conference Presentations.*, Detroit, Michigan, 2006.

[51] Akihama Kazuhiro, Takatori Yoshiki and Inagaki Kazuhisa. "Mechanism of the Smokeless Rich Diesel Combustion by Reducing Temperature". In *SAE Technical Paper*, volume 2001-01-0655, 2001.

[52] Huestis Edwin, Erickson Paul A. and Musculus Mark P. B. "In-Cylinder and Exhaust Soot in Low-Temperature Combustion Using a Wide-Range of EGR in a Heavy-Duty Diesel Engine". In *SAE Technical Paper*, volume 2007-01-4017. SAE International, 2007.

[53] Noehre Christof, Andersson Magnus, Johansson Bengt and Hultqvist Anders. "Characterization of Partially Premixed Combustion". In *SAE Technical Paper*, volume 2006-01-3412, 2006.

[54] Colban Will F., Miles Paul C. and Oh Seungmook. "Effect of Intake Pressure on Performance and Emissions in an Automotive Diesel Engine Operating in Low Temperature Combustion Regimes". In *SAE Technical Paper*, volume 2007-01-4063. SAE International, 2007.

[55] Ogawa Hideyuki, Miyamoto Noboru, Shimizu Hajime and Kido Shingo. "Characteristics of Diesel Combustion in Low Oxygen Mixtures with Ultra-High EGR". In *SAE Technical Paper*, volume 2006-01-1147. SAE International, 2006.

[56] Cheng A. S, Upatnieks A. and Mueller C. J. "Investigation of fuel effects on dilute, mixing-controlled combustion in an optical direct-injection diesel engine". *Energy and Fuels*, Vol. 21 n^o 4, pp. 1989–2002, 2007.

[57] Amorim Rogerio. *Combustion por difusion de baja temperature en motores diesel de pequeña cilindrada*. PhD Thesis. Universitat Politecnica de Valencia, Departamento de Maquinas y Motores Termicos, 2010.

[58] Benajes Jesus, Molina Santiago, Novella Ricardo and Amorim Rogerio. "Study on low temperature combustion for light-duty diesel engines". *Energy and Fuels*, Vol. 24, pp. 355–364, 2010.

[59] Benajes Jesus, Molina Santiago, Novella Ricardo and Belarte Eduardo. "Evaluation of massive exhaust gas recirculation and Miller cycle strategies for mixing-controlled low temperature combustion in a heavy duty diesel engine". *Energy*, Vol. 71, pp. 355–366, 2014.

[60] Ryan Thomas W. and Callahan Timothy J. "Homogeneous Charge Compression Ignition of Diesel Fuel". In *SAE Technical Paper*, volume 961160, 1996.

[61] Takeda Yoshinaka, Keiichi Nakagome and Keiichi Niimura. "Emission Characteristics of Premixed Lean Diesel Combustion with Extremely Early Staged Fuel Injection". In *SAE Technical Paper*, volume 961163, 1996.

[62] Walter Bruno and Gatellier Bertrand. "Development of the High Power NADITM Concept Using Dual Mode Diesel Combustion to Achieve Zero NOx and Particulate Emissions". In *SAE Technical Paper*, volume 2002-01-1744, 2002.

[63] Akagawa Hisashi, Miyamoto Takeshi, Harada Akira, Sasaki Satoru, Shimazaki Naoki, Hashizume Takeshi and Tsujimura Kinji. "Approaches to Solve Problems of the Premixed Lean Diesel Combustion". In *SAE Technical Paper*, volume 1999-01-0183. SAE International, 1999.

[64] Hasegawa Ryo and Yanagihara Hiromichi. "HCCI Combustion in a DI Diesel engine". In *SAE Technical Paper*, volume 2003-01-0745, 2003.

[65] Iwabuchi Yoshinori, Kawai Kenji, Shoji Takeshi and Takeda Yoshinaka. "Trial of New Concept Diesel Combustion System - Premixed Compression-Ignited Combustion". In *SAE Technical Paper*, volume 1999-01-0185, 1999.

[66] Suzuki Hisakazu, Koike Noriyuki, Ishii Hajime and Odaka Matuo. "Exhaust Purification of Diesel Engines by Homogeneous Charge with Compression Ignition Part 1: Experimental Investigation of Combustion and Exhaust Emission Behavior Under Pre-Mixed Homogeneous Charge Compression Ignition Method". In *SAE Technical Paper*, volume 970313, 1997.

[67] Yanagihara H., Sato Y. and Minuta J. "A simultaneous reduction in NOx and soot in diesel engines under a new combustion system (Uniform Bulky Combustion System -UNIBUS)". In *17th International Vienna Motor Symposium*, pp. 303–314, 1996.

[68] Hashizume Takeshi, Miyamoto Takeshi, Hisashi Akagawa and Tsujimura Kinji. "Combustion and Emission Characteristics of Multiple Stage Diesel Combustion". In *SAE Technical Paper*, volume 980505. SAE International, 1998.

[69] Su Wanhua, Lin Tiejian and Pei Yiqiang. "A Compound Technology for HCCI Combustion in a DI Diesel Engine Based on the Multi-Pulse Injection and the BUMP Combustion Chamber". In *SAE Technical Paper*, volume 2003-01-0741. SAE International, 2003.

[70] Helmantel Arjan and Denbratt Ingemar. "HCCI Operation of a Passenger Car Common Rail DI Diesel Engine With Early Injection of Conventional Diesel Fuel". In *SAE Technical Paper*, volume 2004-01-0935. SAE International, 2004.

[71] Buchwald Ralf, Brauer Maximilian, Blechstein Andre, Sommer Ansgar and Kahrstedt Jorn. "Adaption of Injection System Parameters to Homogeneous Diesel Combustion". In *SAE Technical Paper*, volume 2004-01-0936. SAE International, 2004.

[72] Su Wanhua, Wang Hui and Liu Bin. "Injection Mode Modulation for HCCI Diesel Combustion". In *SAE Technical Paper*, volume 2005-01-0117. SAE International, 2005.

[73] Andre M., Walter B., Bruneaux G., Foucher F. and Mounaim-Rousselle C. "Optimizing Early Injection Strategy for Diesel PCCI Combustion". In *SAE Technical Paper*, volume 2009-01-2731. SAE International, 2009.

[74] Pinchon P., Walter B., Reveille B. and Miche M. "New concepts for diesel combustion". In *THIESEL Conference Proceedings*, 2004.

[75] Fang Tiegang, Coverdill Robert E., Lee Chia-fon F. and White Robert A. "Smokeless Combustion within a Small-Bore HSDI Diesel Engine Using a Narrow Angle Injector". In *SAE Technical Paper*, volume 2007-01-0203. SAE International, 2007.

[76] Ryan, T. W. III and Matheaus A. C. "Fuel Requirements for HCCI Engine Operation". In *SAE Technical Paper*, volume 2003-01-1813. Society of Automotive Engineers, 2003.

[77] Yao M., Zheng Z., Zhang B. and Chen Z. "The Effect of PRF Fuel Octane Number on HCCI Operation". In *SAE Technical Paper*, volume 2001-01-2992, 2004.

[78] Kokjohn S. L., Hanson R. M., Splitter D. A. and Reitz R. D. "Fuel reactivity controlled compression ignition (RCCI): a pathway to controlled high-efficiency clean combustion". *International Journal of Engine Research*, Vol. 12 n^o 3, pp. 209–226, 2011.

[79] Splitter Derek, Hanson Reed, Kokjohn Sage, Wissink Martin and Reitz Rolf. "Injection Effects in Low Load RCCI Dual-Fuel Combustion". In *SAE Technical Paper*, volume 2011-24-0047, 2011.

[80] Splitter Derek, Wissink Martin, DelVescovo Dan and Reitz Rolf. "RCCI Engine Operation Towards 60In *SAE Technical Paper*, volume 2013-01-0279, 2013.

[81] Splitter Derek A. and Reitz Rolf D. "Fuel reactivity effects on the efficiency and operational window of dual-fuel compression ignition engines". *Fuel*, Vol. 118 n^o 0, pp. 163–175, 2014.

[82] Mancaruso Ezio and Vaglieco Bianca Maria. "UV-Visible Spectroscopic Measurements of Dual-Fuel PCCI Engine". *SAE International Journal of Fuels and Lubricants*, Vol. 4 n^o 2, pp. 271–281, 2011.

[83] Mancaruso Ezio and Vaglieco Bianca Maria. "UV-Visible Imaging of PCCI Engine Running with Ethanol/Diesel Fuel". In *SAE Technnical Paper*, volume 2012-01-1238, 2012.

[84] Mancaruso Ezio and Vaglieco Bianca Maria. "Characterization of PCCI Combustion in a Single Cylinder CI Engine Fuelled with RME and Bio-Ethanol". In *SAE Technical Paper*, volume 2013-01-1672, 2013.

[85] Magno Agnese, Mancaruso Ezio and Vaglieco Bianca Maria. "Combustion Analysis of Dual Fuel Operation in Single Cylinder Research Engine Fuelled with Methane and Diesel". In *SAE Technical Paper*, volume 2015-24-2461, 2015.

[86] Reitz Rolf D. and Duraisamy Ganesh. "Review of high efficiency and clean reactivity controlled compression ignition (RCCI) combustion in internal combustion engines". *Progress in Energy and Combustion Science*, Vol. 46 n^o 0, pp. 12–71, 2015.

[87] Benajes Jesus, Molina Santiago, Garcia Antonio, Belarte Eduardo and Vanvolsem Michel. "An investigation on RCCI combustion in a heavy duty diesel engine using in-cylinder blending of diesel and gasoline fuels". *Applied Thermal Engineering*, Vol. 63 n^o 1, pp. 66–76, 2014.

[88] Belarte Eduardo. *Estudio del proceso de combustion premezclada controlada por la reactividad del combustible en un motor de encendido por compresion.* PhD thesis. Universitat Politecnica de Valencia, Departamento de Maquinas y Motores Termicos, 2015.

[89] Desantes Jose M., Benajes Jesus, Garcia Antonio and Monsalve-Serrano Javier. "The role of the in-cylinder gas temperature and oxygen concentration over low load reactivity controlled compression ignition combustion efficiency". *Energy*, Vol. 78 n^o 0, pp. 854–868, 2014.

[90] Sjoberg Magnus and Dec John E. "Effects of Engine Speed, Fueling Rate, and Combustion Phasing on the Thermal Stratification Required to Limit HCCI Knocking Intensity". In *SAE Technical Paper*, volume 2005-01-2125. SAE International, 2005.

[91] Sjoberg Magnus and Dec John E. "Smoothing HCCI Heat-Release Rates Using Partial Fuel Stratification with Two-Stage Ignition Fuels". In *SAE Technical Paper*, volume 2006-01-0629. SAE International, 2006.

[92] Sjoberg Magnus, Dec John E. and Cernansky Nicholas P. "Potential of Thermal Stratification and Combustion Retard for Reducing Pressure-Rise Rates in HCCI Engines, Based on Multi-Zone Modeling and Experiments". In *SAE Technical Paper*, volume 2005-01-0113. SAE International, 2005.

[93] Dec John E. and Sjoberg Magnus. "Isolating the Effects of Fuel Chemistry on Combustion Phasing in an HCCI Engine and the Potential of Fuel Stratification for Ignition Control". In *SAE Technical Paper*, volume 2004-01-0557. SAE International, 2004.

[94] Saxena Samveg and Bedoya Ivan D. "Fundamental phenomena affecting low temperature combustion and HCCI engines, high load limits and strategies for extending these limits". *Progress in Energy and Combustion Science*, Vol. 39 n^o 5, pp. 457–488, 2013.

[95] Westbrook Charles K. "Chemical kinetics of hydrocarbon ignition in practical combustion systems". *Proceedings of the Combustion Institute*, Vol. 28 n^o 2, pp. 1563–1577, 2000.

[96] Dagaut Philippe, Reuillon Marcelline and Cathonnet Michel. "Experimental study of the oxidation of n-heptane in a jet stirred reactor from low to high temperature and pressures up to 40 atm". *Combustion and Flame*, Vol. 101 n^o 1-2, pp. 132–140, 1995.

[97] Held T. J. and Dryer F. L. "An experimental and computational study of methanol oxidation in the intermediate-and high-temperature regimes". *Symposium (International) on Combustion*, Vol. 25 n^o 1, pp. 901–908, 1994.

[98] Tanaka Shigeyuki, Ayala Ferran, Keck James C. and Heywood John B. "Two-stage ignition in HCCI combustion and HCCI control by fuels and additives". *Combustion and Flame*, Vol. 132 n^o 1-2, pp. 219–239, 2003.

[99] Dagaut Philippe, Daly Catherine, Simmie John M. and Cathonnet Michel. "The oxidation and ignition of dimethylether from low to high temperature (500-1600 K): Experiments and kinetic modeling". *Symposium (International) on Combustion*, Vol. 27 n^o 1, pp. 361–369, 1998.

[100] Westbrook C. K., Curran H. J., Pitz W. J., Griffiths J. F., Mohamed C. and Wo S. K. "The effects of pressure, temperature, and concentration on the reactivity of alkanes: Experiments and modeling in a rapid compression machine". *Symposium (International) on Combustion*, Vol. 27 n^o 1, pp. 371–378, 1998.

[101] Ribaucour M., Minetti R., Sochet L. R., Curran H. J., Pitz W. J. and Westbrook C. K. "Ignition of isomers of pentane: An experimental and kinetic modeling study". *Proceedings of the Combustion Institute*, Vol. 28 n^o 2, pp. 1671–1678, 2000.

[102] Kitano Koji, Nishiumi Ryoji, Tsukasaki Yukihiro, Tanaka Toshiaki and Morinaga Masataka. "Effects of Fuel Properties on Premixed Charge Compression Ignition Combustion in a Direct Injection Diesel Engine". In *SAE Technical Paper*, volume 2003-01-1815, 2003.

[103] Kook Sanghoon, Bae Choongsik, Miles Paul C., Choi Dae and Pickett Lyle M. "The Influence of Charge Dilution and Injection Timing on Low-Temperature Diesel Combustion and Emissions". In *SAE Technical Paper*, volume 2005-01-3837. SAE International, 2005.

[104] Kanda Tomohiro, Hakozaki Takazo, Uchimoto Tatsuya, Hatano Jyunichi, Kitayama Naoto and Sono Hiroshi. "PCCI Operation with Early Injection of Conventional Diesel Fuel". In *SAE Technical Paper*, volume 2005-01-0378. SAE International, 2005.

[105] Hardy W. L. and Reitz R. D. "A Study of the Effects of High EGR, High Equivalence Ratio, and Mixing Time on Emissions Levels in a Heavy-Duty Diesel Engine for PCCI Combustion". In *SAE Technical Paper*, volume 2006-01-0026, 2006.

[106] Nevin Ryan M., Sun Yong, Gonzalez Manuel A. and Reitz Rolf D. "PCCI Investigation Using Variable Intake Valve Closing in a Heavy Duty Diesel Engine". In *SAE Technical Paper*, volume 2007-01-0903, 2007.

[107] Manente Vittorio, Johansson Bengt and Tunestal Per. "Partially Premixed Combustion at High Load using Gasoline and Ethanol, a Comparison with Diesel". In *SAE Technical Paper*, volume 2009-01-0944. SAE International, 2009.

[108] Manente Vittorio, Tunestal Per and Johansson Bengt. "Effects of Ethanol and Different Type of Gasoline Fuels on Partially Premixed Combustion from Low to High Load". In *SAE Technical Paper*, volume 2010-01-0871, 2010.

[109] Manente Vittorio, Johansson Bengt, Tunestal Per and Cannella William. "Effects of Different Type of Gasoline Fuels on Heavy Duty Partially Premixed Combustion". *SAE International Journal of Engines*, Vol. 2 n^o 2, pp. 71–88, 2010.

[110] Petersen Benjamin, Miles Paul C. and Sahoo Dipankar. "Equivalence Ratio Distributions in a Light-Duty Diesel Engine Operating under Partially Premixed Conditions". *SAE Int. J. Engines*, Vol. 5 n^o 2, pp. 526–537, 2012.

[111] Chang Junseok, Kalghatgi Gautam, Amer Amer and Viollet Yoann. "Enabling High Efficiency Direct Injection Engine with Naphtha Fuel through Partially Premixed Charge Compression Ignition Combustion". In *SAE Technical Paper*, volume 2012-01-0677, 2012.

[112] Das Adhikary Bishwadipa, Ra Youngchul, Reitz Rolf and Ciatti Stephen. "Numerical Optimization of a Light-Duty Compression Ignition Engine Fuelled With Low-Octane Gasoline". In *SAE Technical Paper*, volume 2012-01-1336, 2012.

[113] Ciatti Stephen, Johnson Michael, Das Adhikary Bishwadipa, Reitz Rolf and Knock Aaron. "Efficiency and Emissions performance of Multizone Stratified Compression Ignition Using Different Octane Fuels". In *SAE Technical Paper*, volume 2013-01-0263, 2013.

[114] Kimura Shuji, Aoki Osamu, Ogawa Hiroshi, Muranaka Shigeo and Enomoto Yoshiteru. "New Combustion Concept for Ultra-Clean and High-Efficiency Small DI Diesel Engines". In *SAE Technical Paper*, volume 1999-01-3681, 1999.

[115] Kimura Shuji, Aoki Osamu, Kitahara Yasuhisa and Aiyoshizawa Eiji. "Ultra-Clean Combustion Technology Combining a Low-Temperature and Premixed Combustion Concept for Meeting Future Emission Standards". In *SAE Technical Paper*, volume 2001-01-0200, 2001.

[116] Kimura S, Ogawa H, Matsui Y and Enomoto Y. "An experimental analysis of low-temperature and premixed combustion for simultaneous reduction of NOx and particulate emissions in direct injection diesel engines". *International Journal of Engine Research*, Vol. 3 n^o 4, pp. 249–259, 2002.

[117] Weall Adam and Collings Nick. "Investigation into Partially Premixed Combustion in a Light-Duty Multi-Cylinder Diesel Engine Fuelled with a Mixture of Gasoline and Diesel". In *SAE Technical Paper*, volume 2007-01-4058, 2007.

[118] Okude Keiichi, Mori Kazutoshi, Shiino Shiroh and Moriya Takeshi. "Premixed Compression Ignition (PCI) Combustion for Simultaneous Reduction of NOx and soot in Diesel Engine". In *SAE Technical Paper*, volume 2004-01-1907, 2004.

[119] Liu Haifeng, Ma Shuaiying, Zhang Zhong, Zheng Zunqing and Yao Mingfa. "Study of the control strategies on soot reduction under early-injection conditions on a diesel engine". *Fuel*, Vol. 139 n^o 0, pp. 472–481, 2015.

[120] Kook Sanghoon, Pickett Lyle M. and Musculus Mark P. B. "Influence of Diesel Injection Parameters on End-of-Injection Liquid Length Recession". *SAE Int. J. Engines*, Vol. 2 n^o 1, pp. 1194–1210, 2009.

[121] Musculus Mark P. B., Miles Paul C. and Pickett Lyle M. "Conceptual models for partially premixed low-temperature diesel combustion". *Progress in Energy and Combustion Science*, Vol. 39 n^o 2-3, pp. 246–283, 2013.

[122] Hildingsson Leif, Persson Hakan, Johansson Bengt, Collin Robert, Nygren Jenny, Richter Mattias, Alden Marcus, Hasegawa Ryo and Yanagihara Hiromichi. "Optical Diagnostics of HCCI and Low-Temperature Diesel Using Simultaneous 2-D PLIF of OH and Formaldehyde". In *SAE Technical Paper*, volume 2004-01-2949. SAE International, 2004.

[123] Murata Y., Kusaka J., Odaka M., Daisho Y., Kawano Daisuke, Suzuki Hisakazu, Ishii Hajime and Goto Yuichi. "Achievement of Medium Engine Speed and Load Premixed Diesel Combustion with Variable Valve Timing". In *SAE Technical Paper*, volume 2006-04-03, 2006.

[124] Horibe Naoto, Takahashi Ken, Kee Sung-Sub, Ishiyama Takuji and Shioji Masahiro. "The Effects of Injection Conditions and Combustion Chamber Geometry on Performance and Emissions of DI-PCCI Operation in a Diesel Engine". In *SAE Technical Paper*, volume 2007-01-1874, 2007.

[125] Warey Alok, Hardy Jean-Paul, Hennequin Manuela, Tatur Marek, Tomazic Dean and Cannella William. "Fuel Effects on Low Temperature Combustion in a Light-Duty Diesel Engine". In *SAE Technical Paper*, volume 2010-01-1122, 2010.

[126] Kalghatgi Gautam, Risberg Per and Angstrom Hans. "Partially Pre-Mixed Auto-Ignition of Gasoline to Attain Low Smoke and Low NOx at High Load in a Compression Ignition Engine and Comparison with a Diesel Fuel". In *SAE Technical Paper*, volume 2007-01-0006, 2007.

[127] Kalghatgi Gautam, Hildingsson Leif and Johansson Bengt. "Low NOx and Low Smoke Operation of a Diesel Engine Using Gasolinelike Fuels". *Journal of Engineering for Gas Turbines and Power*, Vol. 132 n^o 9, pp. 092803–092803, 2010.

[128] Hildingsson Leif, Kalghatgi Gautam, Tait Nigel, Johansson Bengt and Harrison Andrew. "Fuel Octane Effects in the Partially Premixed Combustion Regime in Compression Ignition Engines". In *SAE Technical Paper*, volume 2009-01-2648, 2009.

[129] Hildingsson Leif, Johansson Bengt, Kalghatgi Gautam T. and Harrison Andrew J. "Some Effects of Fuel Autoignition Quality and Volatility in Premixed Compression Ignition Engines". In *SAE Technical Paper*, volume 2010-01-0607, 2010.

[130] Kalghatgi G. T. "The outlook for fuels for internal combustion engines". *International Journal of Engine Research*, Vol. 15 n^o 4, pp. 383–398, 2014.

[131] Manente V., Johansson B. and Cannella W. "Gasoline partially premixed combustion, the future of internal combustion engines?". *International Journal of Engine Research*, Vol. 12 n^o 3, pp. 194–208, 2011.

[132] Solaka Hadeel, Aronsson Ulf, Tuner Martin and Johansson Bengt. "Investigation of Partially Premixed Combustion Characteristics in Low Load Range with Regards to Fuel Octane Number in a Light-Duty Diesel Engine". In *SAE Technical Paper*, volume 2012-01-0684, 2012.

[133] Borgqvist Patrick, Tuner Martin, Mello Augusto, Tunestal Per and Johansson Bengt. "The Usefulness of Negative Valve Overlap for Gasoline Partially Premixed Combustion, PPC". In *SAE Technical Paper*, volume 2012-01-1578. SAE International, 2012.

[134] Borgqvist Patrick, Tunestal Per and Johansson Bengt. "Gasoline Partially Premixed Combustion in a Light Duty Engine at Low Load and Idle Operating Conditions". In *SAE Technical Paper*, volume 2012-01-0687, 2012.

[135] Hanson Reed, Splitter Derek and Reitz Rolf. "Operating a Heavy-Duty Direct-Injection Compression-Ignition Engine with Gasoline for Low Emissions". In *SAE Technical Paper*, volume 2009-01-1442, 2009.

[136] Kalghatgi G. T., Kumara Gurubaran R., Davenport A., Harrison A. J., Hardalupas Y. and Taylor A. M. K. P. "Some advantages and challenges of running a Euro IV, V6 diesel engine on a gasoline fuel". *Fuel*, Vol. 108 n^o 0, pp. 197–207, 2013.

[137] Sellnau Mark, Sinnamon James, Hoyer Kevin and Husted Harry. "Gasoline Direct Injection Compression Ignition (GDCI) - Diesel-like Efficiency with Low CO2 Emissions". In *SAE Technical Paper*, volume 2011-01-1386, 2011.

[138] Solsjo Rickard, Jangi Mehdi, Tuner Martin and Bai Xue-Song. "Large Eddy Simulation of Partially Premixed Combustion in an Internal Combustion Engine". In *SAE Technical Paper*, volume 2012-01-0139. SAE International, 2012.

[139] Fridriksson Helgi Skuli, Hajireza Shahrokh, Sunden Bengt and Tuner Martin. "CFD Investigation on Injection Strategy and Gasoline Quality Impact on In-Cylinder Temperature Distribution and Heat Transfer in PPC". In *SAE Technical Paper*, volume 2013-24-0009, 2013.

[140] Shen Mengqin, Tuner Martin, Johansson Bengt and Cannella William. "Effects of EGR and Intake Pressure on PPC of Conventional Diesel, Gasoline and Ethanol in a Heavy Duty Diesel Engine". In *SAE Technical Paper*, volume 2013-01-2702. SAE International, 2013.

[141] Kaiadi Mehrzad, Johansson Bengt, Lundgren Marcus and Gaynor John A. "Experimental Investigation on different Injection Strategies for Ethanol Partially Premixed Combustion". In *SAE Technical Paper*, volume 2013-01-0281, 2013.

[142] Tuner Martin, Johansson Thomas, Aulin Hans, Tunestal Per, Johansson Bengt and Cannella William. "Multi Cylinder Partially Premixed Combustion Performance Using Commercial Light-Duty Engine Hardware". In *SAE Technical Paper*, volume 2014-01-2680. SAE International, 2014.

[143] Weall Adam and Collings Nick. "Gasoline Fuelled Partially Premixed Compression Ignition in a Light Duty Multi Cylinder Engine: A Study of Low Load and Low Speed Operation". In *SAE Technical Paper*, volume 2009-01-1791, 2009.

[144] Das Adhikary Bishwadipa, Reitz Rolf and Ciatti Stephen. "Study of In-Cylinder Combustion and Multi-Cylinder Light Duty Compression Ignition Engine Performance Using Different RON Fuels at Light Load Conditions". In *SAE Technical Paper*, volume 2013-01-0900, 2013.

[145] Das Adhikary Bishwadipa, Reitz Rolf, Ciatti Stephen and Kolodziej Christopher. "Computational Investigation of Low Load Operation in a Light-Duty Gasoline Direct Injection Compression Ignition [GDICI] Engine Using Single-Injection Strategy". In *SAE Technical Paper*, volume 2014-01-1297. SAE International, 2014.

[146] Kolodziej Christopher P., Ciatti Stephen, Vuilleumier David, Das Adhikary Bishwadipa and Reitz Rolf. "Extension of the Lower Load Limit of Gasoline Compression Ignition with 87 AKI Gasoline by Injection Timing and Pressure". In *SAE Technical Paper*, volume 2014-01-1302. SAE International, 2014.

[147] Sellnau Mark C., Sinnamon James, Hoyer Kevin and Husted Harry. "Full-Time Gasoline Direct-Injection Compression Ignition (GDCI) for High Efficiency and Low NOx and PM". *SAE International Journal of Engines*, Vol. 5 n^o 2, pp. 300–314, 2012.

[148] Sellnau Mark C., Sinnamon James, Hoyer Kevin, Kim Junghwan, Cavotta Marilou and Husted Harry. "Part-Load Operation of Gasoline Direct-Injection Compression Ignition (GDCI) Engine". In *SAE Technical Paper*, volume 2013-01-0272, 2013.

[149] Sellnau Mark, Foster Matthew, Hoyer Kevin, Moore Wayne, Sinnamon James and Husted Harry. "Development of a Gasoline Direct Injection Compression Ignition (GDCI) Engine". *SAE International Journal of Engines*, Vol. 7 n^o 2, pp. 835–851, 2014.

Chapter 3

Experimental setup and theoretical tools

Contents

3.1 Introduction

There are different approaches for experimental combustion engine research depending on the particular purposes of each investigation. The work presented in this thesis is mainly based on results from a single-cylinder research engine combined with several diagnostic and modeling tools. Single-cylinder engine testing is very useful to get a basic understanding of the combustion process and effects of individual parameters, for example fuel injection timings on combustion and engine performance and emissions. So, performing fundamental combustion studies on a single-cylinder engine, without the interference between engine cylinders or the coupling with the air loop and auxiliaries systems, is a good starting point before moving on to more complex combustion research studies such as optical diagnostics of local in-cylinder processes.

Experimental engine testing and optimization which is aimed at improving fuel economy and pollutants emission level for modern IC engines, typically requires performing a large number of studies changing different input parameters, which is highly demanding in terms of money and time. So, defining a proper experimental methodology, as well as the correct selection and application of different post-processing and diagnostic tools, will help in reducing engine testing time and also in improving the quality of the information that can be extracted from the experimental results.

The key to improve engine research and development strongly relies on understanding the processes taking place in the engine combustion chamber. Due to the maturity of CFD modeling and increased computational power, engine simulation is nowadays extensively used, both to predict the engine performance and also to provide optimization guidelines for engine design. Furthermore, with the growing interest on advanced combustion concepts, which involve complex physical and chemical processes as described in Chapter 2, there is an urgent need for further development and application of advanced engine simulation tools with the help of mathematical models and faster computational and processing tools.

3.2 Two-stroke single-cylinder research engine

The design philosophy followed within the POWERFUL Project to conceive this new two-stroke engine prototype, was based on the approach of downsizing a 1460 cm^3 four-cylinder four-stroke diesel engine, by operating

with a two-stroke cycle, to obtain a 730 cm^3 two-cylinder engine with equivalent torque performance as the base configuration. Considering a downsized (heavily loaded) diesel engine, the project was directed towards the more robust solution in terms of mechanical design, which is the poppet valve scavenge type architecture. Considering actual direct injection systems and up-to-date innovative turbocharging and supercharging systems, it was supposed easier to cop with the scavenging and trapping difficulties that are inherent to a poppet valve scavenge type configuration.

3.2.1 Main engine geometric characteristics

The experimental studies presented on this investigation were performed on a single-cylinder version of this innovative two-stroke poppet valve CI engine. The single-cylinder engine was specifically designed and manufactured to operate in two-stroke mode, and it is equipped with a common rail HSDI injection system and a cam-driven Variable Valve Timing system for controlling both intake and exhaust timings. The single-cylinder engine presents the same architecture and geometry as the two-cylinder engine, but its main advantage is that it can be used for studying the fundamental physical phenomena related to the air management and combustion processes, in a more controlled and stabilized environment, without the interference or coupling with the other cylinder or the air charging system. As a reference, Table 3.1 contains the main engine geometrical characteristics of this single-cylinder two-stroke engine.

Three different pistons (with different compression ratios and bowl geometries) were available for the research activities, the first two pistons (HiCR1=17.2 and LoCR1=13.6) were tested along the implementation and optimization of the highly premixed combustion mode, while the other piston (HiCR2=17.8) was evaluated in conventional mixing-controlled diesel combustion and partially premixed combustion modes.

3.2.2 Scavenge architecture and valvetrain system

The combustion chamber has four poppet valves with double-overhead camshafts, and the cylinder head has been specifically optimized and redesigned in the framework of the POWERFUL Project, to ensure a suitable in-cylinder flow pattern during two-stroke operation, in order to optimize the scavenging of burnt gases and to reduce the short-circuit losses of fresh air going directly from the intake into the exhaust.

Engine specifications	
Engine type	Single-cylinder two-stroke CI
Displacement	365 cm^3
Bore x Stroke	76 mm x 80.5 mm
Connecting Rod Length	133.75 mm
Number of Valves	4
Type of scavenge	Poppet-Valve Scavenge Loop
Valvetrain	DOHC with VVA
Compression Ratio	HiCR1=17.2 (HPC)
	LoCR1=13.6 (HPC)
	HiCR2=17.8 (CDC)

Table 3.1. *Engine specifications.*

The first definition of the engine architecture, boost system requirements, combustion chamber geometry and scavenging characteristics of this newly designed two-stroke engine has been reported by Tribotte et al. [1]. An iterative approach combining 1D and 3D multidimensional CFD simulations was employed to evaluate and study the air charging and scavenging process during the cycle for different cylinder head designs using preliminary cam lift laws. Three different geometries were analyzed: a flat-roof cylinder head with a modified intake duct, an intrusive mask between intake and exhaust valves and a staggered roof.

The final geometry of the combustion chamber is based on the design patented by Obernesser et al. [2], and it presents a staggered roof for baffling the flow of air between the intake and exhaust valves, as can be seen in Figure 3.1. In that way, the fresh air flow is forced to follow the path of the cylinder wall towards the bottom of the combustion chamber, creating a tumble aerodynamics (instead of swirl) that improves the scavenging of the burnt gases while keeping short-circuit losses as low as possible during the overlap phase. This geometry provided the best compromise between scavenging efficiency, acceptable permeability, and convenient combustion chamber geometry.

The optimum intake/exhaust camshaft lift laws were defined experimentally prior to this investigation, by testing different alternatives in the single-cylinder engine at a representative medium load/speed condition, while operating with conventional diesel combustion. A total of 7 camshafts profiles (4 for the intake and 3 for the exhaust) with different opening durations and

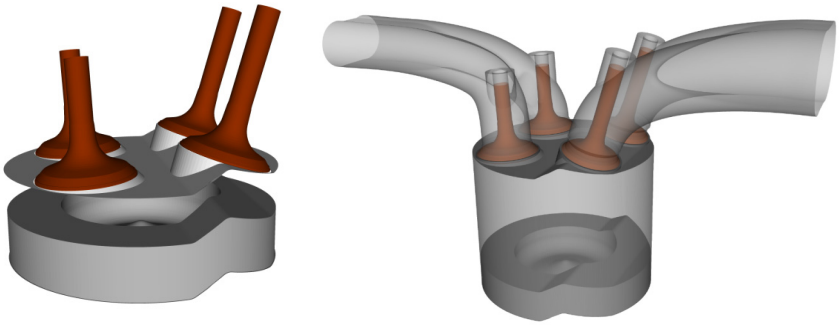

Figure 3.1. *Final cylinder head design. Source: Tribotte et al. [1].*

maximum lifts were evaluated by following a Design of Experiment (DoE) optimization approach, to compare each configuration in terms of the air management characteristics, and also in terms of engine performance. The definition of the most used air management performance parameters typically used to characterize the charging and scavenging process of two-stroke engines, will be detailed in the next subsection 3.5.1.

As a reference, Figure 3.2 shows an example of the DoE optimization for different camshaft configurations, where the air management characteristics of each combination have been compared by means of a trade-off between the internal gas recirculation ratio (IGR) and trapping ratio (TR), and the performance of each configuration has been also evaluated in terms of a trade-off between indicated fuel consumption (ISFC) and TR. Regarding the charging/scavenging relationship, the ideal situation would be to improve the scavenging of burnt gases (decreasing IGR) without punishing the trapping and charging efficiencies (keeping constant TR). However, the experimental results show how trapping ratio unavoidably decreases when decreasing IGR. The lower IGR obtained with the best configuration is around 25 %, and the range of variation is very narrow (from 35 % to 25 %), trending asymptotically to a limit where the IGR cannot be decreased furthermore.

From this preliminary optimization, the optimum camshaft configuration (and final definition) was selected and kept constant for the all studies performed in this investigation. The values of maximum lift and opening duration of the final camshafts definition, as well as the nominal timing for the intake and exhaust are depicted in Table 3.2.

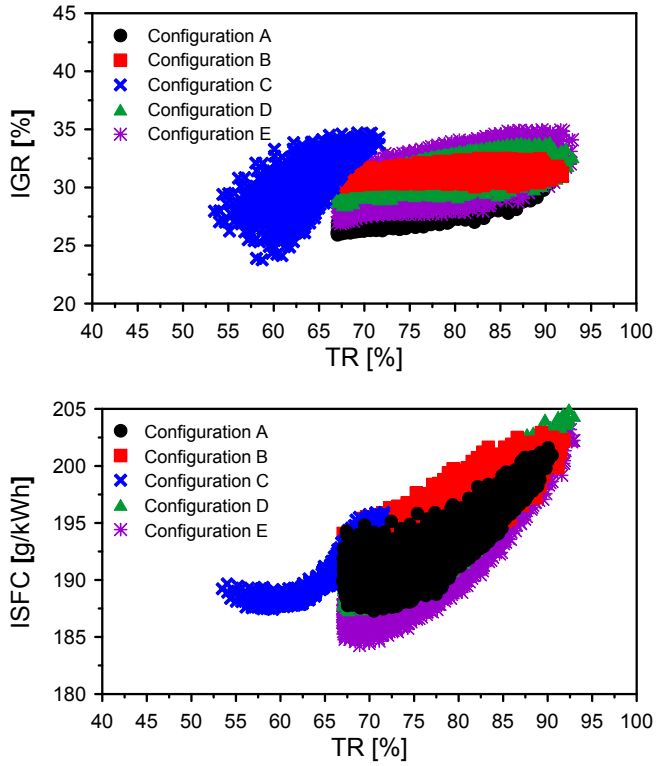

Figure 3.2. *Comparison between different camshaft configurations.*

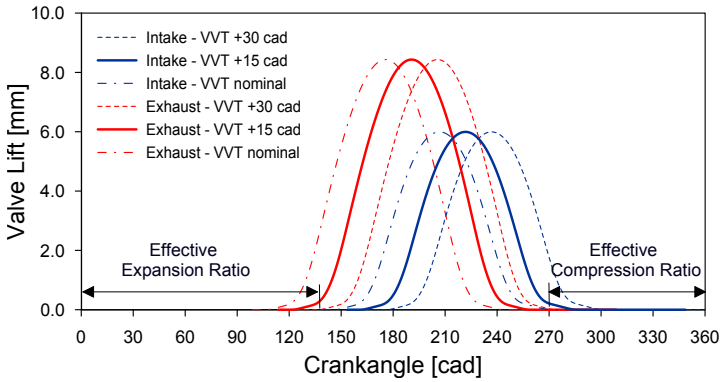

Figure 3.3. *Lift vs crank angle for intake and exhaust valves.*

Final intake and exhaust camshaft definition	
Intake camshaft	Maximum Lift=6 mm
	Opening duration=80 CAD
Exhaust camshaft	Maximum Lift=8.5 mm
	Opening duration=95 CAD
Nominal intake valve timing	IVO=161.9 CAD aTDC
	IVC=251.6 CAD aTDC
Nominal exhaust valve timing	EVO=122.6 CAD aTDC
	IVC=226.9 CAD aTDC

Table 3.2. *Final intake and exhaust camshaft definition.*

The engine is also equipped with a hydraulic cam-driven Variable Valve Timing system, allowing a flexibility of 30 degrees on both intake and exhaust valve timings independently from the mechanical cam timing. The flexibility of the VVT system is shown in Figure 3.3, where the optimized intake and exhaust cam lift laws have been included for the nominal (mechanical phasing at 0°) timing angle and also for two additional positions, intermediate (15°) and maximum (30°) timing angles. Then, the effective compression ratio, overlap between intake and exhaust, and effective expansion ratio can be modified by adjusting the valve timing angles. In this investigation, the key valve timing angles were defined at those crank angle degrees (CAD) where the given valve lift was 0.3 mm. The VVT system advances or retards the valve lift event by rotating the camshaft through a solenoid valve that changes the oil pressure in two internal galleries, depending of the command given by an independent electronic control unit. The ECU requires also the inputs coming from variable reluctance sensors to determine the angular position of both camshafts and also of the crankshaft, for the PID control of the two solenoid valves.

3.2.3 Fuel injection system

The prototype Delphi injection system comes from a common-rail DFI 1.5 that allows up to five independent injections (two pilot injections, one main injection and two post-injections) and the rail pressure can be risen up to 1800 bar when injecting diesel fuel. As a reference, Table 3.3 contains the main characteristics of the injection system used in the single-cylinder two-stroke engine.

The injector nozzles were designed with smaller hole diameters than those currently manufactured for mass production, to assure good atomization of the fuel and also to enhance the physical mixing process, and the number of holes was selected in order to keep the permeability at acceptable levels considering the smaller hole diameters. The match between the optimum injector spray angle and the piston bowl shape was first obtained with 3D CFD calculations, but it was later confirmed by performing specific injector optimization campaigns in the single-cylinder engine, to select the final nozzle configuration. Several piezoelectric injectors (a total of 13) with different mass flow rates (number and diameter of holes) and spray included angles were evaluated to find the best geometry that allowed obtaining the lower emissions level and higher engine efficiency. Figure 3.4 shows a comparison between nozzles in terms of smoke and ISFC, when sweeping the EGR level keeping constant IMEP, and when sweeping SoE2 keeping constant the equivalence ratio. The nozzle geometry selected for CDC operation has 8 holes with a 155° spray cone angle.

In the case of the HPC mode tests, a specially optimized narrow spray cone angle nozzle (60°) was selected, to reduce liquid fuel wetting on the cylinder liner with early injections strategies, therefore improving HPC operation while maintaining a relatively high efficiency. For PPC operation, a slightly lower included angle nozzle (148°) was selected, compared to the optimum nozzle found for conventional diesel operation.

In addition, the characterization of the available nozzles was performed prior to this study, at a suitable range of operating conditions in terms of injection pressure, injector backpressure and injection duration, by measuring the total mass flow rate and the sprays momentum flux in dedicated test rigs, following the methodology described in [3, 4]. The spray angle and penetration were also measured in a high pressure visualization test rig at non-reactive conditions.

3.2.4 Fuels specifications

Two different fuels were selected for the studies presented in this research, a regular fuel pump diesel and a calibrated unleaded gasoline with 95 Research Octane Number (RON). Diesel is used for the analysis and optimization of conventional mixing-controlled diesel combustion (CDC) concept, and also for the study of the highly premixed combustion (HPC) mode, while the gasoline is used for evaluating the partially premixed combustion (PPC) mode.

Injection system specifications	
Fuel injection system	Diesel common-rail HSDI
Injector	Centrally-mounted Piezoelectric injector
Maximum injection pressure	1800 bar (when injecting diesel)
	1200 bar (when injecting gasoline)
Injector mass flow rate	400 ml/min (for the selected nozzles)
Final nozzle definition	A=10 holes 80 μm 60° (HPC)
	B=8 holes 90 μm 155° (CDC)
	C=8 holes 90 μm 148° (PPC)

Table 3.3. *Injection system specifications.*

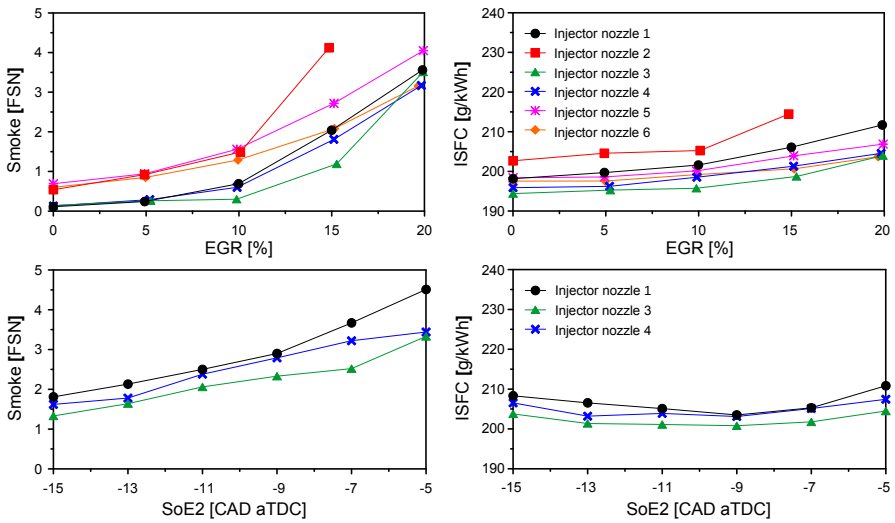

Figure 3.4. *Comparison between different injection nozzles.*

Samples of each fuel were sent to a specialized laboratory to perform the analysis of the most important physical and chemical properties, following the standards given by the ASTM (American Society for Testing and Materials) [5] and the European Regulation (UNE-EN) [6, 7]. In addition, to cope with the lower viscosity of the gasoline, a lubricity additive was added in an amount corresponding to approximately 30 ppm in volume of the total blend, to secure the proper functioning of the injection system. Most important fuel properties are detailed in Table 3.4.

Fuel specifications		
Testing campaign	Diesel CDC and HPC	Gasoline PPC
Test fuel	Regular fuel pump Diesel	Unleaded gasoline RON95
Density (15 °C)	843.3 kg/m^3	758.1 kg/m^3
Kinematic viscosity (40 °C)	2.46 cSt	0.44 cSt
Cetane Number	46.6	–
Research Octane Number	–	94.6
H/C ratio	2.06 mol/mol	1.76 mol/mol
O/C ratio	0 mol/mol	0 mol/mol
Oxygen content	$\leqslant$ 0.5 % m/m	$\leqslant$ 0.17 % m/m
Stoichiometric air/fuel ratio	14.80	14.37
Lower heating value LHV	42.124 MJ/kg	42.82 MJ/kg

Table 3.4. *Injection system specifications.*

Figure 3.5 shows a comparison in terms of mass flow rate and spray momentum flux between diesel and gasoline fuel at a given operating condition (P_{rail}=600 bar and energizing time ET=3000 μs) while keeping the optimum injection hardware for PPC operation (8 holes 90 μm 148°). The lower density of the gasoline is translated into a lower maximum value in the stabilized mass flow rate when compared against diesel fuel keeping the same experimental conditions. This effect has been explained in detail in the work of Domenech [8] and Payri et al. [9]. In the case of the momentum flux, the differences between diesel and gasoline are considered negligible since this parameter is, in general, more dependent on the geometric characteristics of the nozzle and the operating conditions.

From the experimental characterization of the injection system with gasoline fuel, it was also noted that when P_{rail} was increased above 1200 bar, appreciable cavitation was observed in the return line of the injector, which made it difficult to assure a correct measurement of the fuel flow. For this reason, and also to avoid possible failure in the high pressure fuel pump, the maximum P_{rail} was limited to 1000 bar when injecting gasoline with the current injection system.

Obtaining accurate experimental data about the fuel properties and the injection characteristics is of great value to improve the quality of the multidimensional CFD model, and also for performing 1D spray mixing

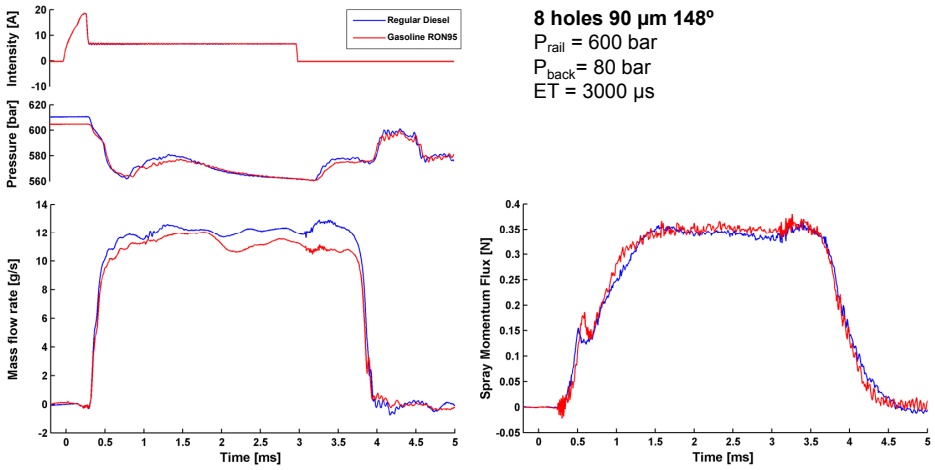

Figure 3.5. *Comparison between diesel and gasoline mass flow rate and spray momentum flux.*

calculations and improving the analysis and diagnostics of the combustion process.

3.3 Test cell characteristics and equipment

3.3.1 Engine dynamometer

The engine is assembled into a fully instrumented test cell, located in the engine laboratory at the Departamento de Máquinas y Motores Térmicos (DMMT) of the Universitat Politècnica de València, where all the experimental studies presented on this research work were performed. Figure 3.6 shows a simplified scheme of the test cell, where the main sub-systems and the single-cylinder research engine are depicted. The location of the most important sensors and probe measurements are also presented in the scheme and described in this section.

The engine speed and torque are controlled by means of an AC electric dynamometer, that has a maximum speed of 9000 rpm and a nominal torque of 120 N m. The dynamometer can act as a break and a generator, dissipating the power generated by the engine in form of heat and electricity that is returned to the grid; or as an electric motor, to start or run the engine in motored (non-firing) conditions. The effective torque of the engine is measured in the

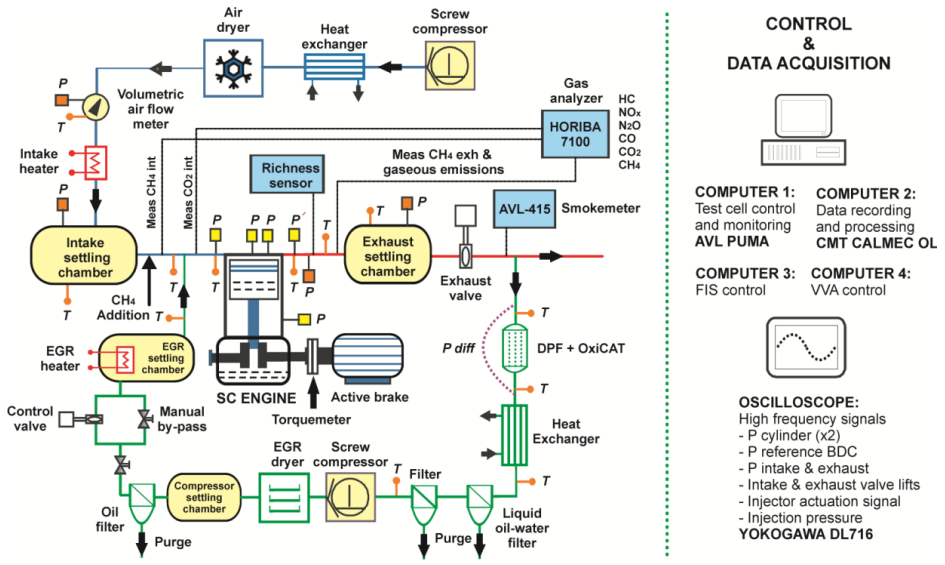

Figure 3.6. *Layout of the single-cylinder engine test cell.*

output shaft of the engine brake with a strain-gage torque meter, while the speed of the engine is measured with an optical angular encoder mounted in the opposite end on the crankshaft.

The engine dynamometer is connected to an AVL EMCOM Engine and Dyno Control with an AVL PUMA software platform, allowing manual and fully automated testing procedures. All the studies presented in this research work were performed at constant engine speed. Therefore, the mean engine speed is controlled by a frequency variator and a PI regulation, that allows a precision of ± 1 rpm. The main characteristics of the engine dynamometer are described in Table 3.5.

3.3.2 Auxiliary systems

Starting with the intake system, an industrial oil-free screw compressor is used to supply pressurized and filtered intake air to the engine. This external compressor can provide a maximum absolute pressure of 4 bar which is higher than the maximum intake pressure required during engine operation. At its maximum operating speed the compressor can supply a continuous flow of 126 L/s. After the air is compressed and filtered, it passes through an horizontal air-to-water refrigeration circuit, where the temperature is lowered

Engine dynamometer specifications	
Type	4 pole AC electric dynamometer
Supplier and model	AMK Type DW3
Nominal Power	38 kW
Nominal Torque	120 N m
Nominal Speed	3000 rpm
Maximum Speed	9000 rpm
Test cell control platform	AVL EMCOM + PUMA

Table 3.5. *Engine dynamometer specifications.*

from approximately 220 °C to 30 °C, before entering a refrigerant air dryer unit, where the air will be dried to remove water vapor.

In the air circuit of the dryer unit, the compressed air first goes into an air-to-air heat exchanger to pre-cool it by the outgoing dry cold air, reducing the heat load of the refrigeration circuit. At the same time, the increase in the temperature of the outgoing dry air helps to prevent posterior re-condensation. Next, the compressed air is further cooled down to the required dew point temperature (3 °C) by the refrigerant circuit in an air-to-refrigerant heat exchanger (evaporator). The resulting condensed water droplets are collected in an integrated water separator, and they are evacuated by an electronic drain. The refrigerant circuit consists of a compressor, a condenser, a filter, and a thermostatic expansion valve.

Once the air is cooled and dehumidified, its volumetric flow rate is measured by a precision Elster G-100 RVG rotary air flow meter, that provides a measurement range between 0.05 to 160 m^3/h with a precision of $\pm 0.1\,\%$ over the measured value. The flow meter integrates pressure and temperature measurements to calculate the air density, and convert the volumetric flow units into mass flow units (in kg/h)

The fresh engine intake air is brought to the desired intake temperature by an electric resistance heater, placed before the entrance of a settling chamber. The volume must be sufficiently large, 250 L in this case, to attenuate the pressure waves caused by the intake process. The pressure and temperature of the fresh air are measured in the intake settling chamber, using a piezoresistive transducer and a K-type thermocouple. After the intake settling chamber, the fresh air is well-mixed with the EGR through a dedicated EGR mixer, and the mean pressure and temperature of the intake mixture (fresh air with EGR)

are measured once again just before entering the engine. These are the values used to control the engine intake charge conditions during the experimental tests.

The intake charge conditions are adjusted and corrected using dedicated PID controllers, the first acting on the external compressor speed to achieve the desired intake pressure with a precision of ± 0.005, and the second acting on the air heater to control the air temperature. In addition, the instantaneous (absolute) intake pressure is measured at the intake port as close as possible to the valve, using an uncooled Kistler 4045A10S piezoresistive sensor, which provides a measurement range from 0 bar to 10 bar.

The exhaust system is relatively simpler compared to the intake system since its main function is to allow the controlled evacuation of the exhaust gases, which are at high pressure and temperature conditions, and also to simulate the back pressure generated at the exhaust line in an equivalent multi-cylinder engine. In the particular case of this two-stroke engine configuration, a positive pressure drop between the intake and exhaust ports, defined as ΔP, is required at all times and over the complete range of engine speeds, to allow the proper scavenging of the burnt gases and minimize the rate of internal gas recirculation (burnt gases which are not expelled out of the cylinder after the exhaust event).

The instantaneous exhaust pressure is measured in the exhaust port as close as possible to the valve, using a water cooled Kistler 4049A10S piezoresistive sensor, that sustains exposure to gas temperatures in excess of 1100 °C, and provides a measurement range from 0 bar to 10 bar. The mean temperature and pressure are also measured in the exhaust manifold close to the engine. A settling chamber (50 L) is placed at the exhaust pipe line to attenuate the pressure waves generated by the pulsating flow during the exhaust event, and to measure once again the mean pressure and temperature. After the exhaust settling chamber, the exhaust pressure is regulated to the desired value by using an electro-pneumatic valve controlled with a PID, that allows a precision of ± 0.005 in the mean exhaust pressure.

A steady flow of EGR is taken from the engine exhaust system downstream the exhaust settling chamber. Considering that the exhaust pressure is lower than the intake pressure, an additional screw compressor is needed to re-compress the flow above the intake pressure level to be able to mix the EGR with the fresh flow. Upstream the EGR compressor, there is a DPF and an oxydation catalyst. Additionally, the flow is cooled with a water-gas heat exchanger, and passes through a series of cyclone filters to remove any

Air path sub-systems specifications	
Compressor Type	Oil-free screw air compressor
Supplier and model	Atlas Copco ZA1-98
Maximum pressure	4 bar (abs)
Flow rate at maximum speed	450 m^3/h
Air dryer type	Refrigerant compressed air dryer
Supplier and model	Atlas Copco FD 380W
Air temperature on the inlet	35 °C
Dew point temperature	3 °C
Intake settling chamber volume	250 L
Exhaust settling chamber volume	50 L
EGR system specifications	
Compressor Type	Oil-free screw air compressor
Supplier and model	Atlas Copco GA 15 VSD
Pressure range	5.5 bar to 12.5 bar
Flow rate range	32 m^3/h to 135 m^3/h
Air dryer type	Integrated in the compressor unit
EGR settling chamber volume	25 L

Table 3.6. *Air path sub-systems specifications.*

remaining particulates, and any liquid water or oil suspended in the flow before entering the compressor.

The EGR compressor unit includes the screw compression stage, an integrated air dryer and a settling chamber. The EGR flow is controlled with a PID acting on a electro-pneumatic flow control valve that allows controlling the EGR rate with a precision of $\pm 0.1\,\%$. There is also an additional bypass that can be manually adjusted. Finally, the compressed and oil-free EGR flow enters an EGR settling chamber (25 L), where there is an internal electrical resistance heater to precisely control the EGR temperature. Temperature measurements are taken at different locations along the EGR route using K-type thermocouples, and the pressure difference at the DPF is monitored to schedule the required regeneration protocols when needed.

The main characteristics of the air path and EGR sub-systems are summarized in Table 3.6.

The single-cylinder engine test cell is equipped with external water and oil cooling circuits, which are independent from the engine functioning. The heat emitted by the engine to the water and oil circuits is later released to the test cell environment, by means of water-to-water and oil-to-water heat exchangers. Both water and oil cooling circuits are also equipped with electric heaters in order to accelerate the warming up of the engine, and to precisely control the fluids temperature during the engine experiments. The oil and water temperatures are maintained constant at $90\,^{\circ}\mathrm{C} \pm 1.5\,^{\circ}\mathrm{C}$ using PID controllers. These temperatures are measured before and after the engine, using Pt100 thermoresistance sensors. The value used as control variable is the one measured at the exit of the engine.

The oil is supplied to the engine by a piston pump, which is driven by an electric motor and a frequency variator. The pump has three pistons, two of them are used for compressing the oil up to the required pressure and supplying it to the engine, while the remaining piston is used as a vacuum pump to assist in the evacuation of the oil out of the engine. The maximum speed allowed by the pump is 4000 rpm, and it can provide 12.5 L of oil when turning at 1000 rpm. A constant oil pressure of 5 bar is required to assure correct hydrodynamic lubrication of all rotating parts, the proper functioning of the hydraulic VVT system, and also the cooling of the piston through two separate oil jets. Specifically in the case of this single-cylinder engine prototype, it is necessary to create a depression of -0.2 bar in the crankcase (below atmospheric pressure), to avoid pressurizing the crankcase which difficult the evacuation of the oil, in addition to creating negative work on the piston. Oil pressure and the absolute pressure at the crankcase are measured using piezoresistive pressure transducers, and they are also recorded at each operating point for safety and monitoring purposes.

The blow-by flow (in m^3/h) is measured using a commercial AVL 442 Blow-by Meter, which utilizes the orifice plate measurement principle to calculate the circulating flow, by measuring the pressure difference upstream and downstream the orifice. At each test, the blow-by measurement is converted to mass flow units (in kg/h) considering the atmospheric pressure and temperature. In this relatively high loaded diesel two-stroke engine, is important to keep track of any drastic increase in the blow-by flow, that can effectively help in detecting wearing problems or excessive leakage/bypass through the piston rings after a long period of running hours.

The fuel is stored in an external tank, that holds the fuel supply and helps maintain its temperature at a level below its flash point. In order for the fuel injection system to fulfill its purpose, the fuel must be safely and

reliably delivered from the tank to the high-pressure components, and it also has to be pre-conditioned within a suitable temperature and pressure range imposed by the injection system. The low-pressure side of the fuel system consists of a number of components including the fuel tank, the fuel balance and the conditioning system. The high-pressure components are responsible for increasing the pressure, metering and delivering the fuel to the combustion chamber. They include a high-pressure pump driven by an external electric motor, the common-rail, the fuel injector and the fuel injection nozzle. An schematic of the fuel circuit is depicted in Figure 3.7.

The fuel consumption of the engine is measured using a Dynamic Fuel Meter AVL 733S, that allows getting a direct measurement of the consumed fuel mass in the desired acquisition time, keeping very high accuracy (around 0.12 %). The fuel consumption is determined using an appropriate weighing vessel linked by a bending beam to a capacitive displacement sensor. Due to the fact that the weighting vessel has to be refilled for each measurement this is a discontinuous measurement principle. The mass of fuel consumed is therefore determined gravimetrically, which means that the density does not have to be determined in addition. The measurement range of the fuel balance is from 0 kg/h to 150 kg/h, however, the fuel flows typically needed during normal operation in this single-cylinder light duty engine are much smaller.

An AVL 753 fuel conditioning system is used for assuring a constant fuel temperature and pressure at the inlet of the high-pressure pump, to minimize the variations in the high-pressure side of the fuel circuit. The temperature is regulated by means of a heater, a fuel-to-coolant heat exchanger and a valve controlled by a PID. As De Rudder states, any rapid change in the temperature supposes a variation in fuel density, and as the circulating volume between the outlet of the gravimetric balance and the inlet of the pump is constant, it results in a change in the mass downstream the balance that leads to an error in the fuel consumption measurement [10]. In addition, if the fuel temperature is not strictly controlled and kept constant along the experiments, the differences in temperature affecting the fuel density, could also modify the injected fuel mass and the spray morphology. This variations in the physical spray characteristics, could lead to a different chemical and thermodynamic state of the fuel-air mixture during the injection and combustion processes, that may have implications on the combustion characteristics and final emissions level [11–13]. In this investigation, the inlet fuel temperature has been kept constant at 35 °C during all the experiments. The temperature is measured using Pt100 thermoresistance sensors, before entering the engine, and later, at the exit of the engine (which is the one used for the PID control).

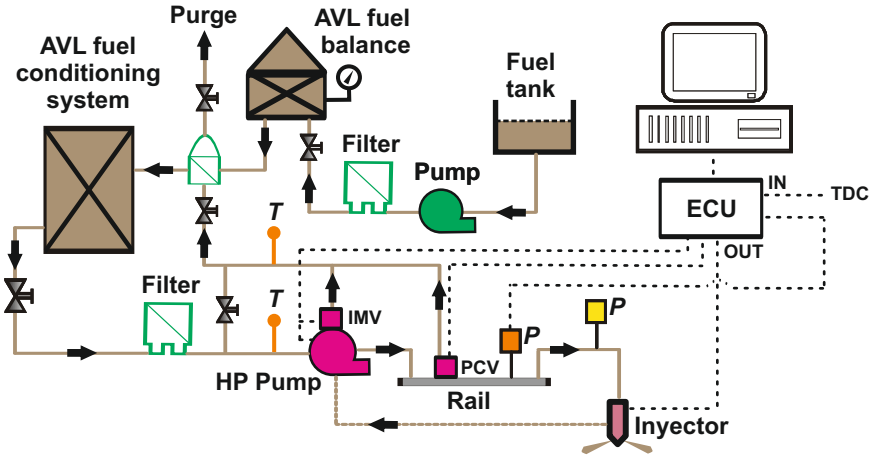

Figure 3.7. *Layout of the fuel circuit.*

The Engine Control Unit (ECU) supplied by Delphi is an opened one, to allow full access for controlling the injection running parameters as desired in a ETAS-INCA environment. The start of energizing (SoE) of the injector command signal and the desired energizing time for each injection event are controlled through the INCA software, which signals the SoE with respect to the timing of piston top dead center (TDC signal) coming from an optical crankshaft angle encoder.

The mean pressure in the rail is measured and controlled by the ECU, by means of a pressure control valve located at one rail extremity (PCV), which is used to spill the excess fuel back to the fuel circuit; or by a inlet metering valve (IMV) located in the high-pressure pump to meter the fuel drawn into the pump, thus avoiding compression of excess fuel to high pressure. Rail pressure control with the PCV installed at the rail is inherently fast because of the proximity of the system input (PCV) and system output (rail pressure sensor), so it is normally preferred during stabilized engine operation.

3.3.3 Gas analysis

Pollutant emissions from the engine are sampled close to the exhaust settling chamber and routed to a state-of-the-art gas analyzer by a heated pipe to ensure gas temperatures above 190 °C. Additionally, there is a sample probe located at a sufficient distance downstream the EGR mixer, to measure

the concentration of CO_2 at the intake, which is required for performing the EGR rate calculation.

Measurements of O_2, CO, CO_2, HC, NO, N_2O, and EGR rate are performed for all the tests by using a Horiba MEXA-7100DEGR gaseous emissions bench. It is actually composed of different gas analyzers depending on the pollutant: flame ionization detector (FID) for total hydrocarbons, heated and vacuum-type chemiluminescence detector (CLD) for oxides of nitrogen, non-dispersive infrared detector (NDIR) for carbon monoxide and intake and exhaust carbon dioxide, and magneto-pneumatic detection (PMA) for oxygen. The working principles behind each gas analyzer are complex and full details can be found in the following references [14–16]. The EGR rate is calculated from the measured volumetric concentrations of CO_2 at the intake ($[CO_2]_{int}$) and at the exhaust ($[CO_2]_{exh}$), according to the following definition:

$$EGR = \frac{[CO_2]_{int} - [CO_2]_{atm}}{[CO_2]_{exh} - [CO_2]_{atm}} \tag{3.1}$$

Prior to each test session, a calibration procedure of the HORIBA analyzers is carried out using reference gases with known concentrations, that are representative for the typical emission range observed in different engines. In such a small engine like the one used in this investigation, the air consumption used for the HORIBA equipment should be taken into consideration, so it has been subtracted from the measured intake flow.

Table 3.7 contains the measured gaseous pollutants along with their corresponding analyzer/method used, as well as the measurement range and the typical tolerance given by the analyzer.

An Universal Exhaust Gas Oxygen sensor (UEGO) is also placed before the settling chamber, to obtain the equivalence ratio at the exhaust. Finally, the sampling for the measurement of the smoke level is taken downstream the exhaust control valve.

The soot content of the exhaust gas is measured with an AVL 415 smoke meter. In this filter-type smoke meter a variable, but exactly defined sampling volume is sampled from the engine exhaust pipe downstream the control valve, and passes through a clean filter paper inside the device. The filtered soot causes blackening on the filter paper which is measured by the photoelectric reflectometer measuring head, and translated to units of Filter Smoke Number (FSN) on a scale from 0-10, with 0 corresponding to an un-blackened filter and 10 to a totally blackened filter.

Pollutant	Analyzer	Range	Tolerance
HC	FID	min. 0 to 10 ppm C	±4 %
		max. 0 to 50 000 ppm C	
NO/NO_x	CLD	min. 0 to 10 ppm C	±4 %
		max. 0 to 10 000 ppm C	
CO	NDIR	min. 0 to 3000 ppm C	±4 %
		max. 0 to 12 vol %	
CO_2	NDIR	min. 0 to 5000 ppm C	±4 %
		max. 0 to 20 vol %	
O_2	PMA	min. 0 to 5 vol %	±4 %
		max. 0 to 25 vol %	

Table 3.7. *Gaseous pollutants measurements.*

The value of smoke (in FSN) can be converted to soot (in mg/m^3) using an empirical correlation proposed by Christian et al. [17], which corresponds to equation 3.2.

$$soot = \frac{1}{0.405} \cdot 4.95 \cdot FSN \cdot e^{(0.38 \cdot FSN)} \tag{3.2}$$

A specifically designed procedure based on the tracer gas method [18, 19] was developed to experimentally measure the trapping ratio (TR) in every test point, using methane (CH_4) as an external gas tracer. First, a controlled concentration of CH_4 (around 1000 ppm) is continuously fed into and mixed with the inlet flow, so the gas divides in the same proportion as the air delivered, when operating at the stabilized engine conditions. The trapped portion of the tracer gas is completely burned in the cylinder during combustion, since the ignition temperature of the tracer gas is much lower than the fuel's ignition temperature. Next, the CH_4 concentration has to be measured at the intake ($[CH_4]_{int}$) and also at the exhaust ($[CH_4]_{int}$) manifolds using a dedicated gas analyzer. The sampling probe in the intake side is located at a sufficient distance downstream the addition point, to assure that the tracer/air mixture has been completely homogenized, but upstream the EGR mixing point. In the exhaust side, there is another independent sampling probe placed before the exhaust settling chamber. Finally, the trapping ratio can be determined from the measured methane concentrations according to equation 3.3

$$\mathrm{TR} = 1 - \frac{Q_{air} + Q_{EGR} + Q_{fuel}}{Q_{EGR} + Q_{air} \cdot \left(\frac{[CH_4]_{int}}{[CH_4]_{exh}} \right)} \tag{3.3}$$

where the EGR mass flow rate (Q_{EGR}) is calculated from the EGR ratio and the fresh air mass flow rate (Q_{air}) as follows:

$$Q_{EGR} = Q_{air} \cdot \left(\frac{EGR}{1 - EGR} \right) \tag{3.4}$$

The trapping ratio indicates what portion of the delivered flow (Q_{del}) is retained in the cylinder at intake valve closing, the rest being "wasted" in the exhaust, so short-circuiting is naturally equal to $(1 - TR)$. Accordingly, the retained (Q_{ret}) and short-circuited (Q_{short}) mass flow rates are obtained from the trapping ratio measurement and the delivered flow, including fresh air and EGR, as follows:

$$\begin{aligned} Q_{ret} &= Q_{del} \cdot TR = (Q_{air} + Q_{EGR}) \cdot TR \\ Q_{short} &= Q_{del} \cdot (1 - TR) = (Q_{air} + Q_{EGR}) \cdot (1 - TR) \end{aligned} \tag{3.5}$$

The calculation method developed to perform the estimation of the residual gas mass, and accordingly IGR, in this two-stroke engine is described in detail in sub-section 3.5.1.

3.3.4 Data acquisition system

The data acquisition system of the test cell is responsible for acquiring signals from various types of sensors and measurement equipment. These can be categorized in two groups: high sampling and low sampling frequency data. For each group, a separate acquisition system is used.

The low frequency system is used to acquire and store the most important data related to the running condition, the engine and test cell monitoring variables, and the experimental average measurements obtained from sensors, dedicated equipment and gas analyzers. These variables are acquired at a frequency of 1 Hz, independently on the engine speed, over a typical measurement period (between one and two minutes) where they are averaged. The measured data is visualized on the test bench during engine operation

Variable	Sensor/equipment	Specification
Engine speed [rpm]	Optical angular encoder	1 to 6000 ±1
Engine torque [N m]	Strain-gauges torque-meter	−200 to 200 ±1
Intake pressure [bar]	Piezorresistive transducer	0 to 10 ±0.001
Exhaust pressure [bar]	Piezorresistive transducer	0 to 10 ±0.001
Intake temperature [°C]	Thermocouple K-type	0 to 1000 ±0.5
Exhaust temperature [°C]	Thermocouple K-type	0 to 1000 ±0.5
Fluid temperature [°C]	Pt100 thermoresistance	−200 to 850 ±0.3
Air flow [m^3/h]	Rotary flow meter	0.05 to 160 ±0.12%
Fuel flow [kg/h]	Dynamic Fuel Meter AVL 733S	0.05 to 150 ±0.12%
Blow-by flow [m^3/h]	Blow-by Flow Meter AVL 442	0 to 4.5 ±1.5%
Equivalence ratio [−]	UEGO NGK Sensor	0.01 to 2 ±0.01%
Pollutant emissions	HORIBA MEXA 7100	see Table 3.7
Smoke level [FSN]	AVL Smoke Meter	0 to 10 ±2%

Table 3.8. *Low frequency measurements.*

using a personalized interface, and it is conveniently stored in a file for post-processing and posterior analysis. As a reference, Table 3.8 contains a summary with some of the relevant mean variables, with their corresponding sensor or measurement equipment, and the range and accuracy given by the device.

The high frequency acquisition is carried out by means of a Yokogawa DL716 digital oscilloscope with 16 channels, which is connected to a PC, to record and store the instantaneous signals coming from different sensors at each measured running condition. The sampling frequency is dependent on the engine speed, so it is automatically adjusted to acquire 1800 points per cycle, corresponding to a resolution of 0.2 CAD, which has been set for the measurements presented in this research work.

An optical encoder mounted in the crankshaft is used to measure the engine speed, and also to send a pulse once every revolution that serves as a reference to the Top Dead Center of the engine (TDC signal). In addition, the encoder sends every 0.5 CAD a pulsed signal to a control box, which is electronically treated to increase the resolution up to 0.2 CAD. With this pulsed signal every 0.2 CAD and the reference TDC pulse as a trigger, the Yokogawa oscilloscope acquires all the data coming from the instantaneous sensors at a high speed. For example, for the tests performed at a running

Signal	Sensor/equipment	Specification
Cylinder pressure [bar]	Piezoelectric sensor	0 to 250 bar
Intake pressure [bar]	Piezoresistive sensor	0 to 10 bar
Exhaust pressure [bar]	Piezoresistive sensor	0 to 10 bar
BDC pressure [bar]	Piezoresistive sensor	0 to 20 bar
Injection pulse [A]	Clamp-on Ammeter	0 to 20 A
Injection pressure [bar]	Piezoresistive sensor	0 to 2000 bar
Camshafts reference [V]	Variable reluctance sensors	0 to 10 V
Angular Speed [−]	Optical angular encoder	1800 pulse/rev, resolution 0.2 CAD

Table 3.9. *High frequency measurements.*

condition of 1500 rpm, the corresponding sampling frequency would be 45 kHz. In addition, the acquisition of all the instantaneous signals are recorded for 100 engine cycles, allowing the analysis of the averaged signals or the cycle-to-cycle variance. As a summary, Table 3.9 contains a list of the selected instantaneous signals, along with the type of sensor used and their range of measurement.

The gas pressure inside the combustion chamber is measured by means of a water cooled piezoelectric sensor (Kistler 6061B), especially suited for thermodynamic investigations in small combustion engines, providing a measurement range from 0 bar to 250 bar along with low sensitivity to thermal shock and good linearity in the whole measurement range. A charge amplifier (Kistler 5011B) converts the electrical charge produced by the piezoelectric sensor into a proportional voltage signal.

The piezoelectric sensor does not provide an absolute measurement of the pressure, so it has to be referenced at some point along the cycle against a piezoresistive sensor. Typically, this is done by matching the cylinder pressure with the intake pressure at a given CAD during the intake stroke. However, in this two-stroke engine the referencing of the cylinder pressure signal is done with an additional piezoresistive pressure sensor, uncooled Kistler 4007BA5F, located at the cylinder liner close to bottom dead center (BDC). This sensor allows measuring the absolute pressure up to 20 bar, at maximum temperatures up to 200 °C.

The instantaneous injection pressure is measured in the high-pressure fuel line between the common-rail and the injector, just before the injector. This

signal is aqcuired using an uncooled piezoresistive sensor (Kistler 4067A2000), which has a measurement range of 0 bar to 2000 bar. Next, it is processed by a charge amplifier (Kistler 4618A) to provide temperature compensation and linearisation of the pressure signal. The injection pulse is also measured and recorded, using a current clamp (Kistler type 2105A) which is fed by an external power supply, then the signal is processed by another amplifier.

The position of the intake and exhaust camshafts, as well as the TDC signal from the crankshaft position sensor, are required for the control and regulation of the VVT system. For this purpose, two variable reluctance sensors are used to generate a TTL signal, that can be compared against the nominal mechanical phasing to determine the angular timing of each camshaft.

3.3.5 On-bench fast post-processing code

Data post-processing involves the manipulation of the data recorded by the high- and low-speed data acquisition systems; and the subsequent calculation of the most important parameters linked to the air management, injection, and combustion processes, as well as the resulting emissions levels and performance indicators. A basic level of data post-processing is done automatically in the engine bench at each test point, for ease of analysis and comparison between a given set of experiments.

In the case of mean engine variables, this task typically includes the calculation of: emissions measurement in mass flow basis or specific units, global exhaust excess air ratio (λ_{exh}) and equivalence ratio (ϕ_{exh}), EGR rate and flow, effective compression and expansion ratios (CR_{eff} and ER_{eff}), indicated and combustion efficiencies (η_{ind} and η_{comb}), specific fuel consumption (ISFC and BSFC), among others.

Performance in terms of engine load, is also calculated directly from the measured cylinder pressure and instantaneous volume to get the indicated mean effective pressure (IMEP), while the brake mean effective pressure (BMEP) is obtained from the engine torque measurement. Main global combustion parameters like peak cylinder pressure (P_{max}), maximum pressure gradient (dP/da_{max}) and combustion stability indicators (CoV_{IMEP} and $CoV_{P_{max}}$) are directly derived from the analysis of the cylinder pressure signal.

A simpler heat release calculation method was adopted in the data post-processing code to get the apparent RoHR on-line at the test bench for each measured test, and correspondingly, the start of combustion (SoC) and the combustion phasing (CA50) defined as crank angle of 50 % accumulated heat released. Additional information about the apparent heat release calculation

can be found in the works of De Rudder [10]. It is worth to point out, that a more complex method is implemented in an in-house combustion diagnostic software (CALMEC) which is used posteriorly to the engine tests to calculate the rate of heat release, considering different sub-models for heat transfer losses, mechanical deformation of the cylinder and blow-by losses. A detailed description of the combustion diagnostic software CALMEC is found in the following section 3.5.2.

A practical tool for estimating the mass of residuals that are not expelled during the exhaust event and remained trapped in the cylinder, was specifically developed for the two-stroke engine application under development, to perform the calculation of the most important air management parameters, including: trapping ratio (TR), charging and scavenging efficiencies (η_{scav} and η_{char}), internal gas recirculation ratio (IGR), total trapped mass (m_{IVC}), oxygen mass fraction and temperature at IVC ($Y_{O_2,IVC}$ and T_{IVC}); and finally, the in-cylinder air/fuel ratio (AFR_{IVC}), effective excess air ratio ($\lambda_{IVC,eff}$) and effective equivalence ratio ($\phi_{eff,IVC}$). This tool is integrated in the data post-processing code, to perform on-line air management analysis at each test point directly on the test cell during normal engine operation. More details about this IGR estimation will be given in section 3.5.1.

3.4 Engine testing procedure

As it was just described in the previous section 3.2, the two-stroke single-cylinder research engine facility provides a great flexibility in the control of parameters which take part during the tests. The engine operation not only requires a fine and independent control over the different auxiliary systems (intake, exhaust, EGR, oil and fuel circuits), but also the proper management and control of the injection system and the variable valve timing system. As a consequence, the greater complexity in the experimental facility added to the larger number of engine settings that has to be simultaneously controlled and registered, may difficult the diagnosis of errors in the tests and the detection of any drift or deviation in the measurement equipment. Therefore, it is very important to define a specific methodology to identify and rapidly detect possible sources of experimental errors before and during test execution.

Accordingly, to improve the accuracy and guarantee the quality of the experimental results presented on this investigation, the correct functioning and repeatability of the experimental facility have been carefully checked every testing day, by following a strict monitoring and detection protocol. Keeping record of this protocol helps in detecting malfunctioning or possible failures on

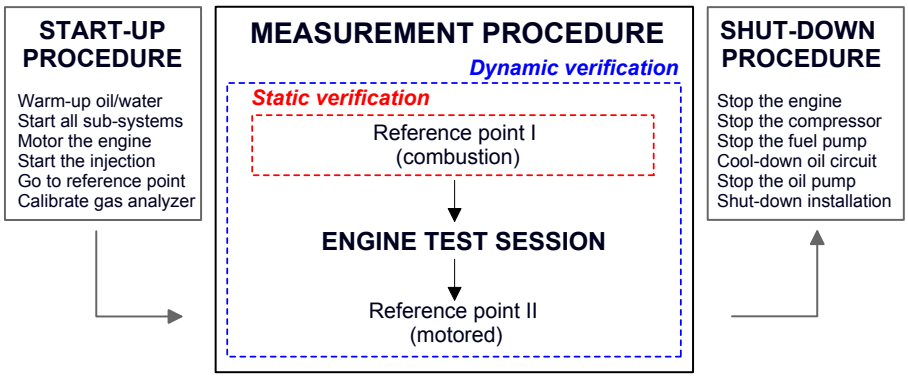

Figure 3.8. *Testing procedure.*

the measurement equipment or auxiliary systems, while it also allows reveling deviations or drifts in the engine behavior during a given period of time.

The procedure followed in this investigation for every engine test session, of typically 7-8 hours duration, can be divided in several steps as depicted in Figure 3.8. In a first step, all the engine sub-systems are started and checked according to the start-up procedure. The oil and water circuits are pre-heated close to (but below) their stabilized operation temperature before starting the engine. Simultaneously, the intake air compressor and the fuel pump are started, and the intake pressure is set to a value slightly higher than the atmospheric (typically around 1.15 bar). In a second step, the engine is first run and brought up to speed in motored conditions, while being driven by the engine dynamometer, while simultaneously the intake pressure, exhaust pressure and oil pressure are regulated up to the settings required for the reference point. Next, the injection equipment is activated to start the combustion. In the meanwhile, the emission gas analyzers are calibrated using special calibration gases by following the required procedure. Once the HORIBA equipment is calibrated and the oil and water have reached their working temperature (90 °C), the engine is brought to the reference point settings, which are representative of a stabilized low or medium load point, with a pilot and a main injection. At this point, the facility is ready for starting the static verification according to the measurement procedure.

The proposed monitoring and detection protocol has been adapted from the methodology proposed in the works of Benajes et al. [20] and Molina [21], which is composed by two types of verifications: a static verification, in which

the engine setting is fixed at the same reference point in different testing days, and a dynamic verification, that allows detecting errors in fresh intake airflow rate, fuel mass flow rate, EGR ratio, and exhaust oxygen concentration during test execution regardless the operating point.

In this investigation, a set of low-frequency variables that quantifies the operation of the engine and auxiliary equipment have been selected to be checked during this first verification, i.e: fresh air flow rate (Q_{air}), injected fuel mass (m_{fuel}), engine torque, P_{max}, IMEP and ISFC, pollutants emissions (NO_x, HC, CO, and smoke), TR and $\phi_{eff,IVC}$, among others.

For the implementation of this static verification on the test facility, it is necessary to develop a control chart for each controlled parameter. In such a way, a short isolated statistic study of each controlled parameter can be performed, calculating the average of the measured values (μ), the standard deviation (σ), and the upper and lower control limits defined with a 95 % confidence interval, which are going to determine if the reference point is acceptable and the experimental facility is operating correctly. As a reference, Figure 3.9 shows an illustrative example of the control charts for a set of 30 reference points measured in a period of two months.

Once the static verification has been performed, it is assumed that all the parameters have been validated and they are correctly measured at the start of the testing time, so the next step is to begin with the measurement campaign for the given set of points planned for that engine test session.

The measurement procedure starts by first stabilizing the engine settings to their required values for the given operating condition. Next, the feeding valve for injecting the tracer gas (CH_4) in the intake flow is opened, until reaching a concentration around 1000 ppm in the intake, once it has been stabilized, the CH_4 concentrations at intake and exhaust manifolds are simultaneously measured and recorded to perform the trapping ratio calculation. Then, the feeding valve is closed to cut the supply of methane to the engine. If all the engine variables are stabilized, the acquisition of all time-averaged (low frequency) and instantaneous (high frequency) measurements is done typically during a time period of one to two minutes. Once the acquisition has finished and the information has been transmitted to the main central computer, the data post-processing code is run to obtain all derived parameters regarding combustion (IMEP, CA50) and air management process (TR, IGR, AFR_{IVC}). The acquisition of the data is performed at least three times, to check the precision of the measurements and also to assure the stability of the measured engine behavior.

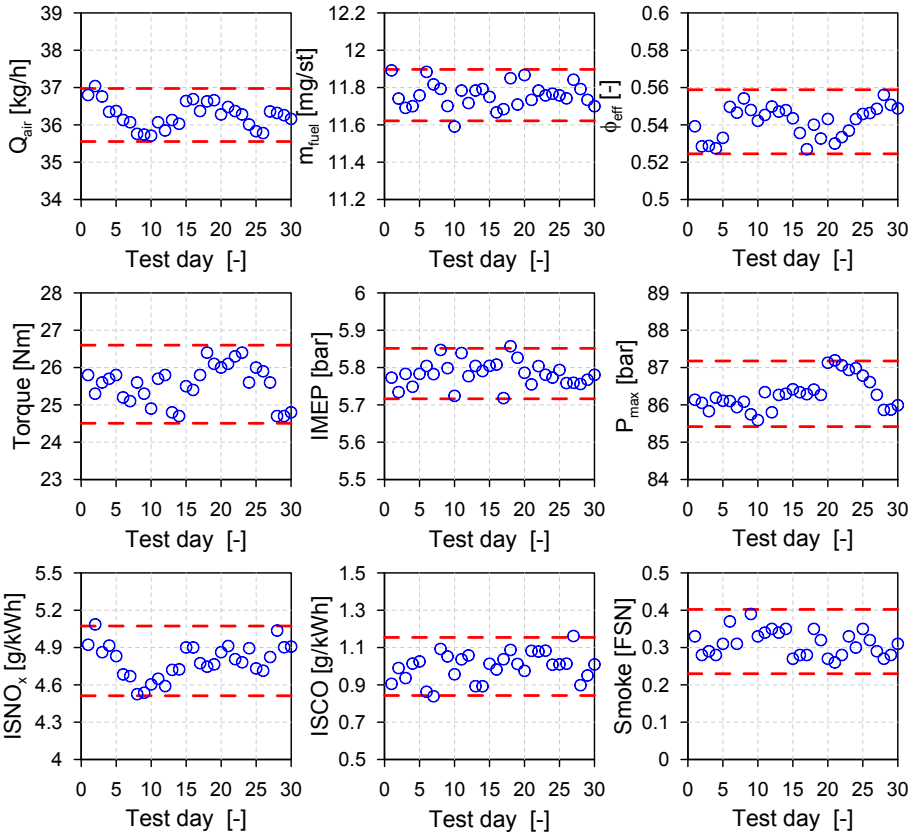

Figure 3.9. *Static verification.*

Performing a dynamic verification during test execution is quite useful for detecting errors in some relevant and sensitive operation variables, such as the fresh intake air flow rate, the fuel mass flow rate, EGR ratio, the exhaust oxygen concentration and the exhaust global equivalence ratio.

An example of some of the methods used for the dynamic verification is shown in Figure 3.10, in the case of an EGR sweep measured during an arbitrary engine test session.

For instance, an error in the EGR rate measurement or in the fresh air flow measurement could have been spotted by a deviation in the total intake delivered flow (Q_{del}), shown in Figure 3.10.a, which has to be independent of the EGR rate, and has to remain constant when all other air management

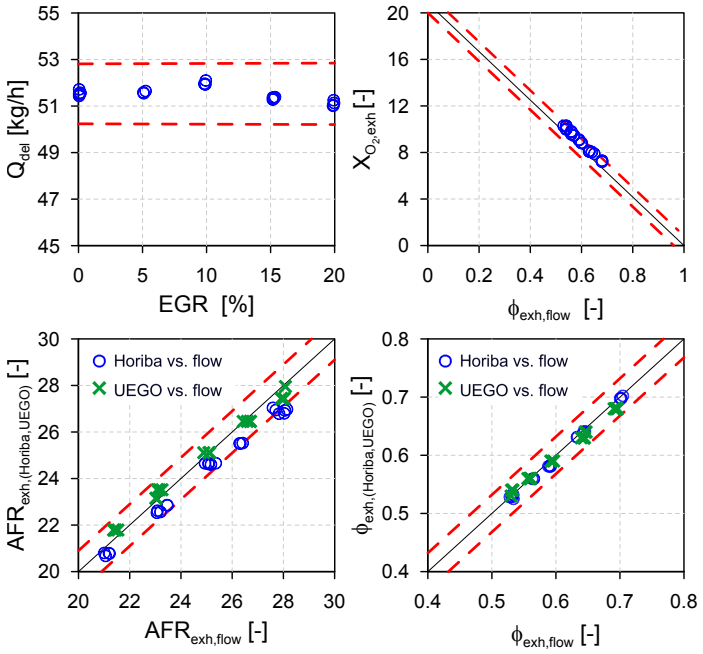

Figure 3.10. *Dynamic verification.*

settings are kept unchanged. The second plot shown in Figure 3.10 relates the oxygen molar concentration ($X_{O_2,exh}$) at the exhaust with the equivalence ratio, according to the expression shown below:

$$X_{O_2,exh} = X_{O_2,air} \cdot (1 - \phi) \qquad (X_{O_2,air} = 20.84\%) \tag{3.6}$$

For the case shown in Figure 3.10.b, ϕ_{exh} is computed from the measured air and fuel flows. Note that all the points should follow this linear relationship between $X_{O_2,exh}$ and ϕ_{exh}, so if any deviation outside the control limits is detected, it may indicate an error in the measurement of $X_{O_2,exh}$ (if the point has displaced vertically above or below the line), or an error in the equivalence ratio that may come from the measured air and fuel flows (if the point has displaced horizontally to the right or left). If the first verification of the total delivered flow was correct, which confirms the measurement of EGR and air flows, the deviation in ϕ_{exh} is probably caused by an error in the fuel flow. The last verification is to compare the global air/fuel ratio and the equivalence ratio at the exhaust obtained from three different sources: from the UEGO oxygen

sensor, from the 5-gas method using the pollutants measured by the HORIBA, and from the measured fresh air and fuel flow rates using the stoichiometric air-fuel ratio, to check the consistency of the different measurement equipment and detect possible drifts on the derived calculations.

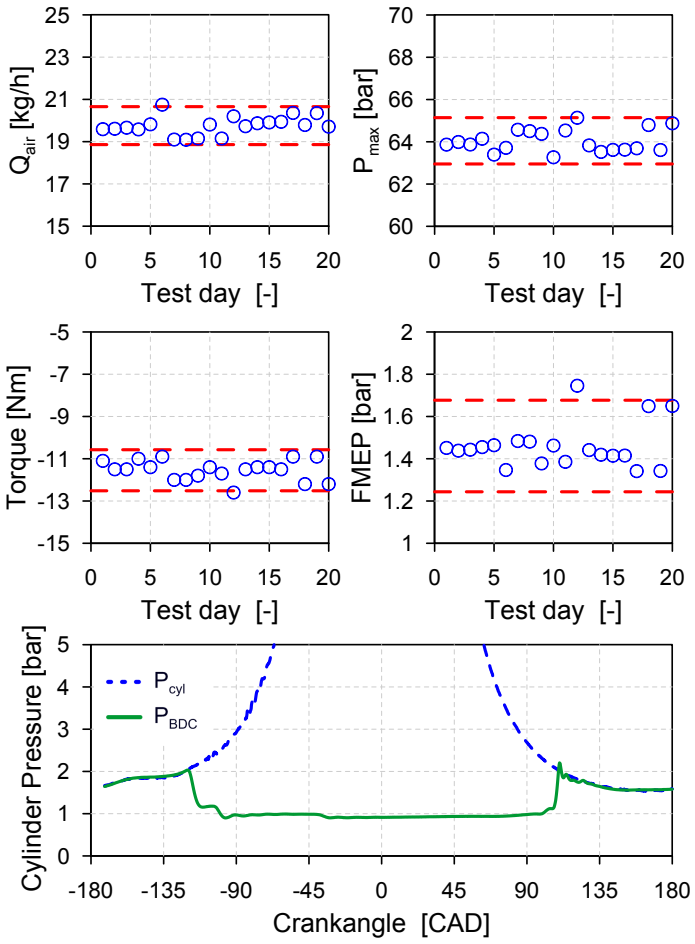

Figure 3.11. *Dynamic verification of motored reference test.*

Once the test plan is finished, the engine is brought to motored operation by removing the injection, and a second reference point is measured without combustion but keeping the same air management settings as the first reference point with combustion. As a reference, Figure 3.11 shows an example of

some control charts typically used for the dynamic verification of the reference motored tests, as well as the verification of the pegging between the cylinder pressure signal measured with the piezoelectric sensor (in blue) and the piezorresistive sensor placed at the BDC (in green).

3.5 Theoretical tools

To fully understand the air management and combustion processes that determine the performance levels of the two-stroke engine under development, this investigation combines a predominantly experimental approach based in single-cylinder engine testing, with a extensive contribution from different diagnostic and modeling tools. This includes the derived calculation of global combustion and air management parameters, zero-dimensional free-spray calculations, as well as the development of a multi-dimensional engine model that is used to complement the analysis of the experimental information.

3.5.1 IGR estimation model

In the two-stroke poppet valves engine under development the high short-circuit losses of intake charge flowing directly to the exhaust system are typically caused by the long overlap period between the intake and exhaust phases, combined with the positive pressure difference between the intake and exhaust mean pressures (ΔP). In addition, the situation is worsened by the proximity between the intake and exhaust valves in the poppet valve scavenge type configuration. The short-circuit losses decrease the trapping efficiency, meaning that only a ratio of the delivered charge is effectively trapped in the cylinder. Moreover, the short-circuit losses consist of fresh air (fuel is injected during close cycle) so the exhaust flow is diluted with air, and the measured air/fuel ratio in the exhaust manifold (AFR_{exh}) is different from the trapped AFR in the cylinder for combustion (AFR_{IVC}).

The correct estimation of the cylinder-charge composition is very important for the thermodynamic analysis of the combustion process of IC engines. In the case of the poppet valve scavenge configuration, the residual gas mass strongly depends on valve train parameters and operating conditions, which means that they must be taken into account not only for the simulation and the analysis of the combustion process, but also for controlling the engine.

Some of the conventional air management performance parameters typically used in a two-stroke engine context, that will be frequently discussed

along this research are: the trapping ratio, the internal gas recirculation ratio, the charging and scavenging efficiencies, the in-cylinder air/fuel ratio and the effective equivalence ratio. Their definitions are included in the set of equations 3.7.

$$\left.\begin{aligned} \mathrm{TR} &= \frac{m_{ret}}{m_{del}} \\ \mathrm{IGR} &= \frac{m_{res}}{m_{IVC}} \\ \eta_{char} &= \frac{m_{ret}}{m_{theor}} \\ \eta_{scav} &= \frac{m_{ret}}{m_{IVC}} \\ AFR_{IVC} &= \frac{m_{air,ret}}{m_{fuel}} \\ \phi_{eff,IVC} &= \frac{AFR_{stoich}}{AFR_{IVC}} \end{aligned}\right\} \quad \text{Main air management definitions} \tag{3.7}$$

The trapping ratio (also known as trapping efficiency) is a measure of the success of trapping the supplied air with a minimum of waste. Therefore, it is defined as the retained mass (m_{ret}) divided by the delivered mass (m_{del}). The charging efficiency compares the retained mass against the theoretical mass (m_{theor}) that would be possible to enclose in the cylinder volume at BDC calculated at reference conditions. On the other hand, the scavenging efficiency evaluates the success in clearing the cylinder of residual gases from the preceding cycle, so is defined as the fraction of retained mass (m_{ret}) in the total cylinder charge at IVC (m_{IVC}). Accordingly, the IGR is then defined as the ratio between the residual gases (m_{res}) trapped from the previous combustion cycle and the total cylinder charge (m_{IVC}) trapped at IVC. Finally, the in-cylinder air/fuel ratio (AFR_{IVC}) is calculated as the ratio between the usable air retained in the cylinder (excluding the air present in the IGR) and the injected fuel mass, whereas the effective equivalence ratio ($\phi_{eff,IVC}$) is obtained from the stoichiometric air/fuel ratio (AFR_{stoich}) and the AFR_{IVC}.

In contrast to measuring fresh air and fuel flows, no standard sensor exists for measuring trapped mass composition, so the residual gas mass or IGR cannot be measured directly in the running engine keeping relatively simple methods. Previous experimental studies found in the literature regarding the measurement of residuals in IC engines are usually based on differences in gas concentrations between fresh gas, cylinder charge or exhaust

gas. The analysis of CO_2 is often used as an indicator of the IGR. For some methods, the gas composition is sampled directly in the exhaust port close to the valve [22, 23], and for other methods, it is directly sampled in the cylinder [24–27]. However, both approaches involve dedicated equipment (fast gas analyzers and/or fast gas sampling valves) which are typically costly prohibitive for engine testing, and also specific measurement procedures (like running the engine in skip-fired mode) so it is difficult to obtain a fast measurement of IGR during normal engine operation. Moreover, in the case of cylinder gas sampling, assuming a homogeneous composition across the cylinder volume is mandatory, so the local sample is representative of all cylinder gas composition, which may not be the case in a two-stroke engine, particularly with the proposed poppet valves architecture.

It is therefore difficult and it requires a lot of effort to determine experimentally the residual gas mass, so different approaches have been developed in the past to predict or estimate it as accurately as possible. Generally, these methods can be classified depending on their increased complexity and computational cost:

- *Simulation of the gas exchange process using three-dimensional fluid-dynamics (CFD) models.* This is the most suitable calculation approach for predicting the complex (and three-dimensional) gas transfer processes happening in a two-stroke engine. By solving the fluid-dynamics during the open cycle the total cylinder charge and the residuals mass can be calculated with relatively high accuracy. However, the CFD model has to be validated against experimental data and properly fed with the detailed engine geometry and adequate boundary conditions to reproduce the real engine behavior. This is a costly approach in terms of setup and computational time, so it is not really a practical solution for the pre-development and optimization phase, neither for performing a fast estimation of the IGR ratio on the test bench.

- *Simulation of the gas exchange process using one-dimensional fluid-dynamics models.* One-dimensional flow calculations can be carried out much faster compared to CFD calculations, and they still take into account the dynamic flow effects since the mass transfer is described by the unsteady Euler equations (conservation of mass, momentum and energy). However, the complex (three-dimensional) internal aerodynamics of the flow during the open cycle is not considered, so it requires a fine-tuned scavenging curve as input for each operating condition, which changes depending on the VVT timing and the

particular engine settings. Consequently, to build a simplified 1D model of a two-stroke engine it is necessary to choose and assume a fixed scavenging law, otherwise, it has to be fitted to reproduce the measured engine data at each test point, so the model can be used only like a diagnostic (but not predictive) tool. In addition, a detailed engine characterization is also needed (accurate lengths and diameters of runners, flow discharge coefficients...) to improve the accuracy of the results when predicting the gas transfer processes for this particular two-stroke engine architecture.

- *Quasi-steady thermodynamic gas exchange analysis.* This zero-dimensional approach considers the intake-exhaust manifolds and the engine cylinder as reservoirs of finite volume, which are transiently filled and emptied for calculating the gas exchange process during an engine cycle. This approach is typically known as Filling and Emptying method. The mass and energy equations for an open system are resolved for each volume at each time-step, and the calculation of the mass exchange rate between the intake/exhaust system and the engine cylinder is typically done with the Saint-Venant and Wantzel equation for isentropic flow through an orifice. Pressures in the intake and exhaust volumes are typically assumed to be constant in the simplest case, but the model can be also fed with the dynamic pressures measured experimentally for the intake/exhaust ports and in-cylinder as boundary conditions. Usually, deviations in the flow coefficients and valve lifts are the main sources of error. But more importantly, this approach neglects the one-dimensional inertial effects and also requires assuming a constant scavenging law, so it is not appropriate for an engine where these effects are relevant, as in the case of the two-stroke engine under development.

- *Simplified thermodynamic estimation.* This approach provides a relatively robust but very fast calculation for giving an estimation of the residual gas fraction, that can be effectively used during engine testing with reasonable CPU run time. It is based on the mass and energy balances at IVC, combined with mean pressure and temperature values acquired during engine operation and some geometrical aspects of the engine. However, it implies performing strong hypothesis and assumptions which can have a significant impact on the accuracy and precision of this method.

For this investigation, a thermodynamic approach was selected to develop a simplified model for the on-line estimation of the IGR directly on the test

bench during test execution. This thermodynamic model has been integrated into the data post-processing code available at the engine test bench. The complexity of pulsating flow during gas exchange is ignored and, instead, the mass and energy balances are applied at intake valve closing (IVC) to calculate total trapped mass and residual gas mass, according to equations 3.8.

$$\begin{aligned} m_{IVC} &= m_{ret} + m_{res} \\ H_{IVC} &= H_{ret} + H_{res} \end{aligned} \tag{3.8}$$

The different considerations that were made for obtaining the terms in equation 3.8 are listed below as follows:

- In-cylinder mass is related to cylinder volume, pressure, and temperature through the ideal-gas equation of state. Instantaneous volume at IVC (V_{IVC}) has been indirectly calculated through the crank slider with pin offset equation, using nominal crank position (angle). Cylinder pressure at IVC (P_{IVC}) is taken from the signal experimentally measured with the piezoelectric pressure transducer, after it has been referenced (pegged) using the BDC absolute pressure. Finally, the specific gas constant of the trapped charge at IVC (R_{IVC}) is assumed to be constant and approximately equal to the value corresponding to fresh air (287 J/kg K) for ease of calculation.

- Perfect gas behavior is assumed for the gas mixture to calculate gas thermodynamic properties. For an ideal thermodynamic process, the specific heats at constant volume (Cv) and pressure (Cp) are typically assumed to be constant; even when they are pressure- and temperature dependent in reality. Accordingly, constant values of Cp_{int} equal to 0.998 kJ/kg K and Cp_{exh} equal to 1.041 kJ/kg K are kept for the specific heat capacities of the fresh intake and exhaust gas, respectively, to simplify the calculation at the test bench. Note that a gas mixture typically has multiple components (different species) so mixture-averaged quantities, pressure- and temperature dependent, would have to be well-defined for computing the gas thermodynamic properties.

- The retained masses of fresh air ($m_{air,ret}$) and EGR ($m_{EGR,ret}$) are known variables obtained from equation 3.5, since the trapping ratio is experimentally measured by the tracer gas method at each operating point, as it was previously explained in section 3.3.3.

Performing all the required substitution of different terms and operating between the equations, the final expression used to calculate the residual gas mass becomes:

$$m_{res} = \frac{Cp_{int}}{Cp_{exh}} \cdot \left(\frac{P_{IVC} \cdot V_{IVC}}{R_{IVC} \cdot T_{res}} \right) - \frac{Cp_{int}}{Cp_{exh}} \cdot m_{air,ret} \cdot \left(\frac{T_{air,ret}}{T_{res}} \right) - m_{EGR,ret} \cdot \left(\frac{T_{EGR,ret}}{T_{res}} \right) \tag{3.9}$$

To resolve this equation it is necessary to make the following additional assumptions and simplifications:

- For on-line estimation of the IGR directly on the test bench, the temperatures of the retained charge ($T_{air,ret}$ and $T_{EGR,ret}$) before being mixed with the residuals, are assumed to be equal to the mean temperatures measured for the fresh air and EGR flows, while neglecting dynamic heating and heat losses during the induction phase. Next, the in-cylinder charge temperature at IVC results from adding the sensible enthalpies of both the retained and residual fractions, as stated in equation 3.8. Note that in the simplest case, one could directly assume that the temperature at IVC is equal to the measured intake temperature. Reported investigations following this approach (keeping $T_{IVC} = T_{int}$) estimated an error in the IGR of approximately 5%, in the case of four-stroke engines where the residuals represent a small ratio compared to the total mass. However, this error is expected to be larger as the fraction of IGR is increased, as in the case of the two-stroke poppet valve configuration.

- The last and strongest approximation needed to compute m_{res} according to equation 3.9, is to assume that the temperature of the residuals (T_{res}) is equal to the mean temperature measured at the exhaust manifold. However, particularly for this two-stroke engine architecture with relatively high short-circuit losses, the temperature in the exhaust manifold is expected to be comparatively lower than the temperature of the residuals. So, T_{res} is estimated using equation 3.10, derived from a complementary mass and energy balance at the exhaust manifold, taking into account the flow and the temperature at the exhaust (T_{exh}) measured before the EGR extraction point, and the short-circuited flow and temperature (T_{short}) given by the mixture of intake fresh air and EGR.

$$T_{res} = \frac{Cp_{exh} \cdot (m_{del} + m_{fuel}) \cdot T_{exh} - Cp_{short} \cdot m_{short} \cdot T_{short}}{Cp_{exh} \cdot (m_{del} + m_{fuel} - m_{short})} \tag{3.10}$$

After calculating the residual gas mass (m_{res}), the total trapped mass in the cylinder (m_{IVC}) and the charge temperature at the start of the close cycle (T_{IVC}), are derived from the mass balance shown in 3.8 and the ideal gas law, respectively. Next, other parameters like the IGR ratio, scavenging efficiency, and effective in-cylinder AFR and equivalence ratio can be completely defined.

3.5.2 Combustion diagnosis

The information about the time-resolution of the thermodynamic variables of the cylinder gas is very valuable for the diagnostics of the combustion process. For combustion laboratory studies, the diagnostic methods use the experimental pressure signal as input data and, after averaging, filtering, and referring to absolute pressure and crank angle values, solve the heat release law (time evolution of heat release fraction), and the instantaneous gas temperature average along the combustion chamber by combination of both the first principle of thermodynamics and the equation of state. These are typically zero-dimensional and single-zone models, hence, do not take into account the air entrainment, vaporization of fuel droplet and spatial variation of mixture composition and temperature. However, the analysis of global combustion parameters such as the start of combustion or the combustion phasing is still valid since they are directly related to the instantaneous evolution of the energy released by the progress of the combustion, independently from the local conditions where this energy is being released. Additionally, single-zone models are advantageous because of their simplicity and their wide usage in engine testing for monitoring global combustion parameters.

The RoHR analysis and derived combustion-related parameters that are presented in this work are calculated using CALMEC, an in-house internal combustion engine combustion diagnosis software [28–30]. This model requires different measured instantaneous signals, such as the in-cylinder pressure and the reference pressure at BDC; as well as other engine working conditions (mass flows, temperatures). Then, the first law is applied considering the combustion chamber as an open system because of blow-by and fuel injection. It uses the ideal gas equation of state to calculate the mean gas temperature in the chamber. The RoHR calculation also includes sub-models for considering heat transfer losses, mechanical deformation of the cylinder and blow-by losses.

A thorough discussion of the fundamental hypothesis of the method, as well as a sensitivity analysis to study the influence of measurement errors and estimated parameters on combustion diagnosis, can be found in the works of Lapuerta [30] and Payri [31]. The main hypothesis behind this model are briefly described as follows:

- The pressure in the combustion chamber is assumed to be uniform. This hypothesis is valid because the flow speed and flame propagation speed is much lower than the speed of sound
- The fluid in the chamber is considered a mixture of air, fuel and stoichiometric burned products. Although it is assumed the uniformity of composition and temperature of the mixture, it is important to emphasize that the model considers three species (air, fuel and burned gases) at the time of evaluating the thermodynamic properties of the gas enclosed in the cylinder. In addition, to consider combustion products burning at stoichiometric conditions is valid in a diffusive flame, since the fuel is primarily burned in a reaction surface with local stoichiometric air/fuel ratio. Note that this might not be necessarily true for premixed combustion.
- Perfect gas behavior is assumed for the gas mixture. Mölenkamp showed the validity of this assumption in the pressure and temperature ranges of diesel engines [32]. However, this hypothesis may be argued when applied to gaseous fuel. Lapuerta compared the results of a similar combustion model but using different state equations for the gaseous fuel, and the study showed that the differences in mean temperature and energy release are relatively small [30], yet they could be relevant if the results are used to predict emissions formation.
- Correlations based on the temperature are used to calculate sensible internal energy of the gas mixture.
- The internal energy is calculated considering the mean gas temperature. This is the hardest hypothesis since burned products are much hotter than mean temperature at the combustion beginning, even though later they become closer.
- The heat transmitted to the walls is calculated utilizing a modified heat transfer coefficient obtained with Woschni's expression [33–35]. An additional heat transfer nodal model is used to calculate the different wall temperatures (piston, liner, cylinder head) [36, 37].

Assuming the previous hypotheses, the model resolves the first-law of thermodynamics, presented in equation 3.11, at time-steps defined by the angular resolution of the cylinder pressure signal (0.2 CAD).

$$\Delta HRL = m_{cyl}\cdot\Delta u_{cyl}+\Delta Q_w+p\cdot\Delta V-(h_{fuel,inj}-u_{fuel,g})\cdot\Delta m_{fuel,evap}+R_{cyl}\cdot T_{cyl}\cdot\Delta m_{bb} \tag{3.11}$$

The different terms in the energy balance considered in equation 3.11 at each computational time-step are listed below as follows:

- ΔHRL. Energy released by the fuel assuming constant calorific power along the combustion process.
- $m_{cyl} \cdot \Delta u_{cyl}$ Variation in internal sensible energy experienced by the gas enclosed in the control volume.
- ΔQ_w. Heat transfer between the gas enclosed in the control volume and the combustion chamber walls that surrounds it.
- $p \cdot \Delta V$ Work done by the gas enclosed in the control volume over the piston surface during the calculation interval. The instantaneous volume is the sum of the combustion chamber volume, the volume displaced by the piston (depending on crank angle) and the mechanical deformations (estimated by a sub-model) produced by the gas pressure and the inertial efforts.
- $(h_{fuel,inj} - u_{fuel,g}) \cdot \Delta m_{fuel,evap}$. Flow work of the injected fuel, evaporation and heating up to the gas temperature. The fuel enthalpy refers to the injection conditions whereas fuel internal energy refers to the evaporated fuel at in-cylinder conditions.
- $R_{cyl} \cdot T_{cyl} \cdot \Delta m_{bb}$. Energy lost by the control volume due to blow-by losses through the piston rings. For the determination of the blow-by mass loss m_{bb} an isentropic discharge through a nozzle connecting the cylinder with the carter was supposed, in combination with a coefficient that is adjusted by comparison with experimental measurement of blow-by.

From the calculated heat release law (HRL) and the derivative of the energy released (RoHR), along with the injection mass flow rate, the following global injection-combustion related parameters are derived:

- SoE: Angle corresponding to the start of energizing of the injector in the measured injection pulse signal. There is an hydraulic delay of approximately 1.5 CAD to 2 CAD before the SoE and the real start of injection (SoI).
- SoI: Angle corresponding to the start of injection in the mass flow rate profile.
- EoI: Angle corresponding to the end of injection in the mass flow rate profile.
- SoC: Angle where the combustion starts to release energy.
- ID: Ignition delay, defined as the angular difference between the SoC and the SoI.
- Mixing time: Angular difference between the SoC and the EoI.
- CA50: Center of gravity of combustion, corresponding to the angle where the 50 % of the energy has been released.
- CA10, CA75, CA90: Angles where the 10 %, 75 % and 90 % of the energy has been released.
- EoC: In this investigation the end of combustion has been defined as the angle where 90 % of the energy has been released.
- Combustion duration: Angular difference between the EoC and the SoC.

3.5.3 Adiabatic flame temperature estimation

As it was previously described, the 0D single-zone model used for calculating the RoHR is based on the assumption of an uniform temperature along the combustion chamber. However, as it was discussed in section 2, the formation and destruction of pollutants is driven by physical and chemical processes affected by the evolution of local conditions, in terms of mixture composition and temperature. So, to qualitatively compare some general trends observed in the pollutants, specially in terms of NO_x, it appears more appropriate to estimate the maximum temperature achieved during the combustion process.

A good qualitative indicator of the maximum local combustion temperature would be to estimate the adiabatic flame temperature (T_{ad}), assuming

that the combustion process in a diesel engine is adiabatic and that the reaction is complete. The adiabatic temperature can be defined for two different processes; considering a combustion at constant pressure, or at constant volume. The following hypothesis have to be made for the calculation of T_{ad}.

- The combustion develops at approximately constant pressure at each time-step of the calculation. This is a simplification to the characteristic mixing-controlled combustion process occurring in a diesel engine. So if a fuel-air mixture is burnt in an adiabatic process at constant pressure, then the absolute enthalpy of the reactants in the initial state (at unburnt temperature) should be equal to the absolute enthalpy of the products at the end of the reaction (at adiabatic temperature).

$$H_{reac}(T_{unburnt}) = H_{prod}(T_{ad}) \tag{3.12}$$

- The maximum adiabatic flame temperature occur in a region of local equivalence ratio equal to stoichiometric. This hypothesis is true for diffusive diesel combustion, where the flame develops in a thin reaction zone at stoichiometric mixture conditions. However, in the case of highly premixed or partially premixed diesel combustion, this hypothesis might not longer be valid, since the reaction zone occurs in a wider range of equivalence ratios.

- The thermodynamic system is considered at all times as a mixture of ideal gases. Then, it is possible to calculate the properties of the mixture, including the enthalpy, like the weighted sum of each species, with the equations shown in 3.13.

$$\begin{aligned} H_{reac}(T_{unburnt}) &= \sum_{i=1}^{k} n_i \cdot \overline{h}_i(T_{unburnt}) \\ H_{prod}(T_{ad}) &= \sum_{j=1}^{m} n_j \cdot \overline{h}_j(T_{ad}) \end{aligned} \tag{3.13}$$

n_i represents the mole number of reactant i, n_j the mole number of product j in the mixture, and $\overline{h}_i(T_{unburnt}$ is the specific enthalpy of reactant i, while $\overline{h}_j(T_{ad})$ is the one for product j. These specific enthalpies of each species are calculated according to the next equations 3.14.

$$\overline{h}_i(T_{unburnt}) = \overline{h}^o_{i,form} + \int_{T=298}^{T=T_{unburnt}} \overline{c}_{p,i}(T) \cdot dT$$
$$\overline{h}_j(T_f) = \overline{h}^o_{j,form} + \int_{T=298}^{T=T_{ad}} \overline{c}_{p,j}(T) \cdot dT \quad (3.14)$$

Where $\overline{h}^o_{i,form}$ and $\overline{h}^o_{j,form}$ corresponds to the standard enthalpy of formation (at $T = 298.15\ K$ and $p = p_{ref}$), and $\overline{c}_{p,i}(T)$, $\overline{c}_{p,j}(T)$ to the specific heat capacity at constant pressure, calculated by polynomial equations.

- N-dodecane ($C_{12}H_{26}$) is used as surrogate fuel, since their properties are well known and reasonably similar to those of diesel fuel.
- To close the calculation it is necessary to estimate an initial temperature of the reactants ($T_{unburnt}$) at each calculation interval. So the temperature of the reactants is assumed to evolve adiabatically as the pressure in the chamber increases due to the combustion process and piston movement.

Finally, a 13-species equilibrium approach at constant pressure was resolved to arrive at the maximum adiabatic flame temperature, as developed by Way [38]. Since the composition of the products has to be calculated at each time-step, but they depend on the calculated value, the adiabatic temperature is resolved following an iterative calculation process.

3.5.4 1D Spray evaporation and mixing modeling

The spray mixing process in non-reactive and reactive conditions is going to be simulated at selected test points by means of a 1D free-spray model, in order to study qualitatively the spatial distributions of properties within the spray (velocity, temperature, density, mixture fraction, ...) as a function of time. This simplified model is useful to gain some insight into the relation between injection and mixing processes, with a lower computational time and cost compared to more complex multi-dimensional CFD calculations. A thorough description of this model, along with the validation against experimental data was reported by Pastor [39] for inert conditions, and by Desantes [40] for reactive conditions.

As a reference, Figure 3.12 shows a schematics of the main inputs and outputs of this 1D spray model. The main hypothesis behind this model are

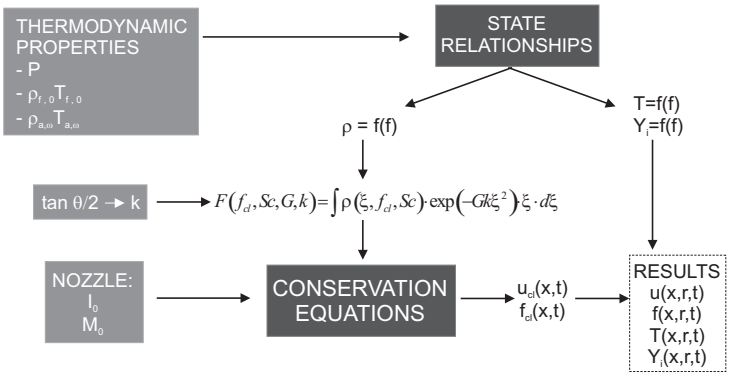

Figure 3.12. *Schematics of the 1D free-spray model. Source: Pastor et al. [39].*

thoroughly discussed in the works of García [41] and Pastor [39], but they can be briefly summarized in the following items:

- Symmetry on the spray axis, i.e., no air swirl.
- A fully-developed turbulent flow is assumed, which means that self-similar radial profiles can be defined for the conserved variables, so the ratio of any conserved variable divided by the centerline value does not depend on the axial coordinate. A Gaussian radial distribution function is used, which is valid for steady inert atmospheric gas jets [42], as well as for developed diesel fuel sprays at typical engine conditions [43]. Under transient injection conditions, some kind of similarity can also be assumed, as shown in [44].
- Locally-homogeneous flow is assumed [45], so it exists a local equilibrium both in thermal and velocity conditions. This allows for a consideration of the spray as a gas jet.
- Pressure is assumed to be constant all over the spray, and thus compressibility effects are neglected.
- Local density is calculated under the assumption of ideal mixing, therefore neglecting compressibility effects.

This tool is used for calculating the mixing process right before the start of combustion, to study relative trends of in-cylinder fuel and air premixing before the SoC, only in selected points with single injection strategies, so the

injection process can be still assumed as a non-reactive spray. The analysis performed by means of this 1D spray model, includes estimating the total spray penetration, the maximum liquid length during the injection event, and the temporal evolution of local equivalence ratio in the axis of the spray, with particular emphasis in the equivalence ratio distribution at the start of combustion.

The main physical properties for the fuel, considering hexadecane and iso-octane as proper surrogates for diesel and gasoline, were extracted from reliable database sources such as NIST [46]. The spray gas surrounding is considered as a perfect mixture of air and exhaust gas in a given ratio provided by the measured EGR rate. The injection mass flow rate and the spray momentum flux, which are the boundary conditions at the injection orifice, were obtained by means of the experimental detailed characterization of the injector used for this research work. The surrounding gas thermochemical conditions (pressure, temperature, density and composition) were calculated with CALMEC, from the experimental results available after testing the engine at the selected operating conditions. Finally, the spray cone angle is the unique calibration parameter of the 1D spray model, and it was estimated from the fuel and surrounding gas conditions adapting the expression suggested by Naber and Siebers [47].

In order to validate the model predictions, the actual spray evolution was characterized by performing dedicated tests installing the injector in a visualization test rig, controlling the injection and surrounding gas according to the experimental setup and methodology described in [48, 49]. Afterwards, recorded images of the spray evolution were processed to obtain an experimental averaged spray angle and penetration profile. Figure 3.13 includes the validation of the 1D spray model against these experiments by comparing the estimated/measured spray cone angles, and finally by introducing the estimated angle and all other boundary conditions to check the estimated/measured spray penetration fit. Figure 3.13 shows a good agreement between the experiments and the model predictions.

3.5.5 Multi-dimensional combustion modeling

Instead of describing engine processes empirically, as in classical thermodynamically-based analyses, comprehensive computer codes are now extensively used in engine research. Multidimensional CFD modeling has become a key enabling technology in the optimization process of modern IC engines, as for the development of advanced combustion concepts, specially

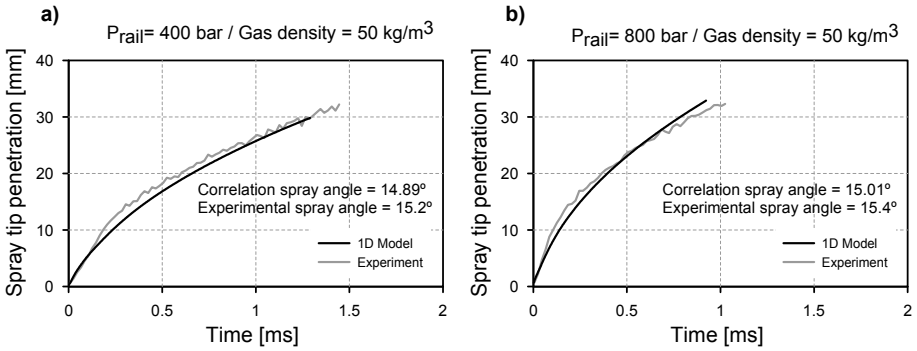

Figure 3.13. *Validation of the 1D free-spray model against experimental results in terms of spray angle and penetration for two different injection pressures.*

because it provides a more accurate prediction and study of the behavior of pollutant emissions compared to simplified multi-zone models or chemical kinetics reactor simulations.

The development of multi-dimensional models greatly benefits from closely coordinated companion experiments. Because engine experiments are sometimes difficult to perform in hostile environment and they may be affected by phenomena such as cycle-by-cycle variability, it is of great importance to carefully setup and validate the CFD model against robust experimental data.

The governing Navier Stokes partial differential conservation equations (mass, momentum, and energy) are resolved on a numerical mesh that follows the time-varying engine geometry during each engine cycle. However, different sub-models (atomization, break-up, turbulence, etc) are still required to describe processes that occur on time and length scales that are too small to be resolved in the simulations, so the appropriate choice of sub-models needs to suit the particular application.

For this investigation, a computational model was built by means of the CONVERGE CFD code, developed by *Convergent Science* [50] to perform full coupled open and closed cycle calculations using the full intake/exhaust and cylinder geometries. The model will be used to perform a detailed analysis, and accordingly more accurate quantitative comparisons, of the evolution of the in-cylinder local conditions along the engine cycle, to support and complement the experimentally measured results.

Model Set-up

Full coupled open and closed cycle computations using the full intake/exhaust and cylinder geometries are setup since the combustion chamber is non-symmetric. The mesh geometry is automatically generated by the CFD code during the calculation process, within a defined combustion chamber geometry that fix the limits of the computational domain. The right-hand side of Figure 3.1 contains a sketch of the computational domain at the intake valve closing (IVC) angle. The code uses a structured Cartesian grid with base cell size of 3 mm. Three additional grid refinements linked to flow velocity and temperature are performed by means of an adaptive mesh refinement (AMR) as well as a fixed three level refinement within the spray region. Figure 3.14 shows the generated mesh, in a plane cutting the spray axes for two different instants during an injection near TDC, and during piston expansion.

Two baseline operating conditions that were measured in the single-cylinder engine are used to set-up and validate the CFD model. The first case corresponds with a mixing-controlled combustion of diesel, and the second to a partially premixed combustion using a RON95 gasoline as fuel. Accordingly, two different fuel surrogates, diesel2 available in CONVERGE and a primary reference fuel blend of 95% iso-octane and 5% n-heptane (PRF95), are selected to reproduce the physical properties of diesel and gasoline, respectively.

The injection rate profile was generated from the experimental database already available after the injector characterization (mass flow rate and spray momentum flux) performed in dedicated test rigs. The diesel-like injection process is simulated by the standard Droplet Discrete Model (DDM) [51], with a wall-film model to account for spray/wall interactions. Then, spray atomization and break-up are simulated by means of the Kelvin-Helmholtz-Rayleigh-Taylor (KH-RT) model [52], with a distribute injected parcels evenly throughout the cone spray, along with the O'Rourke model for droplet turbulent dispersion and collision, and the Frossling droplet evaporation model.

Turbulent flow is modeled using a RANS approach, by means of a renormalization group (RNG) k-ε model [53]. The Angelberger [54] wall-function model is used to resolve the wall-bounded flows, turbulence generated near-wall region, and account for wall heat transfer. This model accounts for both quasi-isothermal flow (for example, in intake pipes and compression during engine computations) and non-isothermal wall flow (for example, in the combustion chamber during combustion and in exhaust pipes).

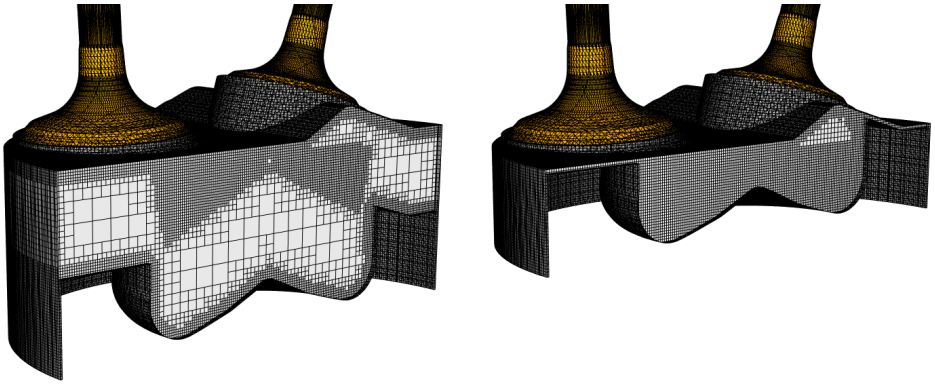

Figure 3.14. *Mesh refinement for an early injection event placed at* SoE -40 CAD aTDC *(left) and for an injection event near TDC at* SoE -2 CAD aTDC *(right).*

Concerning combustion modeling, a direct integration of detailed chemistry approach was used by means of the CONVERGE code and the SAGE solver. To accelerate the solution of detailed chemical kinetics, the multi-zone model [55] solves detailed chemistry in zones, i.e., groups of cells that have similar thermodynamic state. In a two-dimensional zoning strategy, the zoning is done based on two variables: the temperature and the equivalence ratio of the cells, in intervals of 5 K and 0.05 respectively.

For the baseline calculation with conventional diesel combustion, N-heptane is used simulate the ignition behavior of diesel fuel, with a reduced kinetic mechanism composed by 42 species and 168 reactions. For the PPC baseline calculation, a chemical mechanism of a PRF95 is used as surrogate to reproduce the ignition characteristic of the 95 octane gasoline. A well-validated skeletal reaction mechanism for PRF oxidation derived from the ERC-Multichem mechanism [56], with 45 species and 152 reactions was used for the fuel chemistry representation.

In particular, both mechanisms include the thermal path for NO_x formation according to the extended Zeldovich mechanism, and the N_2O path for accounting the NO_x formation at low temperatures, where the latter starts to gain relevance. A classical 2-step phenomenological soot model is used, with the Hiroyasu soot formation model [57] combined with a Nagle-Strickland-Constable (NSC) model [58] for soot oxidation.

Initialization, regions and boundary conditions

There are different options to initialize the physical variables such as velocity, pressure, temperature and species, for starting the calculation in CONVERGE: first, to specify uniform values for the entire geometry; second, to specify values for different regions of the domain if it is divided into regions; third, to use map fields by specifying three-dimensional location specific values, allowing each cell to be initialized individually.

For this investigation, it has been chosen to specify initialization values for the different individual regions of the computational domain. Three different regions are defined in the model for the fluid phase: *region 0* corresponding to the cylinder, *region 1* to the exhaust port and *region 2* to the intake port control volumes, respectively. Accordingly, the boundaries associated to each region are set as *fixed* walls (liner, ports, head...), *moving* surfaces (piston and valves) or *inflow/outflow* boundaries. For each boundary two types of conditions for initializing the partial differential conservation equations can be chosen: Dirichlet (specified value) and Neumann (specified first derivative value), as it is shown in equations 3.15 and 3.16, respectively.

$$\varphi = f \tag{3.15}$$

and

$$\frac{\partial \varphi}{\partial x} = f \tag{3.16}$$

where φ is a solved quantity (pressure, energy, velocity, species) and f is the specified value or specified derivative on the boundary. It is common to set the value of f is equal to zero for initializing the calculation. Other boundary conditions can be also specified (for example law-of-the-wall) but they are typically special cases of Neumann or Dirichlet. Table 3.10 summarizes the main boundary conditions used for the CFD calculations presented in this investigation.

The calculation is initialized at the exhaust valve opening timing (EVO), where the open cycle starts, and the values for the boundary conditions at this timing are defined either from experimental data directly measured at the single-cylinder engine, or from calculated data derived from the combustion diagnostics code (CALMEC). The mean wall temperatures of each boundary, as well as the fluid mean thermodynamic state (initial pressure and temperature) and its composition (mass fraction of each species) for each region at the EVO, are taken from the available results derived from the combustion diagnostics code.

Variable	Boundary condition	Value
Velocity	Law-of-the-wall	0 for fixed walls
		value* for moving surface (from law)
	Neumann	0 for inflow/outflow boundaries
Pressure	Neumann	0 for fixed/moving walls
	Dirichlet	value* for inflow/outflow boundaries (from experimental pressure)
Temperature	Law-of-the-wall	value* for fixed/moving walls (from CALMEC)
	Dirichlet	value* for inflow (from experiments)
	Backflow Dirichlet	value* for outflow (from experiments)
Species	Neumann	0 for fixed/moving walls
	Dirichlet	value* O_2, N_2, CO_2, H_2O for inflow (from CALMEC)
	Backflow Dirichlet	value* O_2, N_2, CO_2, H_2O for outflow (from CALMEC)
Passive	Neumann	0 for fixed/moving walls
	Dirichlet	1 for inflow
	Backflow Dirichlet	0 for outflow
Turbulent kinetic energy (tke)	Neumann	0 for fixed/moving walls
	Intensity	value* for inflow
	Backflow Intensity	value* for outflow
Turbulent dissipation (eps)	Dirichlet	0 for fixed/moving walls
	Length Scale	value* for inflow
	Backflow Length Scale	value* for outflow

Table 3.10. *Boundary conditions.*

The experimental instantaneous signals for the pressure at the intake and exhaust ports are used to define a temporally-varying pressure boundary condition for the inflow/outflow boundaries. The displacement of the intake/exhaust valves are expressed as a function of the crank angle, according to the given valve lift law, to define the velocity input for the translating moving boundary.

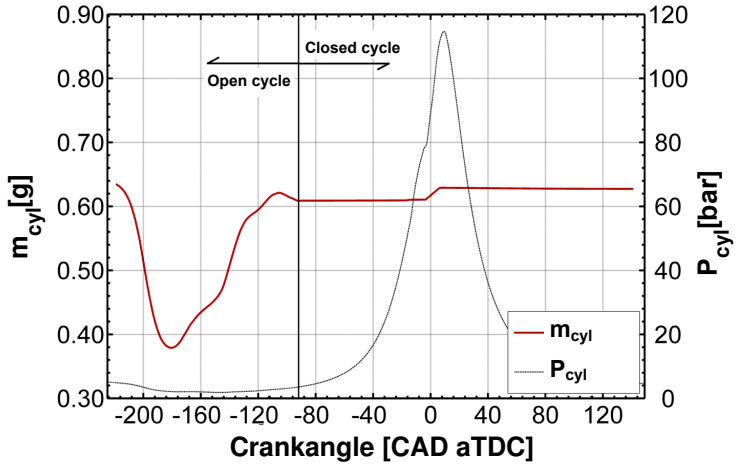

Figure 3.15. *Calculated cylinder mass during a complete engine cycle.*

Calculations run in the complete time gap between the exhaust valve opening (EVO) instants of two consecutive cycles, which corresponds to one full engine cycle.

Figure 3.15 shows the evolution of the calculated cylinder mass during the calculation time, to ensure that one cycle is sufficient to reach convergence between the initialized trapped mass value at EVO and its final calculated value after simulating the full cycle. The final trapped mass at the end of the calculation deviates in less than 5% compared to the initialized value, so multiple cycle approach was not implemented in this work to reduce computational time.

Model Validation

The validation of the CFD model was performed at two baseline operating conditions, the first case corresponds with a mixing-controlled combustion of diesel, and the second to a partially premixed combustion using a RON95 gasoline as fuel.

The quality of the model was evaluated by comparing its combustion and emissions results with those obtained experimentally in the engine. Figure 3.16 compares the CFD and experimental cylinder pressure and RoHR profiles.

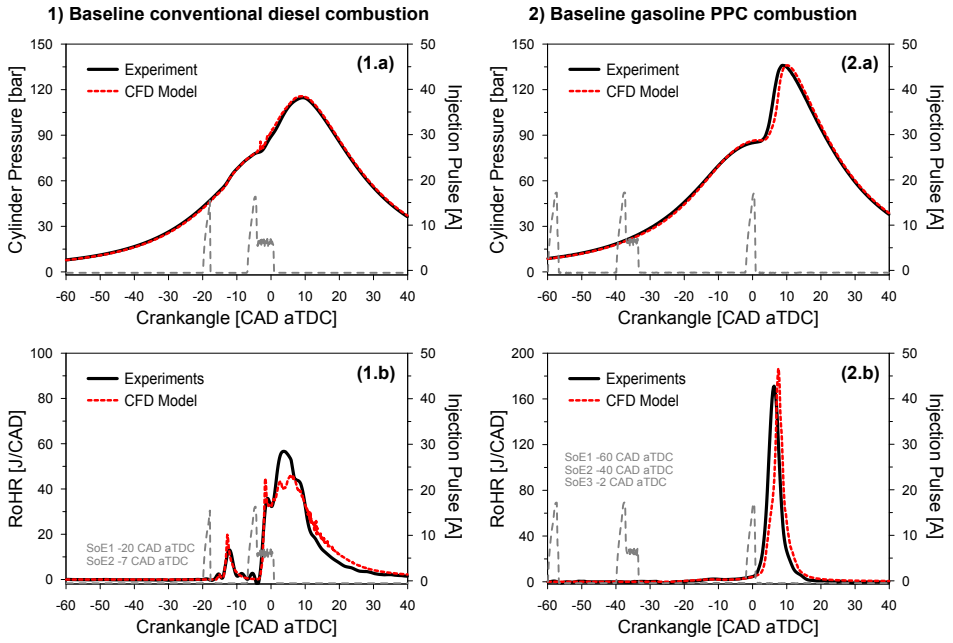

Figure 3.16. *Calculated and measured cylinder pressure and RoHR profiles for CDC (left) and Gasoline PPC (right) Baseline operating conditions.*

According to these results the experimental cylinder pressure evolution is correctly reproduced by the CFD model, however, there are some divergences observed in the RoHR profile, even after several attempts were carried out in order to improve its fit. Despite these differences, the CFD model performance is considered as suitable for being used along this research work, for improving the fundamental understanding of the air management and combustion processes in this two-stroke architecture.

Table 3.11 compares the key combustion and emission output results between experiments and the CFD model.

In general, predictions levels are in range compared to the measured data, but a clear difference in *HC* and *CO* emissions is detected in the case of gasoline PPC operation. After checking this result, it appears that the CFD model is not able to properly evaporate and burn the liquid film attached on the combustion chamber surfaces, what may explain the overestimation of these two pollutants when operating with the gasoline PPC concept and an early injection strategy. For future activities, a crevice model should be

	Baseline CDC		Baseline PPC	
	CFD	Experiment	CFD	Experiment
P_{max} [bar]	114.73	114.70	138.48	138.30
dP/da_{max} [bar/CAD]	5.90	4.50	17.79	17.78
CA50 [CAD aTDC]	7.82	6.10	7.40	6.30
η_{ind} [%]	45.06	45.75	46.92	46.76
NO_x [mg/s]	5.56	5.90	0.61	0.60
Soot [mg/s]	0.087	0.067	0.007	0.035
HC [mg/s]	0.01	0.30	12.03	9.14
CO [mg/s]	4.75	3.75	18.01	16.51

Table 3.11. *CFD model validation in CDC and gasoline PPC.*

incorporated to the calculation to account for blow-by losses and the fuel accumulated in the combustion chamber crevices. In the case of conventional diesel combustion, in the selected operating condition both liquid wall film and HC emissions are at very low levels, so the experiment-CFD model difference is considered to be acceptable.

3.6 Conclusions

This chapter introduced the most relevant features of the poppet valve two-stroke HSDI engine that has been developed in the framework of the POWERFUL Project. Similarly, the main geometrical characteristics and sub-systems of the single-cylinder research version of this two-stroke engine concept have been thoroughly described in section 3.2; along with the technical specifications of the fuels used in this investigation.

The details of the experimental facility used in this investigation were also explained in detail in section 3.3, including the different auxiliary systems needed to supply air, fuel, coolant and lubricating oil to the single-cylinder engine, as well as the required measurement equipment and sensors that are installed to sample pollutants emissions, and acquire and store the most important information related to the engine running condition and the test cell monitoring variables. Regarding the dedicated measurement and calculation procedures that were specifically developed for the study of the air management process on this two-stroke engine, it is interesting to remark the experimental measurement of the trapping ratio based on the tracer gas

method, as well as the thermodynamic estimation of the IGR and the cylinder-charge composition which is very important for the posterior analysis of the combustion process.

Furthermore, details about the testing procedure followed during the experimental test campaigns performed in the single-cylinder engine has been introduced in section 3.4, along with an example of the proposed static and dynamic verification protocols, that were used to ensure the correct measurement and repeatability of the experimental data that is reported in this investigation.

Finally, the theoretical tools that are going to be used to support the analysis of the experimental results were also reviewed in detail in section 3.5, with particular focus on the main hypothesis and assumptions that had to be made to obtain these theoretical models, as well as their field of application and their limitations. Special emphasis has been made to the multidimensional CFD model of the two-stroke engine under study, including the setup and validation of the model both in CDC and gasoline PPC operation.

The next two chapters will now focus on the analysis of the results obtained in the single-cylinder two stroke engine operating with these different combustion modes in order to fulfill the objectives defined in section 1.4 from Chapter 1. The definition of the methodology used to define the experimental studies and to perform the analysis and optimization of the results, will be briefly described at the beginning of each of the following two chapters, since it has been specifically developed to study in detail each particular combustion mode.

Bibliography

[1] Tribotte Pascal, Ravet Frederic, Dugue Vincent, Obernesser Philippe, Quechon Nicolas, Benajes Jesus, Novella Ricardo and De Lima Daniela. "Two Strokes Diesel Engine - Promising Solution to Reduce CO2 Emissions". *Procedia - Social and Behavioral Sciences*, Vol. 48, pp. 2295–2314, 2012.

[2] Obernesser Philippe, Quechon Nicolas and Servant Cedrid. *Two-stroke engine e.g. two-stroke diesel engine, has air deflector located downstream of part of seat in intake valve of intake duct, and directing air flow from intake duct towards lower part of combustion chamber*. France Patent FR20080053623, 2009.

[3] Payri R., Salvador F. J., Gimeno J. and Bracho G. "A new methodology for correcting the signal cumulative phenomenon on injection rate measurements". *Experimental Techniques*, Vol. 32 n^o 1, pp. 46–49, 2008.

[4] Payri R., Garcia J.M., Salvador F. and Gimeno J. "Using spray momentum flux measurements to understand the influence of diesel nozzle geometry on spray characteristics". *Fuel*, Vol. 84 n^o 5, pp. 551–561, 2005.

[5] *ASTM D1298-99 standard test method for density, relative density (Specific Gravity), or API gravity of Crude Petroleum and Liquid Petroleum Products by Hydrometer Method.* ASTM International, West Conshohocken, PA, 1999.

[6] *UNE-EN 228:2013. Combustibles para automocion. Gasolina sin plomo. Requisitos y metodos de ensayo.* ASOCIACION ESPANOLA DE NORMALIZACION Y CERTIFICACION (AENOR), 2013.

[7] *UNE-EN 590:2014. Combustibles para automocion. Combustibles para motor diesel (gasoleo). Requisitos y metodos de ensayo.* ASOCIACION ESPANOLA DE NORMALIZACION Y CERTIFICACION (AENOR), 2014.

[8] Domenech V. *Estudio de nuevas estrategias para el control de la combustion en modos parcialmente premezclados en motores de encendido por compresion.* PhD thesis. Universitat Politecnica de Valencia, Departamento de Maquinas y Motores Termicos, 2013.

[9] Payri Raul, Garcia Antonio, Domenech Vicent, Durrett Russell and Plazas Alejandro H. "An experimental study of gasoline effects on injection rate, momentum flux and spray characteristics using a common rail diesel injection system". *Fuel*, Vol. 97 n^o 0, pp. 390–399, 2012.

[10] De Rudder Korneel. *An approach to low temperature combustion in a small HSDI diesel engine.* PhD thesis. Universitat Politecnica de Valencia, Departamento de Maquinas y Motores Termicos, 2007.

[11] Hoppie L. O. "The Influence of Initial Fuel Temperature on Ignition Delay". In *SAE Technical Paper*, volume 820356. SAE International, 1982.

[12] Kubota Masaru, Yoshida Koji, Shoji Hideo and Tanaka Hidenori. "A Study of the Influence of Fuel Temperature on Emission Characteristics and Engine Performance of Compression Ignition Engine". In *SAE Technical Paper*, volume 2002-32-1777. SAE International, 2002.

[13] Chen G. "Study of fuel temperature effects on fuel injection, combustion, and emissions of direct-injection diesel engines". *Journal of Engineering for Gas Turbines and Power*, Vol. 131 n^o 2, 2009.

[14] Degobert Paul. *Automobiles and Pollution.* Editions Technip, 1995.

[15] Martyr A.J. and Plint M. A. *Engine Testing, 3rd Edition Theory and Practice.* Butterworth-Heinemann, 2007.

[16] *Instrumentation and techniques for exhaust gas emissions measurement. SAE Standards J254.* 1993.

[17] Christian R., Knopf F., Jasmek A. and Schindler W. "A new method for the filter smoke number measurement with improved sensitivity". *MTZ Motortechnische Zeitschift*, Vol. 54, pp. 16–22, 1993.

[18] Olsen D, Hutcherson G, Wilson B and Mitchell C. "Development of the Tracer Gas Method for Large Bore Natural Gas Engines: Part 2 Measurement of Scavenging Parameters". *Journal of Engineering for Gas Turbines and Power*, Vol. 124 n^o 3, pp. 686–694, 2002.

[19] Olsen D, Hutcherson G, Wilson B and Mitchell C. "Development of the Tracer Gas Method for Large Bore Natural Gas Engines: Part 1 Method Validation". *Journal of Engineering for Gas Turbines and Power*, Vol. 124 n^o 3, pp. 678–685, 2002.

[20] Benajes J. V., Lopez J. J., Novella R. and Garcia A. "Advanced Methodology for improving testing efficiency in a single-cylinder research diesel engine". *Experimental Techniques*, Vol. 32 n^o 6, pp. 41–47, 2008.

[21] Molina Santiago. *Influencia de los parametros de inyeccion y la recirculacion de gases de escape sobre el proceso de combustion en un motor Diesel*. PhD thesis. Universitat Politecnica de Valencia, Departamento de Maquinas y Motores Termicos, 2003.

[22] Davis P. W. and Peckham M. S. "Cycle-by-Cycle Gasoline Engine Cold Start Measurement of Residual Gas and AFR Using a Fast Response CO&CO2 Analyzer". In *SAE Technical Paper*, volume 2008-01-1649, 2008.

[23] Regitz S. and Collings N. "Study of Cycle-By-Cycle Air-to-Fuel Ratio Determined from the Exhaust Gas Composition and a Novel Fast Response Device Based on a Wide Band Lambda Sensor". In *SAE Technical Paper*, volume 2008-01-2439, 2008.

[24] Albert B. P. and Ghandhi J. B. "Residual Gas Measurements in a Utility Engine". In *SAE Technical Paper*, volume 2004-32-0029, 2004.

[25] Schwarz F. and Spicher U. "Determination of Residual Gas Fraction in IC Engines". In *SAE Technical Paper*, volume 2003-01-3148, 2003.

[26] Kolmel A., Spicher U., Dusterwald R. and Wytrykus F. M. "Analysis of Mixture Conditions Close to Spark Plug Location using a Time Resolved Gas Sampling Valve". In *SAE Technical Paper*, volume 982473. SAE International, 1998.

[27] Welling Orian and Collings Nick. "UEGO Based Measurement of EGR Rate and Residual Gas Fraction". In *SAE Technical Paper*, volume 2011-01-1289, 2011.

[28] Lapuerta M. *Un modelo de combustion fenomenologico para un motor Diesel de inyeccion directa rapido*. PhD thesis. Universitat Politecnica de Valencia, Departamento de Maquinas y Motores Termicos, 1988.

[29] Armas O. *Diagnostico experimental del proceso de combustion en motores Diesel de inyeccion directa*. PhD thesis. Universitat Politecnica de Valencia, Departamento de Maquinas y Motores Termicos, 1998.

[30] Lapuerta M., Armas O. and Hernandez J. J. "Diagnosis of DI Diesel combustion from in-cylinder pressure signal by estimation of mean thermodynamic properties of the gas". *Applied Thermal Engineering*, Vol. 19 n^o 5, pp. 513–529, 1999.

[31] Payri F., Molina S., Martin J. and Armas O. "Influence of measurement errors and estimated parameters on combustion diagnosis". *Applied Thermal Engineering*, Vol. 26 n^o 23, pp. 226–236, 2006.

[32] Molenkamp H. "Zur Genavigkeit der Brenngesetzrechnung eines Dieselmotors mit Nichtunterteiltem Brennraum". *MTZ Motortechnische Zeitschift*, Vol. 37 n^o 7-8, pp. 285–291, 1976.

[33] Woschni G. "A Universally Applicable Equation for the Instantaneous Heat Transfer Coefficient in the Internal Combustion Engine". In *SAE Technical Paper*, volume 670931. SAE International, 1967.

[34] Woschni G. "Die Berechnung der Wandverluste und der thermischen Belastung der Bauteile von Dieselmotoren". *MTZ Motortechnische Zeitschift*, Vol. 31 n^o 12, pp. 491–499, 1970.

[35] Payri F., Margot X., Gil A. and Martin J. "Computational Study of Heat Transfer to the Walls of a DI Diesel Engine". In *SAE Technical Paper*, volume 2005-01-0210. SAE International, 2005.

[36] Torregrosa A., Olmeda P., Degraeuwe B. and Reyes M. "A concise wall temperature model for DI Diesel engines". *Applied Thermal Engineering*, Vol. 26 n^o 11-12, pp. 1320–1327, 2006.

[37] Degraeuwe B. *Contribution to the thermal management of DI Diesel engines.* PhD thesis. Universitat Politecnica de Valencia, Departamento de Maquinas y Motores Termicos, 2007.

[38] Way R. "Methods for determination of composition and thermodynamic properties of combustion products for internal combustion engine calculations". *Proceedings of the Institution of Mechanical Engineers*, Vol. 190, pp. 686–97, 1976.

[39] Pastor Jose V., Javier Lopez J., Garcia Jose M. and Pastor Jose M. "A 1D model for the description of mixing-controlled inert diesel sprays". *Fuel*, Vol. 87 n^o 13-14, pp. 2871–2885, 2008.

[40] Desantes J. M., Pastor J. V., Garcia-Oliver J. M. and Pastor J. M. "A 1D model for the description of mixing-controlled reacting diesel sprays". *Combustion and Flame*, Vol. 156 n^o 1, pp. 234–249, 2009.

[41] Garcia-Oliver J.M. *Aportaciones al estudio del proceso de combustion turbulenta de chorros en motores diesel de inyeccion directa.* PhD thesis. Universitat Politecnica de Valencia, Departamento de Maquinas y Motores Termicos, 2004.

[42] Muniz L. and Mungal M. G. "Effects of heat release and buoyancy on flow structure and entrainment in turbulent nonpremixed flames". *Combustion and Flame*, Vol. 126 n^o 1-2, pp. 1402–1420, 2001.

[43] Kim T. and Ghandhi J. B. "Characterization of evaporating diesel sprays using exciplex laser-induced fluorescence". *Atomization and Sprays*, Vol. 13 n^o 5-6, pp. 535–559, 2003.

[44] Boree Jacques, Atassi Nidal, Charnay Georges and Taubert Lutz. "Measurements and image analysis of the turbulent field in an axisymmetric jet subject to a sudden velocity decrease". *Experimental Thermal and Fluid Science*, Vol. 14 n^o 1, pp. 45–51, 1997.

[45] Faeth G. M. "Evaporation and combustion of sprays". *Progress in Energy and Combustion Science*, Vol. 9 n^o 1-2, pp. 1–76, 1983.

[46] Linstrom P.J. and Mallard W.G. *NIST Chemistry WebBook, NIST Standard Reference Database Number 69.* National Institute of Standards and Technology, Gaithersburg MD, 20899. http://webbook.nist.gov., 2011.

[47] Naber Jeffrey D. and Siebers Dennis L. "Effects of Gas Density and Vaporization on Penetration and Dispersion of Diesel Sprays". In *SAE Technical Paper*, volume 960034, 1996.

[48] Payri R., Salvador F. J., Gimeno J. and Novella R. "Flow regime effects on non-cavitating injection nozzles over spray behavior". *International Journal of Heat and Fluid Flow*, Vol. 32 n^o 1, pp. 273–284, 2011.

[49] Desantes Jose M., Payri Raul, Pastor Jose M. and Gimeno J. "Experimental characterization of internal nozzle flow and diesel spray behavior. Part I: Non evaporative conditions.". *Atomization and Sprays*, Vol. 15 n^o 5, pp. 489–516, 2005.

[50] Senecal P. K., Richards K. J., Pomraning E., Yang T., Dai M. Z., McDavid R. M., Patterson M. A., Hou S. and Shethaji T. "A New Parallel Cut-Cell Cartesian CFD Code for Rapid Grid Generation Applied to In-Cylinder Diesel Engine Simulations". In *SAE Technical Paper*, volume 2007-01-0159. SAE International, 2007.

[51] Dukowicz J. K. "A particle-fluid numerical model for liquid sprays". *Journal of Computational Physics*, Vol. 35 n^o 2, pp. 229–253, 1980.

[52] Beale J.C. and Reitz R.D. "Modeling Spray Atomization with the Kelvin-Helmholtz/Rayleigh-Taylor Hybrid Model". *Atomization and Sprays*, Vol. 9 n^o 6, pp. 623–650, 1999.

[53] Han Zhiyu and Reitz Rolf D. "A temperature wall function formulation for variable-density turbulent flows with application to engine convective heat transfer modeling". *International journal of heat and mass transfer*, Vol. 40 n^o 3, pp. 613–625, 1997.

[54] Angelberger C., Poinsot T. and Delhay B. "Improving Near-Wall Combustion and Wall Heat Transfer Modeling in SI Engine Computations". In *SAE Technical Paper*, volume 972881. SAE International, 1997.

[55] Babajimopoulos A, Assanis D N, Flowers D L, Aceves S M and Hessel R P. "A fully coupled computational fluid dynamics and multi-zone model with detailed chemical kinetics for the simulation of premixed charge compression ignition engines". *International Journal of Engine Research*, Vol. 6 n^o 5, pp. 497–512, 2005.

[56] Brandl S., Graf B. and Rust A. "NVH Challenges and Solutions for Vehicles with Low CO2 Emission". *SAE Int. J. Passeng. Cars - Mech. Syst.*, Vol. 5, pp. 1084–1090, 2012.

[57] Hiroyasu H. and Kadota T. "Models for Combustion and Formation of Nitric Oxide and Soot in Direct Injection Diesel Engines". In *SAE Technical Paper*, volume 760129, 1976.

[58] Nagle J and Strickland-Constable RF. "Oxidation of carbon between 1000 - 2000 C". In *Proceedings of the Fifth Carbon Conference*, volume Proceedings of the Fifth Carbon Conference, pp. 154–164, 1962.

Chapter 4

Conventional diesel combustion in the poppet valve two-stroke engine

Contents

4.1 Introduction

As it was introduced in Chapter 3, the control of the air management and in-cylinder conditions on the two-stroke poppet valve scavenge type architecture is fundamental for both combustion development and final engine cycle efficiency, increasing significantly the complexity of the engine optimization and calibration tasks; mainly because there are multiple air management actuation levers to be controlled aside from the usual injection settings. Therefore, it is important to establish a proper experimental methodology when optimizing the combustion/emissions characteristics of this complex two-stroke engine.

Departing from this background, this chapter focuses on the evaluation of this newly-designed two-stroke engine concept considering air management, combustion, pollutant emissions and engine performance. Additionally, this research work aims to improve the understanding of the relation between the gas exchange process and the most important combustion-related parameters, which will determine the final exhaust emissions levels and engine fuel consumption.

4.2 Operating conditions and optimization targets

The required power output of the final two-cylinder engine definition is set to 45 kW while keeping constant torque from 1000 rpm to 3000 rpm. The evaluation of the performance, fuel consumption and exhaust emissions of the single-cylinder version of the poppet valve two-stroke engine concept is carried out on six different points ranging from low to high load operation. The part load points are selected to be representative operating conditions of the vehicle consumption in NEDC cycle simulations, while operating with the two-cylinder engine definition, as depicted in Figure 4.1.

The pollutant emissions and noise targets imposed along the evaluation of combustion concepts in the two-stroke engine, corresponds to the levels measured on an equivalent four-stroke diesel engine in terms of unitary displacement and geometry, keeping the standard mass production engine calibration developed to meet Euro 5 regulation [1]. Table 4.1 shows the selected operating points along with preliminary settings definitions (estimated

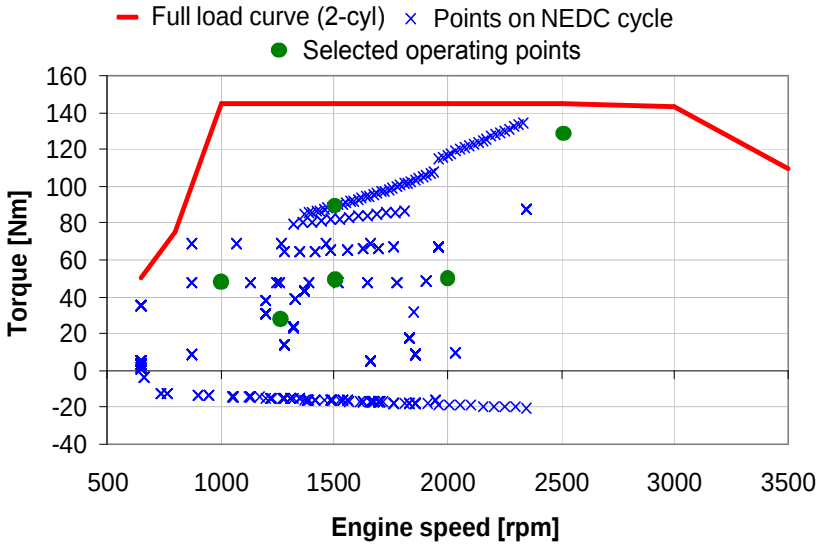

Figure 4.1. *Load requirements of the two-cylinder two-stroke engine and investigated operating points.*

for the single-cylinder research version through 1D GT-Power simulations), and the expected targets/limits in terms of combustion noise and exhaust emissions.

4.3 General methodology of the studies

In order to evaluate the performance of the two-stroke engine concept on a strictly controlled test environment, it was necessary to define a fast and efficient experimental test methodology, which was based on isolating the optimization process of the air management parameters from that of the injection parameters. This optimization is focused on finding the most suitable in-cylinder conditions necessary to fulfill the emission limits, especially in terms of NO_x and smoke, while minimizing the fuel consumption as much as possible. The optimization methodology was divided in two steps:

- Optimization of the air management settings by means of the Design of Experiment (DoE) and Surface Response Method (RSM) statistical techniques, to find proper in-cylinder conditions for a given operating

	Point 1	Point 2	Point 3	Point 4	Point 5	Point 6
Engine speed [rpm]	1250	1000	1500	2000	1500	2500
Torque [N m]	12.5	25	25	25	45	65
IMEP [bar]	3.1	5.1	5.5	5.8	10.4	15.1
BMEP [bar]	2.15	4.3	4.3	4.3	7.7	11.2
EGR rate [%]	20	20	20	20	15	15
Air mass flow [kg/h]	17	17.5	27	35	51.5	102
Fuel mass flow [kg/h]	0.40	0.57	0.87	1.21	1.68	4.00
Intake pressure [bar]	1.2	1.3	1.5	1.7	2.4	3.6
NO_x [mg/s]	0.45	0.75	0.75	0.55	2.15	28.2
HC [mg/s]	0.8	0.4	0.65	1.35	0.65	1.3
CO [mg/s]	4.95	1.95	4.4	9.1	18.65	3.7
Smoke [FSN]	1.44	0.96	0.56	0.73	4.6	0.27
Noise level [dB]	84.2	85.8	89.9	90.2	88.3	91.5

Table 4.1. *Operating points and expected performance and emissions targets for the single-cylinder two-stroke engine.*

point, while keeping constant injection settings. This will allow identifying the most important cause/effect relations and interactions between the air management parameters, the in-cylinder conditions, and consequently, combustion development and exhaust emissions. This approach provides more information with reduced number of tests compared to a more conventional parametric "one-factor-at-a-time" optimization approach, since it is possible to use response surface models to perform multi-objective optimization techniques [2–5].

- Parametric studies of the injection settings, at the global optimum point found with the DoE optimization while keeping constant air management settings. Since the relationship between the injection and the combustion processes in CDC are better-understood, a parametric approach is selected to perform the fine-tuning of the injection strategy focusing on the optimum combustion phasing and the final emissions levels.

As a reference for the reader, a detailed description of the proposed optimization methodology as well as a practical example to illustrate the analysis approach used along this investigation is presented in the Appendix A at the end of this chapter.

4.4 Preliminary study of the gas exchange process

As it was previously introduced in Chapter 3, the two-stroke engine under development offers a high flexibility in terms of controlling different air management settings, increasing significantly the complexity of engine optimization and calibration; mainly because there are multiple air management actuation levers to be controlled aside from the usual injection settings. As it was previously mentioned, the main issue typically found for poppet valve scavenge type configuration is how to cope with the compromise that inherently exist between achieving good scavenging and exhausting of the burnt gases out of the cylinder, while meeting the charging and trapping characteristics that are needed to get the proper fresh cylinder charge required for the combustion process [6–10].

So, to achieve a complete understanding of the CDC operation in the two-stroke engine under development, an in-depth understanding of the gas exchange process is consequently required.

Therefore, to identify and better understand the main trade-offs that are inherent to the poppet valve two-stroke architecture, a first experimental study of the gas exchange process has been designed to analyze the air management strategy solely and its main interactions with indicated efficiency and fuel consumption, without taking into consideration the optimization of the pollutant emissions at this initial stage. As a complement to this study, a detailed analysis of the cylinder flow pattern is carried out by means of the CFD model to provide additional information about the main temporal and spatial characteristics defining the scavenge process in this two-stroke engine.

4.4.1 Experimental characterization of the air management process

4.4.1.1 Overview of the study

The main air management settings chosen as factors for the air management DoE are the intake pressure (P_{int}), the difference between mean intake and exhaust pressures (ΔP), the intake VVT position (VVT_{int}), and the valve overlap duration ($Olap$). The exhaust pressure (P_{exh}) is defined accordingly from the intake pressure and the ΔP, while the exhaust VVT position (VVT_{exh}) is obtained from the intake valve timing and the overlap duration. The EGR rate is set equal to zero, since controlling NO_x emissions is not the main focus of this preliminary study. The engine operating condition

chosen corresponds to Point 5 with 1500 rpm and 10.4 bar of IMEP. The most relevant experimental conditions, in terms of air management and injection settings are described in Table 4.2.

Engine settings						
T_{int}	P_{int}	ΔP	P_{exh}	$VVT_{(int,exh)}$	$Olap$	EGR
[°C]	[bar]	[bar]	[bar]	[CAD]	[CAD]	[%]
35	min: 2.3	min: 0.5	1.4	min: (5,0)	58.4	0
	max: 2.7	max: 0.9	2.2	max: (15,30)	78.4	
IMEP	m_{fuel}	P_{rail}	SoE1	SoE2	SoE3	$\%fuel$
[bar]	[mg/st]	[bar]	[CAD]	[CAD]	[CAD]	[%]
≈ 10.4	19.3	1200	-17	-10	-	13/87/0

Table 4.2. *Engine settings for preliminary study of the air management process using DoE and RSM techniques.*

The ranges of variation for the air management settings selected as factors in the DoE are highlighted in gray in Table 4.2, and they were selected based on previous calculations that were made prior to this investigation using a 1D wave action model, combined with the knowledge gained from performing fast screening parametric tests on the single cylinder engine. The 36 points given by the DoE test plan were measured keeping the injection pressure (P_{rail}) at 1200 bar, while using 2 injection events, one small pilot injection of 2.6 mg/st placed at -17 CAD aTDC, and a main injection of 16.7 mg/st placed at -10 CAD aTDC. The total fuel injected mass (m_{fuel}) was set at the central point of the DoE to achieve the load target of 10.4 bar IMEP, and it was subsequently fixed for the rest of the points of the DoE.

After all the points of the DoE test matrix have been measured in the single cylinder engine, the statistical analysis of the mathematical models for different measured responses is performed following the optimization methodology presented in Appendix A. The different response models will not only serve to provide guidelines for optimization, but also for understanding the physical phenomena and existing relationships/trade-offs between air management settings (DoE factors) and the charging and scavenging process, and consequently, over the in-cylinder conditions, which are fundamental for posterior combustion optimization specially in terms of emissions levels and engine efficiency.

4.4.1.2 RSM and trade-off analysis

Figure 4.2 shows the response surfaces for TR, Q_{del} (which in this case is equal to Q_{air} since EGR is set to zero) and IGR, as function of the air management input factors. For plotting the response surface against two selected inputs, for instance $Olap$ and ΔP; the remaining two other inputs, which would be P_{int} and VVT_{int} in this case, are kept constant at their mid-range value.

As it was expected, the two-stroke poppet valve architecture inherently exhibits lower trapping efficiencies compared to a traditional four-stroke engine. The experimental data showed how all measured points in the DoE test plan were comprised inside a range of variation from 60 % to 90 % of trapping ratio. This typical characteristics of the two-stroke engine is primarily given by a combination of the positive ΔP between the intake and exhaust, along with the long overlap durations that are needed to attain good exhaust and scavenging of the burnt gases out of the cylinder, which added to the proximity between the poppet valves; makes it very difficult to balance the air charging and scavenging of the cylinder with the short-circuit losses [6, 11].

According to Figure 4.2, increasing ΔP results in a strong reduction in trapping ratio that is reflected in an increase in Q_{del} levels, from 43 kg/h to 71 kg/h, by the unavoidably increment of the short-circuit losses due to the cylinder flow path generated by the masking surface. Note that the direction of the axis for the Q_{del} plots has been reversed for allowing proper graphic representation of the response surface. Keeping suitable trapping ratio levels consequently would require decreasing valve $Olap$, to counteract the effect of high ΔP, since the overlap also has a strong influence over the short-circuited mass flowing from the intake to the exhaust.

Concerning the IGR ratio, the experimental results show how decreasing TR, therefore increasing Q_{del}, improved the scavenging of burnt gases out of the cylinder decreasing IGR from 36 % to 30 %, until a practical lower limit (around 30 %) was reach, from which further reductions in TR did not translate in better scavenging process. Moreover, the sacrifice in TR was much higher than the improvement observed in terms of IGR reduction, so it appears to be a strong trade-off between trapping and scavenging efficiencies that needs to be addressed when optimizing the air management settings. The intake pressure has a slight influence but much lower than that of ΔP and $Olap$, increasing TR and Q_{del} but also IGR with higher P_{int}; while VVT_{int} showed almost no effect over TR and Q_{del}, but a slightly higher impact on IGR, for a combination of early VVT_{int} and high values of P_{int}.

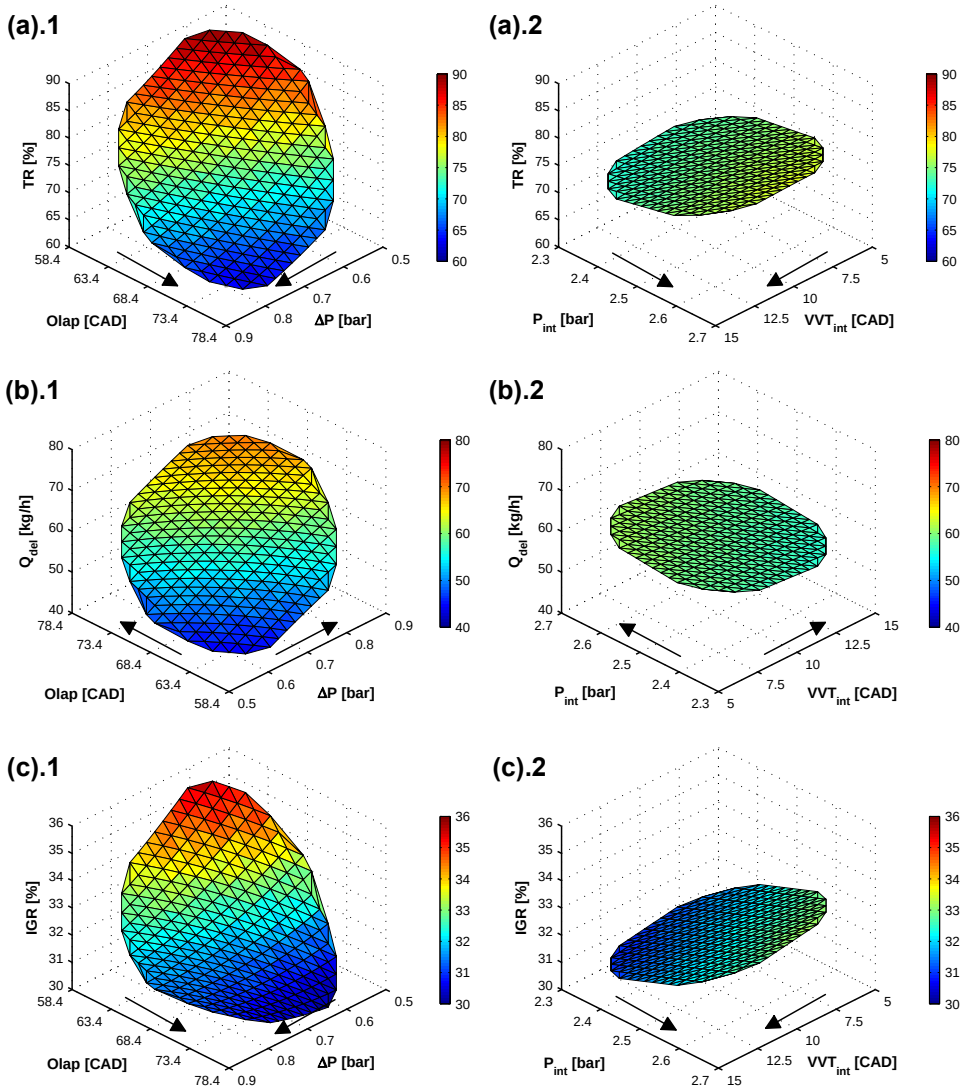

Figure 4.2. *Response surfaces for (a) trapping ratio (*TR*), (b) delivered flow rate (Q_{del}) and (c) IGR ratio (*IGR*) as function of the air management input factors.*

Another way to analyze the information derived from the DoE is to perform a trade-off analysis between different responses by plotting all the points (discretized in a fine grid) in the DoE space within the boundaries of the model. For instance, Figure 4.3 shows the relationship between TR and Q_{del},

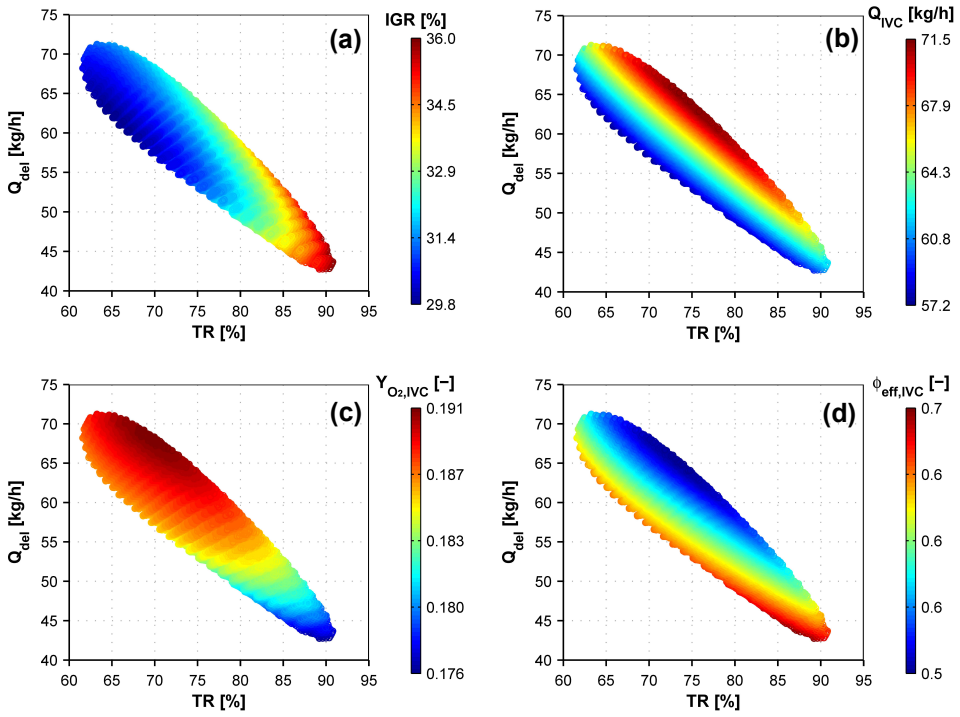

Figure 4.3. *Trade-off analysis for (a)* IGR*, (b) total cylinder charge Q_{IVC}, (c) in-cylinder oxygen concentration $Y_{O_2,IVC}$ and (d) effective equivalence ratio $\phi_{eff,IVC}$ as function of* TR *and Q_{del}.*

along with the IGR and the total cylinder charge (Q_{IVC}), and subsequently with the oxygen concentration at IVC ($Y_{O_2,IVC}$) and the effective equivalence ratio ($\phi_{eff,IVC}$).

Figure 4.3(a) corroborates the trade-off that exists between TR, Q_{del} and IGR which was previously introduced in Figure 4.2. The lowest values of IGR (in the range of 30 %) are obtained at the points with high Q_{del} and low TR, corresponding to the combination of high $Olap$ (over 72 CAD), medium-to-high ΔP (ranging from 0.65 bar to 0.8 bar), medium-to-low P_{int} (lower than 2.5 bar) and relatively late VVT_{int} (later than 10 CAD aTDC). However, Figure 4.3(b) reveals that the highest values of Q_{IVC}, which will translate into higher in-cylinder density and enhanced mixing conditions, are obtained for the points exhibiting a compromise between TR and Q_{del}. So, Q_{IVC} is maximized at the expense of slightly higher IGR, keeping TR in the range of 68 % to 75 % and Q_{del} around 68 kg/h to 60 kg/h, which corresponds to points

with relatively high ΔP (above 0.7 bar), mid-range values of $Olap$ (around 68.4 CAD) and highest P_{int} (2.6 bar to 2.7 bar). Accordingly, Figure 4.3(c) confirm how increasing Q_{IVC}, also increases the oxygen concentration at IVC due to a higher amount of fresh air trapped in the cylinder ($Q_{air,ret}$). Finally, this increase in $Q_{air,ret}$ is also reflected in lower values of $\phi_{eff,IVC}$, as it is shown in Figure 4.3(d), which in addition corresponds to the zone within the DoE space with the most favorable in-cylinder conditions for enhancing the combustion process.

As it was introduced in Chapter 2, the conventional diesel combustion process is highly sensitive to the in-cylinder conditions, particularly to $Y_{O_2,IVC}$ and $\phi_{eff,IVC}$, which have a strong impact over the combustion characteristics and the formation and oxidation processes of pollutants emissions. This close relationship between the in-cylinder conditions and the combustion process, as well as the consequent impact over the emissions level, engine performance and final efficiency will be described in detail in the next section. However, in the case of the current DoE study it is still very interesting to analyze the impact of the air management settings over the engine performance in terms of indicated efficiency (η_{ind}) and ISFC, excluding the effect of EGR, which will be studied in detail in the next section.

Figure 4.4 shows the response surfaces for indicated efficiency (η_{ind}) and indicated specific fuel consumption (ISFC), as function of the air management input factors. The experimental data points measured along the DoE test plan shows that η_{ind} and ISFC are comprised in a range between 44 % to 48 % and 179 g/kW h to 193 g/kW h, respectively, with the optimum values found at the points with high ΔP, medium-to-high $Olap$, high P_{int} and late VVT_{int}. The indicated efficiency, and accordingly the ISFC, are conditioned by several factors: such as CA50, combustion duration and heat transfer losses during the cycle; which are given by the combustion process and are particularly sensitive to $Y_{O_2,IVC}$ and $\phi_{eff,IVC}$, but also the cycle configuration itself; which is sensitive not only to the combustion process but also to the lengths of the expansion and compression strokes given by the exhaust and intake valve closing timings, EVC and IVC respectively. Keep in mind that the EVC timing is controlled by the VVT_{exh}, which in the case of this DoE is given by the VVT_{int} position and the valve overlap, so the latest possible EVC timing is obtained for the combination of the latest VVT_{int} position and highest value of $Olap$.

Note that the lowest ISFC, or accordingly the highest η_{ind}, is found at the region with highest delivered air flow rate Q_{del} and lowest TR, where the scavenging process was improved so the IGR is at its possible minimum

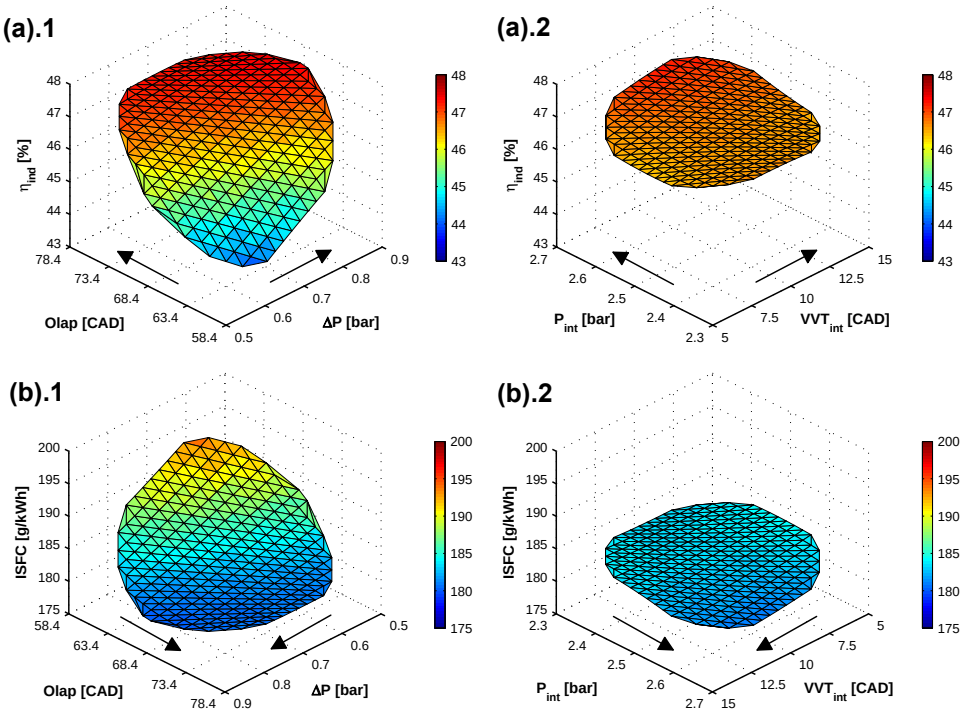

Figure 4.4. *Response surfaces for (a) η_{ind} and (b)* ISFC *as function of the air management input factors.*

value, nevertheless, this is achieved at the expense of increasing short-circuit losses which can be seen as "wasting" compressed intake air flowing directly into the exhaust. So, considering that the two-cylinder engine concept presents a double stage supercharging system, with a mechanical volumetric charger set downstream to a waste-gaste turbocharger [12, 13], it is valuable to estimate the energetic cost required to achieve the intake conditions, to obtain an approximation of the expected or "equivalent" indicated specific fuel consumption (denoted as $ISFC_{corr}$) which could be obtained on the two-cylinder engine. $ISFC_{corr}$ is calculated according to equation 4.1, by multiplying the ISFC measured in the single-cylinder engine with a factor that considers the effective power demanded by the supercharger ($Pw_{eff,SC}$) that would be taken from the indicated power (Pw_{ind}) delivered to the crankshaft.

$$ISFC_{corr} = ISFC \cdot \frac{Pw_{ind}}{Pw_{ind} - Pw_{eff,SC}} \tag{4.1}$$

This correction is useful for estimating qualitatively the increase in BSFC expected at the two-cylinder engine with fully assembled air charging system, and to avoid conditions which are not feasible in the two-cylinder engine due to very high pressure ratios or extremely high air flow rates, which would imply a high penalty in BSFC because of the high power demanded by the supercharger.

In order to provide a fast approximation of $ISFC_{corr}$ if all air loop devices were present, the effective power required by the supercharger is estimated by resolving simple mass and energy balances on the turbine, compressor and supercharger, considering the experimentally measured data (temperature, pressure and mass flow rates) as inputs for the calculation. The following assumptions were made to simplify the calculation:

- A constant value of 60 % efficiency is assumed for all the air loop devices. This simplification is slightly optimistic specially for points with low pressure ratios and low flow rates. However, it is still considered to be reasonable to get a qualitative estimation of the compression work, since at the moment of this investigation the real operating maps for the devices were not available.
- Atmospheric pressure (1 bar absolute) is set at the inlet of the first compression stage, neglecting any pressure drop in the filter system.
- A pressure of (1.2 bar absolute) is set at the outlet of the turbine, assuming there are some pressure drops after the turbine from the other components of the exhaust system.
- The temperature at the inlet of the first compression stage is equal to the exhaust temperature experimentally measured in the exhaust manifold. This assumption considers that the turbine will be placed as close as possible to the engine. Nevertheless, this assumption is somewhat balanced since the exhaust temperature is expected to be relatively lower in the single-cylinder engine compared to the two-cylinder engine.

Figure 4.5 shows the trade-off that exists between ISFC and the estimated $ISFC_{corr}$, along with the in-cylinder conditions: IGR, Q_{IVC}, $Y_{O_2,IVC}$ and $\phi_{eff,IVC}$. As it was previously mentioned, the lowest ISFC values are obtained at the region where the lowest IGR and highest Q_{IVC} are found, as it can be seen in Figure 4.5, where the in-cylinder conditions are favorable for combustion with a high $Y_{O_2,IVC}$ and low $\phi_{eff,IVC}$. However, these conditions are achieved with *Olap* higher than 70 CAD and ΔP above 0.8 bar, where

Q_{del} is at its maximum, therefore demanding a high power from the air loop devices, which in turn translates into the highest values obtained for $ISFC_{corr}$.

Moreover, the relationship between ISFC and $ISFC_{corr}$ within the DoE space depends on the combination between the four air management settings, but it is particularly influenced by the combination of $Olap$ and ΔP. For example, decreasing $\phi_{eff,IVC}$ by increasing $Olap$ (retarding EVC) but keeping low values for ΔP and medium-to-low values of P_{int}, will initially decrease both ISFC and $ISFC_{corr}$, until reaching a minimum in terms of $ISFC_{corr}$, from where further reductions in ISFC will not compensate any longer the increase in power demanded by the supercharger due to the higher Q_{del}, so $ISFC_{corr}$ will consequently start to increase. An additional factor that also increases $Pw_{eff,SC}$, consequently worsening $ISFC_{corr}$, is the fact that retarding EVC decreases the exhaust temperature (because the gases are cooled down to a lower temperature due to the longer expansion stroke), which will decrease the power delivered by the turbine, so in turn the compressor will have a lower pressure ratio output, requiring additional power on the supercharger to achieve the desired P_{int}.

Another example, is the case of points with low ΔP and medium-to-low $Olap$, where even when Q_{del} is at its lowest value, the worsened combustion conditions (high $\phi_{eff,IVC}$ and low $Y_{O_2,IVC}$) combined with earlier EVC lead to the highest value of ISFC, so the lower compression work does not compensate the losses in indicated efficiency, resulting in an increase in $ISFC_{corr}$. So, optimizing $ISFC_{corr}$ demands a good combination of initially medium-to-low ISFC with also medium-to-low Q_{del} to avoid too high power demands on the air management devices. Based on the previous results, the global efficiency of this two-stroke engine concept (specially in the case of the twin-cylinder engine) is expected to be extremely sensitive to the performance of the turbocharger and supercharger devices, reason why it should be carefully taken into consideration during future stages of engine development.

4.4.1.3 Model validation and optimization

The aim of the optimization process is to locate the points within the boundaries of the DoE which comply with the proposed optimization targets, which can be: finding the best possible combination in terms of emissions and ISFC, minimizing ISFC, or in the case of the current study, balancing the trade-off between ISFC and $ISFC_{corr}$. The optimization methodology and the accuracy of the predictions obtained with the response's models are

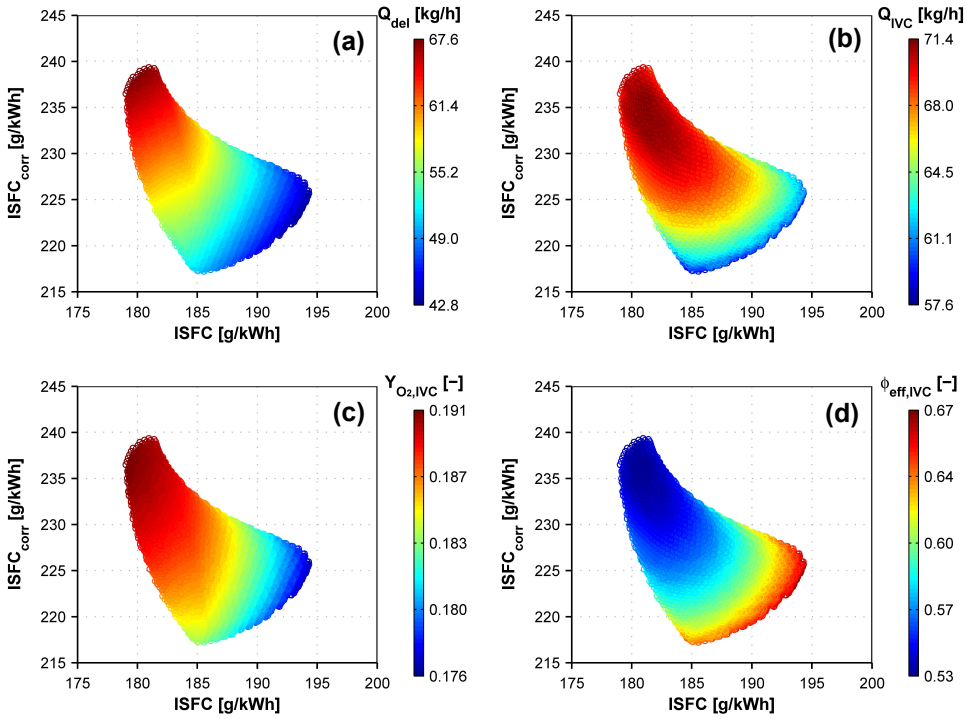

Figure 4.5. *Trade-off analysis for (a)* IGR*, (b) total cylinder charge Q_{IVC}, (c) in-cylinder oxygen concentration $Y_{O_2,IVC}$ and (d) effective equivalence ratio $\phi_{eff,IVC}$ as function of* ISFC *and $ISFC_{corr}$.*

validated by measuring experimentally different optimum points on the single-cylinder engine. Table 4.3 summarizes the air management settings of the final optimum point, that provided the best compromise between ISFC and $ISFC_{corr}$; while Table 4.4 shows the predicted and experimental results along with their corresponding percentage error between them.

Optimum DoE: Best trade-off ISFC/$ISFC_{corr}$				
P_{int} [bar]	ΔP [bar]	P_{exh} [bar]	$VVT_{(int,exh)}$ [CAD]	*Olap* [CAD]
2.45	0.5	1.95	(11,22)	74.4

Table 4.3. *Air management settings for the optimum point found during the optimization process.*

Optimum DoE: Best trade-off ISFC/$ISFC_{corr}$			
Responses	Predicted	Measured	Error [%]
Q_{del} [kg/h]	52.73	52.89	0.30
TR [%]	75.36	76.16	1.06
IGR [%]	30.6	30.9	0.98
Q_{IVC} [kg/h]	57.25	58.32	1.86
$Y_{O_2,IVC}$ [%]	18.51	18.51	0.03
$\phi_{eff,IVC}$ [–]	0.6457	0.6394	0.97
η_{ind} [%]	46.81	46.43	0.81
ISFC [g/kW h]	182.6	184.1	0.82
$ISFC_{corr}$ [g/kW h]	215.4	217.7	1.06

Table 4.4. *Validation of response models at the optimum point for the air management DoE study.*

These results confirm how the percentage of error between the predicted and measured responses is extremely low, below 2 % for every response. Thus, it has been proven that the testing methodology, the statistical analysis and the optimization criteria have been performed with high accuracy, providing the main guidelines to find the optimum operating conditions for achieving the expected optimization objectives.

4.4.2 CFD modeling of the air management process

The CFD model is used to calculate the conditions previously found along the DoE optimization at Point 5, keeping the settings shown in Table 4.3, to provide additional information about the main temporal and spatial characteristics of the air management process in this two-stroke engine. Figure 4.6 shows the temporal evolution of the experimental intake/exhaust and cylinder pressures, as well as the cylinder pressure obtained with the CFD model, along an engine cycle making emphasis on the gas exchange process. The valve timing angles (EVO, IVO, EVC and IVC) have been also included as a reference for the reader, so the open cycle is comprised between the EVO and IVC and the overlap period is comprised between the IVO and the EVC.

Three main sequential stages can be identified as follows:

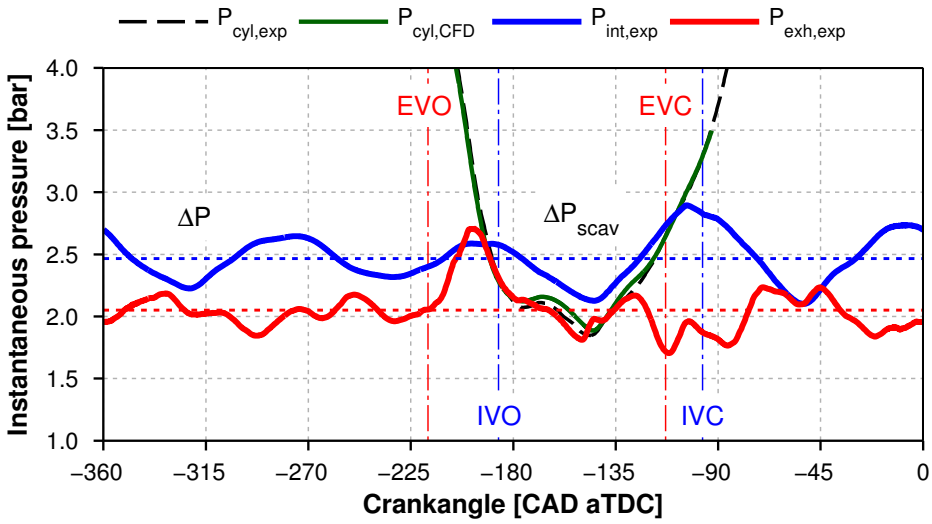

Figure 4.6. *Temporal evolution of intake/exhaust and cylinder pressures along an engine cycle.*

- Blow-down stage: Instants after the EVO, part of the cylinder mass is exhausted due to the high pressure drop between the cylinder and the exhaust manifold, so at the end of this process the cylinder and exhaust pressures equal.

- Scavenge stage: The IVO sets the beginning of the scavenge stage, where both intake and exhaust valves are simultaneously opened during the overlap period. In this case, due to the particular intake/exhaust valve timings the scavenge stage starts practically when the cylinder and exhaust pressures match.

- Supercharging stage: After the EVC, the cylinder pressure diverges from the exhaust pressure and increases progressively until reaching the intake pressure level. This is the time available for increasing the fresh air trapped mass and then cylinder gas density. In this stage it is also possible to observe some back-flow of trapped cylinder gases back to the intake duct.

The instantaneous difference between intake and exhaust pressures during the scavenge stage (which has been denoted as ΔP_{scav}) controls the correct air breathing, while the mean intake/exhaust pressure difference along the

whole engine cycle (already defined as ΔP) primarily determines the power demanded by the supercharger as it was already mentioned. Accordingly, increasing ΔP_{scav} which is strongly affected by the acoustic on the intake and exhaust, but also by the air management settings, promotes the replacement of the cylinder burnt gas by the fresh air needed for combustion and then improves engine ISFC. But as a counterpart, reducing ΔP along the cycle is mandatory to decrease the demanded compression power, and consequently keep $ISFC_{corr}$ as low as possible. The control of the previous trade-off mainly relies on the optimization of the engine acoustics for reducing ΔP while maintaining a suitable ΔP_{scav}. Note that at this operating condition ΔP_{scav} is almost constant during the whole overlap period which is desirable, but it still remains at a lower value than the cycle ΔP which is not the ideal situation to improve scavenging and control $ISFC_{corr}$.

Focusing in the supercharging stage, it is beneficial to produce an overpressure at the time of IVC by properly tuning the intake acoustics, as can be seen in Figure 4.6, to virtually increase the engine boosting at the final stage of the charging process and consequently increase the fresh air trapped mass. It is a challenge to properly tune the intake and exhaust manifolds geometries (lengths and diameters) to provide optimum acoustic behavior at the entire rpm range [6, 14], so the single-cylinder engine was particularly optimized for the mid-to-low engine speed range (below 2000 rpm) where most of the NEDC operating points are found, at the expense of sacrificing some performance at higher engine speeds.

The most important results concerning the global air management parameters obtained from the CFD calculation are shown in Figure 4.7; where the upper plot contains the calculated instantaneous intake/exhaust mass flow rates, as well as the short-circuited mass flow rate; while the bottom plot shows the scavenging law obtained for the given air management conditions by plotting the evolution of the burnt gas fraction in the exhaust $Y_{burnt,ehx}$ as function of the burnt gas fraction in the cylinder $Y_{burnt,cyl}$ along the open cycle.

Figure 4.7.(a) shows that the effect of engine acoustics on the exhaust flow rate is much more important than its impact on the intake flow rate, indicating that a correct tuning of the exhaust line is one fundamental factor for controlling the proper emptying and scavenging of the burnt gases. Additionally, at the end of the scavenge stage, between -135 CAD aTDC and -110 CAD aTDC, the majority of the exhausted flow is actually short-circuited fresh intake mass, so the short-circuit flow rate approaches the exhaust flow rate curve.

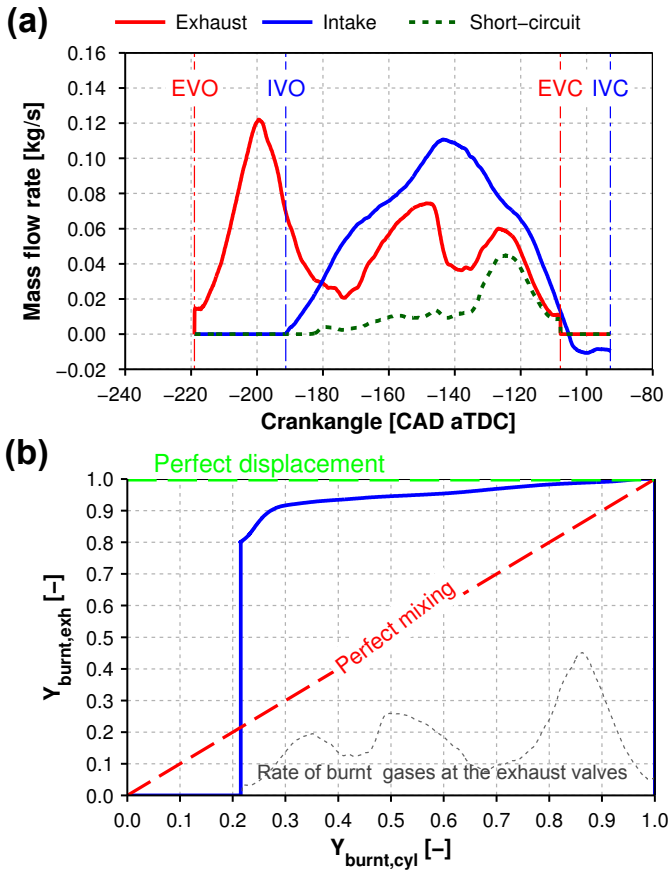

Figure 4.7. *Temporal evolution of global air management parameters. (a) Intake, exhaust and short-circuit mass flow rate. (b) Scavenging law.*

The evolution of the cylinder flow pattern during the scavenge stage in a section perpendicular to the symmetry axis at 1 mm from the cylinder head is shown in Figure 4.8. In this sequence of figures, pure residual gas is traced in red and corresponds to $Y_{fresh,cyl}$ equal to 0, while pure intake gas is marked in blue and corresponds to $Y_{fresh,cyl}$ equal to 1, so mixtures of both flows at a given fractions adopt values between 0 and 1.

The shape of the scavenging curve is an important feature characteristic of the cylinder head geometry. In this regard, Figure 4.7.(b) confirms that the cylinder head masking designed for this poppet valve two-stroke engine is actually effective to avoid the extreme short-circuit of fresh flow towards the exhaust side at least during the first half of the scavenge process. Figure 4.8

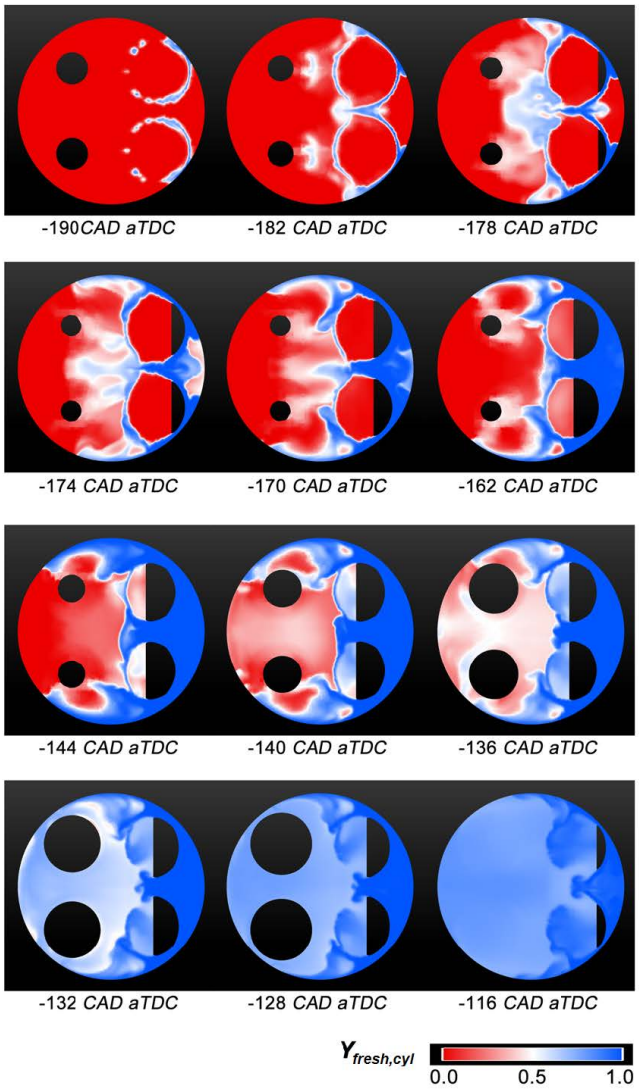

Figure 4.8. *Evolution of the cylinder flow pattern during the scavenge stage in a cut perpendicular to the symmetry axis at* 1 mm *from the cylinder head.*

confirm how initially the cylinder head masking avoids the direct short-circuit of intake gas, but the cylinder fluid-dynamics makes it possible for the intake gas to reach progressively the exhaust valves in the region close to the cylinder liner wall. Therefore, during the late scavenge stage the exhaust valve is

already surrounded by a gas mixture with high fraction of intake gas, so the cylinder head making is no longer effective. As a result, there is a breakpoint in the trend followed by the scavenging law near the end of the scavenge stage, from which the short-circuit losses starts to increase, which is reflected in a fall on the burnt gas concentration at the exhaust, confirming what was previously evidenced in the instantaneous mass flow rate across the valves. Closing the exhaust valves near this timing is convenient to avoid massive short-circuit losses and a dramatic fall in the trapping ratio.

Despite the loss of trapping efficiency at the late stage of the scavenging period, the scavenging curve given by this specifically optimized cylinder head geometry is much better than the theoretical perfect mixing curve (diagonal black line in the plot) or to what would be provided by a conventional four-stroke diesel flat cylinder head [12]. Keep in mind that even when the scavenging characteristics are specific to a given cylinder head design, the exploitation of this curve depends on the operating point and is conditioned by the air management settings.

To close the analysis of the air management process, Figure 4.9 shows the evolution of the cylinder flow pattern during the scavenge stage in two sections parallel to the symmetry axis at the center of the top and bottom valves near the end of the scavenge stage.

The spatial distribution of $Y_{fresh,cyl}$ evidences that a relatively homogeneous mixture of the residual gas and intake fresh gas is obtained at the end of the scavenge, where the mean fraction of fresh gases in the mixture ranges around 0.75-0.8. Nevertheless, there is a zone with slightly higher fraction of residual gas in the central area of the cylinder, caused by the tumble aerodynamics created by the masking on the cylinder head that forces the intake flow to travel close to the walls, thus, producing a stagnation zone with lower velocities in the core of the volume.

4.5 Analysis and optimization of the combustion process during CDC operation

After performing a preliminary analysis of the main characteristics defining the gas exchange process on this two-stroke engine architecture, the following studies will be focused on finding the most suitable in-cylinder conditions necessary to fulfill the emission limits in terms of NO_x and smoke, while minimizing indicated fuel consumption as much as possible, for different operating points selected from Table 4.1. Based on this objective, and

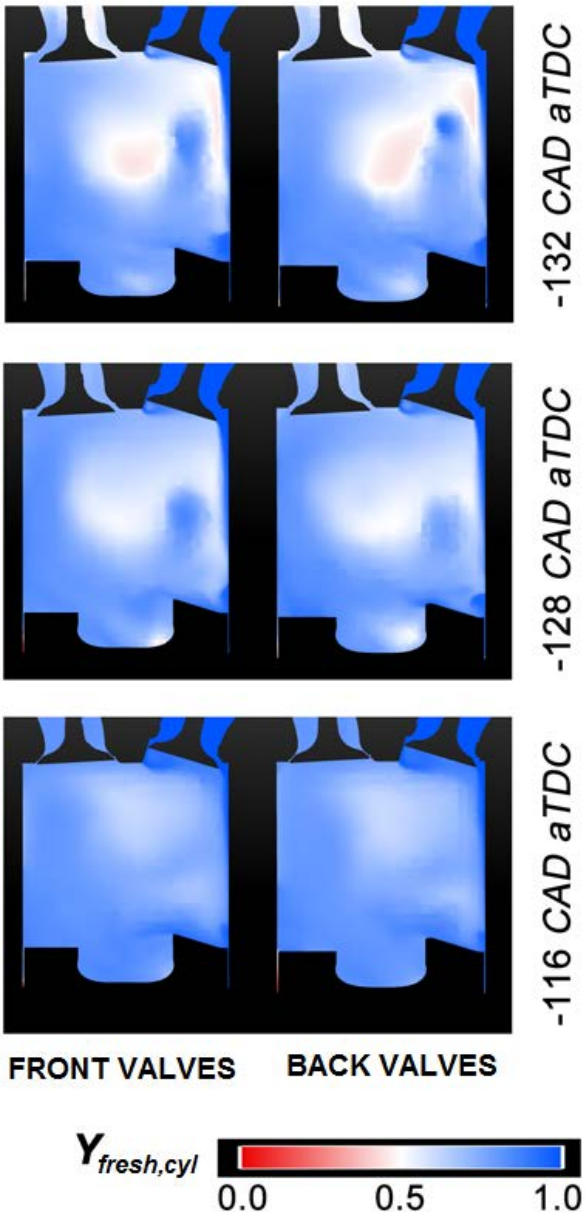

Figure 4.9. *Evolution of the cylinder flow pattern during the scavenge stage in two cuts parallel to the symmetry axis at the center of the top and bottom valves (end of scavenge stage).*

following the experimental methodology proposed in section 4.3, dedicated test campaigns for studying the air management characteristics have been carefully designed in order to find the optimum air management and injection settings to achieve the expected performance and emissions targets detailed in Table 4.1.

4.5.1 Medium load operation

4.5.1.1 Overview of the study

The engine operating condition representative of medium load operation corresponds to Point 5 with 1500 rpm and 10.4 bar of IMEP. The four factors chosen for this new DoE are the EGR rate (EGR), intake pressure (P_{int}), ΔP, and valve overlap ($Olap$). As it was demonstrated previously, the intake valve timing does not show a strong influence over the air management process and consequently over the final in-cylinder conditions, so it was kept constant at its optimum value obtained along the first DoE optimization, which corresponded to VVT_{int} equal to 13. Accordingly, the VVT_{exh} is defined from the intake timing (fixed) and the valve overlap duration (given by the DoE test plan).

The ranges of variation for the air management settings included as factors in the DoE as well as the main injection settings are included in Table 4.5.

The tests are performed keeping a constant injection pressure of 1000 bar and with two injection events, one small pilot injection of 2.0 mg/st placed at −21 CAD aTDC, and a main injection, for which the injected quantity and timing (SoE2) are slightly adjusted to maintain a constant value of 10.4 bar IMEP with CA50 phased at 6.8 CAD aTDC. Intake temperature is kept constant at 35 °C, while oil and water temperatures are also maintain constant at 90 °C.

The pollutant emissions and noise limits imposed along this evaluation of the performance of the two-stroke engine concept corresponds to the values shown in Table 4.1 for Point 5.

As a reference for the reader, a summary of the main results derived from the detailed analysis of the air management and combustion process, that will be described in the next subsections for this medium load condition (1500 rpm and 10.4 bar of IMEP), has been also included in the works of Benajes et al. [15].

Engine settings CDC - Medium Load Point 5						
T_{int}	P_{int}	ΔP	P_{exh}	$VVT_{(int,exh)}$	$Olap$	EGR
[°C]	[bar]	[bar]	[bar]	[CAD]	[CAD]	[%]
35	min: 2.4	min: 0.5	1.7	(13,18)	min: 70	min: 15
	max: 2.6	max: 0.7	2.1	(13,28)	min: 80	max: 25
IMEP	m_{fuel}	P_{rail}	SoE1	SoE2	SoE3	$\%fuel$
[bar]	[mg/st]	[bar]	[CAD]	[CAD]	[CAD]	[%]
10.4	$\approx 20.4^*$	1000	-21	-7^*	-	$10/90/0^*$

Table 4.5. *Engine settings for the DoE optimization at Point 5. *Both* m_{fuel} *and* SoE2 *have been slightly adjusted at some points of the DoE to keep constant values of* IMEP *and* CA50*.*

4.5.1.2 Discussion of results and trade-off analysis

4.5.1.2.1 Global air management characteristics

As it was previously discussed in section 4.4, both the TR and accordingly Q_{del} (which in this case is a mixture of fresh air and EGR) are two highly sensitive parameters to the air management settings. In the case of this new DoE, TR ranges from 63 % to 80 %, while Q_{del} ranges from 53 kg/h to 66 kg/h.

The trade-off between TR and Q_{del}, as well as the influence of the two most influential factors (ΔP and $Olap$) over the key air management parameters, are analogous to what was previously seen in Figure 4.2 for the first DoE. Accordingly, increasing ΔP and $Olap$ results in a decrease in TR and a consequent increase in Q_{del} by the higher short-circuit losses. So, to assure suitable trapping ratio levels is it necessary to keep medium-to-low values for both $Olap$ and ΔP. Intake pressure has slight effects on trapping ratio as it was previously shown, while the EGR rate shows a very small effect (that can be considered as negligible) over the trapping ratio as it was expected. Note that when introducing a given percentage of EGR, the fresh air flow is substituted accordingly by burnt gases to get the desired EGR rate, so the total Q_{del} is kept constant.

The previous study showed how decreasing TR improved the scavenging of burnt gases out of the cylinder, until reaching a lower limit, from which decreasing IGR furthermore was not possible. For this DoE study, the ranges for the air management parameters were predefined in advance to assure the lowest percentage of IGR. Within these ranges, IGR remained approximately

constant at levels of around 26 % to 27 %.

4.5.1.2.2 In-cylinder conditions

Focusing on the in-cylinder conditions, Figure 4.10 shows the response surfaces for Q_{IVC}, $Y_{O_2,IVC}$ and $\phi_{eff,IVC}$, as function of the air management input factors. The total cylinder charge Q_{IVC} is maximized at points with TR near its minimum and Q_{del} near its maximum, with values ranging between 66 % to 68 % and 63 kg/h to 65 kg/h, respectively. This condition is attained at the regions that exhibit relatively high values of ΔP in the range of 0.65 bar to 0.7 bar, medium-to-low values of *Olap* ranging between 76 CAD to 73 CAD and high P_{int} between 2.55 bar to 2.6 bar, as can be seen in Figure 4.10.(a).

Figure 4.10.(b) confirm how for this DoE $Y_{O_2,IVC}$ is primarily controlled by the EGR, as it was expected, so the effects of ΔP and *Olap* over $Y_{O_2,IVC}$ become less relevant because of the ranges chosen for the inputs. The cylinder effective equivalence ratio $\phi_{eff,IVC}$ is affected by both the EGR and P_{int}, as it can be seen in Figure 4.10.(c), but also by ΔP, whereas the *Olap* plays a much smaller role compared to the other three inputs. Note that the conditions with higher $Y_{O_2,IVC}$ and lower $\phi_{eff,IVC}$ are expected to provide the best environment for the combustion process, however, it is necessary to find a new compromise between $Y_{O_2,IVC}$, $\phi_{eff,IVC}$ and Q_{IVC} in order to attain the required targets in terms of NO_x and soot emissions.

4.5.1.2.3 Analysis of the combustion process

The combustion process showed a high sensitivity with respect to the cylinder conditions, and accordingly, to the air management process. Within the measured points of the DoE, the maximum cylinder pressure ranges from 105 bar to 115 bar, and it is phased around 8.4 CAD aTDC to 9.6 CAD aTDC. This maximum cylinder pressure is mainly determined by Q_{IVC}, as can be seen in Figures 4.11.(a) and (b), but is also affected by the cylinder absolute pressure at the IVC which is controlled by both the scavenging process and the *Olap*. The maximum pressure gradient ranges from 3.9 bar/CAD to 4.7 bar/CAD, while combustion noise ranges from 86 dB to 88 dB, which is in all cases lower than the expected target for this operating point, and is mainly influenced by the pilot injection and the ignition delay. Combustion duration traced by $CA90 - CA10$ is extended for conditions with lower

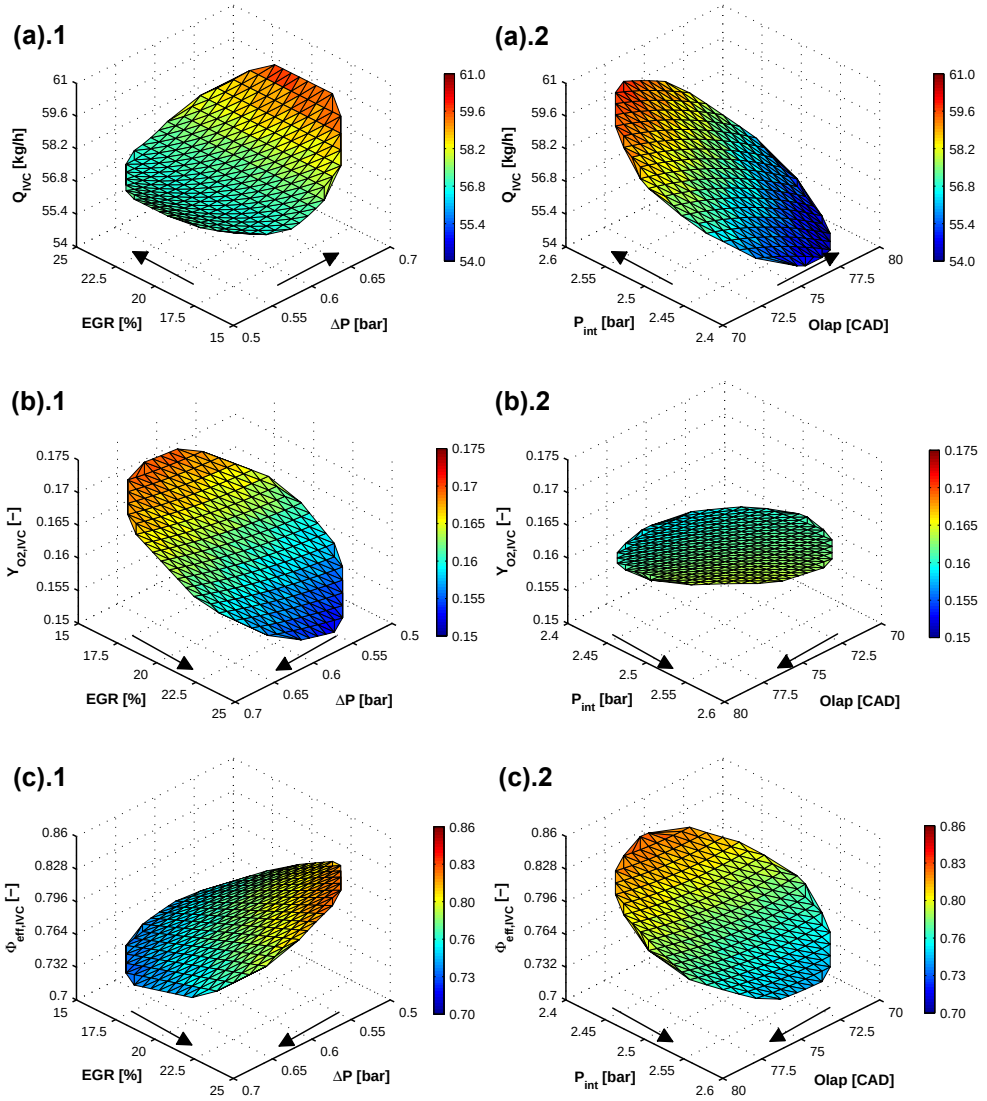

Figure 4.10. *Response surfaces for (a) total cylinder charge (Q_{IVC}), (b) in-cylinder oxygen concentration ($Y_{O_2,IVC}$) and (c) effective equivalence ratio ($\phi_{eff,IVC}$) as function of the air management input factors.*

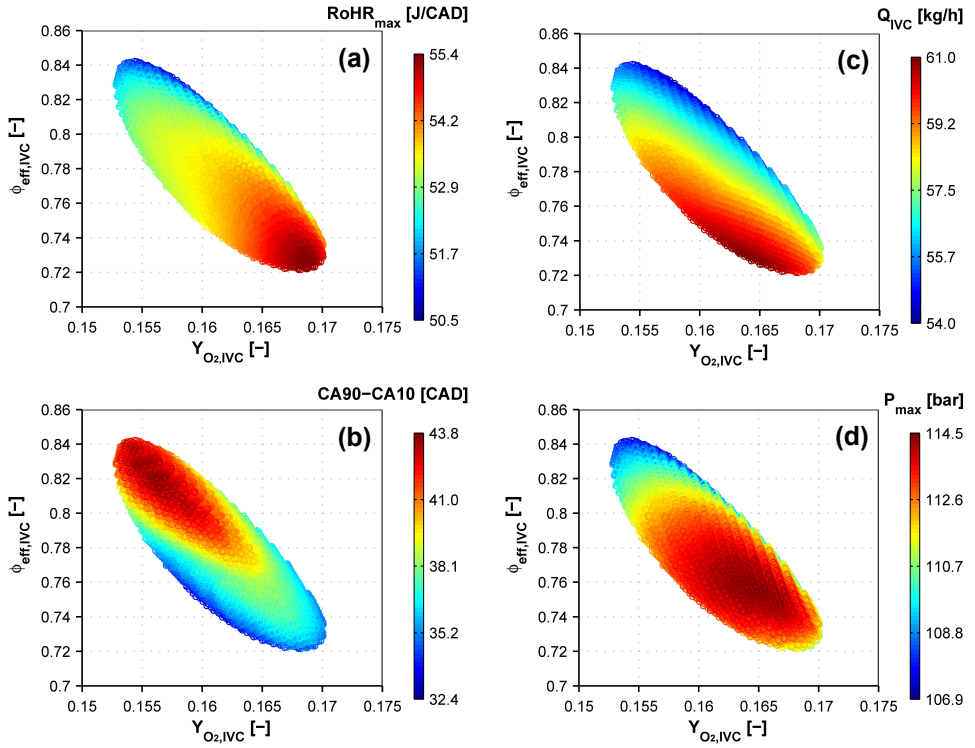

Figure 4.11. *Combustion characteristics: (a) total cylinder charge Q_{IVC}, (b) peak cylinder pressure P_{max} (c) peak rate of heat release $RoHR_{max}$ and (d) combustion duration as function of $Y_{O_2,IVC}$ and $\phi_{eff,IVC}$.*

$Y_{O_2,IVC}$ and high $\phi_{eff,IVC}$, as it was expected, and the slower and worsened combustion process is also reflected in a lower maximum on the RoHR, as confirmed by Figures 4.11.(c) and (d). Finally, combustion stability traced by CoV_{IMEP} remains below 1.2 % in all the DoE space, which is in the range of the levels typically observed for CDC operation.

It is more interesting to understand the relationship between the cylinder conditions and the combustion-related parameters, that are directly linked to the formation and destruction of pollutant emissions, specially in terms of NO_x and soot emissions, which are the two main responses to be optimized in this DoE. As it was discussed in Chapter 2, the thermal mechanisms involved in NO_x formation are chemically controlled and mainly determined by combustion temperature and oxygen availability at the flame periphery [16, 17]. Accordingly, studying local conditions in the cylinder during the combustion process is very important to calculate the local

reaction temperatures with precision, and make a reasonable prediction on NO_x emissions. Nevertheless, to keep the analysis of the main experimental trends on the basis of intuitive and easily obtainable parameters, a simplified approach have been chosen at this stage of engine optimization, which is based on calculating the peak adiabatic temperature ($T_{ad,max}$) at equivalence ratio 1, to qualitatively describe the trends followed by the maximum theoretical reaction temperature, which is expected to be the main factor linked to the formation of NO_x at high temperature diesel combustion. A similar analysis can be found in the works of Novella [18] and Kolodziej [19], both for mixing-controlled diesel combustion and diesel LTC conditions, so final comparison with experimental results confirms the relation between $T_{ad,max}$ and NO_x at least in qualitative terms. However, the use of advanced CFD models is mandatory if the objective is to perform a detailed analysis or more quantitative comparisons in terms of in-cylinder local conditions.

It is also known how the soot formed inside the flame is oxidized outside the flame around the stoichiometric zone, by the attack of OH-radicals which are thought to be the major mechanism responsible for soot oxidation in near stoichiometric conditions as in the case of diffusion flames. So, the late diffusive stage of combustion, between end of injection (EoI) and end of combustion (EoC), is critical for defining the final soot emissions level since the soot oxidation process is substantially slowed down due to the fast decrease of cylinder gas temperature and density. Accordingly, increasing local temperatures at the late stages of combustion and assuring the presence of oxygen is mandatory to increase the rate of formation of OH-radicals and enhance the soot oxidation chemical process [20, 21]. In this regard, both Novella and Kolodziej used the adiabatic flame temperature at the final stages of combustion to estimate the relative quality of late-cycle soot oxidation [22–24] For this investigation, the adiabatic temperature calculated at the time where 80 % of the fuel has been burnt ($T_{ad,80\%MBF}$) was considered as a suitable tracer of the late-cycle soot oxidation temperature.

Figure 4.12 illustrates the intrinsic relations between the key cylinder conditions, the combustion parameters and the NO_x and smoke emission levels. Figure 4.12.(a) clearly shows how decreasing $Y_{O_2,IVC}$ by increasing EGR rate, or by decreasing ΔP, will decrease $T_{ad,max}$, and consequently NO_x formation, due to the dilution effect of the inert exhaust gas inside the combustion chamber. However, as a counterpart, the reduction in fresh air trapped in the cylinder will increase $\phi_{eff,IVC}$. Additionally, the lower $Y_{O_2,IVC}$ also lead to a consequent reduction in the oxygen concentration and adiabatic temperature at the final stages of combustion, traced by $Y_{O_2,80\%MBF}$ and $T_{ad,80\%MBF}$ respectively, so the soot oxidation process is

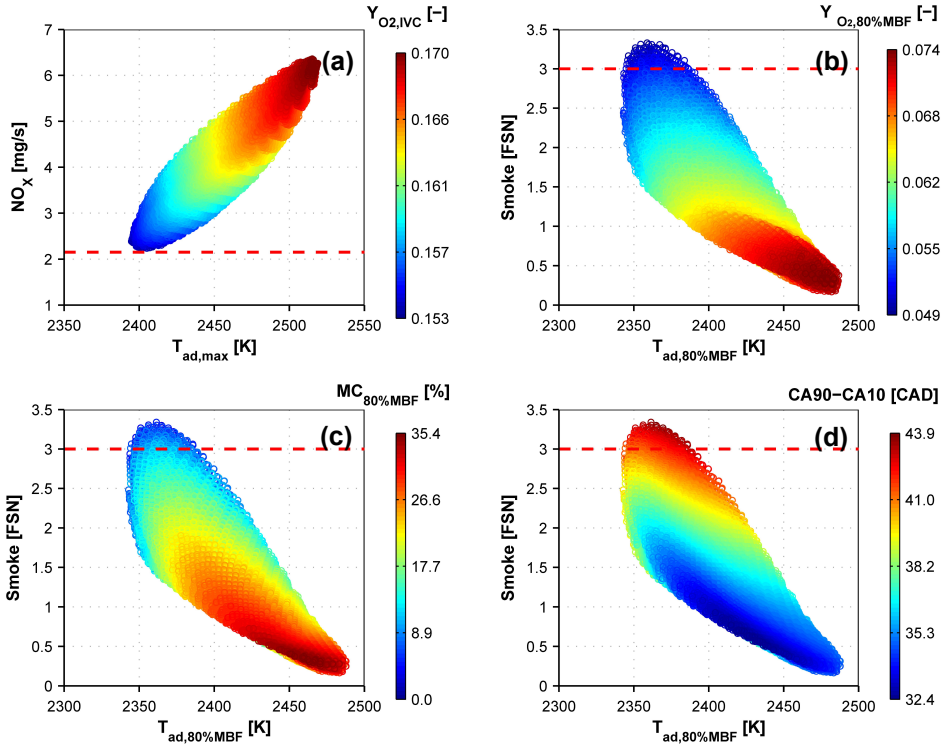

Figure 4.12. *Relation between combustion characteristics and emissions: (a) NO_x as function of $T_{ad,max}$ and $Y_{O_2,IVC}$, (b) smoke as function of $T_{ad,80\%MBF}$ and $Y_{O_2,EVO}$, (c) smoke as function of $T_{ad,80\%MBF}$ and $MC_{80\%MBF}$ and (d) smoke as function of $T_{ad,80\%MBF}$ and combustion duration.*

worsened as it is reflected by the increment in smoke emissions observed in Figure 4.12.(b).

It is worth to remark that soot oxidation is also controlled by other parameters besides the temperature at the final stages of combustion. Previous investigations have shown how for diesel sprays, the mixing process is controlled mainly by the injection parameters, the fuel properties and the in-cylinder conditions, specifically oxygen concentration and gas density [25]. Accordingly, the theoretical characteristic time required for a fuel particle injected in a steady state non-reactive gas jet to reach the stoichiometric conditions can be defined from the following the equation:

$$t_{mix} = K_1 \cdot \left(AFR_{stoich} \cdot \frac{YO_{2,atm}}{YO_{2,cyl}} \right)^2 \cdot \frac{\phi_0}{u_0} \cdot \sqrt{\frac{\rho_{fuel}}{\rho_{cyl}}} \tag{4.2}$$

where $K1$ is a constant that depends on the engine and its configuration, AFR_{stoich} is the stoichiometric air-fuel ratio, $YO_{2,atm}$ and $YO_{2,cyl}$ corresponds to the oxygen mass concentration at ambient conditions and inside the cylinder, u_0 is the injection velocity, ϕ_0 the injector nozzle diameter and ρ_{fuel} and ρ_{cyl} are respectively the density of the fuel and the density of the gas inside the cylinder.

Then, the mixing capacity defined as the inverse of the characteristic mixing time, can be used as a good qualitative indicator of the mixing rate of the spray; as reported in the works of Benajes et al. [21]. For this research in particular, since the injection parameters are kept constant along the tests, it is possible to approximate the mixing capacity as a function proportional to the in-cylinder oxygen concentration and gas density, as reported by Arrègle et al. in [25] for reactive conditions:

$$MC \propto \frac{1}{t_{mix}} \propto \sqrt{YO_{2,cyl} \cdot \rho_{cyl}} \tag{4.3}$$

The mixing capacity was calculated at the time where 80 % of the fuel has been burnt ($MC_{80\%MBF}$), to qualitatively represent the mixing conditions at the late diffusive combustion stage, which is crucial for the late soot oxidation process.

Figure 4.12.(c) shows how $MC_{80\%MBF}$ is also a key parameter controlling late soot oxidation, so the final smoke emissions can be also decreased by increasing Q_{IVC} and consequently cylinder gas density to improve the mixing conditions. Note that the points are presented as the percentage of improvement compared to the point which has the lowest mixing capacity. The points with high $Y_{O_2,80\%MBF}$ and high density have the highest mixing capacity, which results in an improvement in mixing conditions of around 35 % compared to the worst points, where both $Y_{O_2,80\%MBF}$ and cylinder density are at their lowest values.

It is worth to recall that the mixing capacity will account for the effects of both oxygen concentration and gas density, therefore the mixing rate will increase with higher Q_{IVC}, as it was previously mentioned, but also when combustion ends earlier in the cycle (traced by the combustion duration), so the final stage of combustion occurs at enhanced cylinder conditions, as confirmed by Figure 4.12.(d).

Finally, the NO_x-smoke trade-off will be used to present the range of variation of the most important emissions along the points of the DoE, and for linking the final emission levels to the engine fuel consumption.

4.5.1.2.4 Exhaust emissions and fuel consumption

Focusing on the NO_x-smoke trade-off, NO_x emissions ranges from 6.5 mg/s to 2.2 mg/s along the points of the DoE, while the smoke level sharply increases from 0.15 FSN to 3.18 FSN when NO_x is decreased. Figure 4.13.(a) shows CO emissions as function of the NO_x-smoke trade-off, and it confirms how CO follows the same trend as smoke emissions, so it sharply increases from 1 mg/s up to 22 mg/s when NO_x is decreased, exceeding the required target of 18.65 mg/s. HC emissions remained in the range of typical levels for CDC, but they are slightly above the expected target of 0.65 mg/s, ranging between 0.7 mg/s to 1.1 mg/s, as it is shown in Figure 4.13.(b), which is finally translated in combustion efficiencies above 98.5 % for all the range of the DOE.

In terms of engine performance, Figure 4.13.(c) illustrates how the ISFC is closely related with the emissions levels and therefore with the combustion process. As it was previously described, the points with medium-to-high $T_{ad,max}$ and enhanced mixing process have low smoke emissions, medium-to-high NO_x levels and also low ISFC, mainly because combustion takes place in a favorable environment for the fuel-energy conversion processes, where both $Q_{air,ret}$ and $Y_{O_2,IVC}$ are high and consequently $\phi_{eff,IVC}$ is low.

Figure 4.13.(d) confirms that there exists a trade-off between Q_{del} and $ISFC_{corr}$, but also shows that there is an optimum combination of air management settings that can provide low levels of both ISFC and $ISFC_{corr}$. As it was discussed previously in section 4.4, increasing Q_{del}, mostly by decreasing trapping ratio, causes a sharp increment in $ISFC_{corr}$ despite the almost constant ISFC level. In this case, the higher Q_{del} increases the power demanded by the air management devices, but it is not really used to improve the combustion process since most of the flow is directly bypassed. As a result, $ISFC_{corr}$ increases because the negligible benefits in ISFC does not compensate the increase in power demanded by the air charging devices, especially by the mechanical supercharger.

It is possible to find the cylinder conditions that provide the best compromise between the responses to be optimized, by calculating a merit function using equation A.1 from the Appendix A, for instance between NO_x, smoke and ISFC (denoted as $MF_{NO_x,smoke,ISFC}$), and also between NO_x,

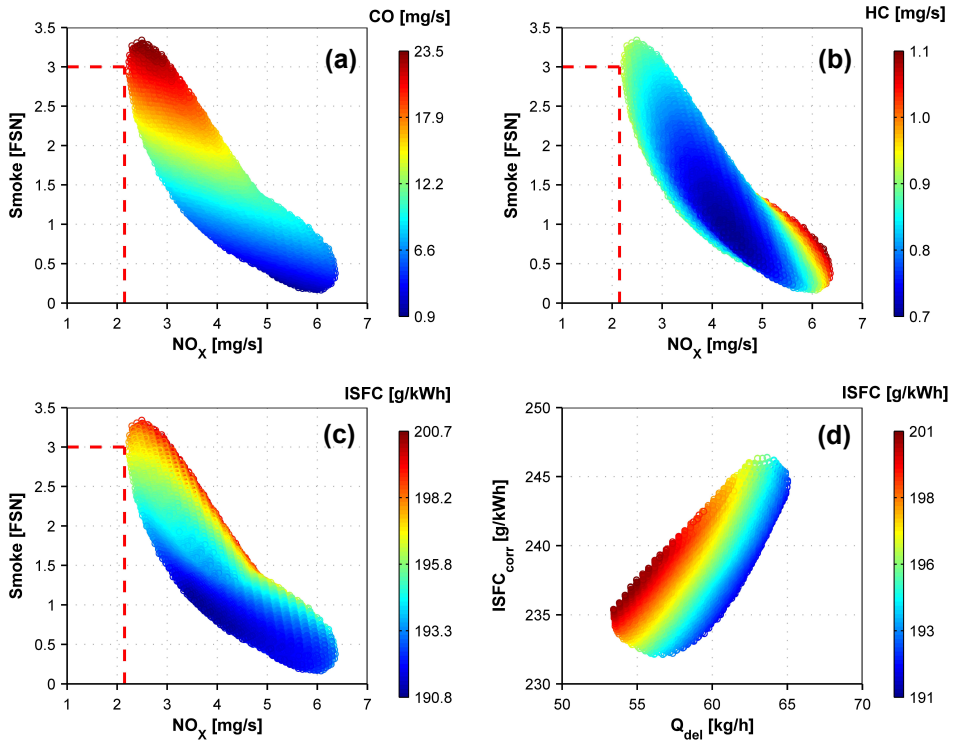

Figure 4.13. *Exhaust emissions and performance: (a) CO as function of NO_x and smoke, (b) HC as function of NO_x and smoke, (c)* ISFC *as function of NO_x and smoke, (d) and* ISFC *as function of Q_{del} and $ISFC_{corr}$.*

smoke and $ISFC_{corr}$ (denoted as $MF_{NO_x,smoke,ISFC_{corr}}$). This function allows for each combination of input parameters to be compared based on a set of desired targets or objectives for the responses. The same weight or emphasis on the optimization was applied for all the responses. Note that larger values of the merit function correspond to those combinations of the responses that better satisfy the desired objectives.

Two different optimization criteria have been selected to calculate the merit functions: first, to find the best trade-off between emissions and fuel consumption; and second, to fulfill the NO_x limit proposed in Table 4.1 while allowing higher smoke level and ISFC. Figure 4.14 shows $MF_{NO_x,smoke,ISFC}$ and $MF_{NO_x,smoke,ISFC_{corr}}$ for the two different optimization criteria.

If the optimization objective is to minimize simultaneously NO_x, smoke and ISFC (first criteria), it is clear how the maximum of the merit functions

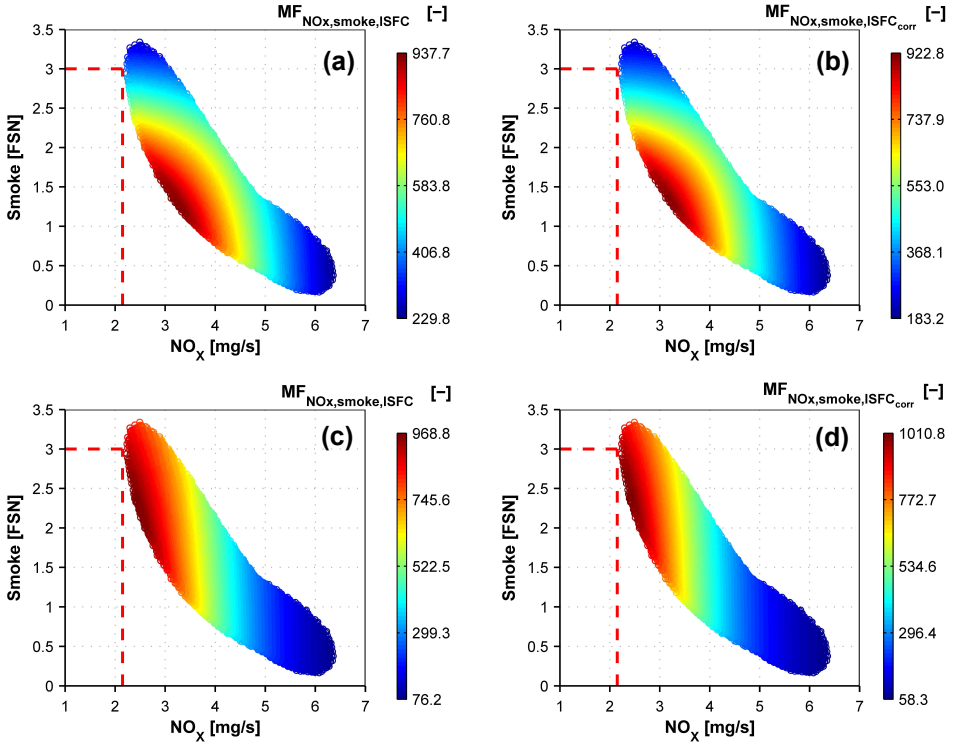

Figure 4.14. *Optimization results: (a) $MF_{NO_x,smoke,ISFC}$, (b) $MF_{NO_x,smoke,ISFC_{corr}}$ for best trade-off between emissions and fuel consumption; (c) $MF_{NO_x,smoke,ISFC}$, (d) $MF_{NO_x,smoke,ISFC_{corr}}$ for minimum NO_x.*

shown in Figure 4.14.(a) is observed at the best compromise between smoke and NO_x emissions, which means that it is possible to balance the NO_x-smoke trade-off without a strong penalty in terms of ISFC. The maximum values of $MF_{NO_x,smoke,ISFC}$ are found in the points with 1.2 FSN of smoke, 3.2 mg/s of NO_x, and 190 g/kWh of ISFC. In the case of $ISFC_{corr}$, even when the optimum point for the NO_x-smoke trade-off does not corresponds to the lowest $ISFC_{corr}$ (237 g/kWh against 232 g/kWh), the best combination between the three responses shown in Figure 4.14.(b) corresponds again with the same corner of the NO_x-smoke trade-off. Then, it is possible to optimize NO_x, smoke and ISFC simultaneously, increasing $ISFC_{corr}$ in less than 5 %.

If the optimization criterion is to minimize NO_x as much as possible, and considering that the targets established in Table 4.1 were 2.15 mg/s and 3 FSN respectively, it is necessary to find the set in-cylinder conditions with lowest $Y_{O_2,IVC}$ to move NO_x emissions closer to the limit. Figures 4.14.(c) and (d)

confirm that the maximum of the merit function is displaced accordingly to the points with lowest NO_x. Unfortunately, this will cause smoke and ISFC to increase up to 3 FSN and 200 g/kWh as it was shown in Figure 4.13.

4.5.1.3 Final optimization

The optimization methodology and model predictions were validated by measuring different optimum points directly on the engine. The experimental results confirm how the percentage of error between the predicted and measured responses is extremely low, below 2 %, so it will not be shown in the case of this DoE. Table 4.6 summarizes the most important engine settings chosen for these optimum points.

Final optimization CDC - Medium Load Point 5						
	P_{int}	ΔP	P_{exh}	$VVT_{(int,exh)}$	$Olap$	EGR
	[bar]	[bar]	[bar]	[CAD]	[CAD]	[%]
OPT1	2.54	0.58	1.96	(13,19)	71.0	25
OPT2	2.58	0.55	2.03	(13,24)	76.0	25
Final	2.58	0.55	2.03	(13,24)	76.0	26.8
	m_{fuel}	P_{rail}	SoE1	SoE2	SoE3	$\%fuel$
	[mg/st]	[bar]	[CAD]	[CAD]	[CAD]	[%]
OPT1	20.6	1000	−21	−8	-	10/90/0
OPT2	20.6	1000	−21	−8	-	10/90/0
Final	20.6	900	−21	−8.5	-	8/92/0

Table 4.6. *Engine settings for the optimum points found during the optimization process.*

The main experimental results in terms of air management, exhaust emissions and engine performance are shown below in Table 4.7. The first optimum point (named OPT1) was found keeping the minimum NO_x criteria, and choosing between the points that provided the maximum values for $MF_{NO_x,smoke,ISFC}$ and $MF_{NO_x,smoke,ISFC_{corr}}$. As it can be seen in Table 4.7, OPT1 has the lowest value of $Y_{O_2,IVC}$ and the highest $\phi_{eff,IVC}$ to achieve a NO_x level of 2.27 mg/s which remains closer but still higher than the expected NO_x target, while smoke level is close to its limit at 2.95 FSN. For the second optimum point (named OPT2) the air management settings were slightly

Final optimization CDC - Medium Load Point 5			
Responses	OPT1	OPT2	Final
TR [%]	73.1	71.3	71.4
IGR [%]	28.4	27.1	26.7
$Y_{O_2,IVC}$ [%]	15.1	15.45	15.19
$\phi_{eff,IVC}$ [−]	0.84	0.80	0.83
P_{max} [bar]	115.3	113.2	111.2
dP/da_{max} [bar/CAD]	4.2	4.5	4.4
Noise [dB]	86.1	87.0	86.4
NO_x [mg/s]	2.27	2.65	2.13
CO [mg/s]	16.36	7.8	13.02
HC [mg/s]	0.92	0.68	0.36
Smoke [FSN]	2.95	1.77	2.99
η_{comb} [%]	99.1	99.54	99.3
η_{ind} [%]	43.53	43.88	43.47
ISFC [g/kW h]	196.3	194.8	196.6
$ISFC_{corr}$ [g/kW h]	235.1	236.7	238.8

Table 4.7. *Main results obtained at Medium Load Point 5.*

modified (towards higher $Olap$ and higher P_{int}) to move closer to the optimum compromise between NO_x, smoke and ISFC; achieving a small improvement in terms of $Y_{O_2,IVC}$ and $\phi_{eff,IVC}$, and consequently, gaining some margin in terms of smoke emissions. Even when NO_x level is increased for OPT2 (2.65 mg/s), it is expected to be decreased down to the required limit after the fine-tuning of the injection settings. Accordingly, the Final optimum point is equivalent to OPT2 in terms of air management settings, except for a small difference in the EGR rate (26.8 instead of 25 %), and new injection settings obtained through a fast parametric optimization of P_{rail} and SoE2. At the end of the optimization process, it was possible to fulfill both NO_x and smoke limits, after decreasing P_{rail} and slightly retarding SoE2 to further decrease NO_x (achieving 2.13 mg/s), accepting a small penalty in terms of smoke, ISFC and $ISFC_{corr}$ (2.99 FSN, 196.6 g/kWh and 238.8 g/kWh respectively). Additionally, both CO and HC as well as the noise level remain below the required limits at the Final optimum, so all the expected targets in terms of combustion and exhaust emissions are successfully satisfied at this operating condition.

Finally, regarding indicated efficiency and fuel consumption, there is a clear penalty at this load condition in terms of η_{ind}, ISFC and $ISFC_{corr}$ when fulfilling the NO_x limits as it was expected, so the final levels obtained after the optimization are comparatively higher to what was previously seen in the first DoE, which focused solely on optimizing the air management characteristics and the final engine efficiency. Nevertheless, the final η_{ind} and ISFC levels obtained at this current stage of engine development are promising since they represented an improvement of 8 % in terms of ISFC compared to the reference four-stroke engine. The final comparison in terms of BSFC will have to be performed on the two-cylinder engine during the final engine calibration with the complete air charging and EGR loops as well as auxiliary systems, to really confirm the benefits of the two-stroke engine configuration against the conventional four-stroke engine.

4.5.2 Extension to high and low load operation

The optimization methodology proposed in the previous subsection 4.5.1 for medium load operation is also applied in an analogous way to the remaining five points detailed in Table 4.1; with the aim of optimizing the fuel consumption and emission levels at each operating condition. In general terms, the experimental results obtained at the other operating points corroborate how the two-stroke architecture have a high flexibility in terms of air management control, valve timing, EGR and intake boosting levels to substantially affect the in-cylinder conditions, and consequently the combustion development which determines final emissions level and indicated efficiency. Since the physical relations between the air management, combustion process and emissions formation are kept regardless the load, and additionally they have been already described in detail for medium load operation, the following subsections will briefly discuss the main differences as well as some interesting aspects observed in CDC when operating at low and high load conditions.

4.5.2.1 Optimization of low load conditions

4.5.2.1.1 Overview of the study

The most important aspects from the optimization of the CDC concept at two different low load points, Point 3 (with 1500 rpm and 5.5 bar of IMEP) and Point 1 (with 1250 rpm and 3.1 bar of IMEP) are going to be briefly summarized below.

According to the proposed optimization methodology, a central composite DoE was performed at each operating point considering the air management parameters included in Table 4.8 and Table 4.9, for Point 3 and Point 1 respectively, together with their ranges of variation. The IMEP target was set at the central point of the DoE and subsequently, the required fuel mass was slightly adjusted (by increasing or decreasing the main injection duration) in order to keep constant IMEP for all the points. Combustion phasing or CA50 was also kept constant at its optimum phasing for all DoE points, so the SoE of the main injection was adjusted to attain the required phasing.

Engine settings - Low Load Point 3						
T_{int}	P_{int}	ΔP	P_{exh}	$VVT_{(int,exh)}$	$Olap$	EGR
[°C]	[bar]	[bar]	[bar]	[CAD]	[CAD]	[%]
35	min: 1.6	min: 0.3	1.1	(13,18)	min: 70	min: 26
	max: 1.7	max: 0.5	1.4	(13,28)	max: 80	max: 36
IMEP	m_{fuel}	P_{rail}	SoE1	SoE2	SoE3	$\%fuel$
[bar]	[mg/st]	[bar]	[CAD]	[CAD]	[CAD]	[%]
5.5	≈ 10.6*	900	-19	-9*	-	21/79/0*

Table 4.8. *Engine settings for the DoE optimization at Point 3. *Both* m_{fuel} *and* SoE2 *have been slightly adjusted at some points of the DoE to keep constant values of* IMEP *and* CA50*.*

Engine settings - Low Load Point 1						
T_{int}	P_{int}	ΔP	P_{exh}	$VVT_{(int,exh)}$	$Olap$	EGR
[°C]	[bar]	[bar]	[bar]	[CAD]	[CAD]	[%]
35	min: 1.3	min: 0.15	1.05	(13,18)	min: 70	min: 18
	max: 1.5	max: 0.25	1.35	(13,28)	max: 80	max: 28
IMEP	m_{fuel}	P_{rail}	SoE1	SoE2	SoE3	$\%fuel$
[bar]	[mg/st]	[bar]	[CAD]	[CAD]	[CAD]	[%]
3.1	≈ 6.6*	450	-15	-5*	-	24/76/0*

Table 4.9. *Engine settings for the DoE optimization at Point 1. *Both* m_{fuel} *and* SoE2 *have been slightly adjusted at some points of the DoE to keep constant values of* IMEP *and* CA50*.*

In the case of the studies at low load, the ranges for the air management parameters were selected using previous knowledge acquired at medium load operation combined with fast-screening tests on the engine. Note that P_{int} and ΔP are accordingly reduced when decreasing the load, while the range for *Olap* is kept the same as for Point 5.

As a reference for the reader, a more thorough description of the trends observed in terms of air management, combustion characteristics and engine performance and emissions for Low load Point 3 (1500 rpm and 5.5 bar of IMEP) can be found in the work of Benajes et al. [26].

4.5.2.1.2 Summary of main trends

Focusing on the air management process, the main effects of the inputs (ΔP, *Olap*, P_{int} and EGR) over the trade-off between Q_{del} and TR are kept regardless the decrease in load, for both Point 3 and 1, with ΔP and *Olap* as the two most influential parameters similarly to what was already seen at medium load conditions. Q_{del} and TR range from 33 kg/h to 42.5 kg/h and 61 % to 78 % for Point 3, and 18 kg/h to 26.5 kg/h and 62.5 % to 73 % for Point 1. IGR remains approximately constant around 32 % to 36 % in the case of the DoE for Point 3, while for Point 1 it ranges from 41 % to 49 %, due to the comparatively lower ΔP used at this very low load condition. The total trapped charge Q_{IVC} is maximized at conditions that exhibit medium-to-low TR and relatively high Q_{del} values, that are given by a combination of high ΔP, medium *Olap* and medium-to-high P_{int}.

Finally, the trends followed by $Y_{O_2,IVC}$ and $\phi_{eff,IVC}$ for the results obtained at Point 3 are analogous to what was previously seen in Figure 4.10 for Point 5, so they are not shown. Accordingly, $Y_{O_2,IVC}$ is influenced mostly by the EGR rate, while $\phi_{eff,IVC}$ results from the combination of all four inputs, being *Olap* the less influential factor. However, in the case of Point 1 the effect of ΔP over the final $Y_{O_2,IVC}$ and $\phi_{eff,IVC}$ becomes as important as the effect of EGR, while *Olap* also gains some relevance, when compared against the trends previously observed for Point 5. So, the flexibility of the two-stroke engine in terms of air management settings to control the in-cylinder conditions is also confirmed at low load operation, where $Y_{O_2,IVC}$ and $\phi_{eff,IVC}$ are varied from 13.7 % to 16.2 % and 0.64 to 0.78 respectively for Point 3, and from 13.1 % to 17 % and 0.51 to 0.73 for Point 1.

Focusing on the combustion process, as the load decreases the effect of the ignition delay period (defined as the difference in CAD between the SoI and the SoC) starts to gain more relevance on the premixed phase

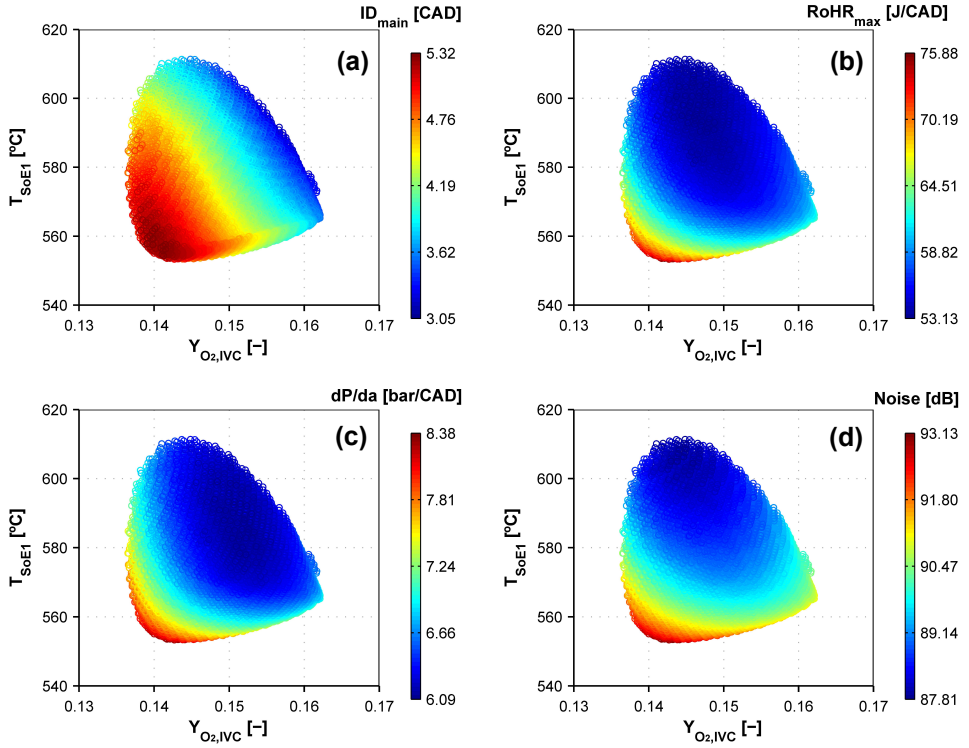

Figure 4.15. *Combustion characteristics: (a) ignition delay of the main injection ID_{main}, (b) $RoHR_{max}$ (c) dP/da_{max} and (d) combustion noise as function of $Y_{O_2,IVC}$ and T_{SoE1} for Low Load Point 3.*

of combustion of the RoHR, consequently affecting the maximum pressure gradient (dP/da_{max}) and the combustion noise, as the mixing-controlled stage of combustion becomes less predominant due to the smaller fuel quantity and shorter injection durations. In this regard, Figure 4.15 shows the ignition delay of the main injection (ID_{main}), $RoHR_{max}$, dP/da_{max} and combustion noise as function of $Y_{O_2,IVC}$ and the mean cylinder gas temperature at the SoE of the pilot injection (T_{SoE1}) for the results obtained at Point 3. Additionally, Figure 4.16 shows the RoHR and injection pulse, in the case of the three experimental points measured along the DoE test plan, that have constant injection timing for both pilot and main injections, but comparatively different $Y_{O_2,IVC}$ and T_{SoE1}.

Figure 4.15.(a) shows how the ignition delay is affected by both $Y_{O_2,IVC}$ and gas temperature during the injection process. So, the points exhibiting a combination of lower T_{SoE1} and comparatively lower $Y_{O_2,IVC}$ have

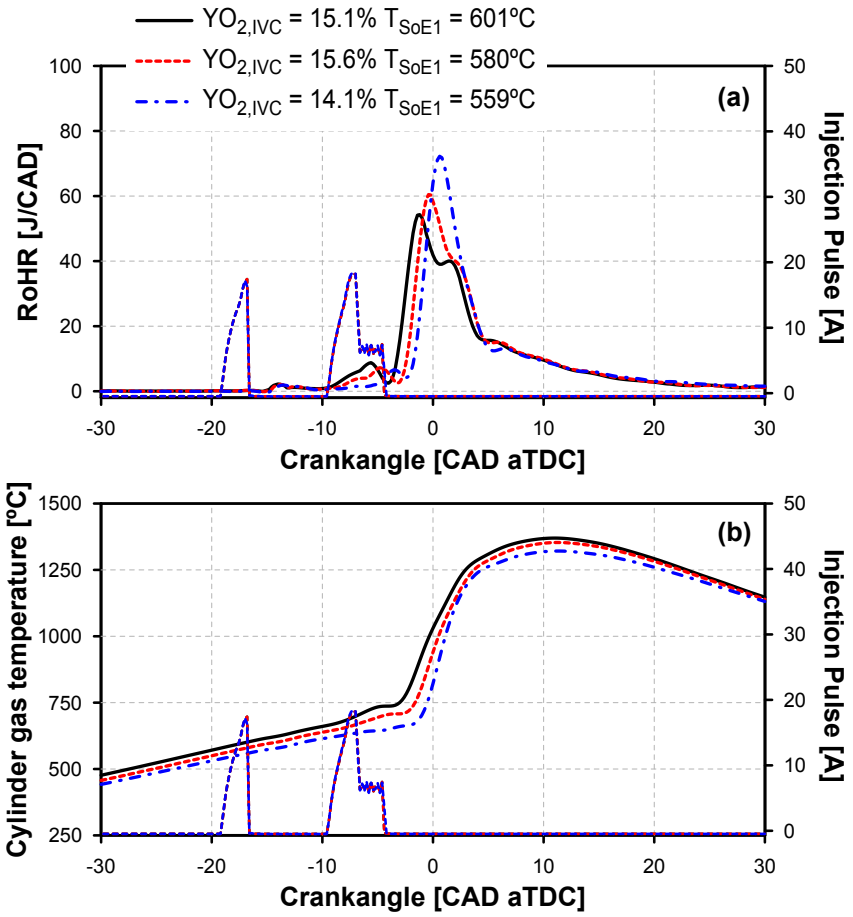

Figure 4.16. *Combustion characteristics: (a) RoHR and (b) Mean cylinder gas temperature for the three different $Y_{O_2,IVC}$ and T_{SoE1} conditions measured at Point 3.*

longer ID_{main}; resulting in a RoHR with predominant premixed combustion phase, as it is confirmed by Figure 4.16 in the case of $Y_{O_2,IVC}$=14.1 % and T_{SoE1}=559 °C. This particular condition exhibited higher $RoHR_{max}$ together with faster and sharper rise in the cylinder pressure; that caused an increase in dP/da_{max}, and consequently in noise level. On the contrary, when the ignition delay is decreased by increasing the $Y_{O_2,IVC}$ or T_{SoE1}, smoother combustion profiles with lower $RoHR_{max}$ and a more distinguished mixing-controlled phase are observed, as in the case of the two other points with

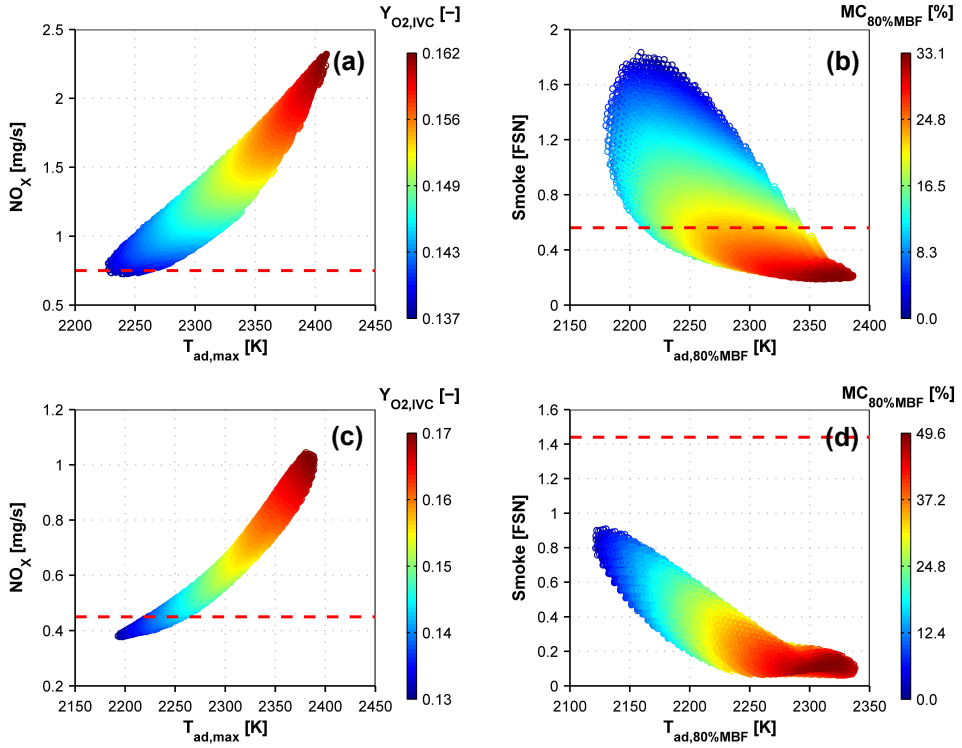

Figure 4.17. *Relation between combustion characteristics and emissions: (a) NO_x as function of $T_{ad,max}$ and $Y_{O_2,IVC}$, (b) smoke as function of $T_{ad,80\%MBF}$ and $MC_{80\%MBF}$ for Point 3, (c) NO_x as function of $T_{ad,max}$ and $Y_{O_2,IVC}$, (d) smoke as function of $T_{ad,80\%MBF}$ and $MC_{80\%MBF}$ for Point 1.*

$Y_{O_2,IVC}$=15.6 % and T_{SoE1}=580 °C, and $Y_{O_2,IVC}$=15.1 % and T_{SoE1}=601 °C, respectively shown in Figure 4.16.

Focusing on the effect of the in-cylinder conditions over NO_x and smoke emissions, Figure 4.17 shows how $Y_{O_2,IVC}$ has to be lowered below 14 %, to decrease $T_{ad,max}$ below 2250 K and slow-down the chemical reactions controlling the thermal NO_x formation. This reduction in $Y_{O_2,IVC}$ is necessary to get NO_x levels as close as possible to the required targets, both in the case of Point 3 and Point 1. However, decreasing $T_{ad,max}$ by increasing EGR or by affecting the air management conditions lead to a decrease in $T_{ad,80\%MBF}$, which slows down the late-cycle soot oxidation process and affect negatively the final smoke emissions. So, the best compromise on the NO_x-smoke trade-off is found at points where $T_{ad,max}$ is relatively low, but the mixing conditions are enhanced so $MC_{80\%MBF}$ is high, favoring the rate of

combustion and the late-cycle soot oxidation process. CO emissions, which are also controlled by the late-cycle oxidation processes, followed the same trend as smoke emissions in the case of the two low load points. This result also corroborates the direct relation between the conditions at the final stages of combustion ($T_{ad,80\%MBF}$ and $MC_{80\%MBF}$), the oxidation processes and the final CO and smoke emission levels.

Finally, the objective of the optimization process is to find the best possible trade-off between NO_x-smoke emissions that fulfill the required targets, while also minimizing ISFC and $ISFC_{corr}$ within the ranges of the DoE. Figure 4.18 shows $MF_{NO_x,smoke,ISFC}$ and $MF_{NO_x,smoke,ISFC_{corr}}$ for Point 3 and Point 1. From Figure 4.18, it is clear how the maximum of the merit functions $MF_{NO_x,smoke,ISFC}$ and $MF_{NO_x,smoke,ISFC_{corr}}$ is observed always at the best compromise between NO_x-smoke emissions for both low load points, which means that it is possible to minimize simultaneously NO_x and smoke without the existence of a trade-off between emissions and consumption.

4.5.2.1.3 Final optimization

At these conditions where the merit functions are maximized, NO_x and smoke levels are as close as possible to the expected limits, but the required levels are not yet achieved in the case of Point 3, whereas for Point 1 they are successfully attained for a group of points within the DoE space. The maximum values of $MF_{NO_x,smoke,ISFC}$ and $MF_{NO_x,smoke,ISFC_{corr}}$ are found at the points with 0.5 FSN of smoke, 1.1 mg/s of NO_x, 188 g/kWh of ISFC and 230 g/kWh of $ISFC_{corr}$ in the case of Point 3; and with 0.2 FSN of smoke, 0.5 mg/s of NO_x, 210 g/kWh of ISFC and 236 g/kWh of $ISFC_{corr}$ in the case of Point 3. Keeping this optimization criterion, a group of optimum points were experimentally measured on the engine to validate the predictions of the mathematical models and to choose the optimum air management settings where the fine-tuning of the injection strategy is performed. Table 4.10 and Table 4.11 summarizes the engine settings and most important experimental results in terms of air management, exhaust emissions and fuel consumption for the optimum points chosen for Point 3.

Table 4.11 shows how the NO_x levels reported at Point 3 for the two selected optimum points (OPT1 and OPT2) exceed the required target of 0.75 mg/s in both cases. However, these two points were chosen based on giving a higher priority to the required smoke limit (0.56 FSN), since further reductions in NO_x are expected to be achieved with the parametric optimization of the injection settings. Combustion efficiency ranges between

Final optimization - Low Load Point 3						
	P_{int} [bar]	ΔP [bar]	P_{exh} [bar]	$VVT_{(int,exh)}$ [CAD]	$Olap$ [CAD]	EGR [%]
OPT1	1.68	0.48	1.2	(13,21)	73.0	35
OPT2	1.68	0.42	1.26	(13,25)	77.0	34
Final	1.68	0.42	1.26	(13,25)	77.0	34
	m_{fuel} [mg/st]	P_{rail} [bar]	SoE1 [CAD]	SoE2 [CAD]	SoE3 [CAD]	$\%fuel$ [%]
OPT1	10.5	900	−19	−9	-	21/79/0
OPT2	10.5	900	−19	−9	-	21/79/0
Final	10.5	860	−21	−4	-	25/75/0

Table 4.10. *Engine settings for the optimum points at Point* 3*.*

Final optimization - Low Load Point 3			
Responses	OPT1	OPT2	Final
TR [%]	67.9	68.3	68.0
IGR [%]	37.3	36.4	35.8
$Y_{O_2,IVC}$ [%]	14.26	14.34	14.30
$\phi_{eff,IVC}$ [−]	0.71	0.72	0.71
P_{max} [bar]	80.7	78.6	68.1
dP/da_{max} [bar/CAD]	7.3	7.9	5.1
Noise [dB]	90.9	91.8	89.4
NO_x [mg/s]	1.09	1.07	0.73
CO [mg/s]	4.57	4.91	5.77
HC [mg/s]	0.41	0.43	0.5
Smoke [FSN]	0.43	0.46	0.38
η_{comb} [%]	99.4	99.4	99.2
η_{ind} [%]	45.6	45.2	47.9
ISFC [g/kW h]	187.6	189.0	178.1
$ISFC_{corr}$ [g/kW h]	229.7	227.1	217.4

Table 4.11. *Main results obtained at Low Load Point 3.*

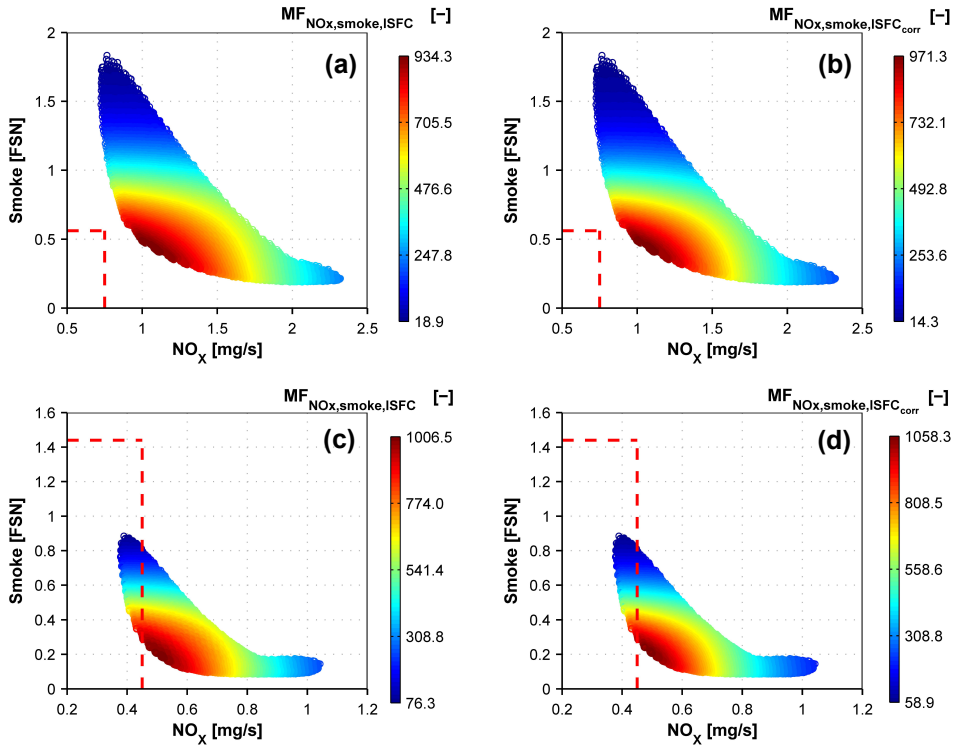

Figure 4.18. *Optimization results: (a)* $MF_{NO_x,smoke,ISFC}$*, (b)* $MF_{NO_x,smoke,ISFC_{corr}}$ *for Point 3; (c)* $MF_{NO_x,smoke,ISFC}$*, (d)* $MF_{NO_x,smoke,ISFC_{corr}}$ *for Point 1.*

99 % to 100 % while noise remains at acceptable levels close to the limit in both cases. In terms of engine performance, OPT1 allows achieving a slightly lower ISFC compared to OPT2, however, OPT2 is the optimum point in terms of $ISFC_{corr}$, so it was selected to continue the optimization process. The Final optimum point that was found after performing the detailed optimization of the injection settings exhibited a slightly lower P_{rail}, earlier pilot injection timing (SoE1) with higher injection quantity (so lower fuel quantity in the main injection), and retarded main injection timing (SoE2) compared to the settings used during the DoE optimization of the air management settings. By keeping these optimized engine settings it is possible to decrease both NO_x and smoke below the required limits (with 0.73 mg/s and 0.38 FSN at the Final optimum), without a penalty in ISFC or $ISFC_{corr}$, which are also improved with the new injection settings (178 g/kWh and 217 g/kWh respectively).

Final optimization - Low Load Point 1						
	P_{int} [bar]	ΔP [bar]	P_{exh} [bar]	$VVT_{(int,exh)}$ [CAD]	$Olap$ [CAD]	EGR [%]
OPT1	1.36	0.15	1.21	(13,27)	79.0	25
OPT2	1.4	0.16	1.24	(13,27)	79.0	26
OPT3	1.36	0.17	1.19	(13,28)	80.0	26
	m_{fuel} [mg/st]	P_{rail} [bar]	SoE1 [CAD]	SoE2 [CAD]	SoE3 [CAD]	$\%fuel$ [%]
OPT1	6.5	450	−15	−6	-	24/76/0
OPT2	6.5	450	−15	−6	-	24/76/0
OPT3	6.5	450	−15	−6	-	24/76/0

Table 4.12. *Engine settings for the optimum points at Point* 1.

Finally, HC and noise limits are also complied, however, CO emissions at this low load condition are slightly higher than the required limit.

In the case of Point 1, Table 4.12 and Table 4.13 summarize the engine settings and most important experimental results in terms of air management, exhaust emissions and fuel consumption obtained at this low load operating condition from the DoE optimization of the air management settings.

In this case, three points (OPT1, OPT2 and OPT3) with slight differences in P_{int}, ΔP, EGR and $Olap$ were selected to be measured on the engine. In terms of NO_x emissions, the required limit of 0.45 mg/s is fulfilled for the three points, as it can be seen in Table 4.13. Smoke, CO and HC emissions are also below the required limits for all the three optimum points, so the final selection is based on engine performance mostly. Combustion efficiency remains at 99 %, while noise limit is also attained in all the points. Finally, OPT3 is selected since it has the lowest ISFC and $ISFC_{corr}$ (208.4 g/kWh and 226.4 g/kWh respectively) from the three measured points. Departing from OPT3, a fast optimization of the injection settings was performed in order to check the optimum combustion phasing in terms of exhaust emissions level and engine performance. In this case, the fine tuning of the injection strategy did not show further improvements in terms of emissions or fuel consumption, so the Final optimum for Point 1 corresponds to the OPT3 obtained from the air management DoE optimization.

Final optimization - Low Load Point 1			
Responses	OPT1	OPT2	Final
TR [%]	68.2	68.1	67.7
IGR [%]	46.3	46.6	44.5
$Y_{O_2,IVC}$ [%]	14.0	14.34	14.62
$\phi_{eff,IVC}$ [−]	0.69	0.66	0.66
P_{max} [bar]	50.9	52.3	50.9
dP/da_{max} [bar/CAD]	3.9	4.1	4.5
Noise [dB]	82.9	83.3	84.3
NO_x [mg/s]	0.42	0.42	0.44
CO [mg/s]	3.3	3.45	3.71
HC [mg/s]	0.54	0.49	0.54
Smoke [FSN]	0.46	0.33	0.33
η_{comb} [%]	99.0	99.0	98.9
η_{ind} [%]	40.2	40.8	41.0
ISFC [g/kW h]	212.5	209.3	208.4
$ISFC_{corr}$ [g/kW h]	229.3	228.4	226.4

Table 4.13. *Main results obtained at Low Load Point 1.*

4.5.2.2 Evaluation of engine performance at full load

4.5.2.2.1 Overview of the study

To evaluate the performance of the two-stroke engine at full load conditions, Point 6 (with 2500 rpm and 15.1 bar of IMEP) is selected to perform a new optimization process and analyze the link between the gas exchange processes, the combustion development and the final emission levels.

But before performing the full engine optimization at this operating point, preliminary screening tests showed how the permeability of this two-stroke engine started to be compromised as the engine speed was increased due to worsened charging and scavenging characteristics, which are negatively impacted not only by the shorter available time to perform the gas exchange process, but also by stronger acoustic wave effects. In addition, the "wasted" cylinder volume occupied by the IGR also gains more relevance at full load conditions, where a proper utilization of the available fresh air trapped in

the cylinder as well as a fast mixing of the injected fuel are limiting factors controlling final soot emissions.

In this regard, a preliminary exploratory study was performed directly on the engine to compare the engine performance at high load/speed conditions; first, keeping unaltered the original exhaust system that has been used along the full engine optimization at medium-to-low load/speed points; and second, after replacing the original exhaust system with a new design which is better suited for high engine speed operation. The air management and injection settings selected for this preliminary evaluation are shown in Table 4.14. However, they are not considered to be optimized until performing a detailed optimization process.

As a reference, Test1 is measured with the original exhaust system, while Test2 is measured after replacing the exhaust system with the new configuration. Since the engine settings used in this study are not optimized, m_{fuel} was kept below the target proposed for Point 6, to avoid excessively high smoke emissions (over 4 FSN) and to keep $\phi_{eff,IVC}$ below 0.8, finally restricting the maximum load attained during these tests.

Figure 4.19 shows the experimental instantaneous pressures at the intake and exhaust manifolds, as well as the cylinder pressure and the main valve timing angles that were experimentally measured with the two different exhaust system configurations at this high load operating condition. For ease of understanding, the instantaneous pressures measured with the original exhaust configuration (Test1) are represented in dotted and light colored lines, while in the case of the adapted exhaust configuration (Test2) the profiles are shown in solid and dark colored lines. Additionally, Table 4.15 shows the most important results in terms of air management and engine performance obtained from this preliminary study.

Focusing on Figure 4.19, in the case of the original exhaust configuration (Test1) there is a noticeable reduction in ΔP_{scav} compared to the mean ΔP caused by an overpressure pulse in the exhaust that arrives in the middle of the scavenging stage, affecting negatively the exhausting of gases out of the cylinder, and consequently decreasing the cylinder head permeability and total fresh trapped mass in the cylinder. By modifying the exhaust system design with new lengths and diameters which are better tuned for high engine speeds, it is possible to shift this overpressure peak in the exhaust trace closer to the end of the scavenging period; therefore, allowing a higher ΔP_{scav} during the overlap period that improves both the exhausting and scavenging of burnt gases.

Preliminary study of exhaust configuration - High Load Point 6						
	P_{int} [bar]	ΔP [bar]	P_{exh} [bar]	$VVT_{(int,exh)}$ [CAD]	$Olap$ [CAD]	EGR [%]
Test1	3.6	1.0	2.6	(5,20)	80.0	0
Test2	3.6	1.0	2.6	(5,20)	80.0	0
	m_{fuel} [mg/st]	P_{rail} [bar]	SoE1 [CAD]	SoE2 [CAD]	SoE3 [CAD]	$\%fuel$ [%]
Test1	24.3	1600	–	−16	–	0/100/0
Test2	24.9	1600	–	−16	–	0/100/0

Table 4.14. *Non-optimized engine settings used for the preliminary study of the exhaust system configuration at Point 6.*

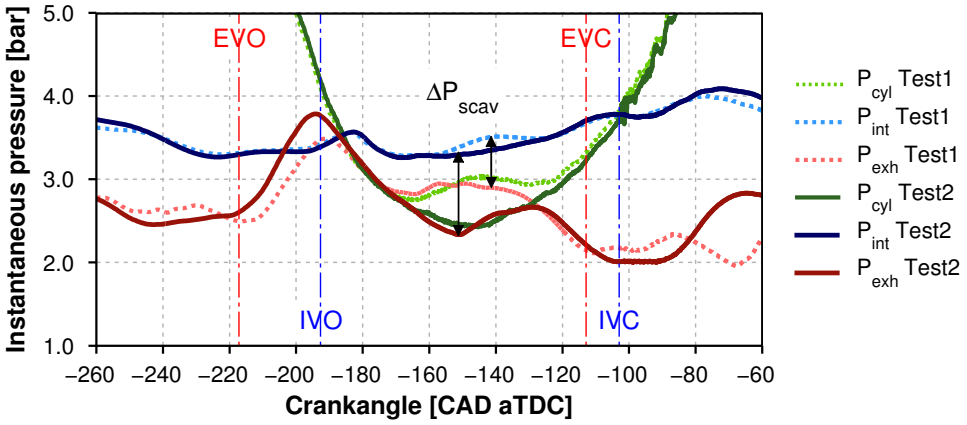

Figure 4.19. *Comparison of instantaneous intake/exhaust and cylinder pressures along the open cycle between original and adapted exhaust system configurations.*

Table 4.15 confirms that Test1 has comparatively lower $Y_{O_2,IVC}$ compared to Test2 due to lower fresh air trapped in the cylinder ($Q_{air,ret}$), which accordingly brings an increase in $\phi_{eff,IVC}$, as a result of the unfavorable acoustic behavior with the original exhaust configuration. The worsened combustion environment at Test1 is reflected in higher smoke and CO emissions, with 1.39 FSN and 14.31 mg/s, respectively, which exceeds the required limits of 0.27 FSN and 3.7 mg/s for Point 6; even when IMEP was kept at 12.05 bar compared to the target set for full load of 15.1 bar. The

Preliminary study of exhaust configuration - High Load Point 6		
Responses	Test1	Test2
Q_{del} [kg/h]	84.6	97.1
TR [%]	84.29	80.71
IGR [%]	32.93	27.9
Q_{IVC} [kg/h]	106.36	108.17
$Q_{air,ret}$ [kg/h]	79.39	86.66
$Y_{O_2,IVC}$ [%]	17.32	18.58
$\phi_{eff,IVC}$ [–]	0.76	0.71
IMEP [bar]	12.05	12.94
NO_x [mg/s]	21.05	21.64
CO [mg/s]	14.31	5.42
HC [mg/s]	1.21	2.23
Smoke [FSN]	1.39	0.45
ISFC [g/kW h]	199.2	190.0
$ISFC_{corr}$ [g/kW h]	227.2	219.1

Table 4.15. *Main results obtained at preliminary study of exhaust configuration at Point 6.*

new exhaust configuration allows increasing cylinder density and $Y_{O_2,IVC}$, due to higher Q_{IVC} and lower IGR, which is translated into higher $Q_{air,ret}$ and lower $\phi_{eff,IVC}$, even with relatively lower TR. The improvement in air management conditions obtained with the new exhaust at Test2 allowed achieving 12.94 bar of IMEP, while keeping smoke and CO at 0.45 FSN and 5.42 mg/s, respectively. Despite the IMEP reported in Test2 is still lower than the required full load target for Point 6, the cylinder conditions and reported emission levels obtained with this new exhaust configuration represent a good starting point for performing the detailed optimization of the engine settings. Therefore, the subsequent DoE optimization of the gas exchange process at Point 6 is performed keeping the new exhaust configuration adapted for high speed operation.

In agreement with the proposed experimental methodology, a central composite DoE was performed at Point 6 considering the air management parameters included in Table 4.16, together with their ranges of variation. Note that both P_{int} and ΔP have been increased compared to the settings used in the preliminary study of the exhaust system, in order to increase

cylinder gas density and $Q_{air,ret}$, to allow injecting the required m_{fuel} to reach 15.1 bar IMEP at the central point of the DoE. Then, m_{fuel} is accordingly adjusted in all the points of the DoE by increasing or decreasing the main injection duration to compensate for slight variations in the IMEP. The injection pressure was also increased to 1700 bar compared to the previous non-optimized settings to improve the mixing process and decrease smoke emissions; while NO_x emissions are controlled using EGR. Additionally, SoE2 at the reference central point was retarded to -10 CAD aTDC, to decrease P_{max} and avoid exceeding the safety limit of 160 bar. This timing was subsequently adjusted in other points of the DoE to keep constant combustion phasing with CA50 at 12.2 CAD aTDC.

Engine settings - High Load Point 6						
T_{int}	P_{int}	ΔP	P_{exh}	$VVT_{(int,exh)}$	$Olap$	EGR
[°C]	[bar]	[bar]	[bar]	[CAD]	[CAD]	[%]
35	min: 3.8	min: 1.25	1.1	(0,5)	min: 70	min: 6
	max: 4.0	max: 1.45	1.4	(0,15)	max: 80	max: 14
IMEP	m_{fuel}	P_{rail}	SoE1	SoE2	SoE3	$\%fuel$
[bar]	[mg/st]	[bar]	[CAD]	[CAD]	[CAD]	[%]
15.1	$\approx 29.8^*$	1700	–	-10^*	-	0/100/0*

Table 4.16. *Engine settings for the DoE optimization at Point 6. *Both m_{fuel} and* SoE2 *have been slightly adjusted at some points of the DoE to keep constant values of* IMEP *and* CA50*.*

4.5.2.2.2 Summary of main trends

Focusing on the air management characteristics, TR ranges between 71.5 % to 78 % within the space of the DoE, with Q_{del} between 116 kg/h to 125 kg/h and IGR from 27 % to 32 %. The maximum value for Q_{IVC} is found at conditions with the highest P_{int}, medium-to-low $Olap$, medium-to-high ΔP, and low EGR, which is the case of points that have approximately 75 % of TR and 122 kg/h to 123 kg/h of Q_{del}. At this conditions $Q_{air,ret}$ and also $Y_{O_2,IVC}$ are maximized, thus providing the minimum $\phi_{eff,IVC}$ observed in this DoE, which is in the range of $0.75-0.76$. The main physical relationships between the air management settings and the cylinder conditions, that were already described for medium and low load conditions, are also kept when

increasing engine speed and load, since they are intrinsic characteristics of this two-stroke engine architecture, so they will not be shown for Point 6.

Figure 4.20 shows the relationship between the cylinder conditions, maximum combustion temperature traced by $T_{ad,max}$ and $T_{ad,80\%MBF}$, and final NO_x and smoke levels reported at this high load point.

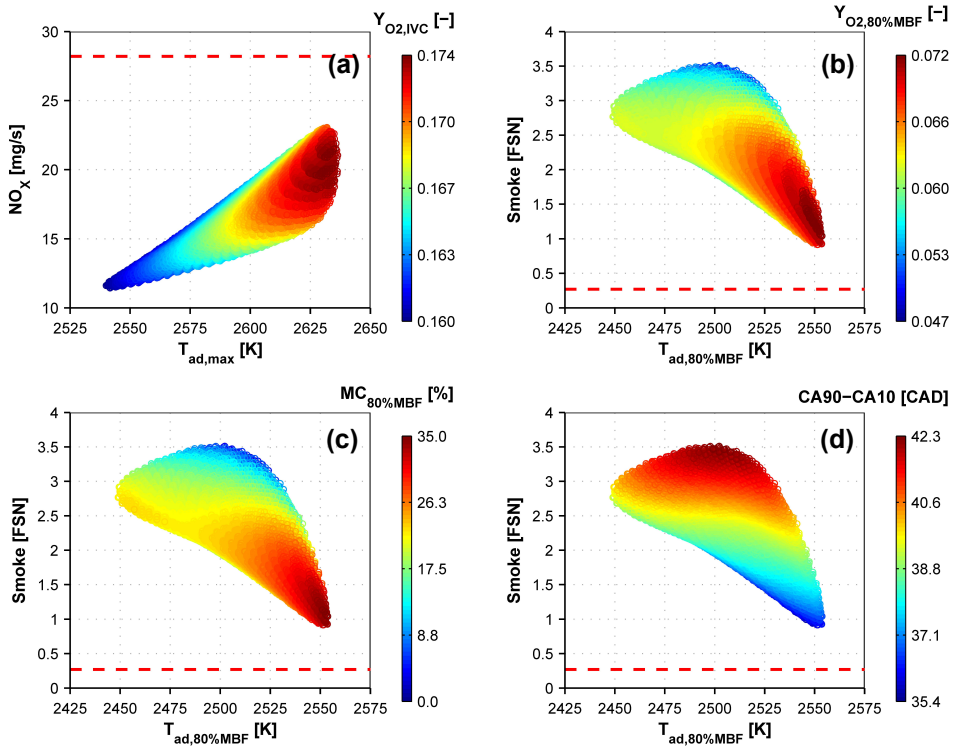

Figure 4.20. *Relation between combustion characteristics and emissions: (a) NO_x as function of $T_{ad,max}$ and $Y_{O_2,IVC}$, (b) smoke as function of $T_{ad,80\%MBF}$ and $Y_{O_2,EVO}$, (c) smoke as function of $T_{ad,80\%MBF}$ and $MC_{80\%MBF}$ and (d) smoke as function of $T_{ad,80\%MBF}$ and combustion duration.*

As it can be seen in Figures 4.20.(a) and (b), NO_x level along the DoE space is always below the reference limit obtained from the equivalent four-stroke engine operating at Point 6, nevertheless, the smoke level always exceeds the reference limit of 0.27 FSN. The poor air charging of the cylinder added to high m_{fuel} and the use of EGR, increases $\phi_{eff,IVC}$ close to stoichiometric combustion, with maximum $\phi_{eff,IVC}$ between 0.85 and 0.9 at the worst points, making it very difficult to achieve smoke emissions below 1 FSN. As it was expected, the smoke/NO_x trade-off cannot be avoided or mitigated

at this high load operating condition. Accordingly, the low smoke area (in the range of 1 FSN to 1.5 FSN) is found at the high NO_x conditions (with NO_x over 20 mg/s) which corresponds to high values of $Y_{O_2,IVC}$ and $T_{ad,max}$, and accordingly high $Y_{O_2,80\%MBF}$ and $T_{ad,80\%MBF}$.

As it was discussed in Chapter 2 and also from the analysis of the experimental results, it is clear how the strong impact of the cylinder thermodynamic conditions on final smoke emissions is the limiting factor when approaching to full load conditions operating in CDC [8, 27]. Therefore, improving the air charging and scavenging characteristics to increase oxygen concentration during all stages of combustion (meaning higher $Y_{O_2,IVC}$ and $Y_{O_2,80\%MBF}$), combined with high cylinder gas density to improve the mixing rate at final stages of combustion (high $MC_{80\%MBF}$) is mandatory to decrease soot formation and enhance the late-cycle soot oxidation processes. The improvement in late-cycle combustion observed in the areas with enhanced cylinder conditions, is also reflected in a shorter combustion duration caused mainly by earlier CA90, as confirmed by Figure 4.20.(d).

Finally, the deterioration of the combustion process and also of the late-cycle oxidation on the zone with high $\phi_{eff,IVC}$ and low $Y_{O_2,IVC}$, has a sharp impact on final CO emissions and also in ISFC, as confirmed by Figure 4.21, where the final trade-off between smoke-NO_x is shown as function of CO, ISFC, $MF_{NO_x,smoke,ISFC}$ and $MF_{NO_x,smoke,ISFC_{corr}}$. Similarly to the trend observed for smoke emissions, CO level is also exceeding the expected target of 3.7 mg/s and is not possible to reach this target in any of the points of the DoE with the current ranges for the air management settings. Finally, the optimization criteria applied for this full load point focused on staying as close as possible to the smoke target. Hence, the maximum of both merit functions $MF_{NO_x,smoke,ISFC}$ and $MF_{NO_x,smoke,ISFC_{corr}}$ are found at the points with lowest smoke emissions, which also corresponds to low values of ISFC (in the range of 192 g/kW h to 195 g/kW h), but relatively higher $ISFC_{corr}$ around 237 g/kW h to 240 g/kW h, coming from the highly demanding condition for the air charging system in terms of P_{int} and ΔP.

4.5.2.2.3 Final optimization

For the final stage of optimization, two different air management conditions were selected to be measured on the engine (denoted as OPT1 and OPT2) which have similar high values for P_{int} and ΔP, the lowest possible value for EGR and two different $Olap$ and VVT_{exh} settings. However, since the smoke limit was not attained within the DoE range, it was interesting to measure

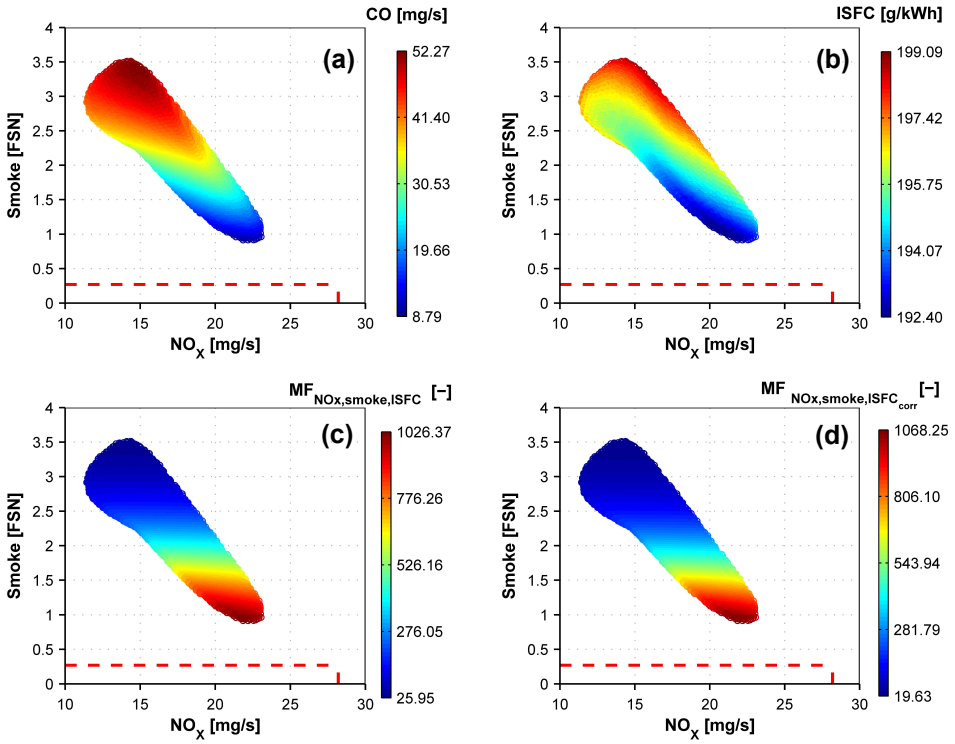

Figure 4.21. *Optimization results: (a) CO, (b)* ISFC*, (c) $MF_{NO_x,smoke,ISFC}$ and (d) $MF_{NO_x,smoke,ISFC_{corr}}$ as function of NO_x and smoke.*

both points without EGR (Final1 and Final2) in order to decrease as much as possible $\phi_{eff,IVC}$, and also slightly adjusting SoE2 without exceeding the safety limit in terms of P_{max}. Table 4.17 and Table 4.18 summarizes the engine settings and most important experimental results in terms of air management, exhaust emissions and fuel consumption obtained at this full load condition.

In terms of NO_x emissions, the required limit of 28.2 mg/s fulfilled in points OPT1 and OPT2, while smoke, CO and HC limits are not attained in any of the four points. Further optimization at this load condition is mandatory to successfully achieve all the emissions targets. In the case of Final2, the slightly higher ΔP and $Olap$ compared to Final1, combined with 0 % of EGR and earlier SoE2, allowed achieving 0.54 FSN of smoke and 6.76 mg/s of CO, while keeping 192.5 g/kW h and 237.3 g/kW h of ISFC and $ISFC_{corr}$, which are the lowest levels reported at this operating condition so far. However, NO_x was consequently increased above the required limit reaching 33 mg/s. In the case

Final optimization - High Load Point 6						
	P_{int} [bar]	ΔP [bar]	P_{exh} [bar]	$VVT_{(int,exh)}$ [CAD]	$Olap$ [CAD]	EGR [%]
OPT1	3.96	1.39	2.57	(0,7)	72.0	6
OPT2	3.96	1.41	2.55	(0,11)	76.0	6
Final1	3.96	1.39	2.58	(0,7)	72.0	0
Final2	3.96	1.42	2.54	(0,11)	76.0	0
	m_{fuel} [mg/st]	P_{rail} [bar]	SoE1 [CAD]	SoE2 [CAD]	SoE3 [CAD]	$\%fuel$ [%]
OPT1	29.4	1700	-	-10.5	-	0/100/0
OPT2	29.5	1700	-	-11	-	0/100/0
Final1	29.8	1700	-	-10	-	0/100/0
Final2	29.3	1700	-	-12	-	0/100/0

Table 4.17. *Engine settings for the optimum points at Point* 6.

Final optimization - High Load Point 6				
Responses	OPT1	OPT2	Final1	Final2
TR [%]	74.3	72.9	74.63	73.2
IGR [%]	32.5	29.8	32.3	30.1
Q_{IVC} [kg/h]	134.13	126.0	135.52	129.17
$Y_{O_2,IVC}$ [%]	16.8	17.17	17.7	17.74
$\phi_{eff,IVC}$ [−]	0.75	0.78	0.72	0.74
P_{max} [bar]	155.33	152.65	154.05	157.04
dP/da_{max} [bar/CAD]	3.92	3.78	3.92	4.30
Noise [dB]	87.9	88.4	88.0	88.8
NO_x [mg/s]	22.6	21.8	28.7	33.1
CO [mg/s]	13.92	13.5	11.4	6.76
HC [mg/s]	1.75	1.54	1.79	1.62
Smoke [FSN]	1.23	1.38	0.91	0.54
η_{comb} [%]	99.57	99.6	99.63	99.73
ISFC [g/kW h]	195.1	194.8	196.4	192.5
$ISFC_{corr}$ [g/kW h]	240.3	239.3	240.4	237.3

Table 4.18. *Main results obtained at High Load Point 6.*

of Final1, NO_x remains just above the limit with 28.7 mg/s while smoke is increased to 0.91 FSN, CO to 11.4 mg/s, and both ISFC and $ISFC_{corr}$ to 196.4 g/kW h and 240.4 g/kW h respectively.

4.6 Concluding remarks

In order to evaluate the performance of the CDC on this two-stroke HSDI CI poppet-valves engine concept on a strictly controlled test environment, it was necessary to define a fast and efficient experimental test methodology, which was based on isolating the optimization process of the air management parameters from that of the injection parameters. This optimization is focused on finding the most suitable in-cylinder conditions necessary to fulfill the emission limits imposed in section 4.2, especially in terms of NO_x and smoke, while minimizing the fuel consumption as much as possible. These limits correspond to the Euro 5 levels measured in an equivalent four-stroke engine with similar unitary displacement and geometric characteristics.

Based on the proposed objective, a dedicate test campaign for studying the air management characteristics was designed in order to easily identify the cause/effect relations of the air management parameters over the in-cylinder conditions, and consequently over combustion development and final exhaust emission levels. Accordingly, a Design of Experiment (DoE) methodology was selected to find the optimum air management settings for each engine operating condition under evaluation. A Central Composite Design (CCD) was used to build the test plan since this design allows modeling the responses using a quadratic equation, taking into account all possible second order interactions between the factors. The main air management settings that were chosen as factors for the DoE optimization are the EGR rate, intake pressure, ΔP and overlap duration.

A summary of the measured final optimum points obtained after the optimization process, in terms of emissions and fuel consumption levels is presented in Table 4.19, as a comparison against the reference levels measured in the four-stroke engine.

From the analysis performed during the optimization of the CDC at different operating conditions, the following main conclusions can be extracted:

- The two-stroke engine architecture proved its potential to have high flexibility in terms of air management control, valve timing, EGR and intake boosting levels to substantially affect the in-cylinder conditions,

	Point 1		Point 3		Point 5		Point 6	
	4-st	*2-st*	*4-st*	*2-st*	*4-st*	*2-st*	*4-st*	*2-st*
Engine speed [rpm]	1250		1500		1500		2500	
IMEP [bar]	3.1		5.5		10.4		15.1	
NO_x [mg/s]	0.45	0.44	0.75	0.73	2.15	2.13	28.2	33.1
CO [mg/s]	4.95	3.71	4.4	5.77	18.65	13.02	3.7	6.76
HC [mg/s]	0.8	0.54	0.65	0.5	0.65	0.36	1.3	1.62
Smoke [FSN]	1.44	0.33	0.56	0.38	4.6	2.99	0.27	0.54
Noise level [dB]	84.2	84.3	89.9	89.4	88.3	86.4	91.5	88.8
ISFC [g/kW h]	237	208.4	210.3	178.1	213.6	196.6	196.37	192.5
$ISFC_{corr}$ [g/kW h]	–	226.4	–	217.4	–	238.8	–	237.3

Table 4.19. *Final comparison between the reference four-stroke (4-st) and the two-stroke (2-st) engines at CDC.*

and consequently the combustion development, which determines final emission levels and indicated efficiency.

- The two-stroke poppet valve architecture inherently exhibits lower trapping efficiencies compared to an uniflow two-stroke engine, due to the combination of positive ΔP between the intake and exhaust and the long overlap durations that are needed to attain good exhaust and scavenge of the burnt gases out of the cylinder, which added to the proximity between the poppet valves; makes it very difficult to balance the air charging and scavenging of the cylinder with the short-circuit losses.

- Concerning the IGR ratio, the experimental results from the preliminary study of the air management process showed how decreasing TR, therefore increasing Q_{del}, improved the scavenging of burnt gases out of the cylinder decreasing IGR, until reaching a practical lower limit (typically around of 30 %), from which further reductions in TR were not translated into a better scavenging process. These results confirm that there is a strong trade-off between trapping and scavenging efficiencies that needs to be addressed when optimizing the air management settings.

- The minimum effective in-cylinder equivalence ratio ($\phi_{eff,IVC}$), is obtained at the point with higher fresh air trapped in the cylinder ($Q_{air,ret}$), which is found at an optimum combination of medium-

to-low TR and medium-to-high delivered flow Q_{del} where the total trapped mass (Q_{IVC}) is maximized. The two most influential factors controlling Q_{IVC} and $Q_{air,ret}$ are the ΔP and the valve overlap. The best combination of TR and Q_{del} is typically obtained at the highest values of ΔP but with the medium-to-low values of *Olap*.

- NO_x emissions can be effectively decreased by reducing $Y_{O_2,IVC}$ and accordingly, $T_{ad,max}$ along the combustion process. In this two-stroke engine, the $Y_{O_2,IVC}$ can be easily controlled by introducing external EGR, but also by affecting the air management conditions with ΔP and *Olap*. However, reducing $T_{ad,max}$ by decreasing the oxygen concentration without compensating with higher in-cylinder gas density leads to a consequent decrease of the temperatures along the late diffusive combustion stage ($T_{ad,80\%MBF}$), resulting in worsened soot oxidation process and higher final soot emissions.

- The final soot level is determined not only by the combustion temperature at the late combustion phase ($T_{ad,80\%MBF}$) but also by the mixing conditions at this slow diffusion stage ($MC_{80\%MBF}$), being both crucial for the late soot oxidation process. A higher Q_{IVC} provides a higher in-cylinder density, enhancing the mixing process and shortening the combustion duration, for which final soot emissions are largely reduced.

- At low to medium loads (from 3.1 bar to 10.4 bar of IMEP) and low speed conditions (from 1250 rpm to 1500 rpm) the emissions and noise limits are fulfilled while ISFC is improved compared to the base four-stroke engine. Optimizing the air management settings is critical to achieve the proper in-cylinder conditions which provide suitable combustion environment to attain high combustion efficiency levels and competitive indicated fuel consumption. At all of these points, it was possible to find the best compromise in terms of NO_x, smoke and ISFC, that allowed fulfilling the expected optimization targets.

- At high load (15.1 bar IMEP) and medium speed (2500 rpm) conditions it was not possible to fulfill the NO_x, smoke, CO and HC emission limits since the combustion process was compromised due to decreased engine permeability. Therefore, a physical limitation to attain full load and high speed operating conditions was identified with the current engine hardware. Important benefits are expected by improving the acoustic characteristics of the intake and especially the exhaust system.

- The results obtained along this chapter, proved how it is possible to reach and even improve the performance of an equivalent CI four-stroke engine with the two-stroke poppet valves engine architecture. The main trends and relations identified along this research are useful to prepare the path towards future optimization of this particular engine concept to comply with more stringent regulations such as EU6.

As a final remark, the methodology presented in this chapter was successfully implemented to optimize the fuel consumption and emission levels of the two-stroke poppet valve engine at the reported engine operating conditions while operating with the CDC mode. The straight and general relations obtained after the analysis of the results confirm how the best approach for understanding the physical processes linked to two-stroke engines, is to switch from particular engine operation settings to the final in-cylinder gas thermodynamic conditions, which later controls the combustion process development and final emission levels and efficiency. Thus, this methodology can be extrapolated to design and develop any kind of two-stroke engine, regardless of its particular architecture or displacement.

Bibliography

[1] *Regulation 715/2007 of the European Parliament and of the Council of 20 June 2007 on type approval of motor vehicles with respect to emissions from light passenger and commercial vehicles (Euro 5 and Euro 6) and on access to vehicle repair and maintenance information.* Official Journal of the European Union, 2007.

[2] Rekab K. and Shaikh M. *Statistical Design of Experiments with Engineering Applications.* Taylor & Francis, 2005.

[3] Eriksson L. *Design of Experiments: Principles and Applications.* Umetrics, 2008.

[4] Mead R., Gilmour S.G. and Mead A. *Statistical Principles for the Design of Experiments: Applications to Real Experiments.* Cambridge University Press, 2012.

[5] Antony Jiju. *Design of Experiments for Engineers and Scientists.* Butterworth-Heinemann, Oxford, 2003.

[6] Blair G.P. *Design and Simulation of Two-stroke Engines.* Society of Automotive Engineers, 1996.

[7] Heywood J.B., Sher E. and Engineers Society of Automotive. *The Two-stroke Cycle Engine: Its Development, Operation, and Design.* Taylor and Francis, 1999.

[8] Payri Gonzalez Francisco and Desantes Jose Maria. *Motores de combustion interna alternativos.* Editorial Reverte, 2011.

[9] Li Zhihua, He Bang-quan and Zhao Hua. "The Influence of Intake Port and Pent-Roof Structures on Reversed Tumble Generation of a Poppet-Valved Two-Stroke Gasoline Engine". In *SAE Technical Paper*, volume 2014-01-1130, 2014.

[10] Duret Pierre. *A new generation of two-stroke engines for the future?* Editions Technip, Pairs, 1993.

[11] Teakle B Philip Robert. *A numerical investigation of a two-stroke poppet-valved diesel engine concept.* Tribology and Materials Technology Group. PhD Thesis. Queensland University of Technology, 2004.

[12] Tribotte Pascal, Ravet Frederic, Dugue Vincent, Obernesser Philippe, Quechon Nicolas, Benajes Jesus, Novella Ricardo and De Lima Daniela. "Two Strokes Diesel Engine - Promising Solution to Reduce CO2 Emissions". *Procedia - Social and Behavioral Sciences*, Vol. 48, pp. 2295–2314, 2012.

[13] Pohorelsky Ludek, Brynych Pavel, Macek Jan, Vallaude Pierre-Yves, Ricaud Jean-Charles, Obernesser Philippe and Tribotte Pascal. "Air System Conception for a Downsized Two-Stroke Diesel Engine". In *SAE Technical Paper*, volume 2012-01-0831, 2012.

[14] Blair G. P. *The Basic Design of Two-Stroke Engines.* SAE International, 1990.

[15] Benajes Jesus, Novella Ricardo, De Lima Daniela and Tribotte Pascal. "Analysis of combustion concepts in a newly designed two-stroke high-speed direct injection compression ignition engine". *International Journal of Engine Research*, Vol. 16 n^o 1, pp. 52–67, 2015.

[16] Dec John E. "A Conceptual Model of DI Diesel Combustion Based on Laser-Sheet Imaging". In *SAE Technical Paper*, volume 970873, 1997.

[17] Kitamura Yasutaka, Mohammadi Ali, Ishiyama Takuji and Shioji Masahiro. "Fundamental Investigation of NOx Formation in Diesel Combustion Under Supercharged and EGR Conditions". In *SAE Technical Paper*, volume 2005-01-0364, 2005.

[18] Novella R. *Estudio de la influencia de los ciclos Atkinson y Miller sobre el proceso de combustion y las emisiones contaminantes en un motor diesel.* PhD thesis. Universitat Politecnica de Valencia, Departamento de Maquinas y Motores Termicos, 2009.

[19] Kolodziej C. *Particulate matter emissions from Premixed Diesel Low Temperature Combustion.* PhD thesis. Universitat Politecnica de Valencia, Departamento de Maquinas y Motores Termicos, 2012.

[20] Tree Dale R. and Svensson Kenth I. "Soot processes in compression ignition engines". *Progress in Energy and Combustion Science*, Vol. 33 n^o 3, pp. 272–309, 2007.

[21] Benajes Jesus, Novella Ricardo, Garcia Antonio and Arthozoul Simon. "The role of in-cylinder gas density and oxygen concentration on late spray mixing and soot oxidation processes". *Energy*, Vol. 36 n^o 3, pp. 1599–1611, 2011.

[22] Benajes J., Novella R., Arthozoul Simon and Kolodziej Christopher. "Particle Size Distribution Measurements from Early to Late Injection Timing Low Temperature Combustion in a Heavy Duty Diesel Engine". In *SAE Technical Paper*, volume 2010-01-1121, 2010.

[23] Payri Francisco, Benajes Jesus, Novella Ricardo and Kolodziej Christopher. "Effect of Intake Oxygen Concentration on Particle Size Distribution Measurements from Diesel Low Temperature Combustion". In *SAE Technical Paper*, volume 2011-01-1355, 2011.

[24] Benajes Jesus, Garcia-Oliver Jose M., Novella Ricardo and Kolodziej Christopher. "Increased particle emissions from early fuel injection timing Diesel low temperature combustion". *Fuel*, Vol. 94 n^o 0, pp. 184–190, 2012.

[25] Arregle J., Lopez J. J., Garcia J. M. and Fenollosa C. "Development of a zero-dimensional Diesel combustion model. Part 1: Analysis of the quasi-steady diffusion combustion phase". *Applied Thermal Engineering*, Vol. 23 n^o 11, pp. 1301–1317, 2003.

[26] Benajes Jesus, Novella Ricardo, De Lima Daniela, Tribotte Pascal, Quechon Nicolas, Obernesser Philippe and Dugue Vincent. "Analysis of the combustion process, pollutant emissions and efficiency of an innovative 2-stroke HSDI engine designed for automotive applications". *Applied Thermal Engineering*, Vol. 58, pp. 181–193, 2013.

[27] Heywood J. B. *Internal combustion engine fundamentals.* Ed. McGraw-Hill Science/Engineering/Math, 1988.

Appendix A

Optimization methodology

A.1 Air management DoE optimization

The practical steps needed for planning and conducting a DoE test campaign can be summarized as follows:

- *Recognition and statement of the optimization target.* In the studies presented on this chapter, the objective of the optimization is typically one of the following: not to exceed standard on pollutants, minimize a given variable like NO_x or ISFC, finding the best compromise between NO_x, smoke and engine efficiency.

- *Selection of the response variables.* This step requires choosing the group of measured engine variables that are going to be modeled along the DoE, with the aim of characterizing the air management and combustion processes, as well as the engine performance indicators in terms of emissions and efficiency that will be posteriorly optimized. For example: Q_{del}, trapping ratio, IGR, $Y_{O_2,IVC}$ and $\phi_{eff,IVC}$, to describe the air management process; P_{max}, dP/da_{max}, T_{ad} and noise, to describe the combustion process; and finally, NO_x, smoke, HC, CO, η_{comb}, η_{ind}, ISFC and $ISFC_{corr}$, as engine performance indicators.

- *Choice of factors and ranges.* The main air management settings that can be chosen as factors for the DoE in this two-stroke engine are: the intake pressure (P_{int}), exhaust pressure (P_{exh} or accordingly the ΔP), the EGR ratio, the timing of each camshaft ($VVT_{(int,exh)}$), or accordingly the valve overlap ($Olap$). For this investigation, the number

of factors has been set to 4 to keep a relatively simple design with reasonable total number of tests. The ranges for each factor are selected based on experience gained prior to this investigation from performing fast screening tests in the engine, and/or from the available information obtained with 1D GT Power calculations done in the first stages of conception and pre-design of the engine.

- *Choice of design.* The type of DoE has to be chosen depending on the number of factors, the assumed form of the influence of a factor on a given response (i.e. linear, quadratic...), and accordingly, the number of levels chosen for the factors. For this investigation, a Central Composite Design (CCD) was selected to build the test plan, to be able to have a polynomial (second degree) mathematical model for the responses, including all possible second order interactions between the factors. The CCD is composed of 3 sequences: a test in the center of the field (at the midpoint of the range of each factor) replicated several times to estimate the variance of repeatability, an orthogonal "full-factorial" design (with 2 levels per factor) that gives the form of the model and the influence of the factors, and finally two additional "star" or axial tests on the axis of each factor at a distance α from the center of the design (selected based on criteria such as rotability) to measure the quadratic effect of the factors and their interactions. The final design gives a test plan with a total of 5 levels for each factor.

- *Test plan execution.* For the selected 4 factors, the CCD test plan gives a total of 36 points, with 12 replicates of the central point, 16 points of the orthogonal design and 8 "star" points. The tests must be performed in the most rigorous way, and in a random run order, to ensure that the model meets certain statistical assumptions and also to reduce possible influence of other "noise" parameters that are not included in the study.

- *Statistical analysis.* After performing the tests, the mathematical models are built and fitted to the data measured for each response. Accordingly, different plots and statistical metrics are generated to assess the fit of the model and evaluate its predictive capability. The results from the fitted model helps to determine which terms of the model have a relevant effect over the measured response, and which terms can be neglected or excluded from the model.

- *Validation of the response models.* The predictive capability of the model is further evaluated by comparing the models estimation against new experimental data, that has not been previously used to built the

models. Validation points are chosen inside the space of the model, but at locations where is necessary to interpolate between the levels for one or more factors.

- *Optimization to achieve the proposed objective.* The statistical models of the different responses are employed to run an automatic optimization algorithm, within the space of the design in order to find the set of points that are able to comply with the proposed optimization targets, while also fulfilling a given set of restrictions or limitations. It also is possible to perform multiple objective optimization, by defining a merit function between the responses that are going to be optimized, assigning different weights to favor the optimization of a given response among the group. For this investigation, different merit functions, i.e. between NO_x and smoke, or between NO_x, smoke and ISFC have been defined according to equation A.1.

$$MF = \frac{1000 \cdot \sum_i(\alpha_i)}{\sum_i \left(\alpha_i \cdot e^{\beta_i \cdot \frac{RV_i - OV_i}{OV_i}} \right)} \tag{A.1}$$

where RV_i is the response value, OV_i is the objective value, and α_i and β_i are coefficients to control the weight of each response in the merit function.

Focusing in the statistical analysis of the responses, there are many different statistics quality indicators that can be used to check the fit of the model and measure its predictive capabilities. For instance, the square of the correlation coefficient (known as R^2) between the set of experimental data and the set of estimated data, indicates that the model is adequate, possessing no significant lack of fit. The closer the value to unity, the better the empirical model fits the actual data. The root mean squared error (RMSE), which is the square root of the mean squared error, represents the standard deviation of the regression, and typically, this is the statistic whose value is minimized during the parameter estimation process. RMSE is minimized when the model gets very close to each data point; so "chasing" the data will therefore improve RMSE. However chasing the data can sometimes lead to strong oscillations in the model between the data points; this behavior can give good values of RMSE but is not representative of the data and will not give reliable prediction values where you do not already have data. This suggest that we should not rely only on R^2 and RMSE to asses overall model quality.

Asides from R^2 and RMSE, a stepwise regression model which minimizes the predicted error sum of squares (PRESS) can be used to eliminated any redundant model terms which results in over-fitting of the models. The PRESS RMSE statistic guards against model over-fitting by testing how well the current model would predict each of the points in the data set if they were not included in the regression. To get a small PRESS RMSE usually indicates that the model is not overly sensitive to any single data point. Finally, the best model for a given engine response is chosen based on the combination of R^2, RMSE and PRESS RMSE statistical metrics.

Table A.1 illustrates an example of the most important statistical metrics that are selected to evaluate the fit of the mathematical models and improve the accuracy of the predictions during the optimization process. The results shown below corresponds to the first DoE discussed in section 4.4 that was performed to study the air exchange process solely without the use of EGR.

Responses	R^2	RMSE	PRESS RMSE
Q_{del} [kg/h]	0.999	0.203	0.275
TR [%]	0.983	0.861	0.911
IGR [%]	0.957	0.377	0.436
Q_{IVC} [kg/h]	0.986	0.477	0.688
$Y_{O_2,IVC}$ [%]	0.965	0.0011	0.0017
$\phi_{eff,IVC}$ [−]	0.967	0.0076	0.0084
NO_x [mg/s]	0.985	0.765	0.817
ISFC [g/kW h]	0.995	0.297	0.43
$ISFC_{corr}$ [g/kW h]	0.995	0.474	0.583
η_{ind} [%]	0.994	0.073	0.105

Table A.1. *Summary of main statistics metrics for different responses models.*

From the statistics metrics shown in Table A.1, R^2 is very close to 1, what would be equivalent to a "perfect fit" between the modeled and the measured data, for the majority of the selected responses which have been measured directly on the engine (such as Q_{del}, TR, NO_x and ISFC); while R^2 is slightly decreased (but still being acceptable) for the post-processed, estimated or derived responses (IGR, $\phi_{eff,IVC}$, $Y_{O_2,IVC}$). It is worth to remark, that the fit of the model would also depend on the observed range of variation for a given response. In the case of some responses like ISFC, noise, smoke, CO and HC emissions, it may be difficult is some cases to assure a perfect fit of the

model if the measured range of variation is small, particularly if the extreme measured values on the data only change in 2 % to 3 % or less compared to the central point of the DoE. In general terms, the statistical analysis is necessary to confirm that the mathematical models are properly fitted to the experimental data, so they can be posteriorly used to analyze the main trends on the engine responses while keeping a high degree of confidence.

Before performing the optimization and trade-off analysis using response surface methods it is also important to estimate the Prediction Error Variance (PEV) to evaluate the precision of the model to predict a given response in areas where there is not any measured data. The prediction is desired to be as reliable as possible throughout the entire DoE space, so a low PEV (close to zero) indicates that good predictions are obtained at a given point or region. In this regard, Figure A.1 shows an example of the model PEV for an arbitrary response as function of two different inputs (depicted as factor 1 and 2), as well as the selected boundary model that is applied for the optimization process.

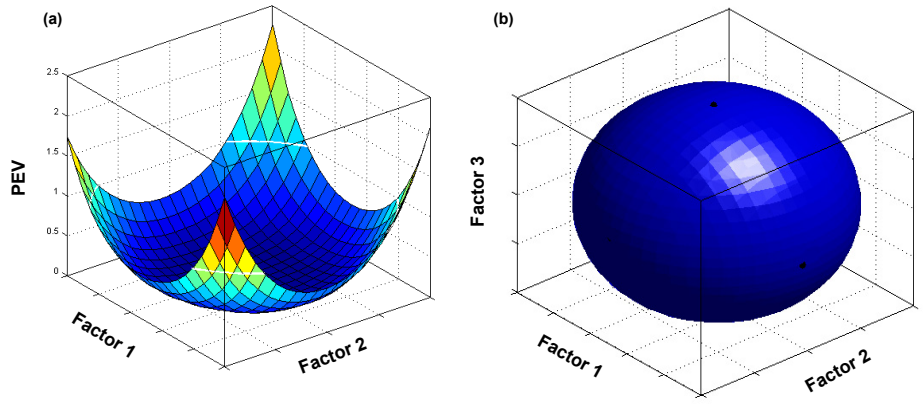

Figure A.1. *Example of predicted error variance and definition of boundary model for an arbitrary response model and the selected CCD test plan.*

As it can be seen in the left plot of Figure A.1, in the particular case of the selected circumscribed CCD, the mathematical models loose predictive power near the corners of the DoE space, in locations that combines simultaneously maximum and/or minimum values of the input factors. So, to ensure a low error in the model's prediction, an ellipsoid boundary model is applied to all the responses models before the optimization process, as it is depicted in the right plot of Figure A.1, by covering all measured points (including "star"

points) but ignoring the corners of the design, where the predictive capability of the models is poor.

Once the boundaries have been defined and the responses models have been properly validated, they can now be used to run the optimization algorithm in order to find the optimum points that comply with the proposed optimization objectives along with the imposed restrictions. The objective of this final stage in the DOE analysis is to find the best trade-off between exhaust emissions, referring to NO_x and smoke mostly, and also considering ISFC and $ISFC_{corr}$. Finally, different optimum point are selected considering the air management settings, and they are measured experimentally on the engine, to check the accuracy on the prediction performed with the statistical models for the selected responses.

A.2 Injection settings parametric optimization

The timing of the main injection (SoE2) is optimized by performing a detailed parametric study, while keeping the optimum air management settings found along the DoE optimization. The objective of this second stage optimization is to check the influence of combustion phasing (CA50) on engine performance and pollutants emissions and perform the final tuning on the emissions levels and final efficiency. The injection pressure (P_{rail}), pilot duration or fuel split ratio ($\%fuel$), and injection dwell between the pilot and the main injection, are also fine-tuned at this stage depending on the needs and particular requirements found at a each operating condition, even-though they have a comparatively smaller influence on the combustion process than the timing of the main injection.

As a reference, Figure A.2 shows an example of the main trends that are typically observed when sweeping simultaneously the timing of the main injection together with the pilot injection, for three different levels of P_{rail}, in the case of a medium to high load operating point. The injection timing SoE1/SoE2 (pilot/main) is swept from $-25/-15$ to $-17/-7$ CAD aTDC, so combustion phasing is shifted between -1 and 9 CAD aTDC. The experimental results evidences that retarding combustion phasing (CA50) by later SoE2, has a very small effect over the in-cylinder conditions (TR, IGR and $\phi_{eff,IVC}$) but a more pronounced effect on exhaust emissions (specially NO_x and smoke), as it is evidenced by Figure A.2. This result corroborates experimentally that there is no strong interaction or coupling between the injection and air management settings, what supports the methodology followed in this research of isolating the optimization of the air

management settings apart from the optimization of the injection settings, confirming that they can be sequentially optimized.

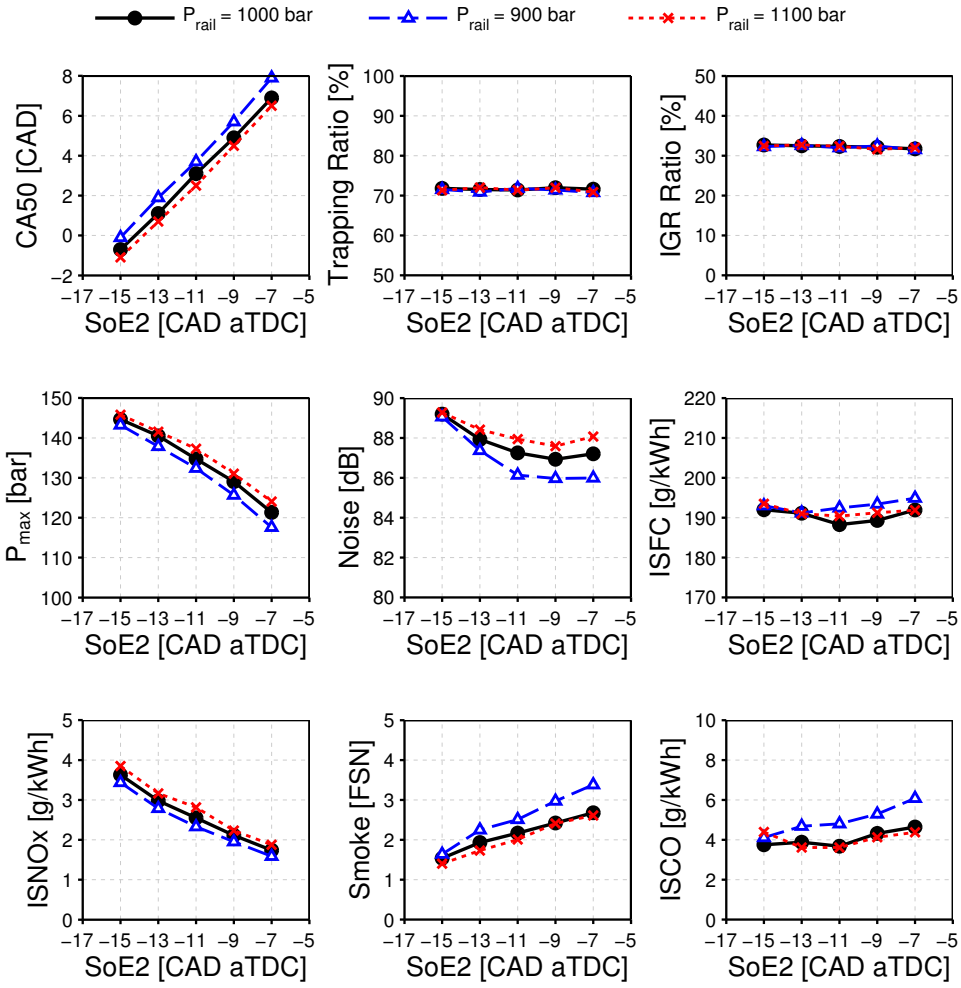

Figure A.2. *Example of main injection timing sweep over air management, combustion and emissions characteristics for different levels of injection pressure.*

In the example shown in Figure A.2, NO_x emissions are decreased when delaying SoE2 as expected, due to the decrease in combustion temperatures when shifting the combustion towards the expansion stroke; while consequently, soot emissions are slightly increased due to a worsened oxidation process at the late stages of combustion. Additionally, CO and HC emissions remain approximately constant or are slightly increased

(specially CO) when shifting the injection towards later timings, which is linked to a reduction in combustion efficiency when delaying combustion phasing later into the expansion stroke. Finally, the influence of injection timing on ISFC is also relatively small, when shifting CA50 around its optimum phasing, so the benefits attained by optimizing combustion phasing are typically expected to be in the range of 2 % to 4 %. Therefore, attaining a breakthrough in terms of reducing the fuel consumption while operating with CDC, is expected to be associated to improvements in the air management characteristics, while injection system plays a secondary role.

Chapter 5

Advanced combustion concepts in the poppet valve two-stroke engine

Contents

5.1 Introduction

As it was introduced in Chapter 2, two main research paths are being followed to develop compression ignition engines, the extreme optimization of the conventional diesel combustion concept and the development of alternative combustion concepts.

From the optimization of CDC operation performed in Chapter 4, it was possible to demonstrate the flexibility of the two-stroke poppet valves engine to control the cylinder conditions and the combustion development, with the aim of improving pollutant emissions and efficiency levels of the traditional four-stroke engine. In this regard, it was possible to fulfill the proposed limits in terms of NO_x and smoke emissions while improving the efficiency level of the reference four-stroke engine, in all load points with the exception of the full load (Point 6), where the combustion process was compromised due to reduced air flow given by a poor acoustic behavior with the current geometries of the intake and exhaust systems. Nevertheless, the characteristic mixing-controlled combustion stage of the CDC concept still represents an important source of NO_x and particulate matter emissions, so the traditional diesel engine will still face important challenges in the near-and-mid term to further decrease these harmful pollutants to comply with future regulations while still keeping their competitive advantage in terms of fuel consumption levels.

Departing from this background, this chapter focuses on exploring the potential and the range of application of advanced combustion concepts in the two-stroke engine under study, with the aim of improving the well-known trade-off inherent to the CDC concept, while keeping competitive levels in terms of efficiency and fuel consumption. Many of these advanced combustion strategies strive for a low combustion temperature and/or increased degree of premixing prior to combustion, to reduce NO_x and PM formation. However, as it was discussed in Chapter 2 there are many practical limitations in terms of mixture preparation, combustion control and final range of operation that are still under investigation before reaching a viable powertrain application.

As a preliminary study of the advanced combustion concepts, the early-injection Highly Premixed Combustion (HPC) using diesel fuel and the single-

injection gasoline Partially Premixed Combustion (PPC) are implemented in the two-stroke engine through a specific set of parametric studies to identify the main limitations and drawbacks of these strategies. Based on this preliminary study, the next stage of the research is then dedicated to the analysis and optimization of the gasoline PPC concept at different load conditions, using multiple injection strategies to allow precise control of the local fuel-air stratification before the onset of ignition and along the combustion process. As mentioned in section 2.3.2 from Chapter 2, the characteristics of the PPC combustion are highly dependent on the mixture preparation prior to ignition; therefore, both the timing and the fuel quantity injected in each injection must be carefully optimized depending on the operating condition. Accordingly, parametric variations of the timing of each injection, with different rail pressures and different fuel split between injections are experimentally performed at the selected operating conditions, to analyze the effect of the injection strategy on the combustion process, exhaust emissions and efficiency levels during PPC operation.

5.2 Preliminary study of premixed LTC concepts in the poppet valve two-stroke engine

The two-stroke engine under development offers an innovative alternative to overcome the load limits of advanced combustion concepts by taking advantage of the intrinsic characteristics of two-stroke engines, since they can attain the full load torque of a four-stroke engine as the addition of two medium load cycles, where the implementation of the premixed LCT combustion concept is more feasible. However, the implementation of kinetically-controlled combustion concepts with highly reactive fuels such as diesel in this two-stroke engine is challenging since even after optimizing the air management process, it intrinsically operates with high IGR levels (as it was already demonstrated in Chapter 4), well over those produced by four-stroke engines operating with a conventional valve timing.

Additionally, the effects of IGR are contradictory since it reduces the oxygen concentration similarly to EGR, but it also increases the temperature during the compression stroke, so the final impact on the reactivity of the mixture will depend on the balance between these two main effects as well as the auto-ignition characteristics of the fuel [1]. However, the two-stroke architecture also provides much higher flexibility to control the IGR rates, as well as the cylinder gas temperature evolution in a wide range by means of the air management settings compared to four-stroke engines [2–4].

Therefore, two-stroke operation has intrinsically much more potential to adjust the cylinder charge thermochemical conditions and consequently affect the combustion environment, which is a key action to control the combustion process and the final emission levels in the frame of both HPC and PPC concepts.

To identify and better understand the main trade-offs and limitations that are inherent to the premixed LTC concepts, a preliminary study of the early-injection HPC with diesel fuel and the single-injection gasoline PPC has been performed in the single cylinder engine, without taking into consideration the expected performance and emissions targets for the operating conditions shown in Table 4.1 at this initial stage of the research.

5.2.1 Implementation of the early-injection Highly Premixed Combustion (HPC) using diesel fuel

5.2.1.1 General methodology of the studies

The potential of the early-injection HPC concept is evaluated based on different parametric studies performed at low engine load, 2 bar of IMEP, and low engine speed, 1250 rpm, to assure safe engine operation while running with the HPC mode, and also because at this low load/speed condition the HPC concept should provide the best results.

Two pistons with compression ratio of HiCR1=17.2 and LoCR1=13.6 respectively, were available for these studies, along with the narrow angle nozzle A=10 holes 80 μm 60°. A sequential approach to the problem is presented according to the next two steps: first, an initial implementation of the HPC concept by advancing the injection event towards the compression stroke; and second, an evaluation of different strategies for improving the performance of the HPC concept considering combustion process (mainly combustion phasing), pollutant emissions, and engine efficiency. This section will only focus on the implementation of the HPC concept, so the parametric optimization of the CR_{eff}, ΔP and $Olap$ will not be presented in this section. Nevertheless, the detailed analysis of these studies has been reported by Benajes et al. in [5, 6].

The implementation of the HPC concept is performed by means of a variation of the injection timing for three different EGR levels (0 %, 20 % and 40 %), sweeping SoE from −10 CAD aTDC (which is a typical timing for CDC) to −70 CAD aTDC, where a highly premixed mixture is expected to be already achieved. A single injection strategy is selected and higher

P_{rail} compared to CDC is used to improve the evaporation and mixing of the diesel fuel when injected in a low density environment such as the found in early stages of the compression stroke. The injected quantity was adjusted at each point to keep the requested constant value of 2 bar IMEP, so it had to be increased in some cases to compensate any loss in indicated efficiency.

The main engine settings selected for this study are shown in Table 5.1.

Engine settings						
T_{int}	P_{int}	ΔP	P_{exh}	$VVT_{(int,exh)}$	$Olap$	EGR
[°C]	[bar]	[bar]	[bar]	[CAD]	[CAD]	[%]
35	2.0	0.4	1.6	(15,10)	65.0	$[0, 20, 40]$
IMEP	m_{fuel}	P_{rail}	SoE1	SoE2	SoE3	$\%fuel$
[bar]	[mg/st]	[bar]	[CAD]	[CAD]	[CAD]	[%]
2.0	$\approx 5.5 - 6.5$*	1000	-	$[-10 \rightarrow -70]$	-	0/100/0

Table 5.1. *Engine settings for the implementation of the HPC concept using diesel fuel. *m_{fuel} have been slightly adjusted at some points to keep constant the* IMEP *value.*

5.2.1.2 Summary of main trends

Focusing briefly on the air management process, which is a key topic for this two-stroke engine as it was already demonstrated in Chapter 4, it is worth to point out that the air management settings were not fully optimized for this particular operating condition, so they were chosen based on prior knowledge acquired from fast screening tests on the engine to assure suitable conditions for HPC operation. A higher P_{int} and ΔP value compared to what would have been used in CDC have been selected, as an attempt to increase cylinder gas density and total trapped mass Q_{IVC}. With this combination of air management settings, Q_{del} and TR values are found to be around 37 kg/h and 80 % for HPC conditions, while IGR is at 50 %. $Y_{O_2,IVC}$ is decreased from 20.4 % for the case without EGR down to 17.2 % when introducing 40 % of EGR.

Figure 5.1 shows the cylinder pressure as well as RoHR profiles obtained when advancing SoE2 from −10 CAD aTDC (CDC) to −70 CAD aTDC, for the baseline study with 0 % of EGR.

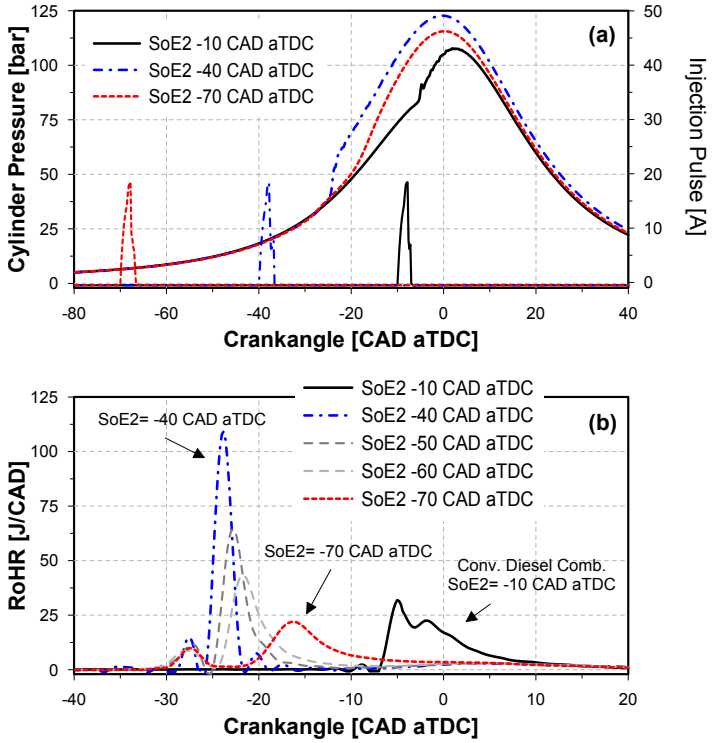

Figure 5.1. *Combustion characteristics: (a) cylinder pressure evolution and (b) RoHR profile for CDC and HPC concepts.*

According to the experimental results, the case with SoE2 equal to -40 CAD aTDC exhibits a sharp increment in the cylinder pressure during the compression stroke around -25 CAD aTDC which comes from an early onset of the combustion process, which is similar to a knocking-like combustion process. The RoHR confirms how combustion is very fast and it is phased too early during the compression stroke, which produces sharp pressure gradients. In this case, the ignition delay does not provide the time required to properly form a sufficiently lean and homogeneous fuel-air mixture and local equivalence ratios at the start of combustion are still too reactive. When the injection is further advanced up to -70 CAD aTDC, the fuel has more time to properly mix with the air before the onset of combustion due to the extended ignition delay, so the charge reactivity is decreased due to a locally leaner and more homogeneous ϕ distribution, resulting in retarded SoC and smoother RoHR due to slower the combustion rate.

Additionally, for the HPC conditions, the RoHR profiles presents a two-stage ignition which is typical of premixed low temperature combustions using diesel-like fuels: a first stage corresponding to the low temperature reactions (LTR) and a second stage of high temperature reactions (HTR). The initial heat release observed in the low temperature zone (less than 850 K) is caused by the first-stage pre-ignition reactions. The experimental results show how the onset of the LTR is observed around 30 CAD before TDC regardless of the SoE2. As the injection timing is advanced from −40 CAD aTDC to −70 CAD aTDC, the peaks of HTR decreased rapidly as a result of lower mixture reactivity.

In order to give more insight into the combustion process and its effect over the indicated efficiency, Figure 5.2 shows the combustion phasing (CA50) along with the pressure gradient (dP/da_{max}), noise and ISFC. CA50 follows the trend already shown in the RoHR, so it is extremely advanced when switching from SoE2 −10 CAD aTDC to −40 CAD aTDC and from this point, it is progressively retarded as SoE2 is advanced beyond −50 CAD aTDC. The use of cooled EGR helped to slightly retard CA50 in most of the points by decreasing $Y_{O_2,IVC}$, and consequently, mixture reactivity; however, the observed effect is comparatively small so it is not enough to shift the combustion phasing closer to TDC. Both pressure gradient and combustion noise are linked to CA50 and combustion rate, so they initially increase for SoE2 −40 CAD aTDC for the case without EGR and then start to gradually decrease as approaching HPC conditions at the earlier timings. Finally, the extremely early combustion phasing combined with a reduction in combustion efficiency, brought a consequent decrease in η_{ind} compared to CDC (which drops from 30 % to 25 %), which is then reflected in an unacceptable increase in ISFC (which goes from 290 g/kW h to 340 g/kW h) when operating with the HPC concept.

Finally, the effect of injection timing on exhaust emissions is shown in Figure 5.3. The reduction in local combustion temperatures when achieving sufficiently lean and homogeneous premixed combustion is the key factor that determines the observed reduction in NO_x emissions since the chemical reactions involved in thermal NO formation has high activation energies, so this thermal NO formation mechanism is highly temperature-dependent. The highest value of NO_x is seen at SoE2 −40 CAD aTDC in the case of EGR=0 % as expected; and afterwards, as injection was further advanced into the compression stroke and HPC conditions were successfully established, NO_x emissions were decreased down to values as low as 0.06 mg/s. Regarding smoke emissions, included also in Figure 5.3.(b), even in CDC the smoke levels were very low at this particular low load condition, so that smoke emissions

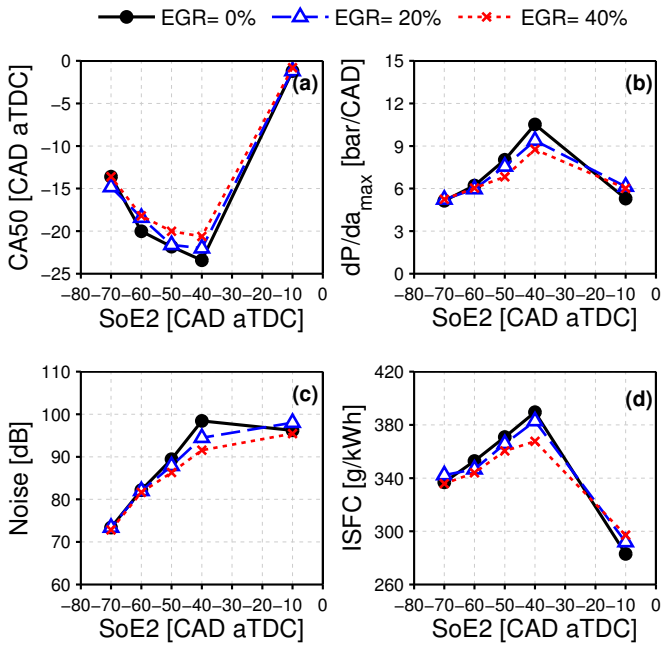

Figure 5.2. *Combustion characteristics: (a)* CA50*, (b)* dP/da_{max}*, (c) noise and (d)* ISFC *as function of* SoE2*.*

were not a critical aspect with the current engine settings selected for these tests. Nevertheless, in HPC conditions where the oxidation temperatures are considerably decreased, the smoke level still remained very low confirming the absence of locally rich mixtures where soot formation is promoted.

The experimental results also confirmed how the reduction in NO_x and smoke emissions is followed by an unavoidable increase in CO and HC emissions, as it can be clearly seen in Figure 5.3.(c), which is in line with the conventional trade-off characteristic of HPC and HCCI concepts [7]. An experimental study coupled with a single-zone modeling study by Dec and Sjöberg [8] confirmed how CO emissions increase dramatically when the local equivalence ratio is lower than 0.2 and also when the local temperature is lower than 1400 K to 1500 K. In the current study, the fuel-air mixture trends to these conditions as the homogeneity increases ($\phi_{eff,IVC}$ ranges between 0.15 and 0.17), explaining the sharp increment in CO observed for SoE2 earlier than -60 CAD aTDC. In the same work [8], the authors also predicts a moderate increment of HC in the same range of local equivalence ratios, so the trend observed in Figure 5.3.(d) for this pollutant might come from

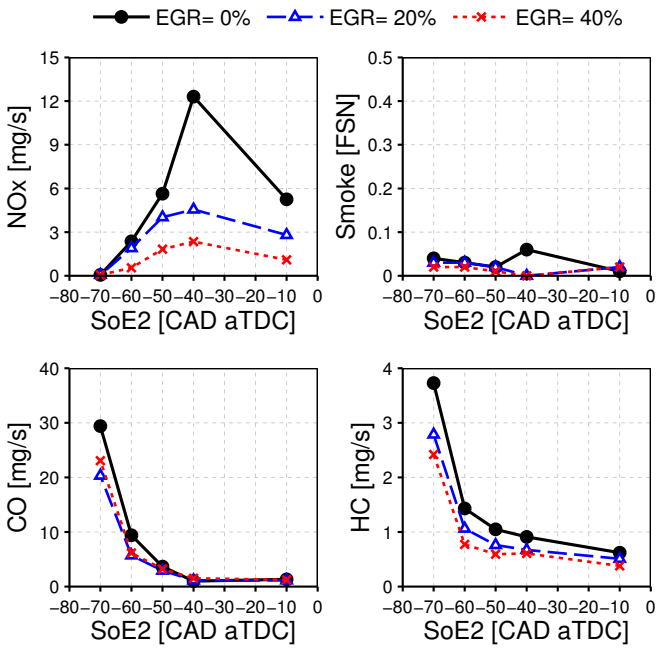

Figure 5.3. *Exhaust emissions: (a) NO_x, (b) smoke, (c) CO and (d) HC as function of* SoE2.

the fuel extremely overmixed with air. Aside from the overmixing effect, liquid fuel impingement onto the piston surface is an additional source of HC, especially for the most advanced SoE2 cases, where the in-cylinder gas densities and temperatures are extremely low along the injection event, worsening the mixing and evaporation processes.

From the experimental results included in Figure 5.3, η_{comb} is substantially decreased even by 10 %, dropping from 99 % to 91 % when switching from CDC to the HPC concept as a direct result of the increment in HC and CO emissions. The expected reduction in NO_x associated to the use of EGR is also observed in Figure 5.3 for the cases with 20 % and 40 % of EGR. But in addition, smoke, CO and HC emissions are also surprisingly decreased when increasing the EGR rate. In these two cases, the injected fuel quantity was slightly decreased compared to the baseline to keep the constant IMEP target, due to an improvement in indicated efficiency given by the slightly later CA50.

The previous study demonstrated how advancing the injection event into the compression stroke to achieve HPC conditions allowed to suppress NO_x and smoke formation reaching near-to-zero levels. However, the typical

drawbacks of this strategy also appeared: too early SoC and CA50, an important reduction in combustion efficiency and excessively high ISFC. The main incompatibility found between the early injection HPC concept and the two-stroke engine architecture under development is the intrinsically high levels of hot IGR, which increases the temperature at IVC compared to four-stroke engines operating with conventional valve timings. The thermal effect of IGR added to the high compression ratio used in this preliminary study, are the two major factors causing the early onset of combustion when using high cetane diesel fuel.

Considering the limitations identified during the implementation of the HPC concept, an additional set of studies was performed in the single-cylinder engine, as an attempt to decrease the temperature of the charge during the compression stroke to shift the onset of combustion as close as possible to TDC. This optimization was based on parametric variations of the CR_{eff}, ΔP and $Olap$ to quantify the effect of the air management settings over CA50 during HPC operation. Afterwards, these studies were also performed with the LoCR1=13.6 piston to quantify the effect of decreasing the geometric compression ratio. The detailed analysis of these studies has been reported by Benajes et al. in [5, 6], so it will not be presented in this section. However, the main findings of this work can be summarized as follows:

- The influence of decreasing the effective compression ratio on combustion phasing and fuel consumption is very limited within the range allowed by the VVT system. For instance, decreasing CR_{eff} from 14.0 to 12.2 by shifting both intake and exhaust valve timings from $VVT_{(int,exh)}$ (15,10) to (30,25), only leads to a delay of the SoC and CA50 by approximately 2 CAD. Note that in this study the $Olap$ is kept constant, so the IGR level and accordingly the T_{IVC} also remained unchanged; therefore, the small delay in SoC is linked only to a small reduction in the gas temperature during compression that is achieved when IVC is delayed later in the cycle.

- Decreasing the temperature at IVC by decreasing as much as possible the IGR through the air management settings (particularly ΔP and $Olap$ which are the two most influential factors) is an interesting option for controlling combustion phasing in HPC conditions, despite the consequent penalty in TR and Q_{del}. In the reported studies, increasing the overlap from 65 CAD to 95 CAD by advancing the intake valve timing while keeping constant the exhaust valve timing, allowed a reduction in IGR from 49 % to 37 %; but additionally, the modified

scavenging process also decreased the pressure at IVC resulting in lower cylinder pressure during compression that further helped retarding the onset of combustion. However, despite the reduction in cylinder gas temperatures, the final effect over the SoC and the CA50 was approximately of 5 CAD in the optimized point, which is still insufficient to produce a suitable combustion process phased around TDC.

- Switching to the lower geometric compression ratio piston LoCR1=13.6 allowed to decrease the final gas temperature near the end of compression in 10 % to 15 % compared to the HiCR1 piston, so it had an impact on the ignition delay as expected. The reduction in compression ratio allowed to delay the SoC and CA50 closer to TDC in about 4 to 5 CAD, even before the optimization of the air management settings. In addition, it helped reaching HPC conditions with a relatively later injection timing compared to the HiCR1=17.2 piston, so that a fairly homogeneous mixture with ϕ lower than 1 was already achieved in the case of SoE2 -40 CAD aTDC providing extremely low levels of NO_x and smoke, along with a smother and slower combustion process with smaller pressure gradients.

- The spray mixing process in non-reactive conditions was simulated by means of a 1-D free-spray model [9, 10] in order to study qualitatively the spatial distributions of properties within the spray (velocity, temperature, density, mixture fraction, ...) as a function of time. Results from these calculations confirmed that in the LoCR1 piston case, even when the mixing process is slower due to the lower density inside the chamber, the longer ignition delay time given by the later SoC provides additional time to properly form a homogeneous and leaner mixture before autoignition, so that the maximum local equivalence ratio at SoC is decreased, and accordingly, the overall reactivity of the charge is much lower compared to the HiCR1 piston case. As a reference for the reader, a comparison of the experimental results obtained with the LoCR1 piston during the SoE2 sweep as well as the analysis derived from the 1-D free-spray model have been reported in [6].

- A simple theoretical analysis based on a polytropic compression adjusted to simulate the measured pressure trace for the reference case with HiCR1, along with a chemical simulation assuming a simplified homogeneous reactor to obtain the RoHR, were carried out to estimate how much the geometric compression ratio should be reduced to achieve a suitable combustion phasing (comparable to CDC with SoE2 -10 CAD aTDC). The geometric compression ratio was reduced

from 17.2 (equal to the reference experimental test conditions) to an extremely low value of 8.2, with the aim of observing the isolated effect of decreasing compression ratio over the in-cylinder gas temperature profile, excluding the air management behavior of the engine. The calculations showed that is necessary to reduce geometric compression ratio below 9 in order to achieve the required SoC angle needed to provide a suitable CA50.

- By combining the LoCR1 piston with optimized settings for ΔP and *Olap*, it was possible to shift CA50 to $-5.4\,\mathrm{CAD\,aTDC}$, which was the closest phasing to TDC observed in all the studies performed. The initial ISFC target of $230\,\mathrm{g/kW\,h}$ was not reached, nevertheless, the relatively better combustion phasing allowed to achieve ISFC values of around $250\,\mathrm{g/kW\,h}$ for the optimum found with the LoCR1 piston, which are close to be competitive compared to other HCCI results reported in the literature in four-stroke engines, and which are in the range of the ISFC initially obtained in CDC with non-optimized engine settings. The variations in ISFC appear as a balance between improving indicated efficiency without punishing too much combustion efficiency. So, the fuel energy losses associated to the sharp reduction in combustion efficiency (which falls to 82 % for the LoCR1 case) and possibly higher liquid fuel impingement onto the piston surfaces mitigates the potential benefits of the HPC concept.

Figure 5.4 summarizes the main achievements obtained during the investigation of the early injection HPC concept in the two-stroke poppet valve single cylinder engine. In this figure, the CDC results are compared with those provided by the HPC concept at the baseline study (SoE2 sweep), and also with the final optimum points found along the parametric optimization of the air management settings.

This research work evidences the potential of the HPC concept using diesel fuel for producing extremely low levels of NO_x and smoke emissions. However, even when operating with well optimized air management settings and adapted engine hardware at a low speed/load condition, the early combustion phasing and the sharp decrease in combustion efficiency given by the high reactivity of diesel fuel and the high cylinder temperatures, are the main drawbacks that compromises the feasibility of this concept for being implemented in the investigated two-stroke engine architecture. Furthermore, as the load increases the intrinsic problems of the HPC concept are further aggravated, restricting the operating range of the concept to extremely low loads.

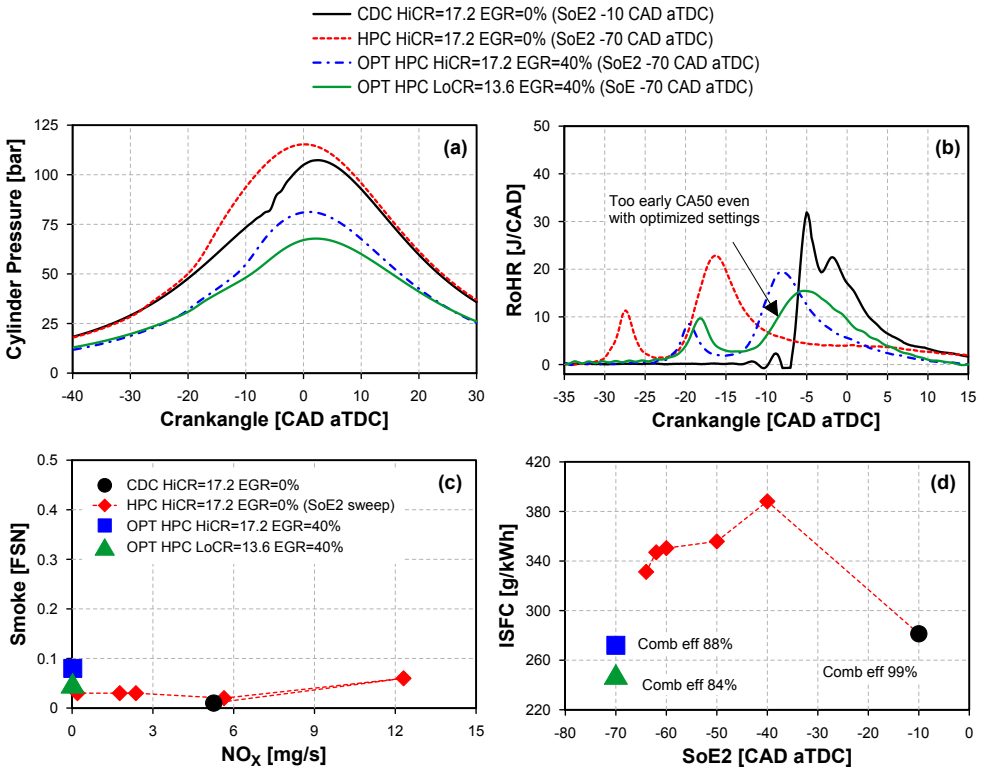

Figure 5.4. *Main outputs of the optimization process of the HPC concept: (a) Cylinder pressure, (b) RoHR, (c) NO_x-smoke trade-off and (d)* ISFC *as function of the injection timing.*

From the previous discussion, it was decided that further investigation of premixed LTC concepts is going to be focused on decreasing the fuel reactivity, while also switching to a partially premixed mixture instead of a nearly homogeneous lean mixture as the one that have been used in HPC studies. On one side, using a fuel with less cetane number (in this case a RON95 gasoline) is expected to help achieving proper combustion phasing in the vicinity of TDC; and on the other side, the local equivalence ratio stratification can allow retaining the control over CA50 with the injection event; which are two major issues to be resolved to improve the results provided by this early-injection HPC concept in the poppet valve two-stroke HSDI engine under development.

5.2.2 Implementation of the Partially Premixed Combustion (PPC) using gasoline fuel

5.2.2.1 General methodology of the studies

The next studies correspond with the preliminary evaluation of the gasoline PPC concept on the two-stroke engine, without performing any in-depth optimization of the engine settings. The operating condition chosen for this experimental test campaign corresponds with a low speed (1200 rpm) and low load (5 bar of IMEP) point, where the implementation of the PPC concept is achievable and safe for this preliminary stage of the research. The engine is operated with the same piston used for the optimization in CDC (HiCR2=17.8) and the wide angle nozzle C=8 holes 90 μm 148° which allows injecting inside the bowl up to −31 CAD aTDC.

A single injection strategy was selected for this preliminary study keeping a fixed fueling rate that provided 5 bar of IMEP, at the initial baseline study with P_{rail}=400 bar and SoE2 equal to −27 CAD aTDC. Then, the injection timing was swept each 2 CAD for each study, in a range defined considering the onset of knocking combustion and keeping the injection of the fuel inside the bowl on one side, and the deterioration of combustion stability and appearance of misfire cycles on the other side.

The impact of in-cylinder gas thermochemical conditions on the performance of the PPC concept has been evaluated by taking advantage of the flexibility of the two-stroke engine. For this first evaluation of the gasoline PPC concept, the air management settings were chosen based on previous knowledge without performing any in-depth DoE optimization, to obtain the required temperature evolution along compression to reach the autoignition temperature of gasoline (around 950 K) near the end of the compression stroke and assure the proper ignition of the cylinder charge. The $VVT_{(int,exh)}$ timings and the ΔP across the engine are used as levers to control the cylinder gas temperature and composition by affecting directly the TR and the IGR, as well as the initial thermodynamic conditions at IVC. For the first parametric test of this study, the gasoline PCC concept is implemented without introducing EGR. Next, the maximum EGR percentage allowed before compromising combustion stability (traced by CoV_{IMEP} and $CoV_{P_{max}}$) was evaluated; first, keeping the same air management conditions as those used in the first test with EGR=0 %, and later, with re-defined air management conditions in order to increase cylinder gas temperatures to permit higher EGR rates, and finally achieve the expected low levels in terms of NO_x emissions. As a reference for the reader, the complete results obtained

from this study can be found in the work of Benajes et al. reported in [11]. Table 5.2 contains the most relevant engine settings used along this preliminary study.

Engine settings						
T_{int} [°C]	P_{int} [bar]	ΔP [bar]	P_{exh} [bar]	$VVT_{(int,exh)}$ [CAD]	$Olap$ [CAD]	EGR [%]
35	1.8	0.25	1.55	(0,15)	80.0	$[0, 14]$
35	1.8	0.2	1.6	(10,15)	70.0	[25]
IMEP [bar]	m_{fuel} [mg/st]	P_{rail} [bar]	SoE1 [CAD]	SoE2 [CAD]	SoE3 [CAD]	$\%fuel$ [%]
≈ 5.0*	10.6	400	-	$[-31 \rightarrow -23]$	-	0/100/0
≈ 5.0*	10.6	400	-	$[-31 \rightarrow -23]$	-	0/100/0

Table 5.2. *Engine settings for the implementation of the PPC concept using gasoline fuel. *m_{fuel} was kept constant along the tests so small differences in* IMEP *are expected.*

5.2.2.2 Summary of main trends

Focusing on the air management characteristics, Figure 5.5 illustrate how the air management settings can be used as levers to control the in-cylinder conditions ($Y_{O_2,IVC}$ and T_{IVC}), by affecting both the TR and the IGR. As it was discussed in Chapter 2, during PPC operation it is necessary to decrease the oxygen concentration of the charge by the introduction of medium-to-high EGR rates to decrease maximum combustion temperature (traced by $T_{ad,max}$) and achieve the required low NO_x levels. The use of relatively high levels of EGR is also necessary to decrease mixture reactivity and slow down the combustion rates, as an attempt to mitigate the high propensity to knocking-like combustion typically found during PPC operation. However, to maintain a high combustion stability while decreasing $Y_{O_2,IVC}$, the air management conditions had to be re-adjusted in the study by decreasing $Olap$ and ΔP to increase both the initial gas temperature and its evolution during the compression stroke, to assure the proper ignition of a less reactive cylinder charge.

In the baseline case with EGR=0 %, the selected air management conditions correspond to a medium-to-small ΔP (0.25 bar) and medium-to-high overlap (80 CAD). These particular air management settings provided

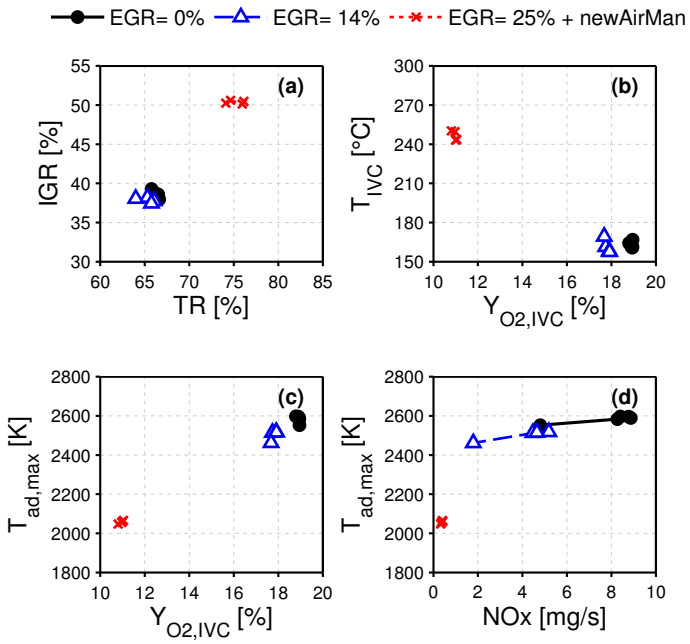

Figure 5.5. *In-cylinder conditions: (a)* IGR *as function of* TR*, (b)* T_{IVC} *as function of* $Y_{O_2,IVC}$*, (c)* $T_{ad,max}$ *as function of* $Y_{O_2,IVC}$*, and (d)* $T_{ad,max}$ *as function of* NO_x*.*

a TR around 66 % and 39 % of IGR, which gives a T_{IVC} and $Y_{O_2,IVC}$ of 160 °C and 19 % respectively. Keeping constant air management settings it was only possible to introduce 14 % of EGR, which corresponds to 17.5 % of $Y_{O_2,IVC}$, before starting to compromise combustion stability and ultimately loose control over the combustion onset. So, to be able to increase EGR up to 25 % and further decrease $Y_{O_2,IVC}$ down to 11 %, while keeping proper combustion stability, it was necessary to decrease both ΔP and *Olap* down to 0.2 bar and 70 CAD. With these new air management settings TR and IGR were increased up to 75 % and 50 % respectively, causing T_{IVC} to increase to 240 °C, what finally increases the temperature along compression assuring the proper ignition of the high octane gasoline.

The path followed to achieve low NO_x emissions during PPC operation is clearly illustrated in Figure 5.5.(c) and (d). At the baseline with EGR=0 %, NO_x emissions are higher than the expected levels, due to the high combustion temperatures ($T_{ad,max}$ over 2400 K) and sharp and fast combustion rate. Next, when introducing 14 % of EGR, the RoHR is softened and shifted

towards the expansion stroke and NO_x emissions are decreased compared to the baseline case as expected, thanks to the lower $Y_{O_2,IVC}$ and lower mixture reactivity. Nevertheless, NO_x levels are still above the target since $T_{ad,max}$ is still higher than 2200 K. For this reason, it is necessary to further increase the EGR rate to decrease $T_{ad,max}$ below 2200 K, and avoid NO_x thermal formation mechanisms to be able to achieve near-to-zero levels in NO_x emissions. Figure 5.5 confirms how these conditions are attained when $Y_{O_2,IVC}$ is decreased down to 11 %, drastically reducing $T_{ad,max}$ to 2060 K and finally reaching 0.3 mg/s of NO_x.

Focusing on the effect of SoE2 on the combustion process, Figure 5.6 shows the cylinder pressure and the RoHR profiles measured at the baseline case (EGR=0 %), along with the injection rates for each SoE2 timing.

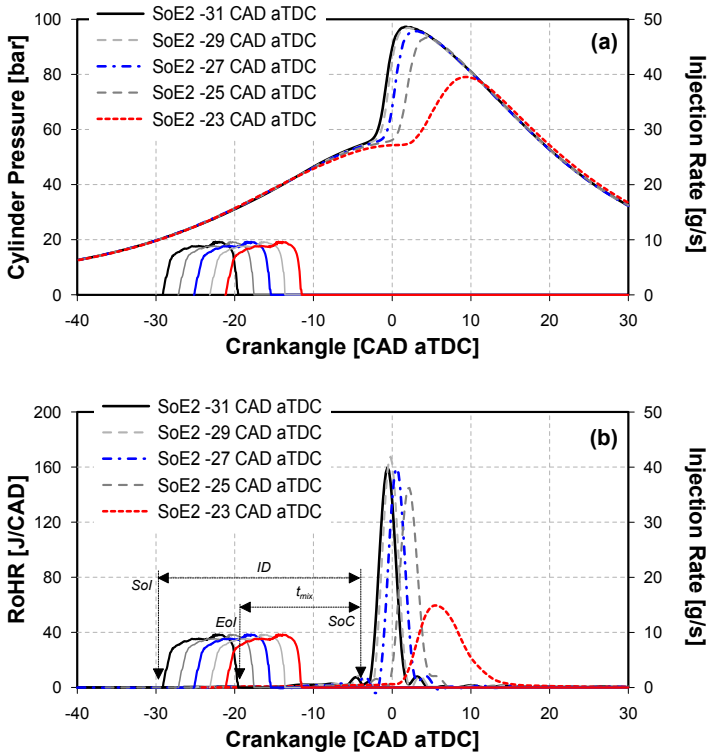

Figure 5.6. *Combustion characteristics: (a) cylinder pressure evolution and (b) RoHR profile for the gasoline PPC concept at the baseline case with* EGR=0 %.

As it is evidenced by the RoHR, the selected air management settings provided suitable in-cylinder conditions to assure reaching the autoignition of the charge close to TDC, which was not possible in the case of diesel HPC combustion. In agreement with the conceptual model of PPCI combustion [12] described in Chapter 2, the injection event is detached from the combustion process (similarly to what was seen in HPC conditions) yielding a positive ignition dwell, to avoid the overly rich mixtures where soot formation is promoted. Then, the mixing time (denoted as t_{mix}) is controlled by the EoI and the SoC. Since the injection event happens at a later timing than in HPC conditions, some degree of stratification in terms of local ϕ is maintained to assure proper ignition of the charge and retain the control over the SoC and CA50 with the SoE2, as it is confirmed by Figure 5.6. Additionally, the combustion process does not exhibit a LTR stage in the RoHR, contrary to what is seen in Figure 5.1 for diesel HPC conditions; since fuels with a branched structure such as the gasoline used in this study or iso-octane, are less conductive to the initial hydrogen abstraction and isomerisation reactions that occur below 850 K, what contributes to their higher resistance to autoignition [13].

Figure 5.7 shows the main combustion characteristics, in terms of CA50, dP/da_{max}, combustion noise and $CoV_{P_{max}}$ as function of SoE2, for the three measured tests with EGR at 0, 14 and 25 %. In general terms, advancing the injection timing earlier in the compression stroke (shifting SoE2 from −23 CAD aTDC to −31 CAD aTDC) increases P_{max}, dP/da_{max}, and advances the CA50 earlier in the compression stroke, increasing the trend towards knocking-like combustion. However, beyond the point of knocking-like combustion it also exist a condition in SoE2 from where a highly premixed mixture is attained and combustion starts to be delayed and softened despite the earlier injection timing. This HPC condition is not attained for the three measured tests with P_{rail}= 400 bar, nevertheless, this effect appeared at the earliest SoE2 when the injection pressure is increased to 600 bar as it was reported in [11].

In terms of the latest SoE2 that can be measured on each test, the experimental results showed that retarding SoE2 gradually increases $CoV_{P_{max}}$ until a limit is reached, from where cyclic dispersion is dramatically increased and misfire cycles start to appear, leading to the lost of control over the combustion process. This condition is observed at CA50 ranging between 8 CAD to 12 CAD because the combustion process fully takes place at the expansion stroke, where temperature and pressure are both decreasing slowing down the chemical reactions.

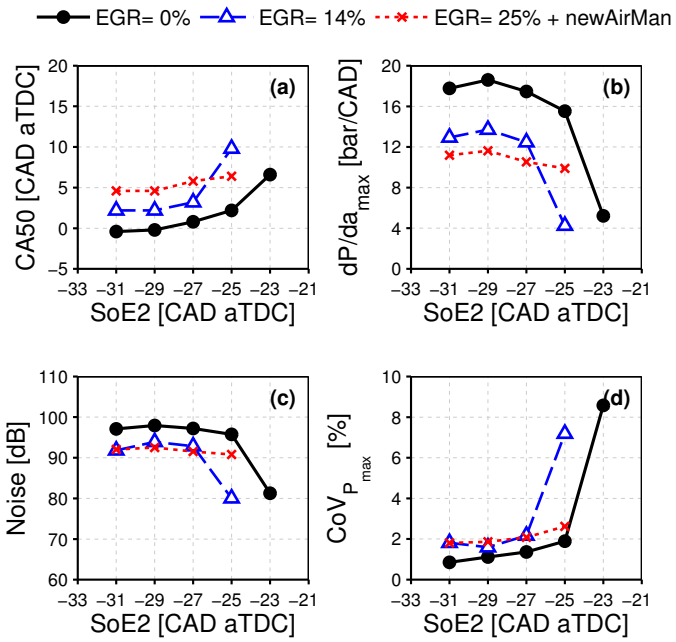

Figure 5.7. *Combustion characteristics: (a)* CA50*, (b)* dP/da_{max}*, (c) noise and (d)* $CoV_{P_{max}}$ *as function of* SoE2*.*

The points with EGR=0 % and SoE2 from −25 to −31 CAD aTDC exhibited the highest dP/da_{max} and noise levels of all three cases, above the threshold value of 15 bar/CAD and close to 100 dB, as a consequence of the abrupt and fast combustion rate previously observed in the RoHR profiles. Even when dP/da_{max} and noise levels exceeded the expected limits, no pressure oscillations typical of knocking combustion were observed in any of the points, and the common knock intensity indicators were below the threshold of knocking combustion. These values are lowered down to 10 bar/CAD and 91 dB due to a lower mixture reactivity when introducing 25 % of EGR, even after the increase in cylinder gas temperatures given by the new air management conditions. This increase in temperatures helped to keep both CoV_{IMEP} and $CoV_{P_{max}}$ below 3 % up to SoE2 −25 CAD aTDC, as it can be seen in Figure 5.7.(d), fulfilling the requirements in terms of combustion stability.

In order to gain insight into the relation between the mixing and combustion processes, the spray mixing process in non-reactive conditions has been simulated for the earliest and latest SoE2 at each level of EGR by means

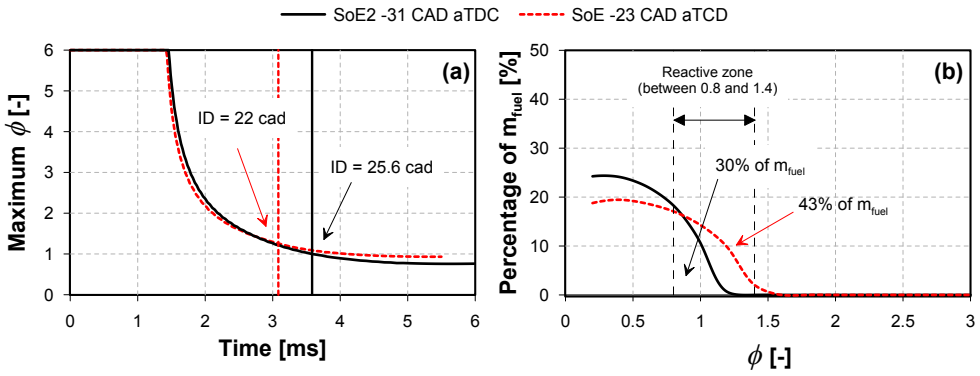

Figure 5.8. *Mixing conditions for* SoE2 −31 CAD aTDC *and* −25 CAD aTDC *(a) Maximum local ϕ as function of time, (b) fuel distribution at* SoC.

of a 1-D free-spray model [9, 10]. As a reference for the reader, a thorough description of this model, along with the validation against experimental data was reported by Pastor [9] for inert conditions, and by Desantes [10] for reactive conditions.

Figure 5.8.(a) shows the estimated maximum local ϕ as a function of time, referred to the SoI, for the baseline with EGR=0 %. The ignition delay for each case is included in this plot as vertical lines. Before the EoI the maximum local ϕ is equal to infinite at the nozzle exit, but for convenience, it was cut to a maximum value equal to 6. On the other hand, Figure 5.8.(b) shows the estimated fuel distribution traced by the percentage of the total injected fuel mass (m_{fuel}) under a given ϕ at the SoC, for the same tests as shown in Figure 5.8.(a). Both plots confirm that overly rich mixtures have been already mixed to ϕ lower than 2 by the time of the SoC, so in agreement with the ϕ-T diagram shown in Figure 2.6 for premixed LTC strategies, the local mixture and temperature conditions are successfully placed on the region that simultaneously avoids both NO_x and soot production zones.

Note how for SoE2 −23 CAD aTDC, the maximum ϕ descends slightly faster compared to the earliest SoE2, as a result of the enhanced mixing process induced by higher density inside the chamber during the injection event; nevertheless, since the ignition delay is shorter for the latest SoE2, a shorter mixing time results in slightly higher maximum ϕ at SoC. Accordingly, advancing SoE2 provides relatively more time to premix the air/fuel mixture, decreasing the percentage of injected fuel mass which is under reactive equivalence ratios (ϕ between 1.4 and 0.8), going from 43 %

for SoE2 −23 CAD aTDC to 30 % for SoE2 −31 CAD aTDC. Nevertheless, the conditions where combustion takes place are quite different between both cases, so even when the mixture at SoC in the case of SoE2 −23 CAD aTDC is more reactive, the combustion starts and progresses along the expansion stroke where pressure and temperature are already decreasing; while in the case of SoE2 −31 CAD aTDC, combustion starts before TDC where temperature and pressure are still increasing and there is still 30 % of the fuel mass near stoichiometric conditions, what might support the differences previously observed in the RoHR profile.

Regarding exhaust emissions, Figure 5.9 shows the measured NO_x, smoke, CO and HC emissions along with the combustion efficiency and the ISFC. As it was previously mentioned, decreasing $T_{ad,max}$ below 2200 K allowed to decrease NO_x emissions near-to-zero levels in the case of 25 % of EGR and new air management conditions, while the smoke level always remains close to zero, regardless of the SoE2 or the in-cylinder conditions; confirming that soot formation is avoided when the maximum ϕ in the combustion chamber is kept lower than 2 by the start of the combustion process.

Despite the drastic decrease in $T_{ad,max}$, the in-cylinder conditions still allowed to ensure high enough temperatures at the late stages of combustion to assure proper CO oxidation and to keep higher η_{comb} than in HPC conditions. Note that combustion efficiency is kept above 95 % in all cases, which is above the common values reported in the literature for medium-to-low loads and high octane fuels [14]. Nevertheless, a sharp increase in CO and HC was observed in the case of latest SoE2 for both EGR 0 % and 14 % caused by the worsened combustion conditions due to delayed CA50 and increased cycle-to-cycle dispersion, what finally punishes combustion efficiency.

Note that in the case of 25 % of EGR and new air management conditions, the higher mean in-cylinder temperatures improved combustion process keeping HC and CO emissions approximately constant compared to the baseline case, providing combustion efficiencies above 98 % even when the maximum combustion temperatures and the oxygen availability are significantly reduced. It is important to remark, that the dominant sources of HC and CO emissions are strongly dependent on the spatial mixture distribution, which is also dependent on the given engine geometry and operating condition [12]. Therefore, detailed CFD simulation of both local mixture conditions and combustion process for this particular two-stroke engine architecture is required to fully support and explain the experimentally measured CO and HC levels.

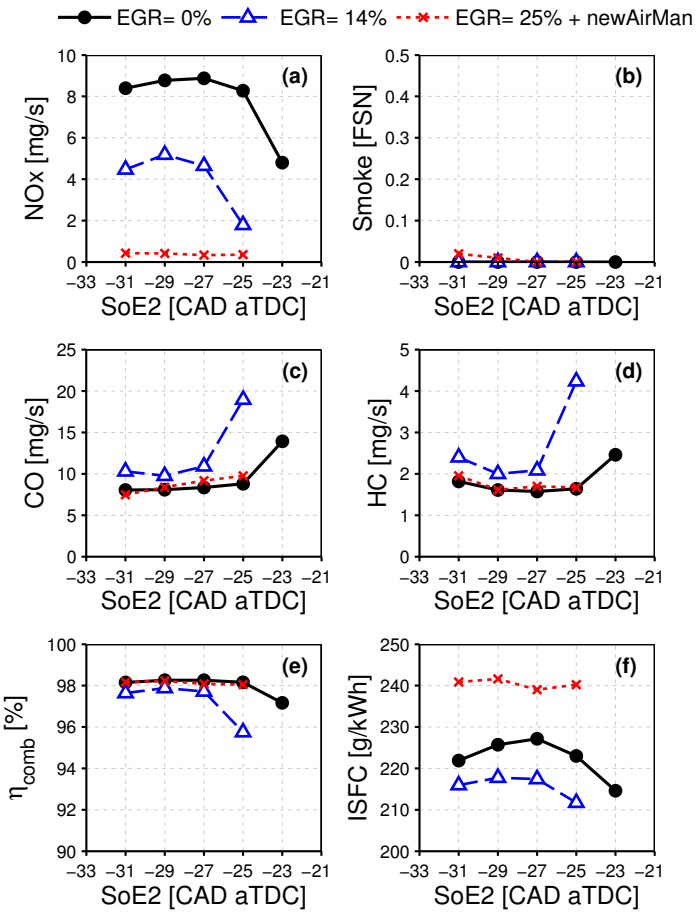

Figure 5.9. *Exhaust emissions and performance: (a) NO_x, (b) smoke, (c) CO and (d) HC, (e) η_{comb} and (f)* ISFC *as function of* SoE2.

Focusing on engine performance, the experimental results in terms of ISFC are depicted in Figure 5.9.(f). Note that the lowest ISFC value (211 g/kW h) and accordingly the highest η_{ind} (40 %) is obtained in the case of EGR=14 % and late SoE2, due to improved CA50 and lowered heat transfer losses given by the smother RoHR profile. On the counterpart, in the case of EGR=25 % and re-defined air management settings both ISFC and η_{ind} were worsened despite the improved CA50, reaching 240 g/kW h and (35 % respectively, due to the differences in the thermodynamic cycle

configuration, the deterioration of the gas adiabatic coefficient (higher burnt gas fraction) and the higher heat transfer losses caused by the higher mean gas temperatures along the cycle. Despite the increase in ISFC observed when going from 0 % to 25 % of EGR, the estimated $ISFC_{corr}$ is finally decreased from 270 g/kW h to 263 g/kW h due to lower Q_{del} and higher temperatures at the inlet of the turbine given by the re-defined air management conditions. Nevertheless, the differences between ISFC and $ISFC_{corr}$ were kept in the range of those observed operating with CDC, since the PPC concept was implemented defining realistic air management conditions, avoiding very high pressure ratios or excessively high air flow rates, which are out of the scope of the practical application in the final engine configuration.

This study confirmed how the PPC concept was successfully implemented in the two-stroke poppet valve engine attaining near-to-zero NO_x and smoke emission levels in a low load point using high ON commercial gasoline, which is difficult to achieve in four-stroke engines without the utilization of dedicated re-breathing or negative valve overlap strategies [15, 16]. In order to evaluate the range of operation of the gasoline PPC concept, a new set of studies was performed at 3 bar and 10 bar of IMEP at 1200 rpm, while keeping a single injection pattern and the same strategy in terms of the air management conditions as the one used at 5 bar IMEP. The detailed discussion of these studies has been reported by Benajes et al. in [17], so it will not be included in this chapter. Nevertheless, as a reference for the reader a short summary of the main findings and conclusions of the implementation of the gasoline PPC concept at 3 bar and 10 bar IMEP are listed below:

- Matching cylinder temperature, oxygen concentration and spray mixing rate is mandatory to achieve stable PPC operation at a given operating condition. A lower limit in terms of mixture reactivity was detected from where combustion could not be sustained any longer without worsening combustion stability. Decreasing oxygen concentration below this limit by further increasing EGR rate is only possible if the air management conditions are re-adjusted (decreasing $Olap$ and ΔP) to increase cylinder temperatures and compensate for this decrease in reactivity.

- It is possible to achieve stable PPC operation with CoV_{IMEP} and $CoV_{P_{max}}$ below 3 % and 4 %, respectively, even at very low engine loads, by keeping the same approach in terms of the air management settings as it was previously described for 5 bar IMEP. Accordingly, IGR level has to be increased up to 50 % while $Y_{O_2,IVC}$ is decreased down to 11 % to keep $T_{ad,max}$ below 2200 K. In the case of 3 bar IMEP reported in [17], near-to-zero levels in NO_x and smoke are reached with 20 % of EGR.

- With a single injection strategy, a transition between PPC and mixing-controlled combustion appeared when increasing the load above 10 bar IMEP depending on the in-cylinder conditions. The intrinsically higher mean gas temperatures combined with a high geometric compression ratio and the physical limitation in maximum P_{rail}, made it difficult to attain enough separation between injection and combustion processes to partially premix fuel-air mixture and avoid overly rich mixtures where soot formation is promoted, while simultaneously maintaining reasonable pressure gradients and low combustion noise. Furthermore, as load increases there is a higher tendency towards knocking-like combustion that makes necessary to decrease IGR as much as possible and to retard the injection event closer to TDC. So, at 10 bar IMEP decreasing simultaneously NO_x and smoke was not possible with the current hardware configuration and a single injection strategy. When a predominant premixed phased is maintained, the high combustion temperatures caused by the abrupt and fast combustion with high dP/da_{max} increased NO_x above the desired targets. On the counterpart, when shifting towards a predominant mixing-controlled phase, soot formation could not be avoided recovering the conventional trade-off be tween NO_x and smoke emissions.

- At 3 bar IMEP the η_{ind} values are found between 32 % to 35 %. The comparatively worst performance of the gasoline PPC concept in the two-stroke engine at this low load condition appeared to be partly explained by the intrinsically higher heat transfer losses, caused by higher mean cylinder gas temperatures along the closed cycle, induced by the high IGR (50 %) that is required to assure proper auto-ignition of the high octane (RON95) gasoline. On the counterpart, η_{ind} was improved when increasing the load, achieving 42 % at 10 bar IMEP as the combustion profile resembles more to a conventional mixing-controlled diffusive combustion, and lower IGR rates are required to assure proper ignition of the cylinder charge. These values are still lower compared to what can be attained operating in CDC, therefore, further optimization of the injection strategy and air management settings is required to fully exploit the benefits of the gasoline PPC concept.

The previous studies demonstrated that the implementation of the PPC concept using a high octane fuel in the two-stroke engine is feasible, reaching low emissions of NO_x and soot, while keeping η_{comb} above 95 % and high combustion stability. In addition, the flexibility provided by the air management settings can be used as an additional lever to control the

combustion environment and extend the range of application of the PPC concept from very low loads up to medium-to-high loads. Nevertheless, even when the results obtained operating with a single injection strategy are already promising, there are still some issues to be further investigated to improve performance of the concept.

In this regard, recent investigations have shown that the use of a multiple injection strategy allows precise control of the fuel-air stratification before the SoC, which affects the timing and strength of auto-ignition as well as the rate and completeness of fuel oxidation throughout the combustion chamber [18–20]. Moreover, Sellnau et al. confirmed the potential of a triple injection strategy for increasing thermal efficiency compared to a single injection strategy thanks to reduced heat losses during the expansion stroke given by a more favorable fuel distribution during combustion which results in less contact between hot combustion gases and the chamber walls [21–23].

Different strategies can be used to improve the performance of the gasoline PPC concept, for instance, combining the intake temperature with the IGR as levers to control the combustion onset, increasing the physical limitation in P_{rail} when injecting gasoline to improve high load operation, or using a fuel with lower octane number to improve low and medium load operation. Nevertheless, the next studies will focused on evaluating the use of multiple injection strategies for both low load and medium load operation. As it was previously mentioned, combustion characteristics are highly dependent on the mixture preparation prior to ignition; therefore, both the timing and the fuel quantity injected in each injection must be carefully optimized depending on the operating condition.

5.3 Analysis of the multiple injection PPC concept using gasoline fuel

After performing the preliminary evaluation of the potential of the diesel HPC and the gasoline PPC concepts on the two-stroke engine under study, the next studies will focused on finding a suitable injection strategy that allows decreasing NO_x and smoke emissions to near-to-zero levels, while improving indicated efficiency as much as possible. The engine is operated with the same hardware used for the optimization of the CDC concept and the implementation of the PPC concept, so with the HiCR2=17.8 piston and the wide angle nozzle C=8 holes 90 μm 148°. Next, three different operating points representative of medium and low load operation have been selected

from Table 4.1: Point 5 with 10.4 bar IMEP and 1500 rpm, Point 3 with 5.5 bar IMEP and 1500 rpm and Point 1 with 3.1 bar IMEP and 1250 rpm. The final objective of these studies is to establish a comparison against the previous results obtained operating with the CDC. As a reference for the reader, a summary of the main results derived from the detailed analysis of the combustion process, that will be described in the next subsections for these three medium-to-low load conditions, have been also included in the works of Benajes et al. [24, 25].

5.3.1 Medium load operation

5.3.1.1 General methodology of the studies

The engine operating condition selected for medium load operation corresponds to Point 5 with 10.4 bar IMEP and 1500 rpm. The fueling rate was fixed in the baseline case at 18.8 mg/st to achieve the targeted IMEP of 10.4 bar with a CA50 of 5 CAD aTDC. Then, m_{fuel} was kept constant for all subsequent tests. Intake air temperature was fixed at 35 °C while oil and coolant were maintained at their working temperature of 90 °C.

Preliminary values for the air management settings were selected using the available mathematical models for the responses that were previously obtained through the DoE optimization methodology while operating in CDC at Point 5. The statistical models were used as a tool to locate optimum air management settings which can provide a given combination of $Y_{O_2,IVC}$ and T_{IVC}, than can ensure the required temperature profile to attain proper auto-ignition of the cylinder charge around TDC. Nevertheless, the final selection and fine-tuning of the air management settings (specially for EGR and ΔP) was done directly at the single-cylinder engine, until low levels for NO_x and smoke emissions were reached while keeping reasonable combustion stability with CoV_{IMEP} below 2 %.

A triple injection strategy was selected for the studies since is expected to help in achieving the load target while avoiding/mitigating the knock tendency that was reported with a single injection strategy. For the reference point (baseline) the injection pattern included a very small first injection placed at SoE1 −60 CAD aTDC, a second (main) injection where most of the fuel is injected at SoE2 −40 CAD aTDC, and a small third injection close to TDC at SoE3 −2 CAD aTDC. This baseline case was used to setup and validate the CFD model during PPC operation with gasoline as fuel, as it was previously shown in Figure 3.16 and Table 3.11 from Chapter 3.

The timing of each injection was swept each 2 CAD for the first study; in a range constraint by the onset of knocking combustion or exceeding the smoke limit (4 FSN) on one side, and the deterioration of combustion stability (CoV_{IMEP} over 3 %) on the other side. Next, the second and third studies focused on evaluating the effect of the injection pressure (P_{rail}) and the fuel mass split between the second and the third injection ($\%fuel$) over the performance of the PPC concept, through additional sweeps of SoE2 for higher and lower levels of P_{rail} and $\%fuel$ compared to the baseline. Table 5.3 shows the main engine settings selected for PPC operation at Point 5.

Engine settings						
T_{int} [°C]	P_{int} [bar]	ΔP [bar]	P_{exh} [bar]	$VVT_{(int,exh)}$ [CAD]	*Olap* [CAD]	EGR [%]
35	2.75	0.71	2.04	(5,20)	78.4	43.5
IMEP [bar]	m_{fuel} [mg/st]	P_{rail} [bar]	SoE1 [CAD]	SoE2 [CAD]	SoE3 [CAD]	$\%fuel$ [%]
≈ 10.4*	18.8	850	[−66 → −54]	−40	−2	20/64/16
≈ 10.4*	18.8	850	−60	[−42 → −34]	−2	20/64/16
≈ 10.4*	18.8	850	−60	−40	[−8 → +2]	20/64/16
≈ 10.4*	18.8	750	−60	[−44 → −38]	−2	20/64/16
≈ 10.4*	18.8	950	−60	[−38 → −34]	−2	20/64/16
≈ 10.4*	18.8	850	−60	[−44 → −40]	−2	20/69/11
≈ 10.4*	18.8	850	−60	[−38 → −34]	−2	20/56/24

Table 5.3. *Engine settings for the analysis of the PPC concept at Point* 5. **m_{fuel} was kept constant along the tests so small differences in* IMEP *are expected.*

Regarding the air management settings, they correspond to considerably higher EGR (43.5 %), higher P_{int} (2.75 bar), higher ΔP (0.71 bar), and higher *Olap* duration (78.4 CAD) compared to the optimum values found operating in CDC. This combination of air management settings, provided 67 % of TR, 67 kg/h of Q_{del} and 35 % of IGR, that are translated into a $\phi_{eff,IVC}$ of 0.83 , and $Y_{O_2,IVC}$ and T_{IVC} of 12 % and 168 °C respectively, and finally a $Y_{O_2,EVO}$ of 4 %. Experimental results demonstrated the small effect of injection settings on the air management characteristics, so the most important gas thermodynamic conditions remained unaltered regardless of the injection timing, P_{rail} or $\%fuel$ between the injections, therefore they will not be shown in the next sections.

5.3.1.2 Effect of injection timing

5.3.1.2.1 Local cylinder conditions

As it was introduced in the preliminary study of the single-injection gasoline PPC concept, in most early-injection PPC strategies the injection event is typically finished before the ignition of the charge, yielding a positive mixing time that promotes pre-mixing of the fuel and air, avoiding the overly rich ϕ zone where soot formation is promoted. The degree of stratification in the mixture in terms of ϕ, which is affected by both the injection strategy as well as the gas thermo-chemical conditions, is used as the main lever to control the onset and development of the combustion process.

In the case of the baseline study at Point 5, the selected injection strategy covers a range typical of early-injection PPC strategies, where the SoE of the two early injections may vary between -70 CAD aTDC to -30 CAD aTDC combined with a late injection event with SoE near TDC which is more likely to the timings used in mixing-controlled diffusive combustion. This range of injection timings will clearly provide different gas thermodynamic conditions depending on the timing of each injection, so the spray behavior and local mixture conditions will be largely affected depending on the environment given at the SoI. Additionally, in the case of low ambient density values, the spray penetration can be large enough so that liquid film can impinge onto the cylinder surfaces forming liquid films. This is particularly important in the case of small bore engines, as the one used in this research, since liquid fuel impingement onto the piston and cylinder surfaces may easily occur, specially when using the wide angle nozzle.

From the previous discussion, it becomes clear that the 1-D free-spray model is no longer sufficient to fully represent the complex local phenomena affecting the spatial fuel distribution during the mixture preparation as well as during the combustion process. Accordingly, the CFD model was used to perform a detailed analysis of the local cylinder conditions (mainly in terms of ϕ and temperature), in order to provide additional insight into the mixing and combustion processes when operating with the gasoline PPC concept and a triple injection strategy at Point 5.

Figure 5.10 shows the local equivalence ratio of the gas mixture in a cross-section throughout the cylinder centerline at different CAD positions, in the case of the baseline study with the earliest and latest SoE2 timings, identified as (a) SoE2=-42 CAD aTDC and (b) SoE2=-34 CAD aTDC respectively.

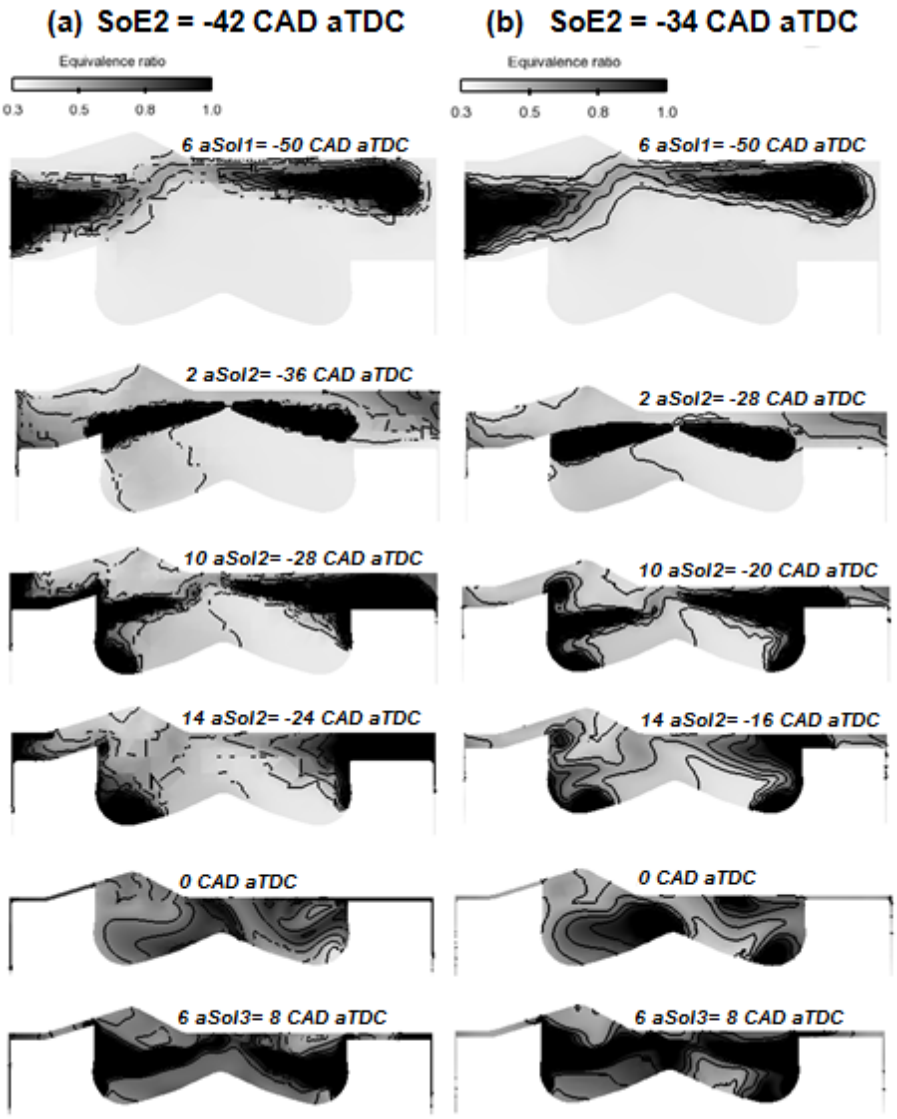

Figure 5.10. *Equivalence ratio distribution for (a)* SoE2 = −42 CAD aTDC *and (b)* SoE2 = −34 CAD aTDC *at different crankangle degrees for the gasoline PPC concept at Point* 5.

The intake valves are located in the left side of the combustion chamber, so the staggered roof in the cylinder head limits the flow of fresh air towards the exhaust valves during the scavenging process, and creates a tumble structure of the flow in counter-clockwise sense, as it was previously shown in section 4.4 in Chapter 4. This tumble-type aerodynamics deflects the sprays on the exhaust side upwards, moving them closer to the cylinder head, which in combination with the piston geometry, gives a non-symmetric distribution in terms of ϕ between the intake and exhaust sides.

The first injection is timed relatively early with SoE1=−60 CAD aTDC when the piston is well below the TDC. The spray is targeted above the piston bowl and, since temperature and density are still low at this CAD, the vaporization of the liquid fuel and spray mixing is less efficient; therefore, the total mass that is injected at this early injection is limited to 16 %, to keep a short pulse and limit the penetration of liquid fuel into the cold squish region. The CFD model confirms that liquid fuel impingement onto the cylinder walls coming from the very early first injection, can be avoided by injecting only a small fraction of the total fuel mass, even when using a 148° included angle nozzle and a relatively high P_{rail} of 850 bar.

After the first early injection, the majority of the injected fuel is mixed in the chamber to an overall lean equivalence ratio. However, by the time when the second injection starts, there are still some zones with ϕ ranging between 0.6-0.8 near the cylinder walls, as it can be seen in Figure 5.10 at 2 CAD aSoI2.

During the second injection event, the spray penetrates the combustion chamber, targeting the top of the piston bowl so the spray is split by the bowl lip, deflecting part of the fuel inside the bowl but also pushing fuel into the cold squish region, which is particularly critical in the flat side of the piston (exhaust side in the right), as shown at 10 CAD aSoI2 for both (a) and (b) cases. Then, the fuel trapped in the squish region takes more time to properly mix with air due to poor air utilization, so it remains at relatively richer ϕ by the time when the third injection starts (around 2 CAD aTDC), while the remaining fuel inside the bowl reaches lean ϕ faster.

Accordingly, advancing SoE2 earlier in the compression stroke helps extending the mixing time available for premixing the charge before the SoC, but at the same time it worsens the fuel/wall interaction between the spray and the piston top land regions, so a higher portion of the fuel remains trapped in the squish region (specially on the exhaust side) at rich ϕ by the time of SoE3, as it can be seen at 0 CAD aTDC in the case of (a) SoE2= −42. On the counterpart, retarding SoE2 closer to TDC as in the case of (b) SoE2= −34, allows keeping a higher percentage of the fuel injected on the second injection

inside the bowl, increasing the regions with ϕ between $1.4 - 0.8$ by the time of SoE3, and consequently increasing overall mixture reactivity compared to earlier SoE2.

A similar spatial mixture distribution as the one shown for the second injection event was reported in the imaging studies performed by Musculus et al. [12] and Petersen et al. [26], previously discussed in section 2.3.2.1 from Chapter 2, in the case of a light duty engine operating with conventional wide-angle injector geometry and typical spray targeting, while running in PPCI conditions with an early injection strategy. Musculus also states that it exist a close connection between this spatial ϕ distribution characteristic of early-injection PPC operation, and the corresponding formation and posterior oxidation of *CO* emissions, which are going to be discussed in detail in the next section.

Finally, once the third and last injection close to TDC has started, the mixture distribution resembles more to a stratified PPCI or late-injection LTC diesel combustion, where the spray may behave as a diffusive flame in a background of already-premixed fuel, depending on the duration of the injection, and the local ϕ distribution along the combustion will vary according to the available mixing time given by the SoC and the mixing rate of the spray. The evolution of ϕ after the EoI of the third injection is more similar to the structure described by Musculus for transient jets after the ramp-down of injection [27], shown in Figure 2.4, with a distribution with centerline ϕ clearly increasing with downstream distance from the injector nozzle.

To complement the analysis of local cylinder conditions, Figure 5.11 shows the temperature distribution in the selected cross-section at different representative crankangle positions along the combustion process (i.e: CA10, CA50 and CA90) and also at an instant well after the EoC during the expansion stroke (40 CAD aTDC), for the case of (a) SoE2=−42 CAD aTDC and (b) SoE2=−34 CAD aTDC respectively. As a reference for the reader, the equivalence ratio is still represented in each figure by contour lines in greyscale, while the temperature is displayed in a color scale.

The temperature required for gasoline auto-ignition (around 950 K) is reached around TDC for the majority of the cylinder charge. Accordingly, the ignition is initiated in the zones having ϕ within the reactive range (0.7-1.1) and the highest local temperature. The late third injection starts at 2 CAD aTDC and continues up to 5 CAD aTDC, while combustion is initiated in the lower area of the bowl at the intake side (left side of combustion chamber) at 4 CAD aTDC in a reactive zone with ϕ between 0.8-1, which results from the fuel injected primarily in the second injection, as it can be

observed in Figure 5.11 at CA10 (4 CAD aTDC. Next, the high-temperature zone characteristic of second-stage ignition processes rapidly progresses into the spray region, first, just in a thin layer at stoichiometric ϕ on the periphery of the flame, but then quickly filling the majority of the jet cross-section, including rich mixtures with ϕ around $2.5 - 2$.

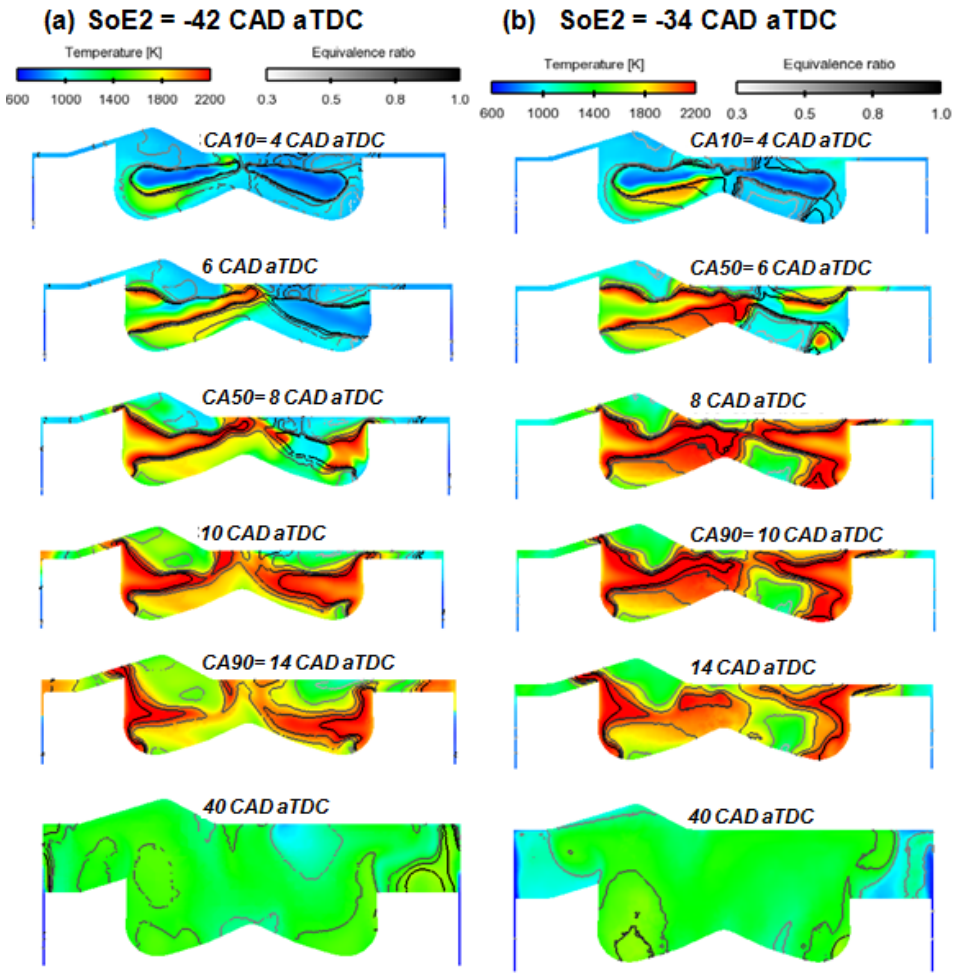

Figure 5.11. *Local temperature distribution for (a)* SoE2 $=-42$ CAD aTDC *and (b)* SoE2 $=-34$ CAD aTDC *at different crankangle degrees for the gasoline PPC concept at Point* 5.

Along the combustion process the maximum temperature is keep below 2300 K thanks to the low $Y_{O_2,IVC}$ given by the high EGR rates, even in the

case of (a) SoE2=34 CAD aTDC, where the higher mixture reactivity coming from the local ϕ distribution increases the combustion rate compared to the earlier SoE2 cases. Then, the relatively low combustion temperatures will allow inhibiting to some extend the thermal NO formation path, which will be reflected in the final NO_x emissions level. Finally, a region with relatively lower temperatures (1300 K to 1600 K) appears near the core of the combustion chamber close to the cylinder head (specially near the intake valves), as well as in the squish region near the cylinder walls, given mainly by the oxidation of leaner mixtures with ϕ between $0.6 - 0.4$. These mixtures may not achieve complete combustion becoming a potential source of HC and CO emissions.

5.3.1.2.2 Combustion characteristics

Switching to effect of the injection timing over the global combustion characteristics, the experimental results showed how sweeping SoE1 has a small effect over the combustion onset and the RoHR profile, as it is experimentally confirmed in Figure 5.12.(a), since only 16 % of the total fuel is injected on this early injection and it creates a fairly homogeneous background of lean ϕ as it was shown in Figure 5.10. Accordingly, the global combustion characteristics (P_{max}, dP/da_{max}, noise and combustion stability) were kept approximately constant regardless of SoE1. Therefore, the analysis will be primarily focused on describing the effects of the timing of the second and third injections, which are mainly controlling the characteristics of the combustion process.

The effect of SoE2 and SoE3 over the RoHR is shown in Figure 5.12.(b) and (c), respectively. SoE2 was swept from -34 CAD aTDC to -42 CAD aTDC being limited by poor combustion stability and appearance of misfire conditions for SoE2 earlier than -42 CAD aTDC and the onset of knocking-like combustion for SoE2 later than -34 CAD aTDC. In the case of SoE3, the timing was sweep between -8 CAD aTDC to 2 CAD aTDC and the range was limited by the onset of knock on earlier SoE3 and high soot emissions on later SoE3.

The RoHR profiles reveal how the second injection controls both the onset of combustion and its phasing (CA50). Specifically, advancing SoE2 shift both SoC and CA50 later in the expansion stroke, as shown in Figure 5.12, causing combustion to become smother and misfire trending; while retarding SoE2 advances both SoC and CA50 closer to TDC, rapidly increasing the propensity of knocking-like combustion.

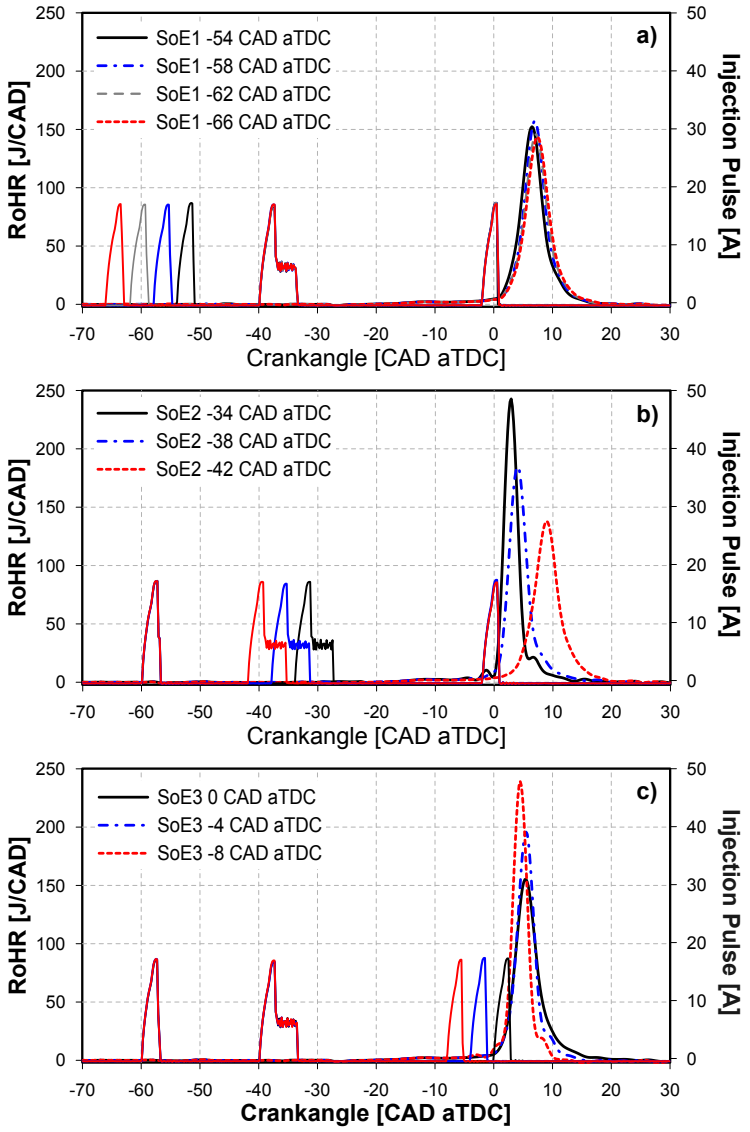

Figure 5.12. *Effect of injection timing (a)* SoE1*, (b)* SoE2 *and (c)* SoE3 *over the RoHR for the gasoline PPC concept at Point* 5*.*

These trends are in agreement with the local temperature distribution obtained for both SoE2=−42 CAD aTDC and SoE2=−34 CAD aTDC with the CFD model.

The experimental results also reveals the small effect of SoE3 over the SoC, which is mainly controlled by the second injection. On the contrary, the influence of SoE3 on the development of the combustion process is still relevant as observed in the RoHR profiles. So, advancing SoE3 increases the ignition delay and the available mixing time, allowing partial mixing of the fuel injected during this late injection event, increasing the reactivity of the global mixture at the SoC, and causing the combustion to trend towards knocking conditions as observed in Figure 5.12.(c). On the contrary, retarding SoE3 shortens the ignition delay and the available mixing time and, as a result, the combustion of the fuel injected in this late injection shifts from a partially premixed process to a mixing-controlled process with the corresponding impact on emissions explained later.

Figure 5.13 shows P_{max}, dP/da_{max}, noise and $CoV_{P_{max}}$ as function of the injection timing for each SoE sweep, confirming how the combustion characteristics are directly linked to the RoHR profile. In the case of the SoE2 sweep; for the latest SoE2 (-34 CAD aTDC) P_{max} is close to 150 bar with an extremely high dP/da_{max} equal to 22 bar/CAD) (being 160 bar 15 bar/CAD the limits recommended to secure engine durability), and noise level over 100 dB, which is caused by the fast and short knock-trending combustion phased near to TDC. On the contrary, for the earliest SoE2 (-42 CAD aTDC) the combustion process is smoother, longer and shifted towards the expansion stroke, with P_{max} equal to 123 bar, dP/da_{max} of 10 bar/CAD and 93 dB of noise level.

An additional effect of retarding combustion phasing later into the expansion stroke by advancing SoE2, is the consequent increase in the cycle-to-cycle dispersion, which is reflected in a noticeable rise in $CoV_{P_{max}}$ for the earliest SoE2 even when CoV_{IMEP} is not substantially affected and remains below 1.5 % in all cases). For cases with earlier SoE2 than -42 CAD aTDC, $CoV_{P_{max}}$ started to rapidly increase, followed by the appearance of misfire cycles and consequent lost of the combustion process.

In the case of the SoE3 sweep, the experimental results corroborates how P_{max}, dP/da_{max} and noise are substantially increased when advancing SoE3; reaching levels of 150 bar, over 20 bar/CAD and 100 dB, respectively, for the earliest SoE3 (-8 CAD aTDC). However, the effect of retarding SoE3 from -2 CAD aTDC (baseline) to later timings, on P_{max}, dP/da_{max} and noise is moderate despite the longer combustion duration. Finally, $CoV_{P_{max}}$ levels assure suitable combustion stability independently from SoE3 and, because similarly to the case of SoC, the cycle-to-cycle dispersion is mostly controlled by the second injection.

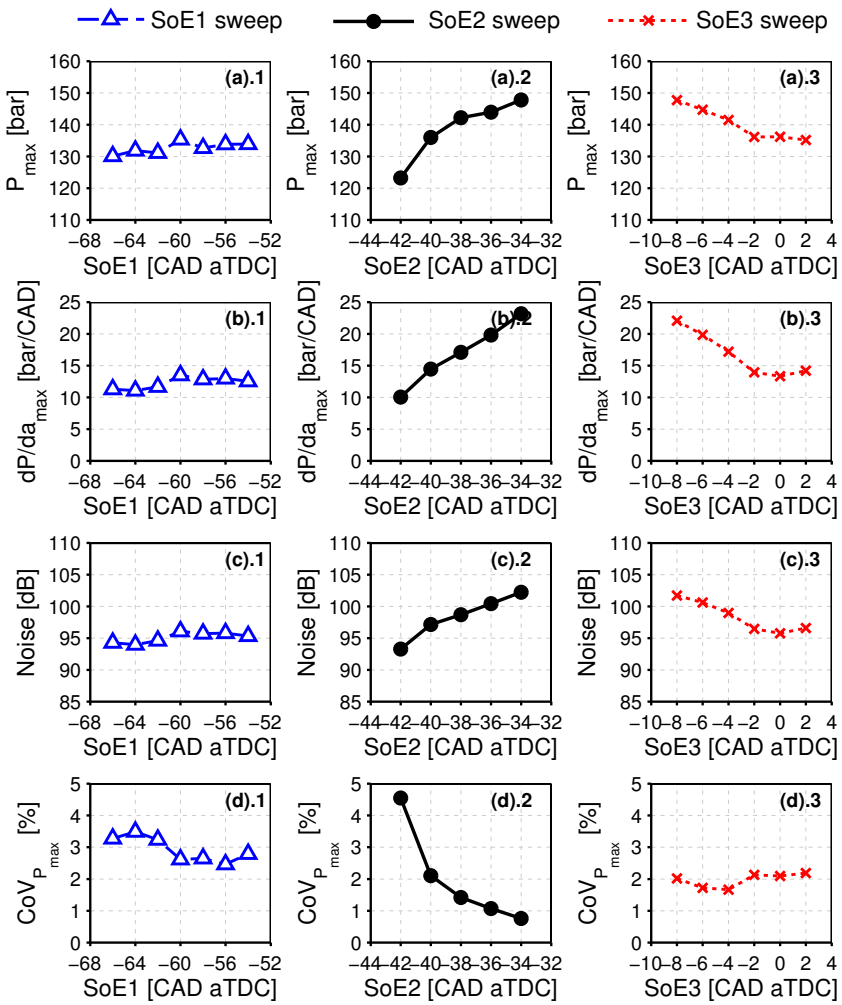

Figure 5.13. *Combustion characteristics: (a) P_{max}, (b) dP/da_{max}, (c) noise and (d) $CoV_{P_{max}}$ for* SoE1, SoE2 *and* SoE3 *sweeps operating with the gasoline PPC concept at Point* 5.

To complement the information about the local mixture conditions, and provide additional insight into the high sensitivity of the combustion process to SoE2 and SoE3 observed in the experimental results; the CFD model was used to build a histogram of fuel mass as function of ϕ, for the baseline study at different SoE2 and SoE3 timings. The reference timings SoE2=−40 CAD aTDC and SoE3=−2 CAD aTDC are then compared against two extreme (earliest and latest) values for SoE2 and SoE3, even when in some cases it was not possible to measure these conditions on the engine due to the appearance of misfire or knocking-like combustion.

Focusing in the effect of SoE2, Figure 5.14 shows a detailed description of the fuel mass at different local ϕ (Figure 5.14.(a)) as well as a histogram of the fuel mass fraction (Figure 5.14.(b)) for the three selected SoE2 timings. This analysis was performed at an instant in time right before SoE3 to avoid undesired interferences from the third injection, therefore, the local ϕ distribution corresponds only to the first and second injection events.

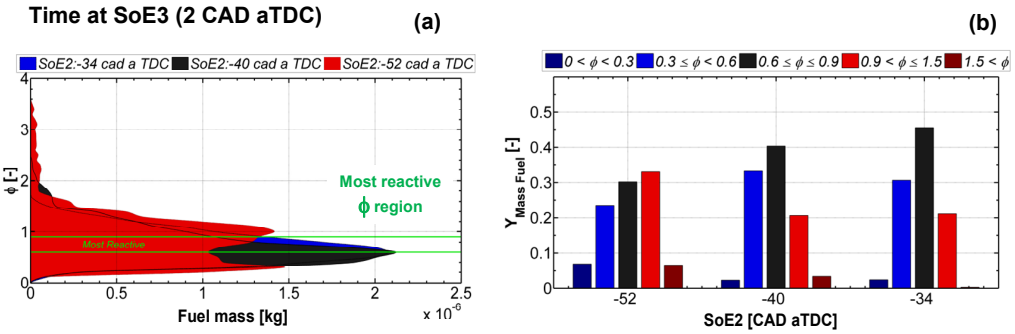

Figure 5.14. *Local conditions evaluated at the time just before* SoE3*: a) equivalence ratio distribution as function of fuel mass, b) histogram of fuel mass fraction for* SoE2 *equal to* −52, −40 *and* −34 CAD aTDC *for the gasoline PPC concept at Point* 5.

Three different SoE2 cases are included: −40 CAD aTDC (reference), −34 CAD aTDC (latest) and −52 CAD aTDC (earliest). Comparing the latest SoE2 with the baseline case, both Figure 5.14.(a) and Figure 5.14.(b) confirm how higher fuel mass is under the most reactive equivalence ratio ($0.6 \leqslant \phi \leqslant 0.9$) due to reduced mixing time and shorter ignition delay of the second injection. The higher reactivity of the mixture at the SoC explains why when retarding SoE2 the combustion rate increases, accordingly enhancing the knock trend, as reflected also by the increase in dP/da_{max}. In the case of the earliest SoE2, it was initially expected to find a local ϕ distribution shifted towards leaner

and then less reactive conditions due to the extended mixing time of the second injection given by the longer ignition delay. However, according to Figure 5.14 and in agreement with the previous analysis of the spatial ϕ distribution, at the earliest SoE2 case the fuel mass under relatively rich equivalence ratios (ϕ>1.5 and 0.9⩽ϕ⩽1.5) is increased compared to the baseline, which is caused by the slower-mixing of the fuel trapped in the squish region; while in contrast the fuel mass under the most reactive zone (0.6⩽ϕ⩽0.9) is consequently decreased due to the smaller fuel quantity that remains inside the bowl.

The result of these calculations also confirm that the reason why it is not possible to measure experimentally the points with SoE2 earlier than −42 CAD aTDC is closely linked to the poor matching between the selected wide angle nozzle and the piston geometry, which have been both optimized for CDC. Nevertheless, this opens a possibility for extending the range of operation of the PPC concept in terms of SoE2 by performing a dedicated optimization of the engine hardware in order to extend the window between knock and misfire extreme conditions.

Switching to the effect of SoE3 over the local mixture conditions, an analogous analysis to extract the local ϕ distribution generated by three different SoE3 is performed but now at the time corresponding to CA10, as it is considered as a suitable tracer of the onset of combustion. Three different SoE3 cases has been selected for comparison: −2 CAD aTDC (reference), −12 CAD aTDC (earliest) and 8 CAD aTDC (latest). Accordingly, Figure 5.15 shows a detailed description of the fuel mass at different local ϕ (Figure 5.15.(a)) and a histogram of the fuel mass fraction (Figure 5.15.(b)) for each SoE3 timing.

For the earliest SoE3 the fuel mass within the most reactive ϕ zone is substantially increased, explaining the higher reactivity of the charge and the faster and sharper RoHR profile trending to knocking-like combustion observed when advancing SoE3. Additionally, the rich zones with ϕ over 1.5 has almost disappeared by the time of CA10, so the soot formation is expected to be very low for early SoE3 conditions. In the case of the baseline SoE3, the third injection is being mixed so there is a clear stratification on local ϕ from rich to lean values, whereas in the case of the latest SoE3, the third injection has not been injected yet, and therefore, the local ϕ distribution corresponds to the mixing conditions of only the first and the second injection.

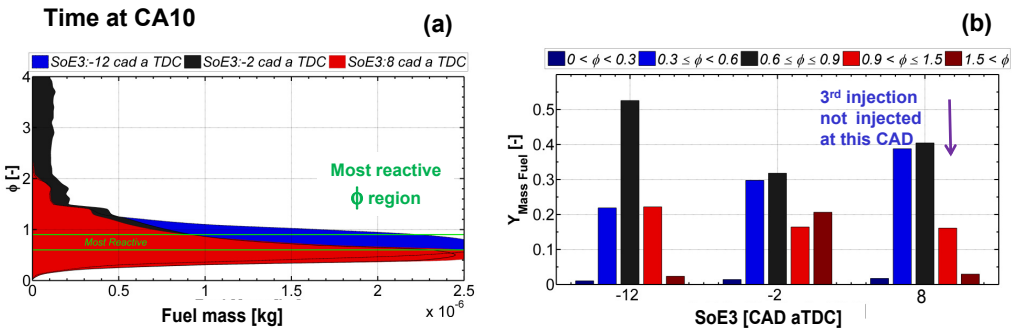

Figure 5.15. *Local conditions evaluated at* CA10*: a) equivalence ratio distribution as function of fuel mass, b) histogram of fuel mass fraction for* SoE3 *equal to* -12*,* -2 *and* 8 CAD aTDC *for the gasoline PPC concept at Point* 5*.*

5.3.1.2.3 Exhaust emissions

Figure 5.16 shows the exhaust emissions experimentally obtained when sweeping SoE1, SoE2 and SoE3. As it can be seen in Figure 5.16, SoE1 has a small impact on exhaust emissions, as it was expected, except for a slight increase in HC for the earliest SoE1 which might be linked to a larger spray penetration due to a slight decrease in cylinder gas density. In general terms, Figure 5.16 confirms that NO_x emissions are very low (below 1 mg/s) in the three studies, while smoke level is also kept comparatively lower than the values reported operating with CDC at this load condition (see Figure 4.13 as a reference).

The reduction in NO_x emissions during PPC operation is mainly attained by decreasing maximum combustion temperatures through the use of high EGR rates, instead of diluting the fuel-air mixture to a homogeneously lean ϕ, like in the case of highly-premixed HPC or HCCI concepts. Then, the thermal formation of NO_x is mainly controlled by $T_{ad,max}$, which is kept below 2400 K during PPC operation. Accordingly, advancing SoE2 brings a slight reduction in NO_x emissions as expected, linked to effect of retarded and softened combustion process with lower $T_{ad,max}$. In the case of smoke emissions, the soot formation appears in the high temperature and rich ϕ regions; so for the current injection strategy, the third (late) injection is the one acting as the main source of soot emissions by increasing local ϕ towards rich conditions during the combustion process. Therefore, the smoke level is also decreased when advancing SoE2 due to the extended ignition delay and therefore increased mixing time available for the third injection.

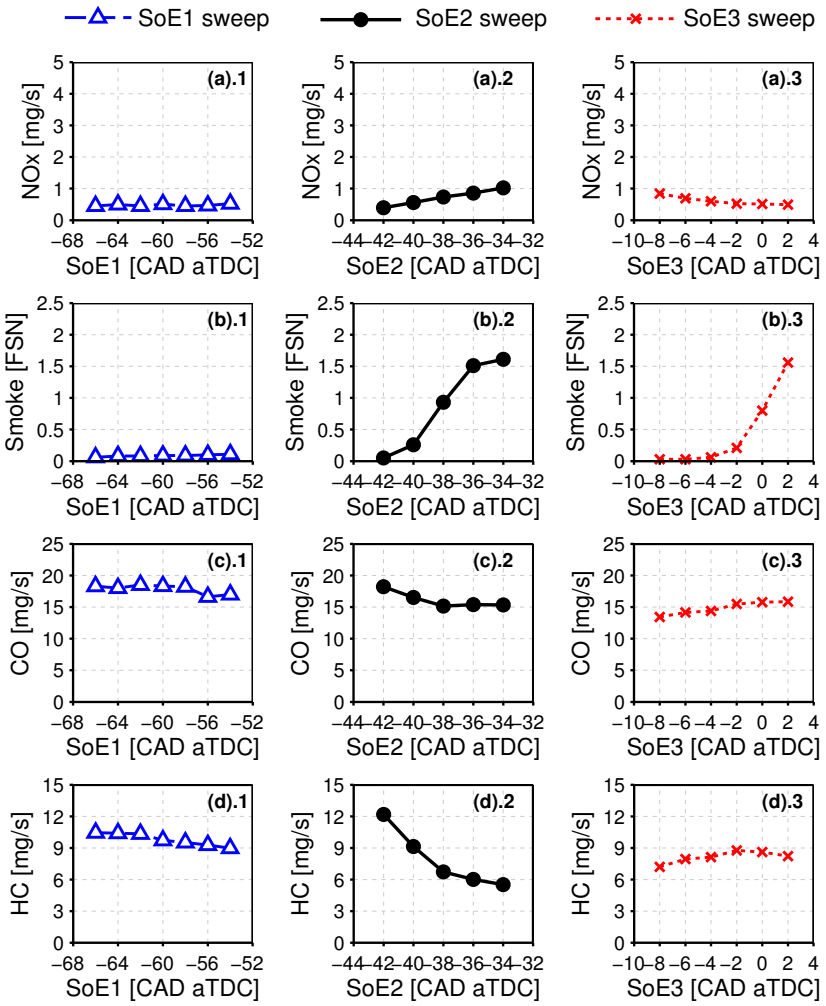

Figure 5.16. *Exhaust emissions: (a) NO_x, (b) smoke, (c) CO and (d) HC for* SoE1, SoE2 *and* SoE3 *sweeps operating with the gasoline PPC concept at Point* 5.

To give more insight about the spatial distribution of NO_x and soot emissions, Figure 5.17 and Figure 5.18 show the instantaneous NO_x and soot concentrations extracted from the CFD model at different crankangle positions, for the cases of (a) SoE2=−42 CAD aTDC and (b) SoE2=−34 CAD aTDC respectively. Additionally, Figure 5.19 shows a different representation of the evolution of the mass of NO (shown in iso-lines) as function of the crankangle and ϕ, for the two selected SoE2 cases.

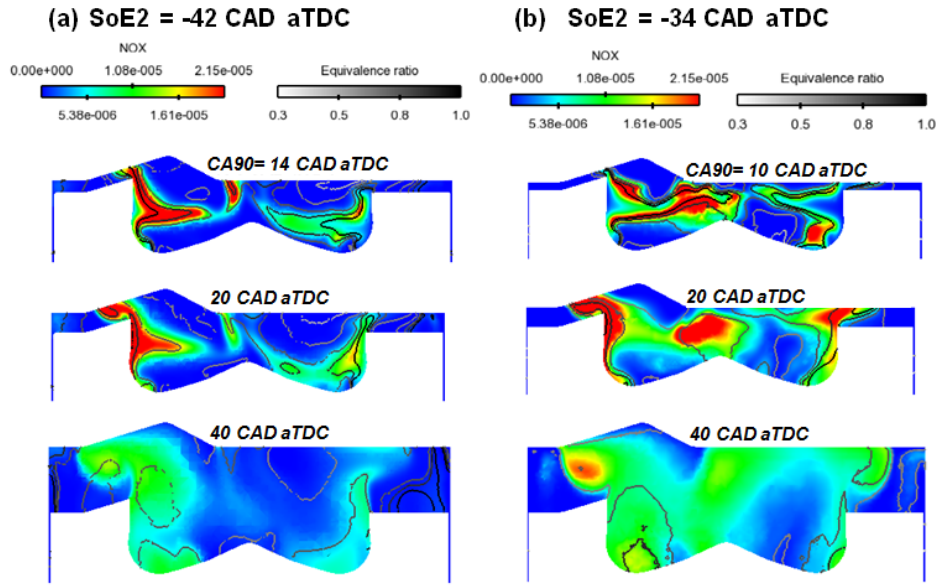

Figure 5.17. *Spatial distribution of NO_x for (a)* SoE2=−42 CAD aTDC *and (b)* SoE2=−34 CAD aTDC *at different crankangle degrees for the gasoline PPC concept at Point* 5.

Figure 5.17 and Figure 5.19 confirms how NO_x is observed during the final stages of combustion, around the CA90, in the reactive ϕ region inside the spray formed by the third injection, where the high temperatures from the combustion process favors the NO_x formation. The mass of NO which later will be transformed to NO_2 and will account for the majority of the NO_x emissions, is formed in the ϕ zone between 0.5 and 1.2, for both the retarded and early SoE2 cases. The lower NO mass shown by the constant mass lines colored in blue for the case of SoE2 −42 CAD aTDC, is a consequence of lower local temperatures, given by the later onset of combustion and retarded CA50 with softened and longer RoHR.

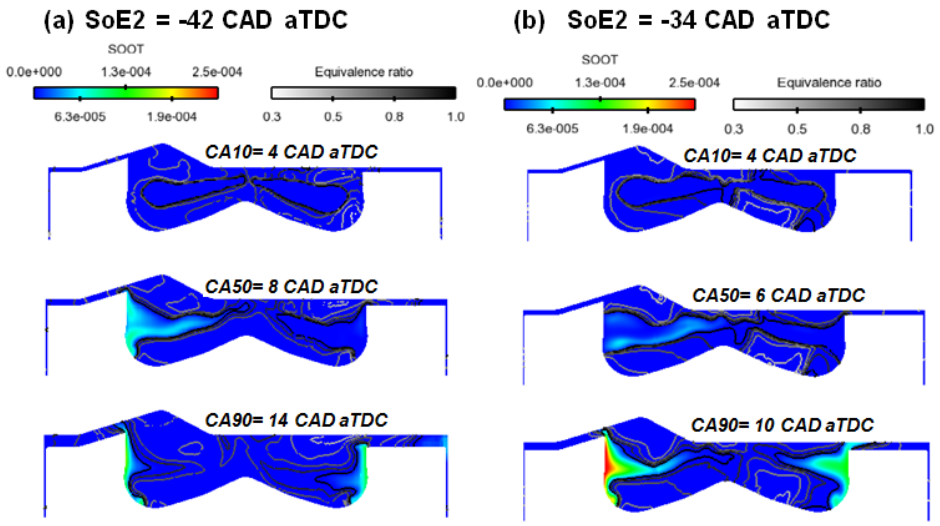

Figure 5.18. *Spatial distribution of soot for (a)* SoE2 = −42 CAD aTDC *and (b)* SoE2 = −34 CAD aTDC *at different crankangle degrees for the gasoline PPC concept at Point* 5.

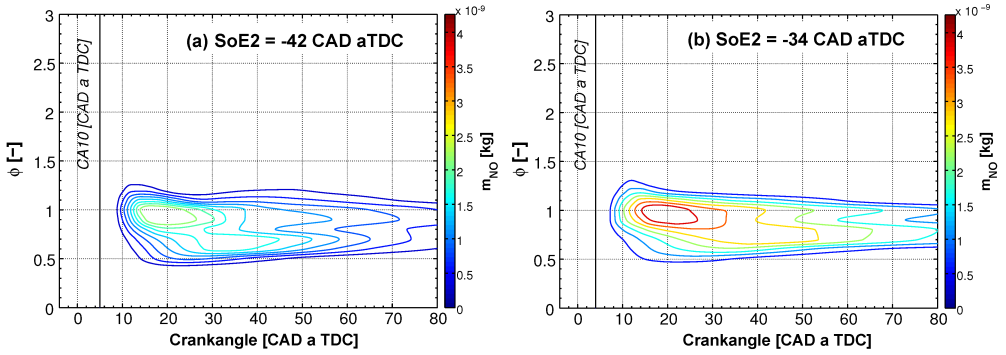

Figure 5.19. *NO mass distribution as function of local* ϕ *and crankangle for (a)* SoE2 −42 CAD aTDC *and (b)* SoE2 −34 CAD aTDC *for the gasoline PPC concept at Point* 5.

Figure 5.18 also confirms how the soot formation is concentrated primarily in the zones with ϕ over 2 in the inner side of the sprays, as it was expected, close to the bowl walls where combustion develops and temperatures are the highest. For the modeled case with SoE2 -42 CAD aTDC, the final soot level is very low, mainly because the fuel injected in the third injection is mixed enough before the SoC, so the extremely high ϕ regions are avoided during combustion.

Focusing in the SoE3 sweep, Figure 5.16.(a).3 confirms how retarding SoE3 decreases NO_x due to the slight reduction in local temperatures caused by the smother and longer combustion process. But on the counterpart, smoke emissions increase, as can be seen in Figure 5.16.(b).3, due to reduced mixing time and extended mixing-controlled stage, recovering the NO_x-smoke trade-off characteristic of the CDC concept. Accordingly, to avoid soot formation it is necessary to retard the SoC or to advance SoE3 to temporary separate this late injection from the combustion event. Note that the final soot level will result from the balance between formation and oxidation processes, so for the triple injection strategy, it will be affected by the local ϕ distribution along the combustion process, given by the timing and fuel mass injected in the second and primarily in the third injection, but also by the mixing rate of the spray and the oxygen concentration and temperature at the final stages of combustion, similarly to what was described for CDC.

Switching to the effect of SoE2 over CO and HC emissions, both pollutants are increased when SoE2 is advanced and accordingly CA50 is delayed, as observed in Figures 5.16(c).2 and 5.16.(d).2. So, it appears a clear trade-off between the levels of NO_x-smoke emissions and the levels of HC-CO. Moreover, the level for both emissions are considerably higher compared to the optimized reference values measured while operating in CDC.

In the case of CO, Figure 5.20 shows the instantaneous spatial CO mass concentration extracted from the CFD model at different crankangle positions, while Figure 5.21 shows the temporal evolution of the mass of CO along the cycle as function of ϕ, for the two selected cases: (a) SoE2=-42 CAD aTDC and (b) SoE2=-34 CAD aTDC.

Two main regions where CO is formed are clearly identified from Figure 5.20 and Figure 5.21. The first region corresponds to the rich ϕ areas (between $1 - 2.5$) located in the inner side of the spray structure, and also in the squish region on the exhaust side; while the second region appears at areas with lean ϕ (between $0.6 - 0.4$) distributed along the core of the combustion chamber close to the cylinder head and in the squish region on the intake side. The CO formed in relatively high ϕ conditions around the spray area will likely

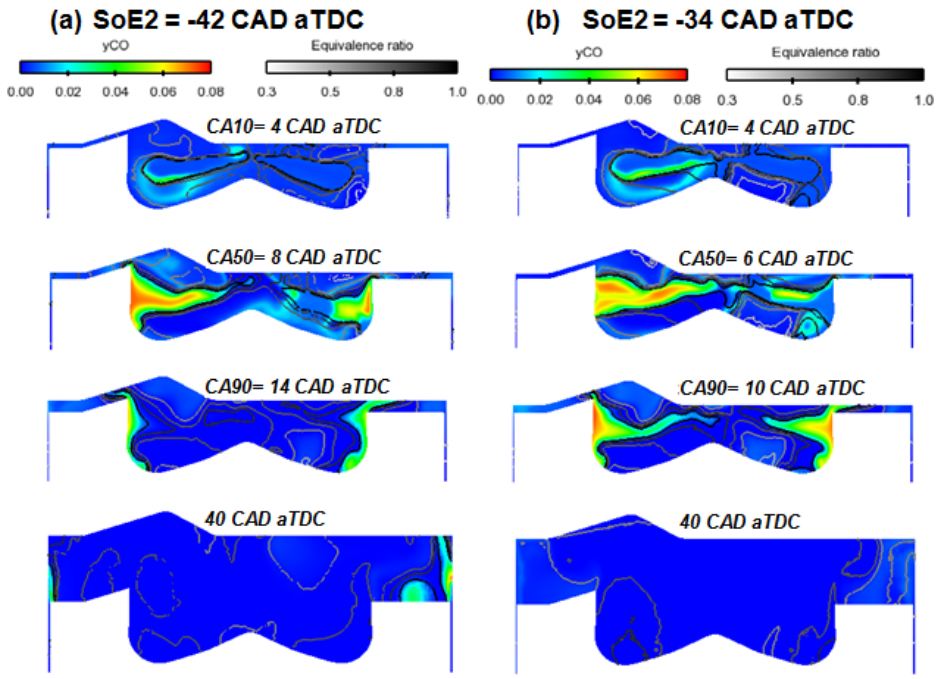

Figure 5.20. *Spatial distribution of CO for (a)* SoE2 = −42 CAD aTDC *and (b)*SoE2 = −34 CAD aTDC *at different crankangle degrees for the gasoline PPC concept at Point* 5.

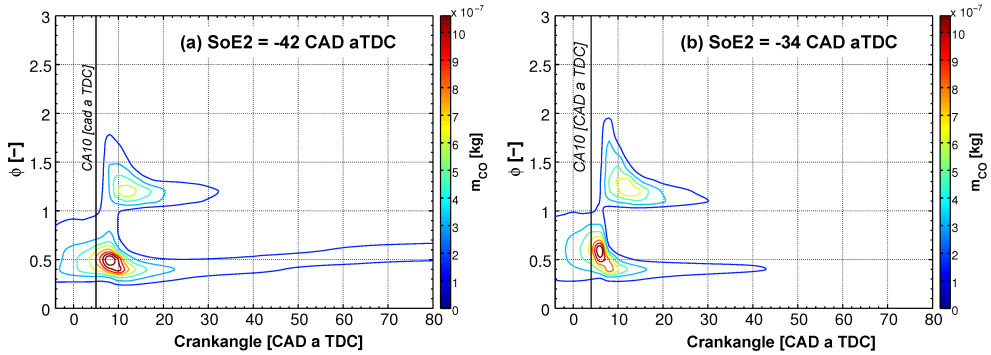

Figure 5.21. *CO mass distribution as function of local ϕ and crankangle for (a)* SoE2 −42 CAD aTDC *and (b)* SoE2 −34 CAD aTDC *for the gasoline PPC concept at Point* 5.

be oxidized along the combustion process; because combustion temperatures are high enough to assure proper CO-CO_2 conversion, as it is confirmed by Figure 5.21 for both SoE2 cases. On the counterpart, the slower reacting, over-lean mixtures located in the squish region and in the central part of the cylinder, with medium-low temperatures in the range of 1500 K and below, may not be properly oxidized, as it was also reported by Musculus et al. in [12]. In the case of SoE2 -42 CAD aTDC shown in Figure 5.21.(a), the CO mass formed in the lean ϕ region, is mainly located in the coldest squish areas near the cylinder walls (as it can be seen in Figure 5.20.(a)). Therefore, the final CO level which results as a balance between formation and destruction processes is consequently increased at early SoE2 due to the poor oxidation of the fuel at these local conditions.

Experimental results shown in Figure 5.16 also evidence a sharp increase in HC emissions for SoE2 earlier than -38 CAD aTDC, which will bring a consequent reduction in combustion efficiency. The CFD model reveals that when the second injection is placed earlier than -36 CAD aTDC (with the current engine hardware) part of the fuel impacting the bowl, piston top-land area and the cylinder liner remains in liquid phase, contributing to an increase in the percentage of fuel film in the walls, as it is shown in Figure 5.22.(a). Part of this fuel can be evaporated later along compression and combustion; however, for SoE2 earlier than -42 CAD aTDC, the fuel film located close to the cylinder liner cannot be properly evaporated; which added to the lower temperatures and slower combustion rate given by the later CA50 will significantly increase HC emissions.

Note that with the current injection settings and selected $\%fuel$, the fuel impingement coming from the first injection can be kept very low (less than 0.5 % of the total m_{fuel}); whereas, the third injection does not contribute to the liquid fuel film on the walls because it is injected near TDC, completely inside the bowl. Finally, the HC and iso-octane mass evolution shown in Figure 5.22.(b), confirms that for early SoE2 timings, almost all the HC emissions are coming from iso-octane that does not reach ignition conditions, mostly located in the squish area near the cylinder walls and cold crevices in the combustion chamber.

Finishing with the effect of SoE3, as it can be seen in Figure 5.16 CO is slightly increased when retarding SoE3 as a result of worse oxidation and slower CO conversion during the late-combustion stage given by the later CA90 and slower combustion rate. HC emissions are also slightly increased when retarding SoE3, but they are still mostly influenced by the first and

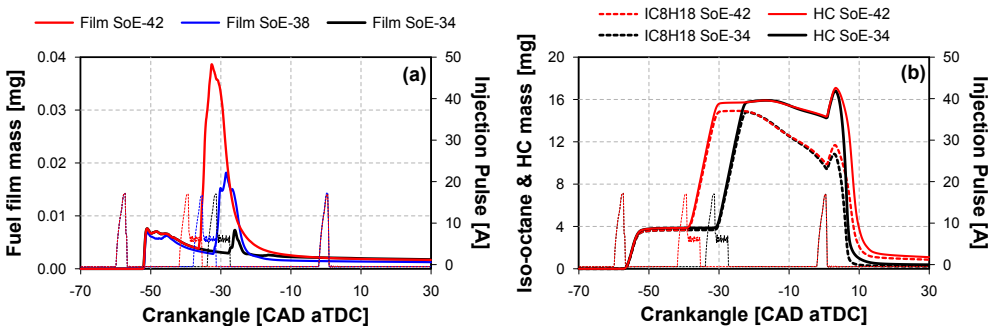

Figure 5.22. *(a) Fuel film mass as function of crankangle for* SoE2 42*,* 38 *and* −34 CAD aTDC *and (b) HC and iso-octane mass for* SoE2 42 *and* −34 CAD aTDC *for the gasoline PPC concept at Point* 5*.*

second injections, so this increase is also probably linked to the slightly worsened combustion efficiency observed with later SoE3.

5.3.1.2.4 Efficiency and fuel consumption

In terms of engine performance, Figure 5.23 shows the measured levels of η_{comb}, η_{ind}, and also ISFC and $ISFC_{corr}$ for the parametric variations of the injection timing of each of the three injections.

In general terms, the experimental results show how combustion efficiency is decreased when operating in PPC mode compared to the levels reported in CDC operation at Point 5, due to the comparatively higher CO and HC emissions. Focusing in the effect of SoE2, Figure 5.23.(a).2 confirms a decrease in η_{comb} when SoE2 is advanced earlier than 38 CAD aTDC which follows the trend observed in CO and HC emissions previously shown in Figure 5.16. However, it remains in levels over 96 % and 97 %, which is in the range of similar results reported in the literature [22, 28] when using high octane fuels.

The indicated efficiency ranges between 46 % to 47.5 % with the lowest values observed for early SoE2 due to the relatively lower η_{comb}. However, this η_{ind} levels correspond to ISFC ranging between 181 g/kW h to 178 g/kW h, which is translated into a 10 % improvement in ISFC compared to the optimum point found in CDC after performing the full optimization of both air management and injection settings. Despite the clear benefits in terms of η_{ind} and ISFC, if the mechanical power demanded by the air loop devices is taken into account, the resultant $ISFC_{corr}$ ranges between 237 g/kW h to

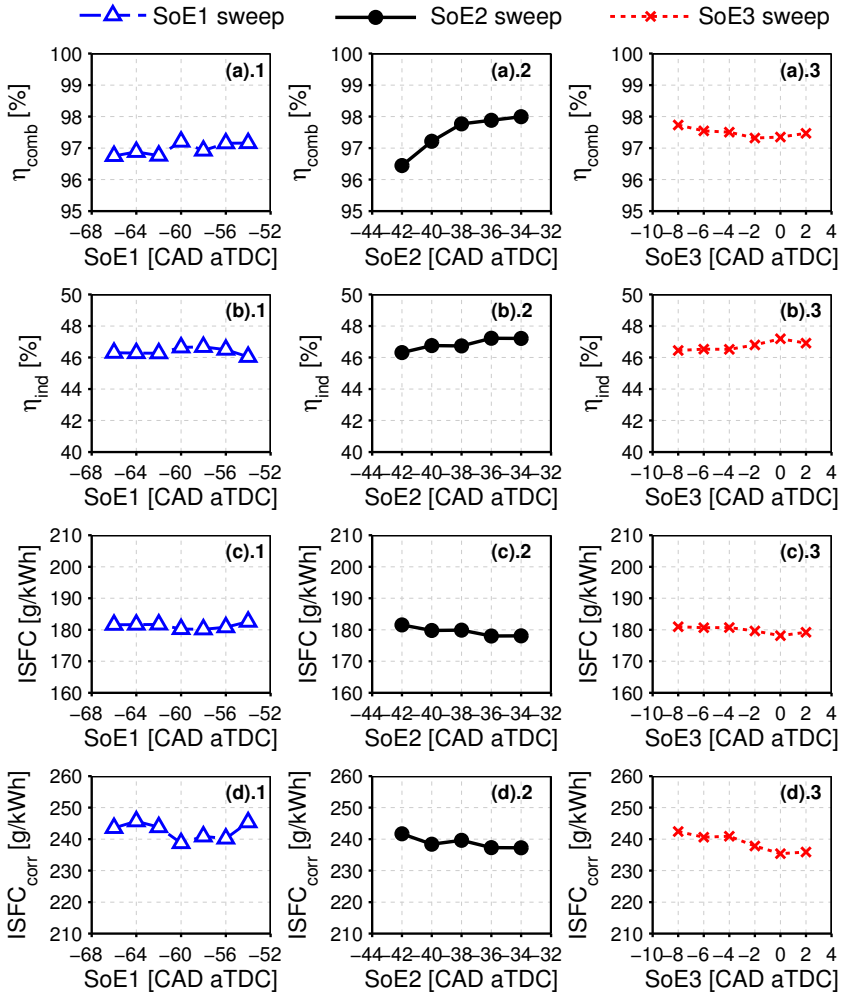

Figure 5.23. *Efficiency and fuel consumption: (a) η_{comb}, (b) η_{ind}, (c)* ISFC *and (d) $ISFC_{corr}$ for* SoE1, SoE2 *and* SoE3 *sweeps operating with the gasoline PPC concept at Point* 5.

241 g/kW h which is similar than the levels reported in CDC, due to the increase in mechanical power demanded by the supercharger to achieve the highly demanding $\phi_{eff,IVC}$ and $Y_{O_2,IVC}$ combination required to operate in PPC.

Focusing solely on the effect of SoE3, Figure 5.23 shows how η_{comb} is always higher than 97 %, while η_{ind} remains at levels around 47 % and neither is substantially affected by SoE3. However, ISFC slightly increases advancing SoE3 due to the fast and short combustion close to knocking conditions, going from 178 g/kW h to 181 g/kW h and as consequence $ISFC_{corr}$ also increases from 236 g/kW h to 242 g/kW h.

5.3.1.3 Effect of injection pressure and fuel split

Two different levels of injection pressure, P_{rail}=750 bar and P_{rail}=950 bar, were compared against the baseline (P_{rail}=850 bar) to study the effect of the mixing rate over the combustion process and pollutant emissions while operating with the gasoline PPC concept and a triple injection strategy.

Figure 5.24 shows a comparison of the RoHR obtained at SoE2 −38 CAD aTDC for the three P_{rail} levels. Additionally, the main combustion characteristics for the SoE2 sweeps at these three different P_{rail} levels are shown in Figure 5.25.

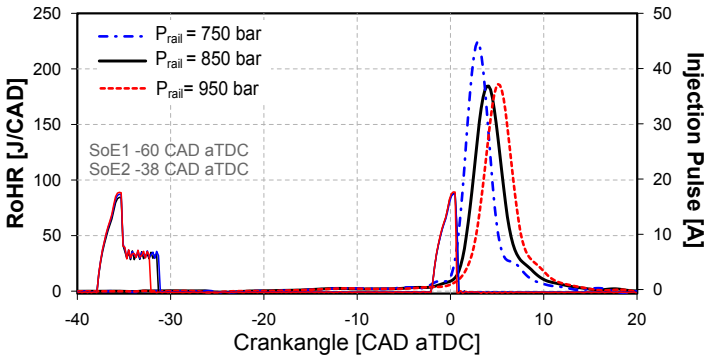

Figure 5.24. *Effect of injection pressure over the RoHR with* SoE2 −38 CAD aTDC *for the gasoline PPC concept at Point* 5.

As it can be seen in both Figure 5.24 and Figure 5.25, slowing down the mixing process by decreasing P_{rail} to 750 bar brought an increase in the overall

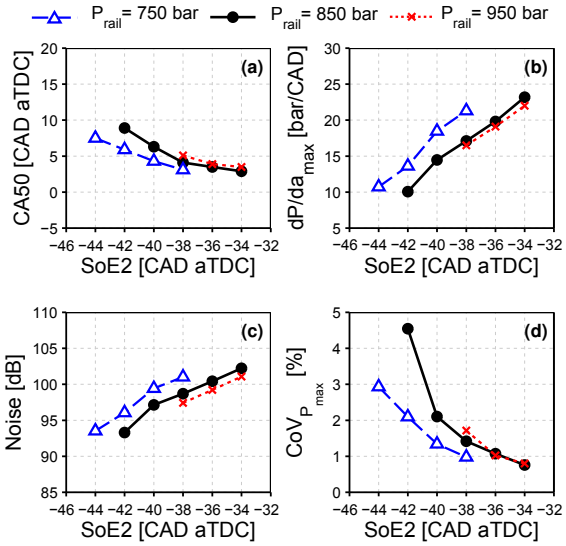

Figure 5.25. *Combustion characteristics: (a)* CA50*, (b)* dP/da_{max}*, (c) noise and (d)* $CoV_{P_{max}}$ *for* SoE2 *sweeps at different* P_{rail} *for gasoline PPC operation at Point* 5*.*

mixture reactivity (by increasing the percentage of fuel mass located in the reactive ϕ zone), that advances both SoC and CA50 consequently shortening combustion duration and increasing the peak of the RoHR compared to the baseline P_{rail}=850 bar. As a result, both dP/da_{max} and noise level, are increased by the earlier combustion phasing as it is confirmed by Figure 5.25.(b) and (c). At P_{rail}=750 bar the latest measured SoE2 was limited to −38 CAD aTDC to avoid the onset of knocking-like combustion and excessively high pressure gradients above 25 bar/CAD.

On the counterpart, increasing P_{rail} to 950 bar allows delaying both SoC and CA50 slightly later into the expansion stroke, allowing a small reduction in dP/da_{max} and noise. However, increasing the mixing rate through higher P_{rail} significantly shortened the window of operation between knocking-like combustion and misfire conditions when sweeping SoE2, so the earliest SoE2 experimentally measured was limited to −38 CAD aTDC to avoid the appearance of misfire cycles and unstable combustion with CoV_{IMEP} over 3 %.

Focusing on exhaust emissions, increasing P_{rail} to 950 bar allowed to decrease smoke emissions compared to the baseline and low P_{rail} case at constant SoE2, as it is shown in Figure 5.26, as the combined effect of faster mixing rate and delayed SoC, which extended the available mixing time for

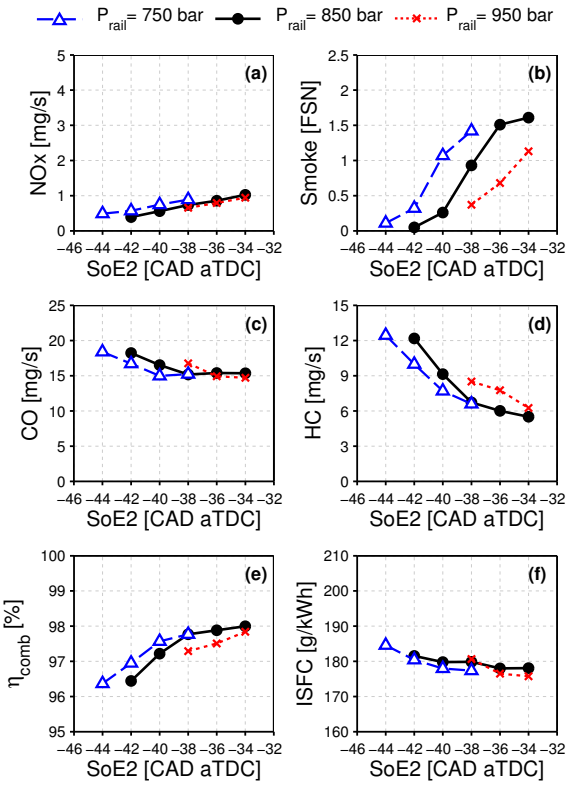

Figure 5.26. *Exhaust emissions and performance: (a) NO_x, (b) smoke, (c) CO, (d) HC, (e) η_{comb} and (f)* ISFC *for* SoE2 *sweeps at different P_{rail} for gasoline PPC operation at Point* 5.

both the second and third injections. On the counterpart, *HC* emissions are slightly higher in the case of P_{rail}=950 bar due to increased spray penetration, consequently worsening the fuel impingement onto the colder wall regions and the squish area.

Figure 5.26 also shows how smoke emissions are increased when decreasing P_{rail} to 750 bar as a consequence of shorter mixing time and worsened mixing conditions of the fuel injected in the late injection, which locally increases rich ϕ zones where soot formation occurs; while NO_x emissions are also increased due to the faster and advanced combustion process with earlier CA50, given by the more reactive local ϕ distribution generated by the worsened mixing conditions also for the early injected fuel. *CO* emissions are slightly lower due

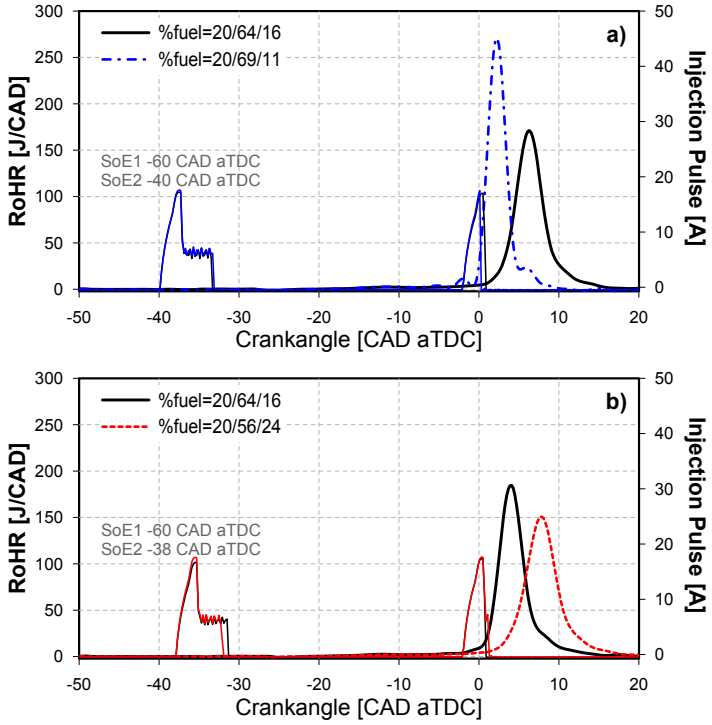

Figure 5.27. *Effect of fuel split over the RoHR with (a)* SoE2 −40 CAD aTDC *and (b)* SoE2 −38 CAD aTDC *for the gasoline PPC concept at Point 5.*

to better oxidation given by the increase in combustion temperatures. As a result of lower HC and CO emissions, η_{comb} is slightly higher in the case of lower P_{rail}. Finally, the injection pressure seems to have a relatively small effect over ISFC, and accordingly, over indicated efficiency, which appeared to be more influenced by the η_{comb} and CA50.

Switching to the effect of $\%fuel$, two additional fuel split distribution between the three injections were experimentally measured to be compared against the baseline, as it was previously shown in Table 5.3. In a first step, part of the fuel is removed from the third injection and it is added to the second, resulting in a $\%fuel$ of 20/69/11; while in a second step, the fuel is removed from the second injection and it is placed in the third, resulting in $\%fuel$ 20/56/24. Figure 5.27 shows the RoHR for the two additional $\%fuel$ cases, obtained at constant SoE2 −40 CAD aTDC and −38 CAD aTDC compared against the baseline. In the case of $\%fuel$ equal

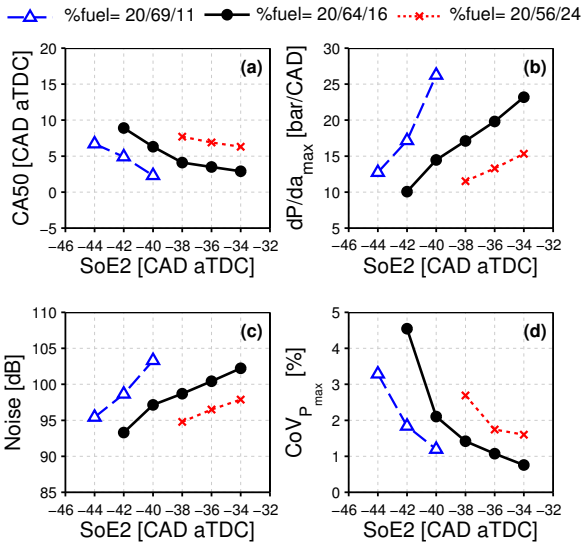

Figure 5.28. *Combustion characteristics: (a)* CA50*, (b)* dP/da_{max}*, (c) noise and (d)* $CoV_{P_{max}}$ *for* SoE2 *sweeps at different* $\%fuel$ *for gasoline PPC operation at Point* 5*.*

to 20/69/11, it was only possible to measure points with SoE2 comprised between −40 CAD aTDC and −44 CAD aTDC; as previously presented in Figure 5.27.a. Moreover, Figure 5.27.c confirms how increasing the fuel percentage in the second injection with respect to the baseline enhanced the knock trend, advancing SoC and shifting CA50 closer to TDC, due to the increase in mixture reactivity given by higher percentage of fuel mass in the reactive ϕ zone. As a consequence, points with SoE2 later than −40 CAD aTDC were not measured due to excessively high dP/da_{max} (over 25 bar/CAD) and noise level above 100 dB).

On the counterpart, decreasing the fuel mass in the second injection while increasing consequently the third injection ($\%fuel$=20/56/24), brought a noticeably reduction in mixture reactivity, so the points with SoE2 earlier than −38 CAD aTDC could not be measured due to poor combustion stability and the appearance of misfire cycles. Moreover, the RoHR profiles for SoE2 −38 CAD aTDC shown in Figure 5.27.c confirmed that in the case of $\%fuel$=20/56/24 CA50 is noticeably delayed further into the expansion stroke, consequently decreasing P_{max}, dP/da_{max} and noise levels; but also extending the mixing-controlled stage of combustion, widening and softening the RoHR as a consequence of the lower combustion rate.

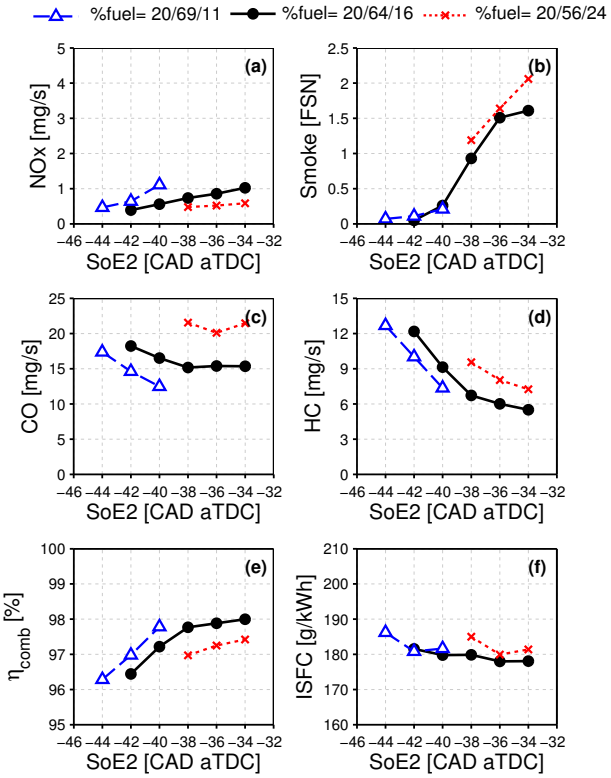

Figure 5.29. *Exhaust emissions and performance: (a) NO_x, (b) smoke, (c) CO, (d) HC, (e) η_{comb} and (f)* ISFC *for* SoE2 *sweeps at different $\%fuel$ for gasoline PPC operation at Point* 5.

Figure 5.29 shows how pollutant emission levels are also affected by the $\%fuel$ between the second and the third injections. In the case of $\%fuel$=20/56/24, soot emissions are increased when compared against the baseline, as a combined effect of higher fuel mass in the late injection which increases local ϕ distribution towards richer conditions by the time of SoC, added to the retarded CA50 and longer combustion duration which worsens late cycle soot oxidation processes. Both *CO* and *HC* emissions are increased for $\%fuel$=20/56/24, when compared against the baseline at constant SoE2; due to the worsened oxidation process and slower energy conversion given by the retarded CA50 phased further in the expansion stroke; while NO_x emissions are decreased also as the straight effect of lower combustion

temperatures. It is worth to remark that if HC emissions are compared at constant CA50, the case with higher fuel in the second injection, which corresponds to $\%fuel$=20/69/11, presents higher HC emissions compared to the baseline and $\%fuel$=20/56/24, due to higher fuel impingement onto the piston top land and squish areas given by the longer second injection event. Finally, Figure 5.29 also confirms how both η_{comb} and η_{ind} are decreased when increasing the mass on the late injection ($\%fuel$=20/56/24) when compared at constant SoE2, as a consequence of the worsened combustion process and extended mixing controlled phase.

5.3.2 Extension to low load operation

The analysis of the main characteristics of the gasoline PPC operation described in the previous subsection 5.3.1 for medium-to-high load conditions is also presented in this subsection for two low load conditions, Point 3 (with 1500 rpm and 5.5 bar of IMEP) and Point 1 (with 1250 rpm and 3.1 bar of IMEP); with the aim of evaluating the fuel consumption and emissions levels and establish a comparison against the optimum points found in CDC. Since the main trends between the air management, combustion process and emissions formation are kept regardless the load, and additionally they have been already described in detail for Point 5, the following subsections will briefly summarize the main trends and highlight some interesting aspects observed during PPC operation at low load conditions.

5.3.2.1 General methodology of the studies

For medium-to-low load points both triple and double injections are evaluated in order to find the most suitable injection pattern. The influence of the injection pressure (P_{rail}) and fuel split between the injections ($\%fuel$) is evaluated aside from the straight effect of sweeping the injection timing.

In the case of Point 3 (5.5 bar IMEP), four different studies were performed using a double injection strategy, in order to investigate the effect of different fuel splits between injections and to compare them against the triple injection strategy used in the baseline case. First, the third injection at -4 CAD aTDC was removed and its mass was added firstly in the second injection ($\%fuel$=16/84/0) and secondly in the first injection ($\%fuel$=32/68/0). Next, the first injection placed at -60 CAD aTDC was removed, and its fuel mass was relocated in the second injection ($\%fuel$=0/84/16) and in the third injection ($\%fuel$== 0/68/32). Table 5.4 summarizes the main engine settings selected for the studies performed at Point 3.

Engine settings						
T_{int} [°C]	P_{int} [bar]	ΔP [bar]	P_{exh} [bar]	$VVT_{(int,exh)}$ [CAD]	$Olap$ [CAD]	EGR [%]
45	1.7	0.32	1.38	(8,8)	63.4	33.5
IMEP [bar]	m_{fuel} [mg/st]	P_{rail} [bar]	SoE1 [CAD]	SoE2 [CAD]	SoE3 [CAD]	$\%fuel$ [%]
$\approx 5.5^*$	10.8	600	$[-66 \rightarrow -54]$	-40	-4	16/68/16
$\approx 5.5^*$	10.8	600	-60	$[-42 \rightarrow -34]$	-4	16/68/16
$\approx 5.5^*$	10.8	600	-60	-40	$[-10 \rightarrow 0]$	16/68/16
$\approx 5.5^*$	10.8	400	-60	$[-46 \rightarrow -38]$	-4	16/68/16
$\approx 5.5^*$	10.8	800	-60	$[-40 \rightarrow -34]$	-4	16/68/16
$\approx 5.5^*$	10.8	600	-60	$[-46 \rightarrow -40]$	w/0	16/84/0
$\approx 5.5^*$	10.8	600	-60	$[-46 \rightarrow -40]$	w/0	32/68/0
$\approx 5.5^*$	10.8	600	w/o	$[-46 \rightarrow -38]$	-4	0/84/16
$\approx 5.5^*$	10.8	600	w/0	$[-48 \rightarrow -40]$	-4	0/68/32

Table 5.4. *Engine settings for the analysis of the PPC concept at Point* 3. $^*m_{fuel}$ *was kept constant along the tests so small differences in* IMEP *are expected.*

In the case of Point 1 (3.1 bar IMEP), a double injection strategy was selected in advance, since a relatively small fuel quantity is injected. So, the first early injection placed at SoE1 −60 CAD aTDC is removed, to avoid excessively high HC emissions, and the fuel is correspondingly divided between the remaining two injections. Additionally, the high resistance to auto-ignition given by the RON95 gasoline increased the sensitivity of the combustion process to the injection strategy making it difficult to keep a stable combustion process with CoV_{IMEP} below 2 %, consequently limiting the range in terms of P_{rail} that could be practically measured in the engine. For that reason, at Point 1 it was only possible to measure two different $\%fuel$ at one level of injection pressure and the effect of P_{rail} will be explained only for Point 3. Finally, Table 5.5 shows the main engine settings selected for the studies performed Point 1.

When decreasing the engine load, decreasing ΔP and $Olap$ is mandatory to increase the IGR ratio and then T_{IVC} until reaching the auto-ignition temperature of the RON95 gasoline (around 950 K) close to TDC and sustain the combustion process. Moreover, the combustion process becomes more sensitive and less tolerant to high EGR rates, so both the intake temperature

Engine settings						
T_{int}	P_{int}	ΔP	P_{exh}	$VVT_{(int,exh)}$	$Olap$	EGR
[°C]	[bar]	[bar]	[bar]	[CAD]	[CAD]	[%]
45	1.3	0.21	1.1	(14,13)	62.4	15
IMEP	m_{fuel}	P_{rail}	SoE1	SoE2	SoE3	$\%fuel$
[bar]	[mg/st]	[bar]	[CAD]	[CAD]	[CAD]	[%]
$\approx 3.1^*$	6.5	400	w/o	$[-36 \rightarrow -26]$	-4	0/60/40
$\approx 3.1^*$	6.5	400	w/o	-30	$[-8 \rightarrow 0]$	0/60/40
$\approx 3.1^*$	6.5	400	w/o	$[-40 \rightarrow -30]$	-4	0/40/60

Table 5.5. *Engine settings for the analysis of the PPC concept at Point* 1. $^*m_{fuel}$ *was kept constant along the tests so small differences in* IMEP *are expected.*

and T_{IVC} are used to compensate the overall decrease in charge reactivity. At Point 3 (5.5 bar IMEP), the decrease in valve overlap and ΔP to 63.4 CAD and 0.32 bar, made possible to increase trapping ratio and IGR to 82 % and 43 %, which added to a relatively high P_{int} and EGR of 1.7 bar and 33.5 %, resulted in 12 % of $Y_{O_2,IVC}$ with 220 °C of T_{IVC} and 0.8 of $\phi_{eff,IVC}$.

At Point 3 (3.1 bar IMEP) where the main priority was to achieve stable PPC operation and assure reliable ignition, the chosen air management settings and particularly the low values for $Olap$ and ΔP (62.4 CAD and 0.21 bar) provided a TR/IGR combination of 81 % and 54 % respectively, while the EGR level was limited to 15 % to keep proper combustion stability with CoV_{IMEP} under 2 %. The final in-cylinder conditions at this low load operation correspond to 0.66 of $\phi_{eff,IVC}$, and 13.8 % and 235 °C of $Y_{O_2,IVC}$ and T_{IVC} respectively. This intrinsic flexibility of the two-stroke engine architecture is a key advantage to achieve PPC conditions over a wide operating range and assure stable combustion even at low loads, where auto-ignition of high octane fuels can be difficult in conventional four-stroke engines.

5.3.2.2 Effect of injection timing

Starting with the effect of the injection timing over the main characteristics of the combustion process, as it was previously described at medium-to-high load conditions (Point 5) when using a triple injection strategy, the timing of the second (and main) injection is controlling both the onset of combustion (SoC) as its phasing (CA50), while the timing of the third (late) injection

controls the combustion rate and its duration, but has a very small influence in the onset of combustion. Figure 5.30 and Figure 5.31 show the effect of SoE2 and SoE3, over the RoHR profile for the two low load operating conditions at the baseline study.

In the case of Point 3 (5.5 bar IMEP), similarly to what was already described for Point 5, both the combustion onset and phasing shift towards the expansion stroke when advancing SoE2, while the RoHR becomes smoother with longer duration and lower peak. On the contrary, retarding SoE2 closer to TDC decreases ignition delay and mixing time, so the local ϕ stratification increases enhancing the reactivity of the mixture. Consequently, both SoC and CA50 are advanced towards the TDC, while combustion is faster with a higher peak in the RoHR.

The influence of SoE3 on the development of the combustion process is still relevant at Point 3, as observed in Figure 5.30.(b). So, advancing SoE3 increases the ignition delay and the available mixing time of the third injection, hence, increasing the reactivity of the global mixture at the SoC causing the combustion to trend towards knocking conditions as observed in Figure 5.12.(c). On the contrary, retarding SoE3 after the SoC shortens the ignition delay and the available mixing time and, as a result, the combustion of the fuel injected in this late injection will start to be burned in a mixing-controlled (diffusive) process.

In the case of Point 1 (3.1 bar IMEP), the RoHR exhibits a combined structure, with an initial premixed phase followed by a mixing-controlled stage, as illustrated in Figure 5.31. The increased stratification in local ϕ, given by the relatively retarded SoE2 and higher fuel amount in the late injection close to TDC, allows assuring higher combustion stability and proper control over CA50 compared to a purely premixed combustion. Since a higher percentage of the fuel is injected in the late injection, the observed effect of SoE2 over the SoC and CA50 became less influential compared to the medium/high load cases, while the effect of the late injection (SoE3 sweep) starts to gain relevance for controlling both SoC and CA50, as confirmed by Figure 5.31.(b).

The main effects of the injection timing over the combustion characteristics are shown in Figure 5.32 and Figure 5.33, for Point 3 and Point 1 respectively.

Similarly to the trends already described at Point 5, in the case of Point 3 (5.5 bar IMEP) excessively high noise levels even over 100 dB are reported when approaching to knocking-like operation, due to the sharp and fast RoHR profile, reaching dP/da_{max} values above 15 bar/CAD which are not feasible for a production engine at this load condition. Nevertheless, by retarding CA50 later into the expansion stroke by advancing SoE2 it is possible to

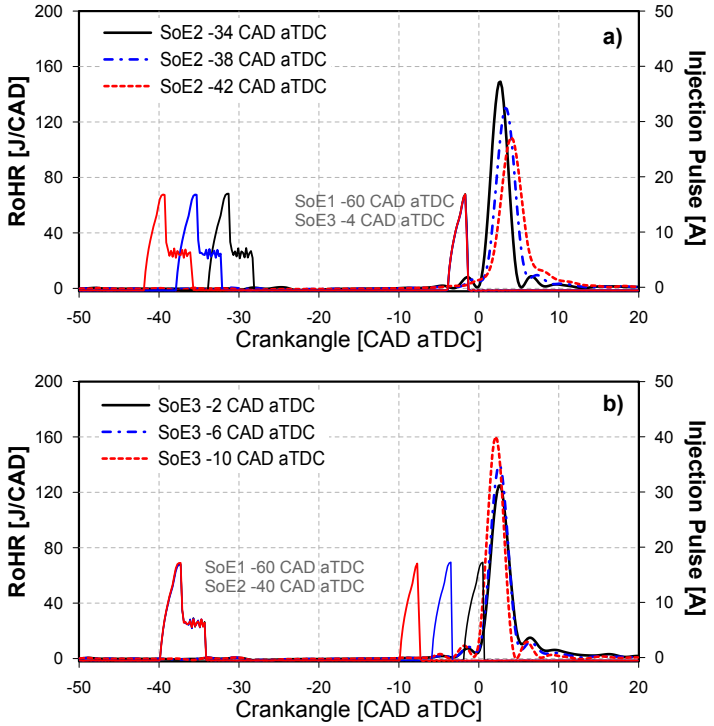

Figure 5.30. *Effect of injection timing (a)* SoE2 *and (c)* SoE3 *over the RoHR for the gasoline PPC concept at Point* 3.

decrease noise and dP/da_{max} down to 95 dB and 10.7 bar/CAD respectively for the baseline case with a triple injection. In the case of Point 1 (3.1 bar IMEP), both noise and dP/da_{max} levels are kept at reasonably low levels, going from 80 dB to 77 dB and from 5 bar/CAD to 2 bar/CAD when sweeping SoE2, mainly because the total injected fuel is burned in two stages combining a first and fast premixed phase and a consecutive mixing-controlled stage.

In terms of combustion stability, both advancing SoE2 earlier in the compression stroke as retarding SoE3 later into the expansion, increased the cycle-to-cycle dispersion in the cylinder pressure close to TDC, which was translated in a rise in $CoV_{P_{max}}$, as it is shown in Figure 5.32 for Point 3. However, in the case of Point 1 the mixed combustion structure with higher percentage of fuel in the late injection allowed to keep the levels of $CoV_{P_{max}}$ below 1 % regardless of the injection timing.

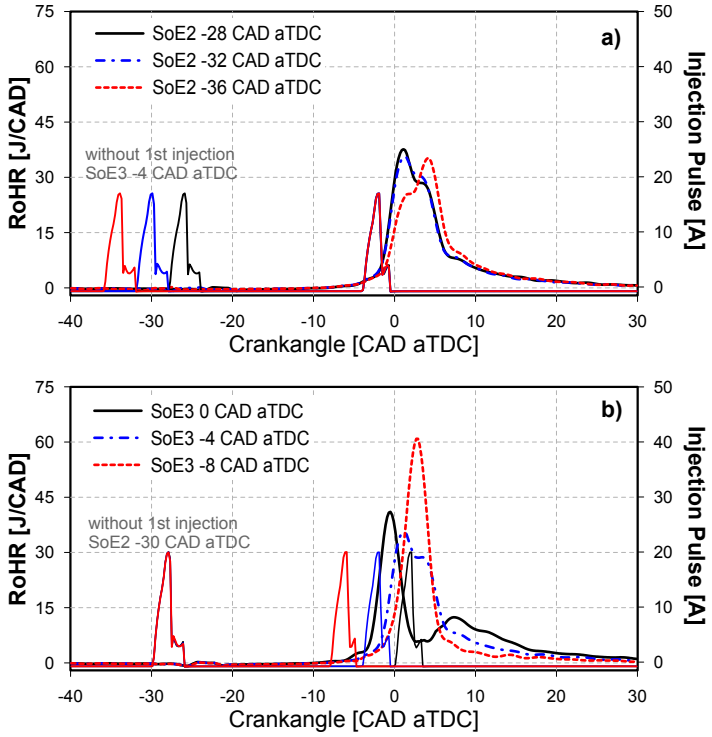

Figure 5.31. *Effect of injection timing (a)* SoE2 *and (c)* SoE3 *over the RoHR for the gasoline PPC concept at Point* 1.

Switching to the effect of the injection timing over the exhaust emissions and fuel consumption, Figure 5.34 and Figure 5.35 summarize the main trends observed at Point 3 and 1 respectively. Previous results obtained at Point 5 already demonstrated how the NO_x/soot trade-off is avoided during PPC operation when the combustion process (thus SoC and CA50) is retarded into the expansion stroke by advancing SoE2.

In the case of NO_x emissions, the thermal NO_x formation is decreased as a result of lower combustion temperature given by the low $Y_{O_2,IVC}$ added to the retarded and slower combustion process; while soot formation is decreased due to the extended mixing times before the SoC. However, when SoE2 is advanced enough so the fuel spray starts to be partially injected outside the bowl, the spray/wall interaction within the piston crown and squish area added to the lower combustion temperatures, worsens the fuel energy conversion and oxidation processes, consequently increasing CO and HC emissions. This

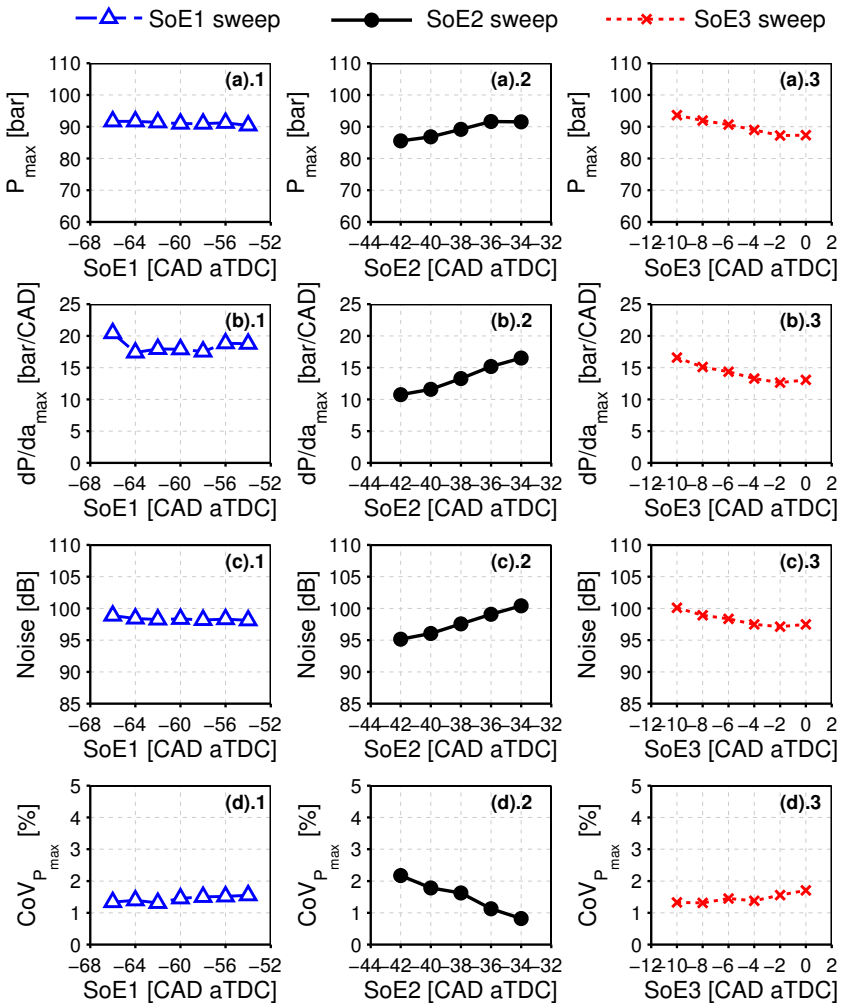

Figure 5.32. *Combustion characteristics: (a) P_{max}, (b) dP/da_{max}, (c) noise and (d) $CoV_{P_{max}}$ for* SoE1, SoE2 *and* SoE3 *sweeps operating with the gasoline PPC concept at Point* 3.

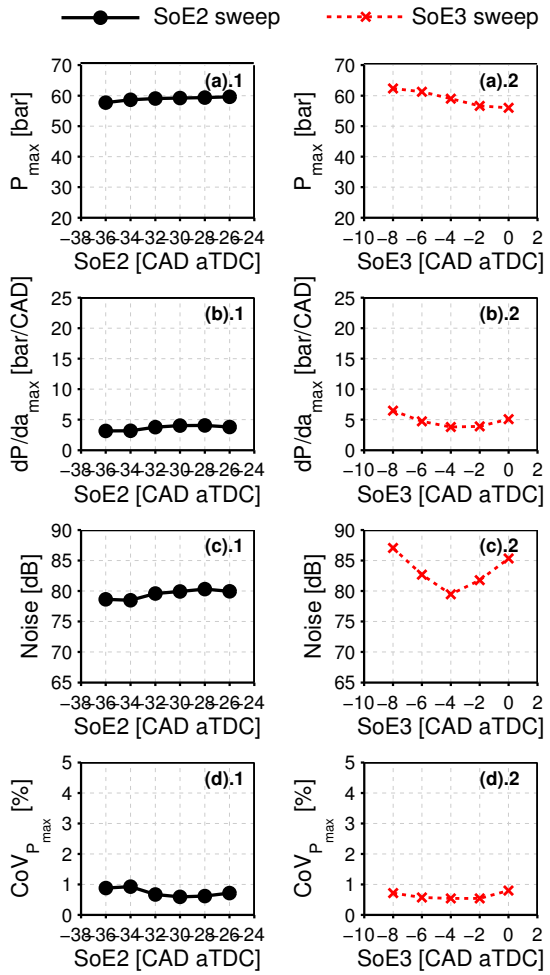

Figure 5.33. *Combustion characteristics: (a) P_{max}, (b) dP/da_{max}, (c) noise and (d) $CoV_{P_{max}}$ for* SoE2 *and* SoE3 *sweeps operating with the gasoline PPC concept at Point* 1.

effect is becomes worsened as the engine load decreases since the cylinder gas density and also the gas temperature are intrinsically lower. Finally, this is translated into a trade-off between NO_x/soot reduction and the deterioration of combustion efficiency (η_{comb}) for the early SoE2 cases.

On the counterpart, advancing SoE3 is effective to decrease smoke level without a significant increase in CO or HC (which are mainly caused by the second injection), but at the expense of higher NO_x, noise and dP/da_{max} levels given by the increased amount of fuel burning in the premixed stage of combustion, as it can be seen in Figures 5.32 and 5.34 for Point 3 and in Figures 5.33 and 5.35 for Point 1.

Finally, the levels obtained in terms of NO_x and smoke for the earliest SoE2 cases are well below the required targets previously shown in Table 4.1 for Point 3 and Point 1; with NO_x and smoke equal to 0.42 mg/s and 0.07 FSN (while the limits are 0.75 mg/s and 0.56 FSN) in the case of Point 3, and 0.3 mg/s and 0.3 FSN (while the limits are 0.45 mg/s and 1.44 FSN) in the case of Point 1. Nevertheless, CO and HC limits are exceeded, with 8.25 mg/s and 7.85 mg/s respectively in the case of Point 3 (against the targets of 4.4 mg/s and 0.65 mg/s); and 6.1 mg/s and 3.32 mg/s in the case of Point 1 (against the targets of 4.95 mg/s and 0.8 mg/s).

In terms of engine performance and efficiency, the measured levels of η_{comb}, η_{ind}, and their corresponding ISFC and $ISFC_{corr}$ are presented in Figure 5.36 and Figure 5.37 for the parametric variations of the injection timing for both Point 3 and Point 1.

In agreement with the trends already described for Point 5, combustion efficiency is decreased when switching to PPC mode compared to the levels found in CDC operation at Point 3 and 1, due to the intrinsically higher CO and HC emissions. Accordingly, advancing SoE2 earlier in the compression stroke brought a decrease in η_{comb} as it was expected, but it still remains above 96 % even for the earliest SoE2 cases. In the case of SoE3 sweep η_{comb} remains approximately constant at a level of 97 % for Point 3 and 98.3 % for Point 1, since CO and HC emissions were not substantially affected by SoE3.

Focusing on the effect of injection timing over indicated efficiency and fuel consumption, Figure 5.36 shows that η_{ind} and ISFC were not substantially affected by SoE2 at Point 3 despite the sharp decrease in η_{comb} found when advancing SoE2, remaining at levels around 42 % and 200 g/kW h; while in the case of SoE3 η_{ind} was slightly decreased from 42 % to 41.2 % by an increase in ISFC from 200 g/kW h to 204 g/kW h when SoE3 is retarded to 0 CAD aTDC. Despite the worse performance in terms of η_{ind} and ISFC compared to the

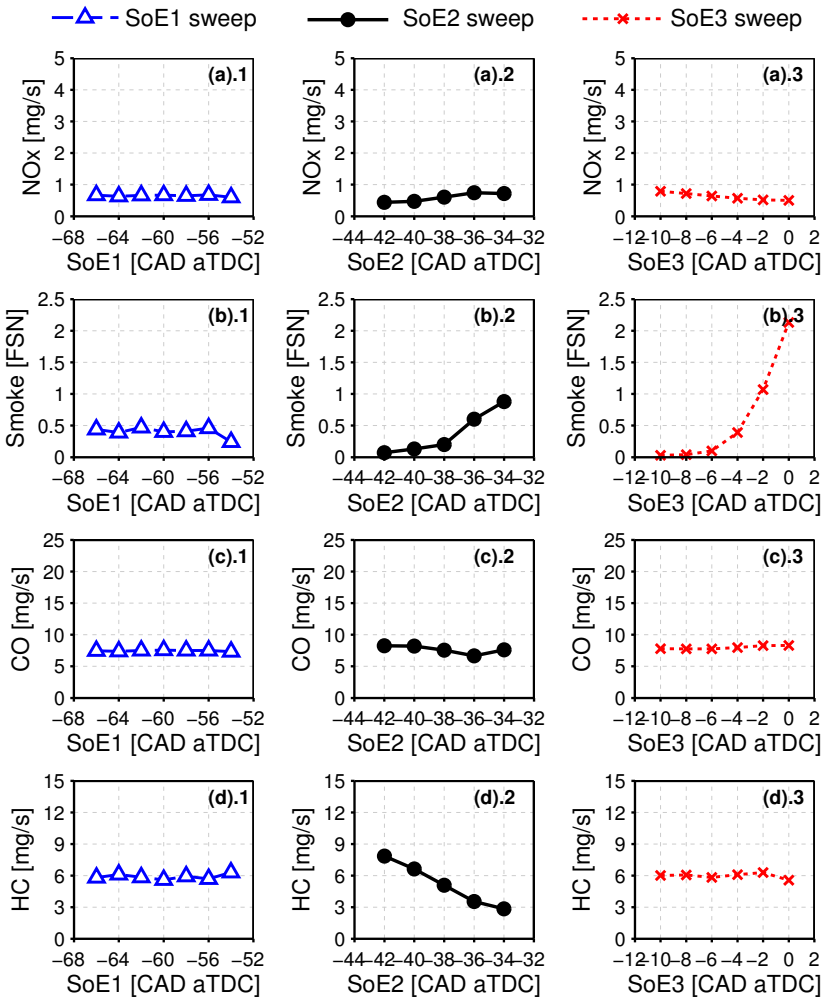

Figure 5.34. *Exhaust emissions and performance: (a) NO_x, (b) smoke, (c) CO, (d) HC, (e) η_{comb} and (f)* ISFC *for* SoE1, SoE2 *and* SoE3 *sweeps operating with the gasoline PPC concept at Point* 3.

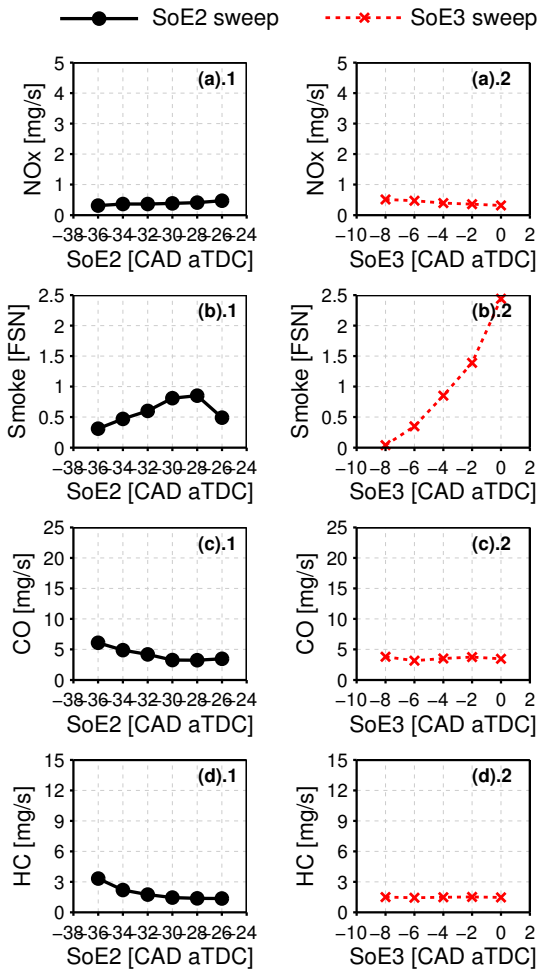

Figure 5.35. *Exhaust emissions and performance: (a) NO_x, (b) smoke, (c) CO, (d) HC, (e) η_{comb} and (f)* ISFC *for* SoE2 *and* SoE3 *sweeps operating with the gasoline PPC concept at Point* 1.

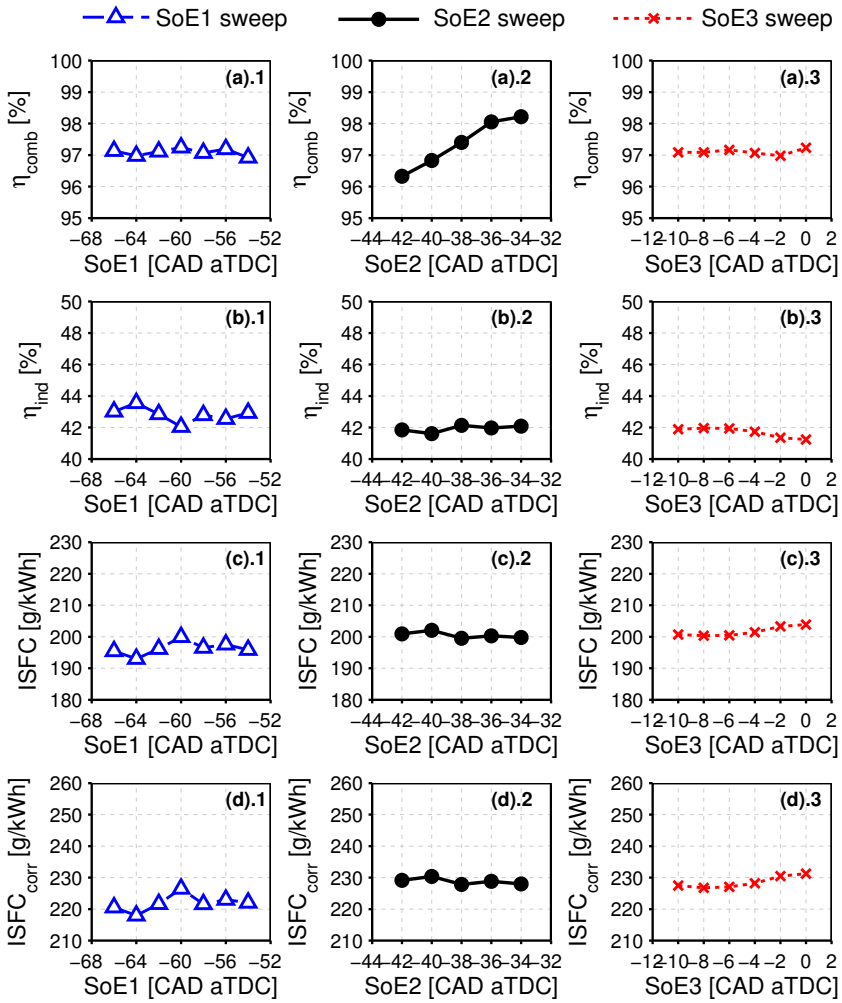

Figure 5.36. *Efficiency and fuel consumption: (a) η_{comb}, (b) η_{ind}, (c)* ISFC *and (d) $ISFC_{corr}$ for* SoE1, SoE2 *and* SoE3 *sweeps operating with the gasoline PPC concept at Point* 3.

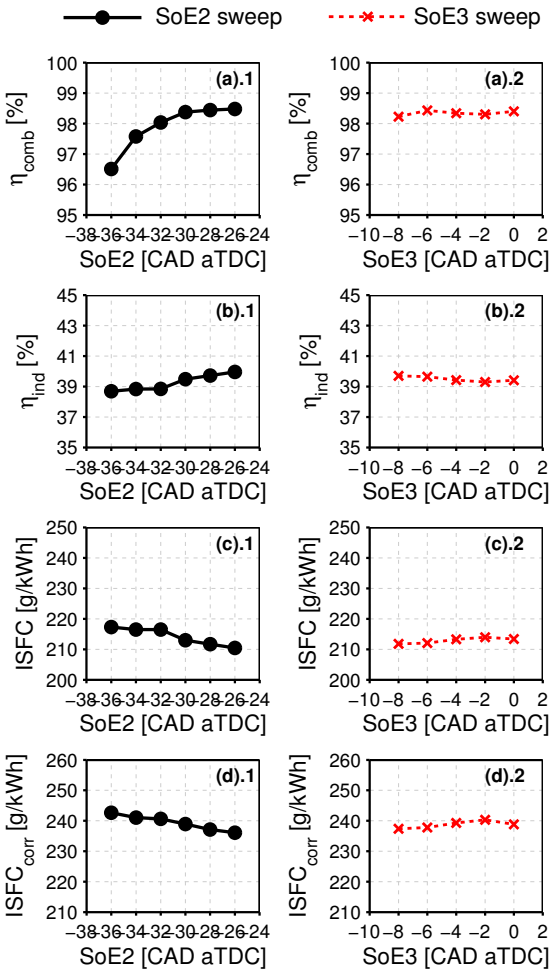

Figure 5.37. *Efficiency and fuel consumption: (a)* η_{comb}*, (b)* η_{ind}*, (c)* ISFC *and (d)* $ISFC_{corr}$ *for* SoE1, SoE2 *and* SoE3 *sweeps operating with the gasoline PPC concept at Point* 1.

fully-optimized CDC condition, if the mechanical power demanded by the air loop devices is taken into account, the resultant $ISFC_{corr}$ is found between 227 g/kW h to 230 g/kW h for Point 3, which is in the range of the levels obtained in CDC, due to the lower ΔP and $Olap$ settings used to decrease $Y_{O_2,IVC}$ and increase IGR and T_{IVC}.

In the case of Point 1, both η_{ind} and ISFC were punished when advancing SoE2 going from 40 % to 38.7 % and from 210 g/kW h to 217.3 g/kW h respectively. On the counterpart, in the case of SoE3 sweep they were only slightly affected when retarding SoE3 going from 40 % to 39.7 % and from 211.8 g/kW h to 213.4 g/kW h respectively. Finally, the combination of ISFC and the given air management conditions at Point 1 brought an increase in $ISFC_{corr}$ compared to CDC, with levels in the range of 236.1 g/kW h to 242.6 g/kW h.

Even when the η_{ind} and ISFC levels observed in the medium-to-low load range operating with the PPC concept using a multiple injection strategy are slightly worse than those observed operating with optimized settings for CDC concept, they are still considered as promising, since they are kept within the range of values reported in the literature on light-duty four-stroke engines running with the PPC concept at low load conditions with lower octane gasoline fuels [14]. Furthermore, Sellnau et al. reported important benefits in efficiency and emissions levels using dedicated engine hardware (piston and injector nozzle) properly optimized for PPC operation compared to using conventional hardware optimized for CDC [22, 28].

5.3.2.3 Effect of injection pressure and fuel split

Starting with the effect of the injection pressure over the combustion process at low load conditions, Figure 5.38 shows a comparison of the RoHR profiles obtained at Point 3 and SoE2 equal to −40 CAD aTDC, for two levels of P_{rail} (lower) 400 bar and (higher) 800 bar along with the baseline case with P_{rail}=600 bar. Additionally, the most important combustion characteristics measured for the three P_{rail} levels when sweeping SoE2 are summarized in Figure 5.39.

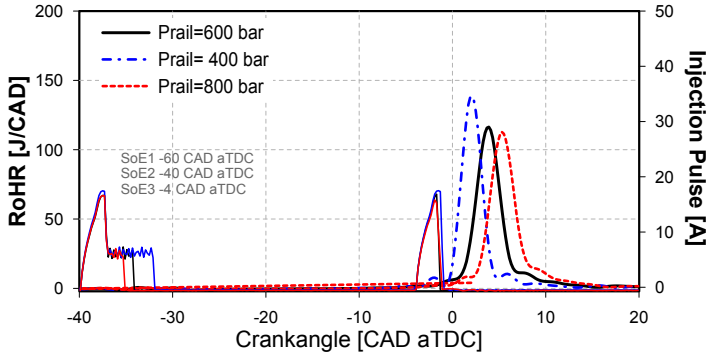

Figure 5.38. *Effect of injection pressure over the RoHR with* SoE2 −40 CAD aTDC *for the gasoline PPC concept at Point* 3.

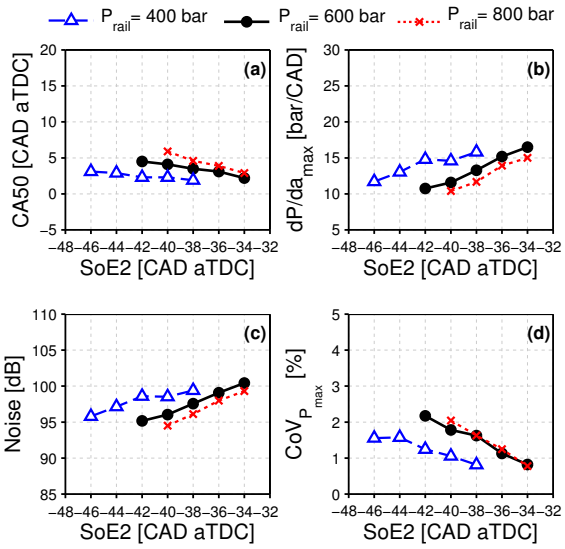

Figure 5.39. *Combustion characteristics: (a)* CA50*, (b)* dP/da_{max}*, (c) noise and (d)* $CoV_{P_{max}}$ *for* SoE2 *sweeps at different* P_{rail} *for gasoline PPC operation at Point* 3.

In agreement to the trends already described for Point 5, increasing the mixing rate through higher injection pressure further reduced the window of operation between knocking-like combustion and misfire when sweeping SoE2.

So, for P_{rail}=800 bar the earliest SoE2 experimentally measured was limited to −40 CAD aTDC due to the appearance of misfire cycles and sharp worsening of combustion stability for earlier SoE2 timings. Nevertheless, a faster mixing rate of the second and third injection, allows shifting some percentage of the fuel located at the most reactive ϕ towards leaner conditions by the time of SoC, which results in slightly retarded SoC and CA50 compared to the baseline P_{rail}=850 bar, and helps decreasing dP/da_{max} and noise levels, as it is confirmed by Figure 5.39.

On the counterpart, decreasing mixing rate by lowering P_{rail} to 400 bar shifted both SoC and CA50 earlier in the cycle, shortening combustion duration and increasing the peak of the RoHR; as it can be seen in Figure 5.38. Thus, P_{max}, dP/da_{max} and noise levels are consequently increased for P_{rail}=400 bar compared to P_{rail}=600 bar and P_{rail}=800 bar cases.

Focusing on exhaust emissions, Figure 5.40.(b) shows how smoke emissions are dramatically increased when P_{rail} is decreased to 400 bar, as a combined effect of shorter mixing time given by the earlier SoC and slower mixing rate of the fuel injected in the late injection, which locally increases rich ϕ zones where soot formation occurs. In addition, NO_x emissions are also increased in the case of P_{rail}=400 bar due to the faster combustion process, caused by the more reactive local ϕ distribution given also by the fuel injected in the early injections. On the contrary, increasing P_{rail} to 800 bar provided a slight reduction in smoke emissions compared to the baseline, while keeping approximately constant levels of NO_x. Nevertheless, HC emissions are higher for P_{rail}=800 bar, as it can be seen in Figure 5.40.(d), specially for the early SoE2 timings, probably because of a higher mass of fuel impinging onto the piston walls and squish area coming from the longer spray penetration with higher P_{rail}. The trends shown in Figure 5.40.(e) in terms of combustion efficiency at this load condition seems to be mostly correlated to the variations observed in HC emissions, since CO emissions were not drastically affected in the measured range of P_{rail}. Finally, the injection pressure seems to have very small effect over ISFC and consequently over η_{ind}, so both remained approximately constant regardless of P_{rail} at this load condition.

Switching to the effect of $\%fuel$, Figure 5.41 shows a comparison of the RoHR profiles obtained at Point 3 for the reference triple injection case with $\%fuel$=16/68/16 along with the four additional $\%fuel$ cases with double injection strategies for SoE2 placed at −40 CAD aTDC. Removing the third injection results in two "early injections" with $\%fuel$=16/84/0 and $\%fuel$=32/68/0 as shown in Figure 5.41.(a), while removing the first injection

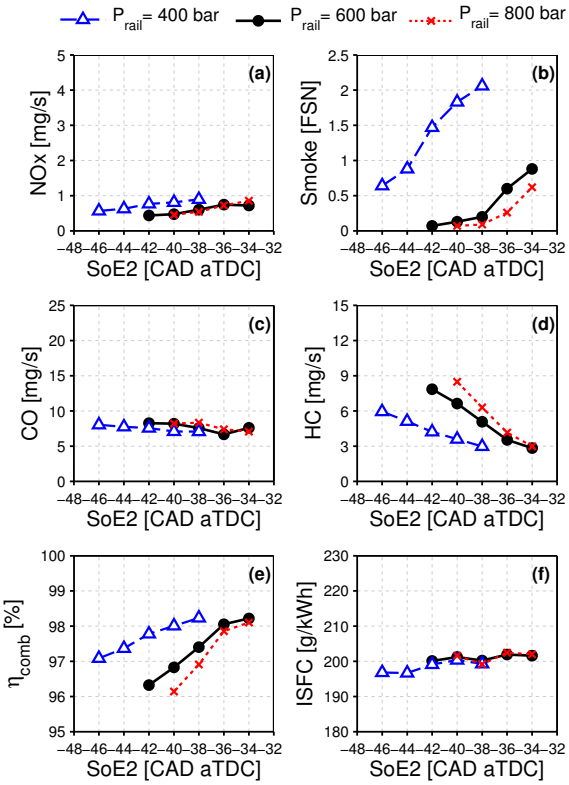

Figure 5.40. *Exhaust emissions and performance: (a) NO_x, (b) smoke, (c) CO, (d) HC, (e) η_{comb} and (f)* ISFC *for* SoE2 *sweeps at different P_{rail} for gasoline PPC operation at Point* 3.

gives two "late injections" with $\%fuel$=0/84/16 and $\%fuel$=0/68/32 as shown in Figure 5.41.(b).

In the case of Point 1, an example of the RoHR profiles obtained at SoE2 −32 CAD aTDC is presented for the two measured fuel split cases with $\%fuel$=0/60/40 and $\%fuel$=0/40/60.

Similarly to what was previously described for Point 5, increasing the mass of fuel injected in the early injections leads to a consequent increase in local mixture reactivity that advanced both the SoC and the CA50 earlier in the cycle, enhancing the trend towards knocking-like combustion compared to the baseline case with a triple injection, as it is confirmed by Figure 5.41.(a) for both $\%fuel$=16/84/0 and $\%fuel$=32/68/0 with SoE2 equal to

−40 CAD aTDC. With these two fuel split distributions, the resulting ignition delay is long enough to allow premixing all the fuel mass that has been injected in the two early injections, so the combustion process occurs completely in premixed conditions without the presence of a late diffusive stage.

Figure 5.41.(b) shows how the combustion advances when the first injection is removed and its fuel is introduced either in the second or in the third injection. This trend appeared to be caused by slight differences in the temperature evolution along the compression stroke, considering that the cooling effect generated by the evaporation of the fuel is modified for each injection pattern. In the case of $\%fuel$=0/84/16, the RoHR is faster with a higher peak due to higher reactivity at SoC resulting from the shorter time to premix the fuel added in the second injection. Focusing on $\%fuel$=0/68/32 where the injection pattern promotes the third injection close to TDC, the peak of the RoHR is lower and combustion duration is longer compared to $\%fuel$=0/84/16 even when combustion starts slightly earlier. This confirms a reduction of the premixed phase and a consequent extension of the mixing-controlled stage analogous to what was previously described in Point 5 when increasing the fuel mass in the third late injection.

Figure 5.43 and Figure 5.44 show the effect of $\%fuel$ over the main global combustion characteristics for the SoE2 sweeps for Point 3 and 1 respectively. In the case of Point 3, the RoHR profiles already confirmed how removing either the first or the third injection resulted in an increase in mixture reactivity that advanced both the SoC and the CA50 earlier in the cycle, enhancing the trend towards knocking-like combustion compared to the baseline case with a triple injection. This is translated into a higher P_{max}, dP/da_{max} and noise levels particularly when increasing the fuel injected in the "early injections", as well as a decrease in $CoV_{P_{max}}$ given by the more reactive and advanced combustion process.

However, it is also interesting to remark that to keep a constant CA50 phased at 4.5 CAD aTDC while removing the first injection, it is necessary to advance SoE2 in 4 CAD, from −42 CAD aTDC to −46 CAD aTDC, in order to match the mixture conditions (given by the local ϕ distribution) with the in-cylinder thermodynamic conditions (T_{IVC} and $Y_{O_2,IVC}$). Therefore, if $\%fuel$=0/68/32 case is compared against the baseline at constant CA50, the higher quantity of the fuel burnt in the mixing-controlled stage will result in a longer combustion duration and lower maximum RoHR, given by a slower combustion rate, that will accordingly help to decrease dP/da_{max} and noise levels down to 5 bar/CAD and 86 dB, as it is confirmed by Figure 5.43.(b) and (d).

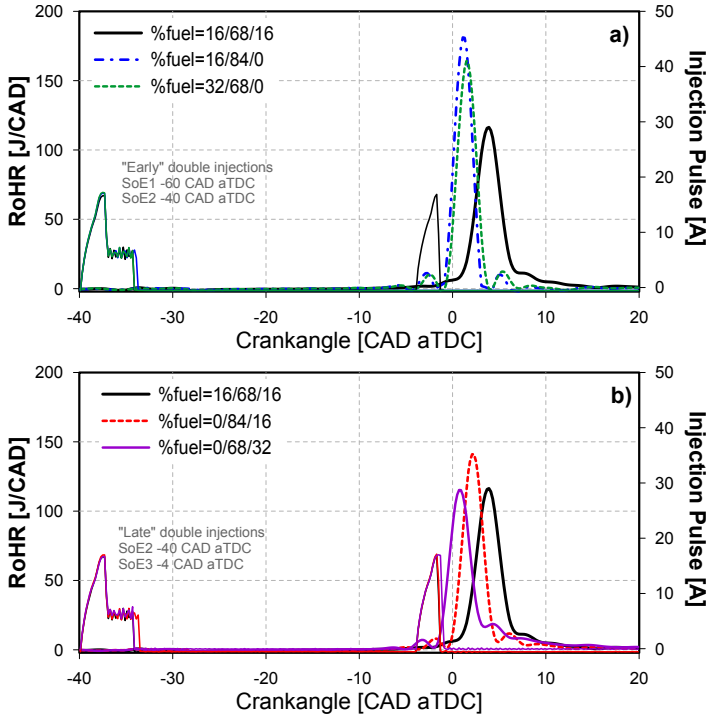

Figure 5.41. *Effect of fuel split over the RoHR (a) removing the first injection and (b) removing the third injection at constant* SoE2 $-40\,\mathrm{CAD\,aTDC}$ *for the gasoline PPC concept at Point* 3.

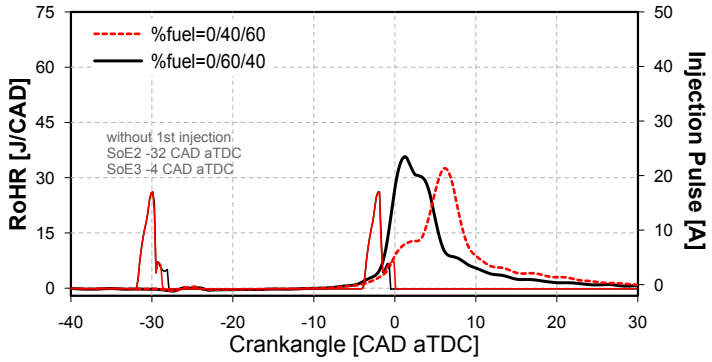

Figure 5.42. *Effect of fuel split over the RoHR at constant* SoE2 $-32\,\mathrm{CAD\,aTDC}$ *for the gasoline PPC concept at Point* 1.

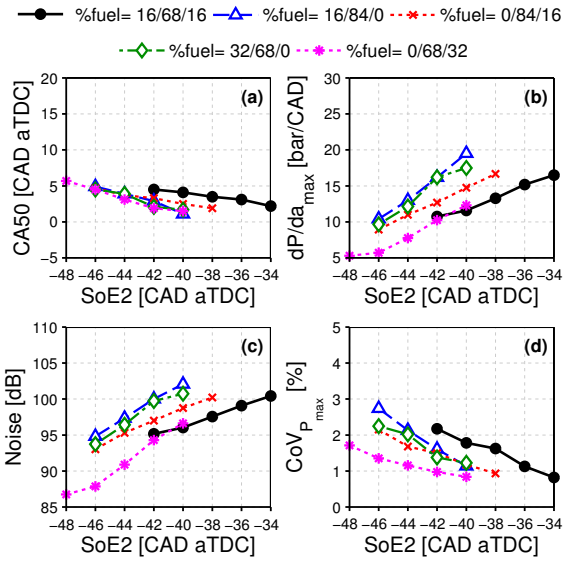

Figure 5.43. *Combustion characteristics: (a)* CA50*, (b)* dP/da_{max}*, (c) noise and (d)* $CoV_{P_{max}}$ *for* SoE2 *sweeps at different* $\%fuel$ *for gasoline PPC operation at Point* 3*.*

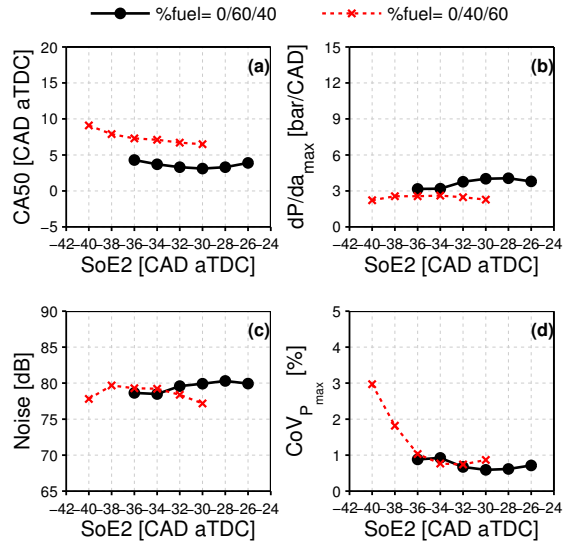

Figure 5.44. *Combustion characteristics: (a)* CA50*, (b)* dP/da_{max}*, (c) noise and (d)* $CoV_{P_{max}}$ *for* SoE2 *sweeps at different* $\%fuel$ *for gasoline PPC operation at Point* 1*.*

For Point 1, injecting the majority of the fuel in the late injection ($\%fuel$=0/40/60) brought a noticeable change in the shape of the RoHR as can be seen in Figure 5.42 while SoC remained constant, decreasing the peak of the first stage of premixed combustion of the fuel injected early during compression, but also delaying the second combustion of the fuel injected close to TDC. This change on the combustion profile results in an increase in the duration of the combustion process and retards the CA50 later into the expansion stroke by approximately 4 CAD aTDC compared to the baseline, as shown in Figure 5.44. The dP/da_{max} and noise levels are slightly lower in the case of $\%fuel$=0/40/60 in most of the measured points, being influenced by the combustion rate and particular shape of the RoHR. Finally, combustion stability represented by $CoV_{P_{max}}$ is punished by the retarded CA50 in the cases with $\%fuel$=0/40/60 and SoE2 equal to -38 CAD aTDC and -40 CAD aTDC, however, the higher fuel burnt in mixing-controlled conditions allowed to sustain the combustion process, unlike the equivalent early SoE2 timings with $\%fuel$=0/60/40 which were not measured due to misfire conditions.

Focusing on exhaust emissions, Figure 5.45 and Figure 5.46 show the trade-off between decreasing NO_x/smoke and reducing η_{comb} when advancing SoE2, for the different $\%fuel$ measured at Point 3 and 1 respectively. In the case of Point 3, when the third injection is removed, $\%fuel$=16/84/0 and $\%fuel$=32/68/0, the smoke level remained below the minimum detection limit in all the measured range of SoE2, as it is shown in Figure 5.45.(b), since the diffusive stage of the combustion is completely avoided as the injected fuel has enough time to be partially premixed before the SoC. However, increasing the fuel injected in the "early injections" brought an increase in NO_x emissions as it was expected, due to the advanced and rapid combustion process with increased knock trend. On the counterpart, removing the first injection and adding the fuel to the third injection, $\%fuel$=0/68/32, caused a sharp increase in smoke level as it can be seen in Figure 5.45.(b), which confirms a higher quantity of fuel burnt in mixing-controlled combustion, which is translated into a worse NO_x/soot trade-off compared to the other $\%fuel$ cases.

Similar effects of $\%fuel$ over NO_x and smoke emissions are observed in Figure 5.46 for Point 1, so it can be stated that, in general terms, the experimental results confirm how both the fuel split between injections combined with the SoE2 can be used as levers to control NO_x and smoke levels by affecting the combustion rate and the shape of the RoHR through the local ϕ distribution and the global mixture reactivity. Therefore, they have to be carefully optimized to attain the optimum CA50 and RoHR profile, that

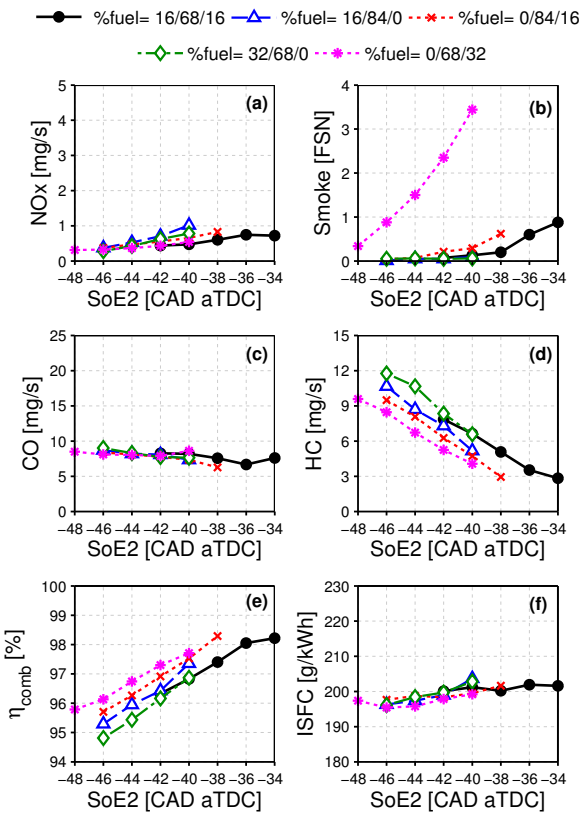

Figure 5.45. *Exhaust emissions and performance: (a) NO_x, (b) smoke, (c) CO, (d) HC, (e) η_{comb} and (f)* ISFC *for* SoE2 *sweeps at different $\%fuel$ for gasoline PPC operation at Point* 3.

allow achieving noise and pressure gradient requirements while meeting the low NO_x/soot target.

Switching to CO and HC emissions, Figure 5.45.(c) and Figure 5.45.(d) show how in the case of Point 3, increasing the fuel mass in the two very early injections brought an increment in HC emissions, while CO emissions were hardly affected. Accordingly, removing the first injection helped in decreasing HC emissions compared to the triple injection case. The lowest levels of HC are obtained in the case of $\%fuel$=0/68/32 as it was expected, since it has the lowest ratio of fuel injected early during the compression stroke. These trends support the hypothesis of the spray/wall interaction as the main source of HC emissions operating in PPC while using early injection events.

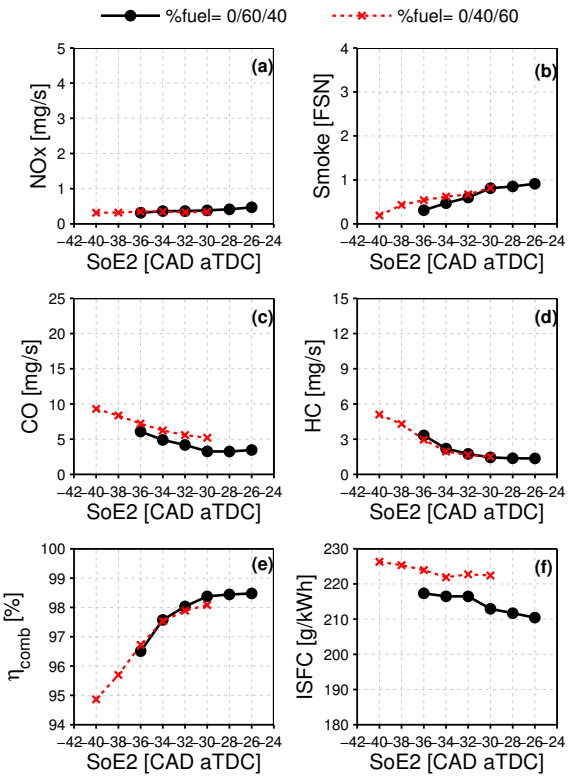

Figure 5.46. *Exhaust emissions and performance: (a) NO_x, (b) smoke, (c) CO, (d) HC, (e) η_{comb} and (f)* ISFC *for* SoE2 *sweeps at different $\%fuel$ for gasoline PPC operation at Point* 3.

The reported levels of combustion efficiency for the different $\%fuel$ cases are well correlated with the observed behavior in HC emissions, therefore, the highest η_{comb} levels are found at $\%fuel$=0/68/32.

At Point 1 a slight increase in CO is observed when increasing the fuel mass of the third late injection ($\%fuel$=0/40/60); while HC emissions appeared to remain unaltered regardless of the $\%fuel$ between the two injections. The increase in CO levels observed for $\%fuel$=0/40/60 is expected to be linked to the worsening of the late-cycle oxidation processes given by the extended mixing-controlled stage with later CA50 and EoC compared to $\%fuel$=0/60/40.

Finishing with the effect of $\%fuel$ over the indicated fuel consumption, Figure 5.45.(f) shows how ISFC is not drastically affected by the $\%fuel$ in the case of Point 3, with the exception of slightly lower ISFC values reported for $\%fuel$=0/68/32 that might be linked to a possible reduction in heat transfer losses given by a combination of a smoother RoHR profile with improved η_{comb}. However, at Point 1 ISFC is increased in the case of $\%fuel$=0/40/60 even when η_{comb} remains approximately constant, so the deterioration of η_{ind} could be caused by a less optimum cycle configuration (cylinder pressure evolution) coming from the slower combustion process with too retarded CA50.

5.3.3 Comparative analysis between gasoline PPC and CDC concepts

An optimum point for gasoline PPC operation in terms of NO_x/soot and noise levels is selected at each operating condition, in order to be compared against well-optimized points obtained operating in CDC after performing the full DoE optimization following the methodology described in Chapter 4. The optimum points measured in CDC were selected to improve Euro 5 emissions levels measured on the equivalent four-stroke engine in terms of unitary displacement and geometry, while also providing the best compromise in terms of indicated fuel consumption. Despite the comparison is not performed keeping iso-NO_x conditions, which could be an attractive alternative, the key benefits/drawbacks of each combustion concept can be clearly observed.

Starting with the higher load condition, Figure 5.47 summarizes the most important pollutant emissions, noise and fuel consumption levels for CDC and PPC optimum points; measured at Point 5, with 10.4 bar IMEP and 1500 rpm. To assure the cylinder conditions required for PPC operation at medium-to-high load conditions it was necessary to increase P_{int}, ΔP and $Olap$ to increase the fresh air trapped mass, allowing the use of a higher EGR rate compared to CDC. Moreover, the triple injection strategy allowed to reduce P_{rail} compared to CDC without punishing smoke emissions, which is interesting for reducing the compression power from the fuel pump.

Operating with the gasoline PPC concept is interesting to decrease simultaneously NO_x and soot emissions down to 0.4 mg/s and 0.05 FSN, compared to 2.1 mg/s and 2.99 FSN obtained in the optimum point for CDC. CO and HC emissions are increased to 18.22 mg/s and 12.1 mg/s which corresponds to η_{comb} around 96.5 %, compared to 13.02 mg/s, 0.36 mg/s and 99 % for CDC, due to the early timing of the first and second injection combined with poor injector nozzle matching for PPC operation. Moreover,

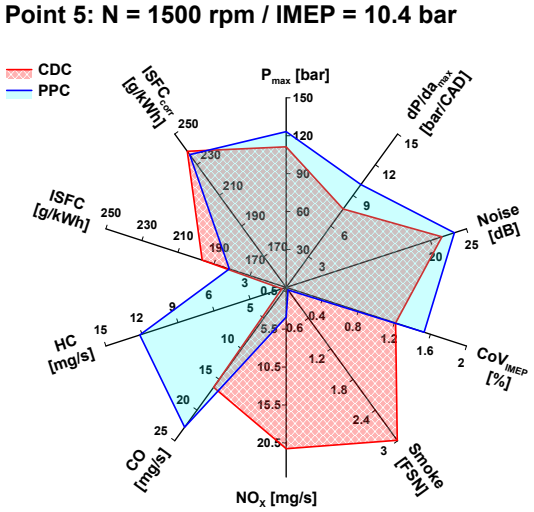

Figure 5.47. *Comparison between optimum points found for CDC and gasoline PPC operation at Point* 5.

combustion noise is noticeably higher when operating in PPC at the medium-to-high load range compared to CDC, increasing from 86.4 dB to 93.3 dB, due to the fast and short combustion process given by the enhanced tendency towards knocking-like combustion.

PPC operation increases η_{ind} from 43 % to 47 %, which corresponds to the highest value observed so far in the engine at this load condition. The increased indicated efficiency is reflected in a reduction in ISFC from 197 g/kW h to 178 g/kW h when operating in PPC, as shown in Figure 5.47. However, if the compression work demanded by the supercharging system is taken into account to correct the ISFC values, the more demanding air management conditions required to achieve higher P_{int}/EGR combination could mask the benefits of PPC operation in terms of indicated efficiency. Therefore, the estimation of $ISFC_{corr}$ is useful for evaluating qualitatively the increase in BSFC expected at the two-cylinder engine with fully assembled air charging system, and also to discard air management conditions which are not feasible due to extremely high pressure ratios or air flow rates. In this case, Figure 5.47 confirms the lower gain observed in terms of $ISFC_{corr}$, going from 239 g/kW h when operating in CDC down to 236 g/kW h when operating with gasoline PPC.

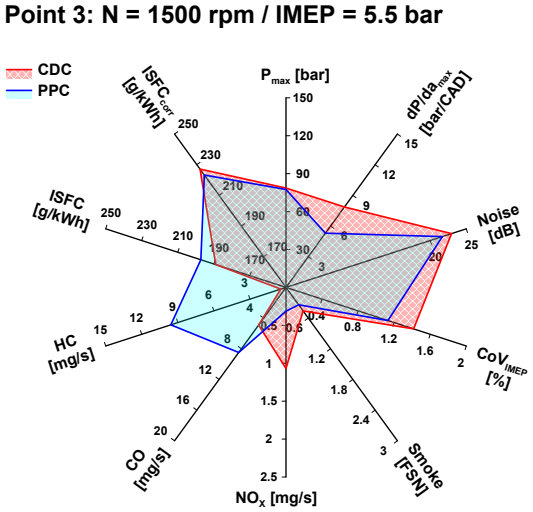

Figure 5.48. *Comparison between optimum points found for CDC and gasoline PPC operation at Point* 3.

When decreasing the load, a combination of slightly higher P_{int} with lower ΔP and earlier timing of the exhaust valve to reduce $Olap$ compared to CDC, is used to assure the required level of IGR to keep a reliable ignition and a high combustion stability during PPC operation.

The most important pollutant emissions, noise and fuel consumption levels for CDC and PPC optimum points; measured at Point 3 and Point 1, are summarized in Figure 5.48 and Figure 5.49 respectively.

At the medium-to-low load range, the lower NO_x/smoke levels obtained when operating with the PPC concept are attained at the expense of increased CO and HCemissions compared to CDC. In the case of Point 3, the benefits in terms of NO_x and smoke are much smaller than the previously obtained at Point 5, with 0.3 mg/s and 0.34 FSN compared to 0.73 mg/s and 0.38 FSN obtained in the optimum point for CDC. On the counterpart, CO and HC are significantly increased up to 8.48 mg/s and 9.58 mg/s when operating with the PPC concept, compared to 5.77 mg/s and 0.5 mg/s at the optimized CDC. In the case of Point 1, NO_x and smoke are kept at 0.3 mg/s and 0.31 FSN when operating with PPC, compared to 0.44 mg/s and 0.33 FSN obtained with CDC; while CO and HC are increased to 6.1 mg/s and 3.32 mg/s, compared to 3.71 mg/s and 0.54 mg/s for CDC.

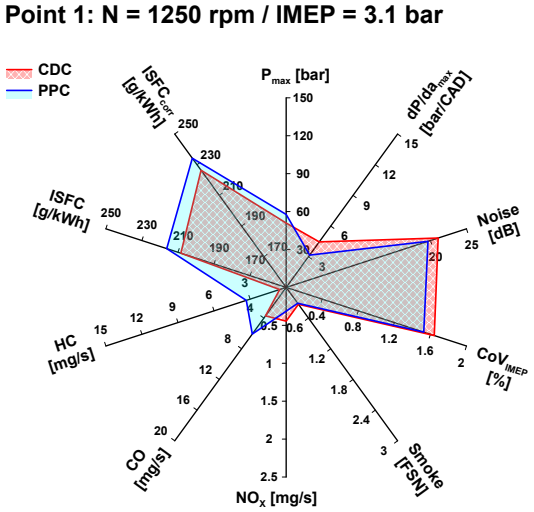

Figure 5.49. *Comparison between optimum points found for CDC and gasoline PPC operation at Point* 1.

Comparing the indicated efficiency values obtained at medium-to-low load between PPC and CDC operation, the η_{ind} with the PPC concept is comparatively lower than the optimum values found in CDC, possibly due to higher heat transfer losses given by the high temperatures at IVC required to ignite the gasoline at low load, combined with the slightly lower combustion efficiency, but also due to the earlier EVO which decreases the effective expansion ratio compared to the CDC with fully optimized air management settings.

Focusing in Point 3, η_{ind} drops from 45 % to 43 % following an increase in ISFC from 189 g/kW h to 197 g/kW h, while $ISFC_{corr}$ still decreases from 227 g/kW h to 224 g/kW h due to slightly lower Q_{del} given by the air management settings, specially lower $Olap$ and ΔP. In the case of Point 1, η_{ind} decreases from 41 % to 39 %, which corresponds to an increase in ISFC from 208 g/kW h to 216 g/kW h, bringing in this case a consequent increase in $ISFC_{corr}$ from 226 g/kW h to 234 g/kW h. Finally, for both Point 3 and Point 1 it is possible to decrease noise level below the measured optimum points for CDC by delaying CA50 and controlling the shape of the RoHR with the fuel split between the injections.

5.4 Concluding remarks

The present chapter focused on evaluating the performance of advanced combustion concepts on the two-stroke HSDI poppet-valves engine concept, with the aim of improving the conventional trade-off in NO_x and soot emissions inherent to the CDC concept, while keeping competitive levels in terms of efficiency and fuel consumption. Due to the complexity of premixed LTC concepts in terms of practical engine operation, linked to the high sensitivity of the combustion process to the charge thermo-chemical conditions as well as the spatial mixture distribution, the experimental test methodology chosen for this chapter was based on a parametric optimization approach, rather than a Design of Experiments optimization methodology. Then, the structure of the chapter is based on different parametric studies carefully designed to improve the understanding on the effect of the injection strategy over the combustion characteristics and its consequent impact on exhaust emissions and engine performance when operating with different premixed LTC concepts.

The two-stroke architecture under development offers the flexibility to operate over the air management settings (by changing P_{int}, ΔP, $VVT_{(int,exh)}$, $Olap$, and EGR) to substantially modify the TR and IGR trade-off; and accordingly change the $Y_{O_2,IVC}$, T_{IVC} and the charge density. Then, in-cylinder gas composition and temperature can be fine-tuned to control to some extend the ignition of the charge and the combustion phasing when operating with advanced (and kinetically-controlled) combustion concepts.

The following conclusions can be summarized from the preliminary implementation of premixed LTC concepts, early-injection HPC with diesel fuel and gasoline PPC with a single-injection strategy, at low speed and load operating conditions:

- The potential of the early-injection HPC concept for producing extremely low levels of NO_x and soot emissions in the two-stroke diesel engine under development has been experimentally confirmed, but even decreasing the geometric compression ratio, the early SoC advances the CA50 towards the compression stroke and the final result is an important reduction in combustion efficiency and excessively high ISFC levels.
- The main incompatibility between the early injection HPC concept using diesel as fuel and the two-stroke engine architecture under development is the high levels of hot IGR, since it increases the in-cylinder gas

temperature along the compression stroke and this is the main cause of the early onset of combustion. Additionally, decreasing the geometric compression ratio cannot reduce the in-cylinder gas temperature as much as needed to attain a well-phased combustion process, since levels below 9 would be required.

- On the contrary, to implement the single-injection PPC concept while switching to a fuel with lower reactivity as in the case of gasoline, it is necessary to retain high IGR levels (around 50 %) to increase temperature along compression and achieve the auto-ignition temperature of the 95 octane fuel around TDC. As load, and then in-cylinder temperature increases, assuring proper combustion stability becomes less problematic, so the IGR can be accordingly decreased down to a minimum, with the aim of extending mixing times and ignition delay as much as possible, and achieve enough separation between the injection and combustion events.

- Matching cylinder temperature, oxygen concentration and spray mixing rate is mandatory to achieve stable PPC operation at a given operating condition. A lower limit in mixture reactivity was detected from where combustion could not be sustained without worsening cyclic dispersion. Decreasing mixture reactivity below this limit was only possible by adjusting the air management conditions to increase cylinder temperature and compensate for this less reactivity.

From the analysis performed during the optimization of the gasoline PPC concept with a triple injection strategy at different operating conditions, the following main conclusions can be extracted:

- The detailed analysis of local conditions is interesting to aid in the understanding of the basic physics involved in the particular combustion process, observed when operating in PPC with multiple injection strategies. From the CFD results, it is evident how the development of the combustion process and pollutant emissions is controlled by local conditions, which are not only sensitive to the air management and injection strategy, but also to the combustion chamber geometry.

- In the three load conditions, operating with the gasoline PPC concept allows decreasing simultaneously NO_x and soot emissions compared to a well-optimized CDC operation points. The reduction in NO_x and soot is more evident at the medium-to-high load range, because the premixed

stage of combustion helps reducing the mixing-controlled or spray driven combustion compared to CDC.

- Soot emissions are greatly determined by the available mixing time for the late injection close to TDC. Therefore, the timing and duration of this injection, as well as the injection pressure and onset of combustion will affect final soot level. The use of a multiple injection strategy combined with the PPC concept allowed to decrease injection pressure compared to CDC without penalties in soot emissions. Additionally, NO_x emissions are reduced by the use of large amounts of EGR with much lower penalties in terms of soot compared to CDC. As a drawback, CO and HC emissions increase compared to CDC, due to increased spray/wall interactions from the early injections added to worsened oxidation processes.

- At medium-to-high loads (as in the case of 10.4 bar IMEP), combustion noise is noticeably higher operating in PPC compared to CDC, due to the fast and short combustion process and enhanced knock trend given by the inherently higher temperatures. Noise is reduced while decreasing NO_x and soot by advancing SoE2 to delay CA50. It could be decreased furthermore to some extent, by delaying SoE3 or increasing the $\%fuel$ in the late injection, but at the expense of an increase in soot emissions.

- At low loads (5.5 bar and 3.1 bar IMEP), it is possible to decrease noise below the levels obtained for CDC, by delaying CA50 with early SoE2, and by controlling the shape of the RoHR with the fuel split between injections.

- The benefits of the PPC concept in terms of indicated efficiency compared to CDC were mostly observed in the medium-to-high load range (10.4 bar IMEP), where a faster combustion process with lower mean gas temperatures allows decreasing heat losses during the cycle.

- At the medium-to-low load range, the indicated efficiency decreases while operating in PPC for both Point 3 and Point 1, possibly due to increased heat transfer losses coming from the use of higher IGR rates combined with lower combustion efficiencies. But also by the earlier EVO timing, which is advanced compared to CDC to keep a high T_{IVC}, and finally decreases the effective expansion ratio possibly causing an additional increase in ISFC.

- It is of great interest to estimate the power demanded by the air loop devices (turbocharger and supercharger) to achieve the required

$Y_{O_2,IVC}/\phi_{eff,IVC}$ combination, and accordingly correct the ISFC to qualitatively predict the penalty expected in the multi-cylinder engine when operating with the PPC concept. The benefits obtained in ISFC at high load operation could be masked if high power is required by the supercharger to achieve the required intake conditions.

As a final remark, there is still a clear room for improving the performances of the PPC concept, in terms of controlling the maximum combustion rate to decrease pressure gradient and noise level, together with increasing combustion efficiency to decrease CO and HC emissions, while impacting also positively η_{ind} as a result of the increment in the energy released by the fuel. Future research can focus mainly in optimizing the local ϕ distribution in the combustion chamber, not only by further DoE optimization of the engine settings, but also by matching the bowl geometry and fuel spray angle (with a slightly narrower included angle) to reduce the propensity for fuel wall wetting during the early injections, and also to improve the mixture preparation particularly for the second injection.

Bibliography

[1] Iijima Akira, Yoshida Koji and Shoji Hideo. "A Comparative Study of HCCI and ATAC Combustion Characteristics Based on Experimentation and Simulations Influence of the Fuel Octane Number and Internal EGR on Combustion". In *SAE Technical Paper*, volume 2005-01-3732. SAE International, 2005.

[2] Zhang Yan, Ojapah Mohammed, Cairns Alasdair and Zhao Hua. "2-Stroke CAI Combustion Operation in a GDI Engine with Poppet Valves". In *SAE Technical Paper*, volume 2012-01-1118, 2012.

[3] Zhang Yan, Zhao Hua, Ojapah Mohammed and Cairns Alasdair. "CAI combustion of gasoline and its mixture with ethanol in a 2-stroke poppet valve DI gasoline engine". *Fuel*, Vol. 109 n^o 0, pp. 661–668, 2013.

[4] Zhang Y. and Zhao H. "Investigation of combustion, performance and emission characteristics of 2-stroke and 4-stroke spark ignition and CAI/HCCI operations in a DI gasoline". *Applied Energy*, Vol. 130 n^o 0, pp. 244–255, 2014.

[5] Benajes Jesus, Novella Ricardo, De Lima Daniela, Dugue Vincent and Quechon Nicolas. "The potential of highly premixed combustion for pollutant control in an automotive two-stroke HSDI diesel engine". In *SAE Technical Paper*, volume 2012-01-1104, 2012.

[6] Benajes Jesus, Novella Ricardo, De Lima Daniela, Quechon Nicolas and Obernesser Philippe. "Implementation of the early injection highly premixed combustion concept in a two-stroke HSDI engine". In *SIA Diesel Powertrain Congress 2012*, volume SIA Diesel Powertrain Congress 2012, Rouen, France, 2012.

[7] Lewis Samuel A., Storey John M. E., Bunting Bruce and Szybist James P. "Partial Oxidation Products and other Hydrocarbon Species in Diesel HCCI Exhaust". In *SAE Technical Paper*, volume 2005-01-3737, 2005.

[8] Dec John E. and Sjoberg Magnus. "A Parametric Study of HCCI Combustion - the Sources of Emissions at Low Loads and the Effects of GDI Fuel Injection". In *SAE Technical Paper*, volume 2003-01-0752, 2003.

[9] Pastor Jose V., Javier Lopez J., Garcia Jose M. and Pastor Jose M. "A 1D model for the description of mixing-controlled inert diesel sprays". *Fuel*, Vol. 87 n^o 13-14, pp. 2871–2885, 2008.

[10] Desantes J. M., Pastor J. V., Garcia-Oliver J. M. and Pastor J. M. "A 1D model for the description of mixing-controlled reacting diesel sprays". *Combustion and Flame*, Vol. 156 n^o 1, pp. 234–249, 2009.

[11] Benajes J., Molina S., Novella R. and De Lima D. "Implementation of the Partially Premixed Combustion concept in a 2-stroke HSDI diesel engine fueled with gasoline". *Applied Energy*, Vol. 122 n^o 0, pp. 94–111, 2014.

[12] Musculus Mark P. B., Miles Paul C. and Pickett Lyle M. "Conceptual models for partially premixed low-temperature diesel combustion". *Progress in Energy and Combustion Science*, Vol. 39 n^o 2-3, pp. 246–283, 2013.

[13] Saxena Samveg and Bedoya Ivan D. "Fundamental phenomena affecting low temperature combustion and HCCI engines, high load limits and strategies for extending these limits". *Progress in Energy and Combustion Science*, Vol. 39 n^o 5, pp. 457–488, 2013.

[14] Solaka Hadeel, Aronsson Ulf, Tuner Martin and Johansson Bengt. "Investigation of Partially Premixed Combustion Characteristics in Low Load Range with Regards to Fuel Octane Number in a Light-Duty Diesel Engine". In *SAE Technical Paper*, volume 2012-01-0684, 2012.

[15] Borgqvist Patrick, Tuner Martin, Mello Augusto, Tunestal Per and Johansson Bengt. "The Usefulness of Negative Valve Overlap for Gasoline Partially Premixed Combustion, PPC". In *SAE Technical Paper*, volume 2012-01-1578. SAE International, 2012.

[16] Sellnau Mark, Moore Wayne, Sinnamon James, Hoyer Kevin, Foster Matthew and Husted Harry. "GDCI Multi-Cylinder Engine for High Fuel Efficiency and Low Emissions". *SAE Int. J. Engines*, Vol. 8 n^o 2, pp. 775–790, 2015.

[17] Benajes J., Novella R., Martin J. and De Lima D. "Analysis of the Load Effect on the Partially Premixed Combustion Concept in a 2-Stroke HSDI Diesel Engine Fueled with Conventional Gasoline". In *SAE Technical Paper*, volume 2014-01-1291, 2014.

[18] Das Adhikary Bishwadipa, Reitz Rolf and Ciatti Stephen. "Study of In-Cylinder Combustion and Multi-Cylinder Light Duty Compression Ignition Engine Performance Using Different RON Fuels at Light Load Conditions". In *SAE Technical Paper*, volume 2013-01-0900, 2013.

[19] Kolodziej Christopher P., Ciatti Stephen, Vuilleumier David, Das Adhikary Bishwadipa and Reitz Rolf. "Extension of the Lower Load Limit of Gasoline Compression Ignition with 87 AKI Gasoline by Injection Timing and Pressure". In *SAE Technical Paper*, volume 2014-01-1302. SAE International, 2014.

[20] Kaiadi Mehrzad, Johansson Bengt, Lundgren Marcus and Gaynor John A. "Experimental Investigation on different Injection Strategies for Ethanol Partially Premixed Combustion". In *SAE Technical Paper*, volume 2013-01-0281, 2013.

[21] Sellnau Mark, Sinnamon James, Hoyer Kevin and Husted Harry. "Gasoline Direct Injection Compression Ignition (GDCI) - Diesel-like Efficiency with Low CO2 Emissions". In *SAE Technical Paper*, volume 2011-01-1386, 2011.

[22] Sellnau Mark C., Sinnamon James, Hoyer Kevin and Husted Harry. "Full-Time Gasoline Direct-Injection Compression Ignition (GDCI) for High Efficiency and Low NOx and PM". *SAE International Journal of Engines*, Vol. 5 n^o 2, pp. 300–314, 2012.

[23] Sellnau Mark, Foster Matthew, Hoyer Kevin, Moore Wayne, Sinnamon James and Husted Harry. "Development of a Gasoline Direct Injection Compression Ignition (GDCI) Engine". *SAE International Journal of Engines*, Vol. 7 n^o 2, pp. 835–851, 2014.

[24] Benajes Jesus, Novella Ricardo, De Lima Daniela and Tribotte Pascal. "Analysis of combustion concepts in a newly designed two-stroke high-speed direct injection compression ignition engine". *International Journal of Engine Research*, Vol. 16 n^o 1, pp. 52–67, 2015.

[25] Benajes J., Novella R., De Lima D. and Tribotte P. "Investigation on Multiple Injection Strategies for Gasoline PPC Operation in a Newly Designed 2-Stroke HSDI Compression Ignition Engine". *SAE Int. J. of Engines*, Vol. 8 n^o 2, 2015.

[26] Petersen Benjamin, Miles Paul C. and Sahoo Dipankar. "Equivalence Ratio Distributions in a Light-Duty Diesel Engine Operating under Partially Premixed Conditions". *SAE Int. J. Engines*, Vol. 5 n^o 2, pp. 526–537, 2012.

[27] Musculus Mark P. B., Lachaux Thierry, Pickett Lyle M. and Idicheria Cherian A. "End-of-Injection Over-Mixing and Unburned Hydrocarbon Emissions in Low-Temperature-Combustion Diesel Engines". In *SAE Technical Paper*, volume 2007-01-0907. SAE International, 2007.

[28] Sellnau Mark C., Sinnamon James, Hoyer Kevin, Kim Junghwan, Cavotta Marilou and Husted Harry. "Part-Load Operation of Gasoline Direct-Injection Compression Ignition (GDCI) Engine". In *SAE Technical Paper*, volume 2013-01-0272, 2013.

Chapter 6

Conclusions and future work

Contents

6.1 Introduction

The research work presented on this thesis represents an important contribution to the first stages of development and optimization of the combustion system of an innovative two-stoke CI engine, that has been designed for small passenger car vehicles.

This final chapter outlines the main conclusions and scientific contributions of this research work, and highlights the most relevant results obtained along the different stages of this investigation, with the aim of proposing new optimization paths to further improve the performance and emissions level of the two-stroke engine concept under development.

In a second step, new possible research directions are formulated together with the recommendation of future tasks and studies, which are based on the knowledge and experience acquired along the practical execution and posterior analysis of the different studies proposed in this investigation.

6.2 Summary and main conclusions of this thesis

Before gathering and summarizing the most relevant outcomes and contributions achieved by this thesis, it might by useful to remind ourselves about the global context and the general objectives proposed for this investigation. As it was discussed in Chapter 1, this research work has been established in a difficult context marked by the growing technological challenges for the automotive industry, which has to be in constant evolution to face and successfully overcome more severe legislations for both traditionally regulated emissions (NO_x, PM, HC and CO) as for CO_2 level, combined with more realistic and dynamic test vehicle procedures. All of this is added to the already complex and rapidly changing regional and global markets, the increasing socio-political concerns about the environmental and health impact of the transportation sector, and the more demanding customer expectations in terms of vehicle fuel consumption and engine performance.

Therefore, the next generation of powertrain concepts must reach incredibly high efficiency levels, while using cost-effective technologies to decrease exhaust emissions both through advanced combustion strategies as well as complex after-treatment systems. As it was introduced in Chapter 2, two main research paths are being followed to develop compression ignition engines, the extreme optimization of the conventional diesel combustion concept and the application of advanced combustion concepts. The idea of developing a two-stroke engine as a possible alternative for future "extremely downsized" powertrains, was proposed in the framework of the "Powertrain for future light-duty vehicles (POWERFUL)" project funded by the European Union, where Renault started a large-scale research project dedicated to the development of a 0.73 L two-stroke two-cylinder CI engine, that then became the base concept used for this investigation.

Despite the technological challenges inherent to two-stroke operation that have been prevented the application of conventional two-stroke engines on the automotive market, they could actually represent a cost-effective solution to downsized modern engines for the small class vehicles, that could meet the pollutants legislation while keeping competitive efficiency levels. Nowadays, achieving this goal has become more feasible thanks to the numerous technical advances found in the areas of HSDI injection systems, advanced boosting technologies and variable valve actuation mechanisms; along with faster and more powerful modeling and control tools, as well as increasing knowledge about the implementation of advanced combustion concepts, which attempt to compete against the traditional SI gasoline and CI diesel combustion systems.

From the literature review performed on Chapter 2 it was possible to understand the fundamental aspects related to the physical and chemical mechanisms occurring inside the combustion chamber of a direct injection CI diesel engine, in the frame of mixing-controlled CDC as well as advanced LTC concepts with high (HCCI and HPC) to moderate (PPCI and PPC) degree of premixing. In the case of CDC, the ignition and combustion of the cylinder charge typically occur while the fuel is still being injected and mixed with the surrounding air, so the combustion rate is controlled by the injection and air entrainment rate into the fuel spray, and the fuel-air mixture spans a wide range of local equivalence rations and temperatures along the combustion process, which promote the formation of both NO_x and PM emissions.

Switching to the review of advanced combustion concepts in CI engines presented in section 2.3 from Chapter 2, most of premixed LTC strategies are typically focused on promoting a sufficiently premixed air-fuel mixture before the onset of ignition; in order to slow down or even avoid the chemical reactions leading to thermal NO_x formation due to a drastic reduction in the local combustion temperatures. In addition, PM formation is hindered by the absence of high local ϕ zones during the combustion process. Nevertheless, the ignition and combustion processes are mainly controlled by the chemical kinetics of the fuel-air mixture, so as the engine load increases, the control over the combustion phasing and rate typically becomes the main challenge for all LTC premixed strategies.

In this regard, the two-stroke engine under development provides much higher flexibility compared to four-stroke engines to control both the charge composition as well as the cylinder gas temperature evolution in a wider range by means of the air management settings. Thus, two-stroke operation has intrinsically much more potential to adjust the charge thermochemical conditions and consequently affect the combustion environment, which is a key action to control the combustion process and the final emission levels in the frame of both conventional diesel operation and advanced premixed combustion concepts.

During the literature review it also became evident that since the automotive market has been fully dominated by the four-stroke engines, only few research work has been carried out in the scope of advanced combustion concepts on two-stroke engines for automotive applications [1–7]. And from those studies, very little efforts have focused on developing a viable poppet-valves two-stroke engine concept for a modern powertrain platform. Therefore, there is a clear opportunity for expanding the current knowledge about two-stroke operation in general; as well as improving the

understanding of the main physical processes governing the air management and combustion characteristics in poppet-valves two-stroke engines, which will finally determine the pollutant emissions and final efficiency level.

From the previous discussion, it can been concluded that there is a major research effort to be done to really foreseen the potential of the two-stroke engine for competing against the well-established four-stroke CI engine, in terms of their respective pollutant emissions and efficiency levels. And similarly, there is a clear research interest on identifying the compatibility of the two-stroke operation in the frame of application of advanced combustion concepts.

Based on the context described, the main objective proposed for this investigation is to **improve the existing understanding and assess the main relationships between the gas exchange and combustion processes in two-stroke poppet-valves engines, and evaluate their impact on exhaust emissions and engine efficiency while operating with CDC and premixed HPC and PPC concepts**. The experimental studies presented on this thesis were performed on a single-cylinder version of this innovative two-stroke poppet valves CI engine currently under development. The single-cylinder engine was specifically designed and manufactured to operate in two-stroke mode, and presents the same architecture and geometry as the final two-cylinder configuration, but it has the advantage that can be used for studying the fundamental physical phenomena related to the combustion and emissions formation processes, in a more controlled environment compared to a multi-cylinder engine.

To achieve this global goal and pursue the specific objectives defined in section 1.4 in Chapter 1, the research work has been divided in two sequential stages:

- Analysis and optimization of the conventional diesel combustion (CDC) in the poppet-valves two-stroke engine at different representative operating conditions, considering the air management and combustion characteristics, pollutants emissions, fuel consumption and efficiency levels.

- Analysis of advanced combustion concepts in the poppet-valves two-stroke engine, for improving the conventional NO_x-PM trade-off inherent to the CDC concept. In a first step, the low thermal homogeneous combustion (LTHC) concept with diesel fuel is implemented to identify its potential for emissions reduction as well as its technological limitations; and in a second step, the partially

premixed combustion (PPC) concept with gasoline fuel is implemented and analyzed in detail, along with the use of multiple injection strategies for extending its operating range and improving its performance.

The detailed description of the most relevant features of this novel two-stroke poppet-valves engine concept were presented in Chapter 3, as well as the main characteristics of the single-cylinder engine facility used in this investigation. As it was discussed in Chapter 3, the precise control over the air management and in-cylinder conditions on this type of engine architecture is fundamental for both combustion development and final engine efficiency, which notably increases the complexity in terms of engine operation and optimization; mainly because there are multiple actuators related to the air management system in addition to the injection settings. Therefore, it was very important to establish an efficiency experimental methodology for optimizing the combustion/emissions characteristics of this two-stroke engine architecture. Additionally, it was necessary to develop specific measurement and calculation procedures for the correct study of the air management process on this two-stroke engine. The following contributions can be highlighted both from the experimental techniques as well as theoretical tools employed in this thesis:

- A procedure based on the tracer gas method, has been developed to experimentally measure the trapping ratio (TR) in every test condition. This procedure requires injecting a controlled concentration of methane (CH_4) in the intake flow during stabilized engine operation with combustion, and measuring simultaneously the resulting concentrations of CH_4 on the intake and on the exhaust pipes using dedicated gas analyzer.

- The development of a practical and fast on-line tool for the estimation of the IGR and the total trapped mass at IVC; as well as for the calculation of the most important global in-cylinder conditions, such as the oxygen mass fraction and temperature at the IVC($Y_{O_2,IVC}$, T_{IVC}) and the effective equivalence ratio ($\phi_{eff,IVC}$).

- The use of a piezoresistive pressure sensor located in the bottom-part of liner to measure the cylinder pressure around BDC, and provide an accurate reference signal for pegging the pressure signal measured with the piezoelectric sensor. A correct and precise measurement of the cylinder pressure at IVC is required both for the IGR estimation model and for the RoHR calculation in the combustion diagnosis software.

- A multidimensional CFD model of the two-stroke poppet-valves engine was developed in CONVERGE, to provide additional insight into the air management and combustion processes in the two-stroke architecture under study, both for CDC as for gasoline PPC operation.

To able to perform an initial optimization of the performances of this two-stroke poppet-valves engine concept in the most efficient way, while simultaneously obtaining important information about the physical phenomena controlling both gas exchange and the combustion processes, it was decided to split the experimental test methodology in two sequential steps as follows:

- Optimization of the air management settings by means of a Design of Experiment methodology, to find the most suitable in-cylinder conditions for a given operating point, while keeping constant the injection settings. Then, the cause/effect relations of the air management parameters over the in-cylinder conditions, and consequently over combustion development and exhaust emissions can be captured within the DoE, providing a valuable information with reduced number of tests compared to the parametrical approach.

- Optimization of the injection settings by means of parametric studies, to check the influence of combustion phasing on engine performance and pollutants emissions, at constant air management conditions that are predefined with the aid of the DoE statistical models.

This optimization methodology was successfully applied in Chapter 4 to optimize the fuel consumption and emissions levels of the two-stroke engine while operating with the CDC concept at six different points ranging from low to high load operation. The straight and general relations obtained after the analysis of the results presented in Chapter 4 confirm how the best approach for understanding the physical processes linked to two-stroke engines, is to switch from particular engine operation settings to the final in-cylinder gas thermodynamic conditions, which later controls the combustion process development and final emissions level and efficiency. Thus, the proposed optimization approach can be extrapolated to design and develop any two-stroke engine, regardless of its particular architecture or displacement. The following conclusions can be extracted from the analysis of the conventional diesel combustion operation presented in Chapter 4:

- From the first experimental study of the gas exchange process performed at Point 5 (10.4 bar IMEP and 1500 rpm) it has been demonstrated how the two-stroke poppet valve architecture typically exhibits low TR values, due to the positive ΔP (between P_{int} and P_{exh}) as well as the long *Olap* duration (in the range of 60 CAD to 80 CAD) that are needed to attain proper exhaust and scavenging of the burnt gases out of the cylinder. The experimental results showed there is a strong trade-off between TR and IGR, so decreasing TR by increasing ΔP and *Olap* (what leads to an increase in delivered flow Q_{del}) improves the scavenging of burnt gases out of the cylinder decreasing IGR, up to a point where the IGR cannot be further reduced (typically around 30 % of IGR) even while TR continues to fall. The minimum effective in-cylinder equivalence ratio ($\phi_{eff,IVC}$) is obtained at the conditions with higher fresh air trapped in the cylinder ($Q_{air,ret}$), which is found at an optimum combination of medium-to-low TR and medium-to-high delivered flow Q_{del} where the total cylinder charge (Q_{IVC}) is maximized. The two most influential factors controlling Q_{IVC} and $Q_{air,ret}$ are the ΔP and the valve overlap, followed by the intake pressure P_{int}. The best combination of TR and Q_{del} is typically obtained at the highest values of ΔP but with the medium-to-low values of *Olap*.

- The indicated specific fuel consumption and the indicated efficiency (ISFC and η_{ind} respectively) are particularly conditioned not only by the typical factors related to the combustion process such as CA50, combustion duration and heat transfer losses; which are affected by the $Y_{O_2,IVC}$ and $\phi_{eff,IVC}$, but also to the thermodynamic cycle itself; which is sensitive not only to the combustion process but also to the lengths of the expansion and compression strokes given by the exhaust and intake valve closing timings, EVC and IVC respectively. The results demonstrated how the optimum ISFC values are achieved at the region that exhibited the lowest $\phi_{eff,IVC}$ and higher $Y_{O_2,IVC}$ values, so the in-cylinder conditions are more favorable for the combustion process; combined with the most retarded EVC timing which gives the longest expansion (power) stroke. Nevertheless, these conditions result in a strong penalty in terms of the demanded power from the air loop devices, consequently increasing $ISFC_{corr}$. The trade-off between ISFC and $ISFC_{corr}$ observed within the DoE depends on the interactions between the four air management settings, but it is particularly influenced by the combination of *Olap* and ΔP.

- Low NO_x emissions levels are attainable by reducing $Y_{O_2,IVC}$ to decrease $T_{ad,max}$ along the combustion process down to 2400 K or below, either by increasing EGR rate or by affecting the air management conditions (i.e. decreasing ΔP and $Olap$). However, reducing $T_{ad,max}$ by decreasing $Y_{O_2,IVC}$ leads to a consequent decrease of the temperatures along the late diffusive combustion stage ($T_{ad,80\%MBF}$) that worsens soot oxidation process resulting in higher final soot emissions (which supports the conventional smoke-NO_x trade-off). Nonetheless, the flexibility of the two-stroke engine can be used to partially counteract this effect, by increasing the total cylinder charge Q_{IVC} with the remaining air management settings, with the aim of increasing cylinder gas density to enhance the mixing process during combustion, which not only helps improving soot oxidation but also increases combustion rate resulting in earlier CA90.

- The air management process is critical to achieve the proper in-cylinder conditions which provide suitable combustion process with low NO_x and smoke emissions, high combustion efficiency and good compromise between ISFC and $ISFC_{corr}$. After performing the optimization process for the selected low-to-medium load points (from 3.1 bar to 10.4 bar of IMEP) and low speed conditions (from 1250 rpm to 1500 rpm), it was possible to fulfill all the emissions and noise limits while improving ISFC compared to the base four-stroke engine. At these points, it was possible to find the best compromise in terms of NO_x, smoke and ISFC, without the existence of a trade-off between the pollutant emissions and the indicated efficiency.

- At high load (15.1 bar IMEP) and medium speed (2500 rpm), it was not possible to fulfill the NO_x, smoke, CO and HC emissions limits since the combustion process was compromised due to decreased engine permeability. Then, a physical limitation to attain full load performance (which was expected to be around 17 bar IMEP) at high engine speeds was identified with the current engine hardware. Important benefits at full load operation could be obtained by improving/optimizing the acoustic characteristics of the intake and especially the exhaust system.

The analysis of advanced combustion concepts in the two-stroke engine under study, presented in Chapter 5, was divided in two sequential stages as follows: in a first step, a preliminary study was performed to implement the early-injection HPC concept with diesel fuel and also the single-injection gasoline PPC concept, with the aim of identifying the main limitations and

drawbacks of these two strategies; and in a second step, the performance of the multiple-injection gasoline PPC concept is evaluated through different parametric studies of the injection settings, which have been specifically designed to analyze and optimize the gasoline PPC concept at the selected load conditions, while providing valuable information about the effect of local fuel-air stratification over the characteristics of the combustion process and its final impact on exhaust emissions and efficiency levels.

The following conclusions can be highlighted from the preliminary study of premixed LTC concepts presented in section 5.2 in Chapter 5:

- It was possible to run the two-stroke engine with diesel fuel and the early-injection HPC concept, but only at low engine speed/load conditions (results shown in section 5.2.1 for 2.1 bar IMEP and 1200 rpm). Switching from CDC to HPC operation allowed drastically decreasing NO_x emissions down to near-to-zero levels, while smoke was already kept low with the selected engine settings. However, operating with the early-injection HPC concept also brought the expected increase in CO and HC emissions, due to the extremely low combustion temperatures combined with the presence of over-mixed lean mixtures which may fail to reach second stage ignition, causing in a sharp decrease in combustion efficiency which drops down to 91 %.

- The high reactivity of diesel fuel added to the intrinsically high IGR rates characteristic of the poppet-valves two-stroke architecture; are the main reasons why it is impossible to attain a properly-phased combustion process during HPC operation, even when using a lower compression ratio piston (13.6 compared to originally 17.2) and optimized engine settings at low load conditions. Therefore, the resulting indicated efficiency level as the observed gains in terms of NO_x-smoke emissions are not sufficient to make the HPC operation competitive against CDC, so the application of this premixed LTC combustion concept on this two-stroke engine was discarded [8, 9].

- In the case of the implementation of the single-injection gasoline PPC concept shown in section 5.2.2, the potential of the two-stroke engine in terms of air management control for assuring stable PPC operation of a high octane gasoline was demonstrated in medium-to-low load conditions (5 bar IMEP and 1200 rpm), which is difficult to achieve in four-stroke engines without the utilization of dedicated re-breathing or negative valve overlap strategies. The timing of the injection event controls both the SoC and the CA50, however, the combustion process

is still controlled by the chemical kinetics and reactivity of the mixture, so it is highly sensitive to the thermodynamic conditions, the charge composition as well as the mixing process.

- To achieve a drastic reduction in NO_x emissions while operating with gasoline PPC concept, it is necessary to introduce medium to high percentages of EGR to decrease $Y_{O_2,IVC}$ and be able to reduce maximum combustion temperatures below 2200 K. Soot formation is hindered by maintaining maximum equivalence ratio below 2 by the time of SoC, which is achieved by detaching the injection and combustion events. At 5 bar IMEP, it was necessary to introduce 25 % of EGR in combination with 50 % of IGR to achieve low NO_x conditions while assuring a stable and well-phased combustion with CoV_{IMEP} around 2 %.

- Between 5 bar to 3 bar IMEP it was possible to achieve low NO_x emissions (below 0.4 mg/s) with near-to-zero smoke level, while retaining 98 % of combustion efficiency and proper combustion stability with CoV_{IMEP} under 3 %, as it has been reported in [10]. However, at higher load (10 bar) a transition between premixed and mixing-controlled combustion was observed when operating with a single-injection strategy, depending on the cylinder conditions, so the conventional trade-off between NO_x and soot emissions was recovered [10]. The results obtained with this preliminary study of the gasoline PPC concept, encouraged the investigation of multiple injection strategies to further extend the successful range of operation of the PPC concept up to high load conditions.

From the analysis performed during the optimization of the gasoline PPC concept with a triple injection strategy at different operating conditions, the following main conclusions can be extracted:

- The experimental results shown in section 5.3.1 confirmed how the timing of the second and main injection (SoE2) controls both the SoC as the CA50, whereas the third late injection has negligible effect over the SoC but has an impact on the combustion rate and duration by affecting the mixing-controlled phase of combustion, so it can be used to control to some extend the CA50 and CA90.

- Advancing SoE2 retards the combustion phasing and softens the RoHR, consequently decreasing P_{max}, dP/da_{max} and noise. The earliest SoE2 was limited by the appearance of misfire cycles, which have been

proven to be linked to the interaction between the spray and the piston bowl. So, the earliest SoE2 timing is constrained by the need of avoiding directing the spray towards the squish region. On the counterpart, the latest SoE2 timing is limited by the onset of knocking-like combustion, and is promoted by the reduced mixing time of the second injection which gives an increase in the mixture reactivity at the SoC.

- By properly optimizing the triple injection strategy at Point 5 (10.4 bar IMEP and 1500 rpm), it is possible to decrease simultaneously NO_x and smoke emissions down to 0.4 mg/s and 0.05 FSN respectively, compared to 2.1 mg/s and 2.99 FSN obtained in the optimum point for CDC. CO and HC emissions are increased to 18.22 mg/s and 12.1 mg/s which corresponds to η_{comb} around 96.5 %, compared to 13.02 mg/s, 0.36 mg/s and 99 % for CDC, due to the early timing of the first and second injection combined with poor injector nozzle matching for PPC operation.

- Combustion noise as well as the maximum pressure gradient (dP/da_{max}) are noticeably increased when operating with the gasoline PPC concept, due to the faster combustion process given by the rapid auto-ignition of a highly reactive mixture compared to the slower mixing-controlled process characteristic of CDC. They can be reduced by advancing SoE2 earlier in the compression stroke, to delay the CA50 later into the expansion, which also simultaneously decreases NO_x and soot. However, CO and HC emissions are notably increased due to higher spray/wall interactions from the two early injections and worsened oxidation process. Another option to further decrease noise and dP/da_{max}, is to delay SoE3 or increase the $\%fuel$ in the late injection, but at the expense of extending the mixing-controlled phase of combustion, consequently leading to an unavoidable increase in soot emissions.

- The benefits of the PPC concept in terms of indicated efficiency compared to CDC were mostly observed in the medium-to-high load range, where a faster combustion process with lower mean gas temperatures allows decreasing heat losses during the cycle. At Point 5, it allowed increasing η_{ind} up to 47 %, which corresponds to the highest value observed so far in the engine at this load condition. The improved indicated efficiency is reflected in a reduction in ISFC from 197 g/kW h for CDC operation to 178 g/kW h when operating in PPC. However, if the compression work demanded by the supercharging system is taken into account to estimate $ISFC_{corr}$, there is a much smaller gain during PPC operation due to the more demanding air management conditions

required to achieve higher P_{int}/EGR combination, which results in a final $ISFC_{corr}$ equal to 236 g/kW h compared to 239 g/kW h when operating in CDC.

- At Point 3 and Point 1 (5.5 bar and 3.1 bar IMEP at 1500 rpm and 1250 rpm respectively), the benefits in terms of NO_x and smoke are much smaller than the previously obtained at Point 5. In the case of Point 3, the NO_x and smoke levels obtained in PPC operation were 0.3 mg/s and 0.34 FSN compared to 0.73 mg/s and 0.38 FSN for CDC. On the counterpart, CO and HC are significantly increased up to 8.48 mg/s and 9.58 mg/s compared to 5.77 mg/s and 0.5 mg/s at the optimized CDC. In the case of Point 1, NO_x and smoke are kept at 0.3 mg/s and 0.31 FSN when operating with PPC, compared to 0.44 mg/s and 0.33 FSN obtained with CDC; while CO and HC are increased to 6.1 mg/s and 3.32 mg/s, compared to 3.71 mg/s and 0.54 mg/s for CDC.

- At low load conditions it is possible to decrease noise below the levels obtained for CDC, by delaying CA50 with early SoE2, and by controlling the shape of the RoHR with the fuel split between injections. At Point 3 and Point 1, the indicated efficiency decreases while operating in PPC compared to fully-optimized CDC operation, possibly due to increased heat transfer losses coming from the use of higher IGR rates combined with lower combustion efficiencies. It is also thought that the earlier EVO timing required during PPC operation, which has to be advanced compared to CDC to keep a high T_{IVC} to assure proper ignition, may also cause an additional increase in ISFC due to comparatively lower effective expansion ratio.

As a final remark, from the conclusions and main contributions made along this thesis it was demonstrated how it is possible to reach and even improve the performance of an equivalent diesel four-stroke engine with the two-stroke poppet-valves architecture, when operating both in CDC as with the gasoline PPC concept. The main trade-offs and physical relationships identified along this investigation are useful to create new research paths focused on the further development and/or thorough optimization of this innovative two-stroke engine concept to comply with future emissions regulations. Additionally, the proposed methodology as well as the experimental tools presented in this thesis can be extrapolated to design and develop any kind of two-stroke engine, regardless of its particular architecture or displacement.

6.3 Future activities and new research directions

A series of observations and suggestions have emerged along the execution of this thesis, that unfortunately could not be considered at the time of the investigation, either due to hardware limitations, time constraints or budget restrictions. Among the key points that could be improved for future studies on the poppet-valves two-stroke engine, and that would potentially help to further improve the results obtained on this thesis, it can be highlighted:

- *DoE optimization of the air management process considering a higher number of factors.* In the current investigation, the central composite design chosen for the DoE optimization was limited to a number of four factors, to keep a reasonably low number of tests and assure the simplicity of the test plan. Nevertheless, it would be interesting to include all the air management settings as independent factors on the DoE (i.e. P_{int}, ΔP, $VVT_{(int,exh)}$, $Olap$, EGR) as well as adding some additional factors such as the ambient temperature and pressure that are known to have an impact on the engine operation and on the final exhaust emissions level.

- *Improve the acoustic behavior of the intake and exhaust systems through dedicated 1D simulations.* The current geometry of the intake and exhaust system, is optimized to favor in some extend the acoustic behavior at the low speed range, however, as it was demonstrated at the high load point 6 (15.1 bar IMEPand 2500 rpm) the combustion process is compromised at full load conditions due to decreased engine permeability which leads to high smoke emissions. Performing dedicated 1D simulations is needed to further improve the engine acoustics at least in a wider range of engine speeds. A correct tuning of the intake and exhaust pressure waves would also help improving the intrinsic trade-off between TR and IGR observed in the poppet-valves architecture.

- *New design of the piston and injector nozzle geometry to improve its compatibility with the gasoline PPC concept.* Matching the bowl geometry and fuel spray angle (with a slightly narrower included angle) is expected to reduce the propensity for fuel wall wetting during the early injections, and also to improve the mixture preparation particularly for the second injection which is critical for the combustion development in PPC operation with a triple injection strategy.

- *New HSDI common-rail system with higher maximum injection pressure.* Increasing the maximum injection pressure of up to 1800 bar to 2000 bar

would help increasing the mixing rate of the spray, providing a positive impact in terms of smoke emissions. This is expected to help achieving the full load performance of the engine without exceeding the smoke limitation under CDC operation, but it would also help extending the range of application of the gasoline PPC concept (with triple injection strategy) up to higher loads by improving the mixing of the late third injection. Keep in mind this would also bring additional side effects on the spray characteristics (i.e. penetration) as well on the combustion process (i.e noise) which would finally impact NO_x, CO and HC.

Furthermore, from the general overview of the strengths and weaknesses of the poppet-valves two-stroke architecture, that have been previously summarized in the main conclusions of this thesis, it is possible to propose new research lines and prospective studies that would further complement and extend the methodologies needed for the development and optimization of future two-stroke light-duty engine concepts for automotive applications. The following new research directions can be proposed for the future development of advanced poppet-valves two-stroke CI engine concept:

- *Experimental measurement of the cylinder gas composition and residual gas fraction.* The correct determination of the trapped gas composition and IGR ratio is a key topic for the development of two-stroke engines as it was demonstrated on this investigation. There are different experimental approaches to determine the cylinder gas composition, but the complexity and high cost of fast sampling valves and fast gas analyzers have prevented the use of these techniques on this thesis. Despite these known difficulties, performing a dedicated study to experimentally measure the residual gas fraction at representative operating conditions (i.e. through $VVT_{(int,exh)}$ and ΔP sweeps at different engine loads) would be an important contribution to properly validate the current estimation of IGR (for 1D, 3D and also 0D calculations) and further improve the development of accurate and fast prediction tools for characterizing the gas exchange process in two-stroke engines.

- *Detailed optimization of the local ϕ distribution in the combustion chamber for gasoline PPC operation by means of CFD simulations.* This study could be realized in parallel with the design of a new piston bowl and injector nozzle geometry as it was previously suggested. Then, a dedicated DoE test plan can be designed to use the CFD model as a predictive tool to further optimize the in-cylinder conditions and the

injection strategy, considering the local mixture distribution and the air utilization inside the combustion chamber as key points to achieve successful PPC operation at different load conditions.

- *Further expansion of the range of operation of both CDC and the gasoline PPC concept to full load and high engine speed conditions.* This activity can be realized if the acoustics of both intake and exhaust systems are carefully optimized to improve engine permeability at high speed conditions, and/or if the current maximum limit in terms of the injection pressure is further increased. For full load gasoline PPC operation, this task could be more difficult to achieve with the current HSDI technology, since the injection system has to be able to inject at high pressures a lower viscosity fuel compared to diesel, without compromising the correct functioning of the fuel pump, and while also preventing fuel cavitation.

- *Investigation of lower octane gasolines for improving the performance of the PPC concept at low load conditions.* Switching to a lower octane gasoline during PPC operation is expected to improve low load operation and the reported indicated efficiency values, by relaxing the requirements in terms of IGR and T_{IVC} while keeping proper combustion stability. This could also help at medium load operation, by increasing the window between knocking and misfire conditions, which would allow performing a DoE optimization the air management settings. Nevertheless, using a lower octane gasoline will have a negative impact at high load operation, where a more reactive fuel will make difficult to attain a proper mixture stratification before the onset of ignition. Accordingly, the effect of fuel octane number on the range of operation of the gasoline PPC concept should be carefully assessed through additional studies at different load conditions.

In addition to the previously suggested research directions, it is worth to make a final comment about the poppet-valves two-stroke architecture itself. Despite this engine configuration provides important benefits in terms of mechanical design and engine reliability compared to two-stroke engines with ports on the cylinder wall, the intrinsic lower permeability given by the limited flow effective area combined with the proximity between the intake and exhaust valves, naturally increases the intake pressure and ΔP requirements compared to an uniflow scavenging architecture. Therefore, there is still a great interest from both the automotive manufacturer's as well as the scientific community to further investigate the feasibility and evaluate the performances of an uniflow two-stroke engine for extremely downsized automotive applications [11].

Bibliography

[1] Osborne R. J., Stokes J., Lake T. H., Carden P. J., Mullineux J. D., Helle-Lorentzen R., Evans J. C., Heikal M. R., Zhu Y., Zhao Hua and Ma T. "Development of a Two-Stroke/Four-Stroke Switching Gasoline Engine - The 2/4SIGHT Concept". In *SAE Technical Paper*, volume 2005-01-1137, 2005.

[2] Iijima Akira, Watanabe Takashi, Yoshida Koji and Shoji Hideo. "A Study of HCCI Combustion Using a Two-Stroke Gasoline Engine with a High Compression Ratio". In *SAE Technical Paper*, volume 2006-32-0043, 2006.

[3] Zhao H. *HCCI and CAI engines for the automotive industry*. Woodhead Publishing in mechanical engineering. Woodhead Pub., 2007.

[4] Dahl Daniel and Denbratt Ingemar. "Valve Profile Adaptation, Stratification, Boosting and 2-Stroke Strategies for Raising Loads of Gasoline HCCI Engines". *SAE International Journal of Engines*, Vol. 5 n^o 3, pp. 1033–1045, 2012.

[5] Zhang Yan, Ojapah Mohammed, Cairns Alasdair and Zhao Hua. "2-Stroke CAI Combustion Operation in a GDI Engine with Poppet Valves". In *SAE Technical Paper*, volume 2012-01-1118, 2012.

[6] Zhang Yan, Zhao Hua, Ojapah Mohammed and Cairns Alasdair. "CAI combustion of gasoline and its mixture with ethanol in a 2-stroke poppet valve DI gasoline engine". *Fuel*, Vol. 109 n^o 0, pp. 661–668, 2013.

[7] Zhang Y. and Zhao H. "Investigation of combustion, performance and emission characteristics of 2-stroke and 4-stroke spark ignition and CAI/HCCI operations in a DI gasoline". *Applied Energy*, Vol. 130 n^o 0, pp. 244–255, 2014.

[8] Benajes Jesus, Novella Ricardo, De Lima Daniela, Dugue Vincent and Quechon Nicolas. "The potential of highly premixed combustion for pollutant control in an automotive two-stroke HSDI diesel engine". In *SAE Technical Paper*, volume 2012-01-1104, 2012.

[9] Benajes Jesus, Novella Ricardo, De Lima Daniela, Quechon Nicolas and Obernesser Philippe. "Implementation of the early injection highly premixed combustion concept in a two-stroke HSDI engine". In *SIA Diesel Powertrain Congress 2012*, volume SIA Diesel Powertrain Congress 2012, Rouen, France, 2012.

[10] Benajes J., Novella R., Martin J. and De Lima D. "Analysis of the Load Effect on the Partially Premixed Combustion Concept in a 2-Stroke HSDI Diesel Engine Fueled with Conventional Gasoline". In *SAE Technical Paper*, volume 2014-01-1291, 2014.

[11] Laget O, Ternel C, Thiriot J, Charmasson S, Tribotte P and Vidal F. "Preliminary Design of a Two-Stroke Uniflow Diesel Engine for Passenger Car". In *SAE Technical Paper*, volume 2013-01-1719, 2013.

Bibliography

Instrumentation and techniques for exhaust gas emissions measurement. SAE Standards J254.
1993. (cited in p. 101)

ASTM D1298-99 standard test method for density, relative density (Specific Gravity), or API gravity of Crude Petroleum and Liquid Petroleum Products by Hydrometer Method.
ASTM International, West Conshohocken, PA, 1999. (cited in p. 91)

Regulation 715/2007 of the European Parliament and of the Council of 20 June 2007 on type approval of motor vehicles with respect to emissions from light passenger and commercial vehicles (Euro 5 and Euro 6) and on access to vehicle repair and maintenance information.
Official Journal of the European Union, 2007. (cited en pp. 4, 141)

Regulation 443/2009 of the European Parliament and of the Council of 23 April 2009 setting emission performance standards for new passenger cars as part of the Community's integrated approach to reduce CO2 emissions from light-duty vehicles.
Official Journal of the European Union, 2009. (cited in p. 5)

European Roadmap. Future Light-Duty Powertrain Technologies and Fuels.
ERTRAC Working Group on Energy and Environment, 2011. (cited en pp. 9, 10)

Comission Regulation 459/2012 of 29 May 2012 amending Regulation 715/2007 of the European Parliament and of the Council and Commission Regulation No 692/2008 as regards emissioos from light passenger and commercial vehicles (Euro 6).
Official Journal of the European Union, 2012. (cited in p. 5)

UNE-EN 228:2013. Combustibles para automocion. Gasolina sin plomo. Requisitos y metodos de ensayo.
ASOCIACION ESPANOLA DE NORMALIZACION Y CERTIFICACION (AENOR), 2013. (cited in p. 91)

Energy Technology Perspectives 2014. Harnessing Electricity Potential.
International Energy Agency IEA Publications, 2014. (cited in p. 3)

Key World Energy Statistics 2014.
International Energy Agency IEA Publications, 2014. (cited in p. 2)

UNE-EN 590:2014. Combustibles para automocion. Combustibles para motor diesel (gasoleo). Requisitos y metodos de ensayo.
ASOCIACION ESPANOLA DE NORMALIZACION Y CERTIFICACION (AENOR), 2014. (cited in p. 91)

Abthoff J., Duvinage F., Hardt T., Kramer M. and Paule M.
The 2-Stroke DI-Diesel Engine with Common Rail Injection for Passenger Car Application.
In *SAE Technical Paper*, volume 981032. SAE International, 1998. (cited in p. 12)

Akagawa Hisashi, Miyamoto Takeshi, Harada Akira, Sasaki Satoru, Shimazaki Naoki, Hashizume Takeshi and Tsujimura Kinji.
Approaches to Solve Problems of the Premixed Lean Diesel Combustion.
In *SAE Technical Paper*, volume 1999-01-0183. SAE International, 1999.
(cited en pp. 45, 46)

Akihama Kazuhiro, Takatori Yoshiki and Inagaki Kazuhisa.
Mechanism of the Smokeless Rich Diesel Combustion by Reducing Temperature.
In *SAE Technical Paper*, volume 2001-01-0655, 2001. (cited en pp. 41, 43)

Albert B. P. and Ghandhi J. B.
Residual Gas Measurements in a Utility Engine.
In *SAE Technical Paper*, volume 2004-32-0029, 2004. (cited in p. 115)

Alkidas Alex C.
Combustion advancements in gasoline engines.
Energy Conversion and Management, Vol. 48 n^o 11, pp. 2751–2761, 2007. (cited in p. 8)

Amorim Rogerio.
Combustion por difusion de baja temperature en motores diesel de pequeña cilindrada.
PhD Thesis. Universitat Politecnica de Valencia, Departamento de Maquinas y Motores Termicos, 2010. (cited in p. 43)

Andre M., Walter B., Bruneaux G., Foucher F. and Mounaim-Rousselle C.
Optimizing Early Injection Strategy for Diesel PCCI Combustion.
In *SAE Technical Paper*, volume 2009-01-2731. SAE International, 2009. (cited in p. 46)

Angelberger C., Poinsot T. and Delhay B.
Improving Near-Wall Combustion and Wall Heat Transfer Modeling in SI Engine Computations.
In *SAE Technical Paper*, volume 972881. SAE International, 1997. (cited in p. 128)

Antony Jiju.
Design of Experiments for Engineers and Scientists.
Butterworth-Heinemann, Oxford, 2003. (cited in p. 143)

Aoyagi Y., Kamimoto T., Matsui Y. and Matsuoka S.
A Gas Sampling Study on the Formation Processes of Soot and NO in a DI Diesel Engine.
In *SAE Technical Paper*, volume 800254, 1980. (cited in p. 40)

Armas O.
Diagnostico experimental del proceso de combustion en motores Diesel de inyeccion directa.
PhD thesis. Universitat Politecnica de Valencia, Departamento de Maquinas y Motores Termicos, 1998. (cited in p. 119)

Arregle J.
Analisis de la estructura y dinamica interna de chorros diesel.
PhD thesis. Universitat Politecnica de Valencia, Departamento de Maquinas y Motores Termicos, 1997. (cited in p. 26)

Arregle J., Lopez J. J., Garcia J. M. and Fenollosa C.
Development of a zero-dimensional Diesel combustion model. Part 1: Analysis of the quasi-steady diffusion combustion phase.
Applied Thermal Engineering, Vol. 23 n^o 11, pp. 1301–1317, 2003.
(cited en pp. 167, 168)

Arregle J., Lopez J. J., Garcia J. M. and Fenollosa C.
Development of a zero-dimensional Diesel combustion model: Part 2: Analysis of the transient initial and final diffusion combustion phases.
Applied Thermal Engineering, Vol. 23 n^o 11, pp. 1319–1331, 2003. (cited in p. 34)

Babajimopoulos A, Assanis D N, Flowers D L, Aceves S M and Hessel R P.
A fully coupled computational fluid dynamics and multi-zone model with detailed chemical kinetics for the simulation of premixed charge compression ignition engines.
International Journal of Engine Research, Vol. 6 n^o 5, pp. 497–512, 2005.
(cited in p. 129)

Beale J.C. and Reitz R.D.
Modeling Spray Atomization with the Kelvin-Helmholtz/Rayleigh-Taylor Hybrid Model.
Atomization and Sprays, Vol. 9 n^o 6, pp. 623–650, 1999. (cited in p. 128)

Belarte Eduardo.
Estudio del proceso de combustion premezclada controlada por la reactividad del combustible en un motor de encendido por compresion.
PhD thesis. Universitat Politecnica de Valencia, Departamento de Maquinas y Motores Termicos, 2015. (cited in p. 47)

Benajes J., Molina S., Novella R. and De Lima D.
Implementation of the Partially Premixed Combustion concept in a 2-stroke HSDI diesel engine fueled with gasoline.
Applied Energy, Vol. 122 n^o 0, pp. 94–111, 2014. (cited en pp. 221, 224)

Benajes J., Novella R., Arthozoul Simon and Kolodziej Christopher.
Particle Size Distribution Measurements from Early to Late Injection Timing Low Temperature Combustion in a Heavy Duty Diesel Engine.
In *SAE Technical Paper*, volume 2010-01-1121, 2010. (cited in p. 166)

Benajes J., Novella R., De Lima D. and Tribotte P.
Investigation on Multiple Injection Strategies for Gasoline PPC Operation in a Newly Designed 2-Stroke HSDI Compression Ignition Engine.
SAE Int. J. of Engines, Vol. 8 n^o 2, 2015. (cited in p. 232)

Benajes J., Novella R., Martin J. and De Lima D.
Analysis of the Load Effect on the Partially Premixed Combustion Concept in a 2-Stroke HSDI Diesel Engine Fueled with Conventional Gasoline.
In *SAE Technical Paper*, volume 2014-01-1291, 2014. (cited en pp. 229, 302)

Benajes J. V., Lopez J. J., Novella R. and Garcia A.
Advanced Methodology for improving testing efficiency in a single-cylinder research diesel engine.
Experimental Techniques, Vol. 32 n^o 6, pp. 41–47, 2008. (cited in p. 108)

Benajes Jesus, Garcia-Oliver Jose M., Novella Ricardo and Kolodziej Christopher.
Increased particle emissions from early fuel injection timing Diesel low temperature combustion.
Fuel, Vol. 94 n^o 0, pp. 184–190, 2012. (cited in p. 166)

Benajes Jesus, Molina Santiago, Garcia Antonio, Belarte Eduardo and Vanvolsem Michel.
An investigation on RCCI combustion in a heavy duty diesel engine using in-cylinder blending of diesel and gasoline fuels.
Applied Thermal Engineering, Vol. 63 n^o 1, pp. 66–76, 2014. (cited en pp. 46, 47)

Benajes Jesus, Molina Santiago, Novella Ricardo and Amorim Rogerio.
Study on low temperature combustion for light-duty diesel engines.
Energy and Fuels, Vol. 24, pp. 355–364, 2010. (cited in p. 43)

Benajes Jesus, Molina Santiago, Novella Ricardo and Belarte Eduardo.
Evaluation of massive exhaust gas recirculation and Miller cycle strategies for mixing-controlled low temperature combustion in a heavy duty diesel engine.
Energy, Vol. 71, pp. 355–366, 2014. (cited in p. 43)

Benajes Jesus, Novella Ricardo, De Lima Daniela, Dugue Vincent and Quechon Nicolas.
The potential of highly premixed combustion for pollutant control in an automotive two-stroke HSDI diesel engine.
In *SAE Technical Paper*, volume 2012-01-1104, 2012. (cited en pp. 210, 216, 301)

Benajes Jesus, Novella Ricardo, De Lima Daniela, Quechon Nicolas and Obernesser Philippe.
Implementation of the early injection highly premixed combustion concept in a two-stroke HSDI engine.
In *SIA Diesel Powertrain Congress 2012*, volume SIA Diesel Powertrain Congress 2012, Rouen, France, 2012. (cited en pp. 210, 216, 217, 301)

Benajes Jesus, Novella Ricardo, De Lima Daniela and Tribotte Pascal.
Analysis of combustion concepts in a newly designed two-stroke high-speed direct injection compression ignition engine.
International Journal of Engine Research, Vol. 16 n^o 1, pp. 52–67, 2015.
(cited en pp. 161, 232)

Benajes Jesus, Novella Ricardo, De Lima Daniela, Tribotte Pascal, Quechon Nicolas, Obernesser Philippe and Dugue Vincent.
Analysis of the combustion process, pollutant emissions and efficiency of an innovative 2-stroke HSDI engine designed for automotive applications.
Applied Thermal Engineering, Vol. 58, pp. 181–193, 2013. (cited in p. 176)

Benajes Jesus, Novella Ricardo, Garcia Antonio and Arthozoul Simon.
The role of in-cylinder gas density and oxygen concentration on late spray mixing and soot oxidation processes.
Energy, Vol. 36 n^o 3, pp. 1599–1611, 2011. (cited en pp. 166, 168)

Blair G. P.
The Basic Design of Two-Stroke Engines.
SAE International, 1990. (cited in p. 156)

Blair G.P.
Design and Simulation of Two-stroke Engines.
Society of Automotive Engineers, 1996. (cited en pp. 11, 144, 146, 156)

Boree Jacques, Atassi Nidal, Charnay Georges and Taubert Lutz.
Measurements and image analysis of the turbulent field in an axisymmetric jet subject to a sudden velocity decrease.
Experimental Thermal and Fluid Science, Vol. 14 n^o 1, pp. 45–51, 1997. (cited in p. 125)

Borgqvist Patrick, Tuner Martin, Mello Augusto, Tunestal Per and Johansson Bengt.
The Usefulness of Negative Valve Overlap for Gasoline Partially Premixed Combustion, PPC.
In *SAE Technical Paper*, volume 2012-01-1578. SAE International, 2012.
(cited en pp. 67, 229)

Borgqvist Patrick, Tunestal Per and Johansson Bengt.
Gasoline Partially Premixed Combustion in a Light Duty Engine at Low Load and Idle Operating Conditions.
In *SAE Technical Paper*, volume 2012-01-0687, 2012. (cited in p. 67)

Brandl S., Graf B. and Rust A.
NVH Challenges and Solutions for Vehicles with Low CO2 Emission.
SAE Int. J. Passeng. Cars - Mech. Syst., Vol. 5, pp. 1084–1090, 2012. (cited in p. 129)

Bruneaux G.
Combustion structure of free and wall-impinging diesel jets by simultaneous laser-induced fluorescence of formaldehyde, poly-aromatic hydrocarbons, and hydroxides.
International Journal of Engine Research, Vol. 9 n^o 3, pp. 249–265, 2008.
(cited en pp. 27, 29, 30, 32)

Bruneaux Gilles.
Mixing Process in High Pressure Diesel Jets by Normalized Laser Induced Exciplex Fluorescence Part I: Free Jet.
In *SAE Technical Paper*, volume 2005-01-2100. SAE International, 2005. (cited in p. 34)

Buchwald Ralf, Brauer Maximilian, Blechstein Andre, Sommer Ansgar and Kahrstedt Jorn.
Adaption of Injection System Parameters to Homogeneous Diesel Combustion.
In *SAE Technical Paper*, volume 2004-01-0936. SAE International, 2004. (cited in p. 46)

Canaan R., Dec J., Green R. and Daly D.
The Influence of Fuel Volatility on the Liquid-Phase Fuel Penetration in a Heavy-Duty D.I. Diesel Engine.
In *SAE Technical Paper*, volume 980510, 1998. (cited in p. 27)

Chang Junseok, Kalghatgi Gautam, Amer Amer and Viollet Yoann.
Enabling High Efficiency Direct Injection Engine with Naphtha Fuel through Partially Premixed Charge Compression Ignition Combustion.
In *SAE Technical Paper*, volume 2012-01-0677, 2012. (cited in p. 50)

Chartier Clement, Aronsson Ulf, Andersson Oivind, Egnell Rolf, Collin Robert, Seyfried Hans, Richter Mattias and Alden Marcus.
Analysis of Smokeless Spray Combustion in a Heavy-Duty Diesel Engine by Combined Simultaneous Optical Diagnostics.
In *SAE Technical Paper*, volume 2009-01-1353. SAE International, 2009. (cited in p. 32)

Chen G.
Study of fuel temperature effects on fuel injection, combustion, and emissions of direct-injection diesel engines.
Journal of Engineering for Gas Turbines and Power, Vol. 131 n^o 2, 2009. (cited in p. 99)

Cheng A. S, Upatnieks A. and Mueller C. J.
Investigation of fuel effects on dilute, mixing-controlled combustion in an optical direct-injection diesel engine.
Energy and Fuels, Vol. 21 n^o 4, pp. 1989–2002, 2007. (cited in p. 43)

Christian R., Knopf F., Jasmek A. and Schindler W.
A new method for the filter smoke number measurement with improved sensitivity.
MTZ Motortechnische Zeitschift, Vol. 54, pp. 16–22, 1993. (cited in p. 102)

Ciatti Stephen, Johnson Michael, Das Adhikary Bishwadipa, Reitz Rolf and Knock Aaron.
Efficiency and Emissions performance of Multizone Stratified Compression Ignition Using Different Octane Fuels.
In *SAE Technical Paper*, volume 2013-01-0263, 2013. (cited en pp. 50, 68)

Co. Daihatsu Motor.
Ltd, Press Information.
In *The 61st International Motor Show (IAA), Frankfurt 2005.*, 2005. (cited in p. 11)

Colban Will F., Miles Paul C. and Oh Seungmook.
Effect of Intake Pressure on Performance and Emissions in an Automotive Diesel Engine Operating in Low Temperature Combustion Regimes.
In *SAE Technical Paper*, volume 2007-01-4063. SAE International, 2007.
(cited en pp. 43, 64)

Correas D.
Estudio Teorico-Experimental del chorro libre diesel isotermo.
PhD Thesis. Universitat Politecnica de Valencia, Departamento de Maquinas y Motores Termicos, 1998. (cited in p. 26)

Curran H. J., Gaffuri P., Pitz W. J. and Westbrook C. K.
A Comprehensive Modeling Study of n-Heptane Oxidation.
Combustion and Flame, Vol. 114 n^o 1-2, pp. 149–177, 1998. (cited en pp. 29, 49)

Dagaut Philippe, Daly Catherine, Simmie John M. and Cathonnet Michel.
The oxidation and ignition of dimethylether from low to high temperature (500-1600 K): Experiments and kinetic modeling.
Symposium (International) on Combustion, Vol. 27 n^o 1, pp. 361–369, 1998.
(cited in p. 49)

Dagaut Philippe, Reuillon Marcelline and Cathonnet Michel.
Experimental study of the oxidation of n-heptane in a jet stirred reactor from low to high temperature and pressures up to 40 atm.
Combustion and Flame, Vol. 101 n^o 1-2, pp. 132–140, 1995. (cited en pp. 49, 50)

Dahl Daniel and Denbratt Ingemar.
Valve Profile Adaptation, Stratification, Boosting and 2-Stroke Strategies for Raising Loads of Gasoline HCCI Engines.
SAE International Journal of Engines, Vol. 5 n^o 3, pp. 1033–1045, 2012.
(cited en pp. 12, 295)

Das Adhikary Bishwadipa, Ra Youngchul, Reitz Rolf and Ciatti Stephen.
Numerical Optimization of a Light-Duty Compression Ignition Engine Fuelled With Low-Octane Gasoline.
In *SAE Technical Paper*, volume 2012-01-1336, 2012. (cited en pp. 50, 68)

Das Adhikary Bishwadipa, Reitz Rolf and Ciatti Stephen.
Study of In-Cylinder Combustion and Multi-Cylinder Light Duty Compression Ignition Engine Performance Using Different RON Fuels at Light Load Conditions.
In *SAE Technical Paper*, volume 2013-01-0900, 2013. (cited en pp. 68, 231)

Das Adhikary Bishwadipa, Reitz Rolf, Ciatti Stephen and Kolodziej Christopher.
Computational Investigation of Low Load Operation in a Light-Duty Gasoline Direct Injection Compression Ignition [GDICI] Engine Using Single-Injection Strategy.
In *SAE Technical Paper*, volume 2014-01-1297. SAE International, 2014. (cited in p. 68)

Davis P. W. and Peckham M. S.
Cycle-by-Cycle Gasoline Engine Cold Start Measurement of Residual Gas and AFR Using a Fast Response CO&CO2 Analyzer.
In *SAE Technical Paper*, volume 2008-01-1649, 2008. (cited in p. 115)

De Rudder Korneel.
An approach to low temperature combustion in a small HSDI diesel engine.
PhD thesis. Universitat Politecnica de Valencia, Departamento de Maquinas y Motores Termicos, 2007. (cited en pp. 99, 107)

Dec John E.
A Conceptual Model of DI Diesel Combustion Based on Laser-Sheet Imaging.
In *SAE Technical Paper*, volume 970873, 1997. (cited en pp. 25, 27, 31, 40, 61, 165)

Dec John E. and Canaan Robert E.
PLIF Imaging of NO Formation in a DI Diesel Engine.
In *SAE Technical Paper*, volume 980147, 1998. (cited in p. 33)

Dec John E. and Coy Edward B.
OH Radical Imaging in a DI Diesel Engine and the Structure of the Early Diffusion Flame.
In *SAE Technical Paper*, volume 960831. SAE International, 1996.
(cited en pp. 29, 30, 33)

Dec John E. and Espey Christoph.
Ignition and Early Soot Formation in a DI Diesel Engine Using Multiple 2-D Imaging Diagnostics.
In *SAE Technical Paper*, volume 950456. SAE International, 1995. (cited in p. 27)

Dec John E. and Espey Christoph.
Chemiluminescence Imaging of Autoignition in a DI Diesel Engine.
In *SAE Technical Paper*, volume 982685. SAE International, 1998. (cited en pp. 27, 29)

Dec John E. and Kelly-Zion Peter L.
The Effects of Injection Timing and Diluent Addition on Late-Combustion Soot Burnout in a DI Diesel Engine Based on Simultaneous 2-D Imaging of OH and Soot.
In *SAE Technical Paper*, volume 2000-01-0238. SAE International, 2000. (cited in p. 39)

Dec John E. and Sjoberg Magnus.
A Parametric Study of HCCI Combustion - the Sources of Emissions at Low Loads and the Effects of GDI Fuel Injection.
In *SAE Technical Paper*, volume 2003-01-0752, 2003. (cited in p. 214)

Dec John E. and Sjoberg Magnus.
Isolating the Effects of Fuel Chemistry on Combustion Phasing in an HCCI Engine and the Potential of Fuel Stratification for Ignition Control.
In *SAE Technical Paper*, volume 2004-01-0557. SAE International, 2004. (cited in p. 47)

Dec John E. and Tree Dale R.
Diffusion-Flame / Wall Interactions in a Heavy-Duty DI Diesel Engine.
In *SAE Technical Paper*, volume 2001-01-1295. SAE International, 2001. (cited in p. 33)

Degobert Paul.
Automobiles and Pollution.
Editions Technip, 1995. (cited in p. 101)

Degraeuwe B.
Contribution to the thermal management of DI Diesel engines.
PhD thesis. Universitat Politecnica de Valencia, Departamento de Maquinas y Motores Termicos, 2007. (cited in p. 120)

Desantes J. M., Pastor J. V., Garcia-Oliver J. M. and Pastor J. M.
A 1D model for the description of mixing-controlled reacting diesel sprays.
Combustion and Flame, Vol. 156 n^o 1, pp. 234–249, 2009. (cited en pp. 124, 217, 226)

Desantes Jose M., Benajes Jesus, Garcia Antonio and Monsalve-Serrano Javier.
The role of the in-cylinder gas temperature and oxygen concentration over low load reactivity controlled compression ignition combustion efficiency.
Energy, Vol. 78 n^o 0, pp. 854–868, 2014. (cited in p. 47)

Desantes Jose M., Lopez J. Javier, Garcia Jose M. and Pastor Jose M.
Evaporative Diesel Spray Modeling.
Atomization and Sprays, Vol. 17 n^o 3, pp. 193–231, 2007. (cited in p. 27)

Desantes Jose M., Payri Raul, Pastor Jose M. and Gimeno J.
Experimental characterization of internal nozzle flow and diesel spray behavior. Part I: Non evaporative conditions.
Atomization and Sprays, Vol. 15 n^o 5, pp. 489–516, 2005. (cited in p. 126)

Domenech V.
Estudio de nuevas estrategias para el control de la combustion en modos parcialmente premezclados en motores de encendido por compresion.
PhD thesis. Universitat Politecnica de Valencia, Departamento de Maquinas y Motores Termicos, 2013. (cited in p. 92)

Dukowicz J. K.
A particle-fluid numerical model for liquid sprays.
Journal of Computational Physics, Vol. 35 n^o 2, pp. 229–253, 1980. (cited in p. 128)

Duret Pierre.
A new generation of two-stroke engines for the future?
Editions Technip, Pairs, 1993. (cited en pp. 12, 144)

Duret Pierre and Moreau Jean-Francois.
Reduction of Pollutant Emissions of the IAPAC Two-Stroke Engine with Compressed Air Assisted Fuel Injection.
In *SAE Technical Paper*, volume 900801, 1990. (cited in p. 12)

Elzen Michel den, Roelfsema Mark, Hof Andries, Botcher Hannes and Grassi Giacomo.
Analysing the emission gap between pledged emission reductions under the Cancun Agreements and the 2C climate target.
PBL Netherlands Environmental Assessment Agency. European Comission Joint Research Centre, 2012. (cited in p. 3)

Enrico Mattarelli, Giuseppe Cantore and Carlo Alberto Rinaldini.
Advances in The Design of Two-Stroke, High Speed, Compression Ignition Engines, volume Chapter 5.
InTech, 2013. (cited in p. 11)

Eriksson L.
Design of Experiments: Principles and Applications.
Umetrics, 2008. (cited in p. 143)

Faeth G. M.
Evaporation and combustion of sprays.
Progress in Energy and Combustion Science, Vol. 9 n^o 1-2, pp. 1–76, 1983.
(cited in p. 125)

Fang Tiegang, Coverdill Robert E., Lee Chia-fon F. and White Robert A.
Smokeless Combustion within a Small-Bore HSDI Diesel Engine Using a Narrow Angle Injector.
In *SAE Technical Paper*, volume 2007-01-0203. SAE International, 2007. (cited in p. 46)

Flynn P.F., Durrett R.P., Hunter G.L., Zur Loye A.O., Akinyemi O. C., Dec John E. and Westbrook Charles K.
Diesel combustion: An integrated view combining laser diagnostics, chemical kinetics, and empirical validation.
In *SAE Technical Paper*, volume 1999-01-0509, 1999. (cited en pp. 25, 28, 29, 31, 32, 61)

Fridriksson Helgi Skuli, Hajireza Shahrokh, Sunden Bengt and Tuner Martin.
CFD Investigation on Injection Strategy and Gasoline Quality Impact on In-Cylinder Temperature Distribution and Heat Transfer in PPC.
In *SAE Technical Paper*, volume 2013-24-0009, 2013. (cited in p. 68)

Galloni E., Fontana G. and Palmaccio R.
Effects of exhaust gas recycle in a downsized gasoline engine.
Applied Energy, Vol. 105 n^o 0, pp. 99–107, 2013. (cited in p. 8)

Garcia-Oliver J.M.
Aportaciones al estudio del proceso de combustion turbulenta de chorros en motores diesel de inyeccion directa.
PhD thesis. Universitat Politecnica de Valencia, Departamento de Maquinas y Motores Termicos, 2004. (cited en pp. 27, 125)

Gimeno J.
Desarrollo y aplicacion de la medida del flujo de cantidad de movimiento de un chorro diesel.
PhD thesis. Universitat Politecnica de Valencia, Departamento de Maquinas y Motores Termicos, 2008. (cited in p. 26)

Han Zhiyu and Reitz Rolf D.
A temperature wall function formulation for variable-density turbulent flows with application to engine convective heat transfer modeling.
International journal of heat and mass transfer, Vol. 40 n^o 3, pp. 613–625, 1997. (cited in p. 128)

Hanson Reed, Splitter Derek and Reitz Rolf.
Operating a Heavy-Duty Direct-Injection Compression-Ignition Engine with Gasoline for Low Emissions.
In *SAE Technical Paper*, volume 2009-01-1442, 2009. (cited in p. 68)

Hardy W. L. and Reitz R. D.
A Study of the Effects of High EGR, High Equivalence Ratio, and Mixing Time on Emissions Levels in a Heavy-Duty Diesel Engine for PCCI Combustion.
In *SAE Technical Paper*, volume 2006-01-0026, 2006. (cited in p. 50)

Hasegawa Ryo and Yanagihara Hiromichi.
HCCI Combustion in a DI Diesel engine.
In *SAE Technical Paper*, volume 2003-01-0745, 2003. (cited en pp. 45, 46)

Hashizume Takeshi, Miyamoto Takeshi, Hisashi Akagawa and Tsujimura Kinji.
Combustion and Emission Characteristics of Multiple Stage Diesel Combustion.
In *SAE Technical Paper*, volume 980505. SAE International, 1998. (cited in p. 46)

Held T. J. and Dryer F. L.
An experimental and computational study of methanol oxidation in the intermediate-and high-temperature regimes.
Symposium (International) on Combustion, Vol. 25 n^o 1, pp. 901–908, 1994. (cited en pp. 49, 50)

Helmantel Arjan and Denbratt Ingemar.
HCCI Operation of a Passenger Car Common Rail DI Diesel Engine With Early Injection of Conventional Diesel Fuel.
In *SAE Technical Paper*, volume 2004-01-0935. SAE International, 2004. (cited in p. 46)

Hermens S.
Influence of diesel injector nozzle geometry on the injection and combustion process.
PhD Thesis. Universitat Politecnica de Valencia, Departamento de Maquinas y Motores Termicos, 2008. (cited in p. 26)

Heywood J. B.
Internal combustion engine fundamentals.
Ed. McGraw-Hill Science/Engineering/Math, 1988. (cited in p. 190)

Heywood J.B., Sher E. and Engineers Society of Automotive.
The Two-stroke Cycle Engine: Its Development, Operation, and Design.
Taylor and Francis, 1999. (cited en pp. 11, 144)

Higgins B, Siebers D and Aradi A.
Diesel-Spray Ignition and Premixed-Burn Behavior.
In *SAE Technical Paper*, volume 2000-01-0940, 2000. (cited en pp. 29, 30)

Hildingsson Leif, Johansson Bengt, Kalghatgi Gautam T. and Harrison Andrew J.
Some Effects of Fuel Autoignition Quality and Volatility in Premixed Compression Ignition Engines.
In *SAE Technical Paper*, volume 2010-01-0607, 2010. (cited in p. 66)

Hildingsson Leif, Kalghatgi Gautam, Tait Nigel, Johansson Bengt and Harrison Andrew.
Fuel Octane Effects in the Partially Premixed Combustion Regime in Compression Ignition Engines.
In *SAE Technical Paper*, volume 2009-01-2648, 2009. (cited en pp. 65, 66, 68)

Hildingsson Leif, Persson Hakan, Johansson Bengt, Collin Robert, Nygren Jenny, Richter Mattias, Alden Marcus, Hasegawa Ryo and Yanagihara Hiromichi.
Optical Diagnostics of HCCI and Low-Temperature Diesel Using Simultaneous 2-D PLIF of OH and Formaldehyde.
In *SAE Technical Paper*, volume 2004-01-2949. SAE International, 2004.
(cited en pp. 59, 60)

Hiroyasu H. and Kadota T.
Models for Combustion and Formation of Nitric Oxide and Soot in Direct Injection Diesel Engines.
In *SAE Technical Paper*, volume 760129, 1976. (cited in p. 129)

Hooper P. R., Al-Shemmeri T. and Goodwin M. J.
Advanced modern low-emission two-stroke cycle engines.
Proceedings of the Institution of Mechanical Engineers, Part D: Journal of Automobile Engineering, Vol. 225 n^o 11, pp. 1531–1543, 2011. (cited in p. 12)

Hoppie L. O.
The Influence of Initial Fuel Temperature on Ignition Delay.
In *SAE Technical Paper*, volume 820356. SAE International, 1982. (cited in p. 99)

Horibe Naoto, Takahashi Ken, Kee Sung-Sub, Ishiyama Takuji and Shioji Masahiro.
The Effects of Injection Conditions and Combustion Chamber Geometry on Performance and Emissions of DI-PCCI Operation in a Diesel Engine.
In *SAE Technical Paper*, volume 2007-01-1874, 2007. (cited in p. 64)

Hu Bing, Musculus Mark P. B. and Oefelein Joseph C.
The influence of large-scale structures on entrainment in a decelerating transient turbulent jet revealed by large eddy simulation.
Physics of Fluids, Vol. 24 n^o 4, pp. 045106, 2012. (cited in p. 37)

Huestis Edwin, Erickson Paul A. and Musculus Mark P. B.
In-Cylinder and Exhaust Soot in Low-Temperature Combustion Using a Wide-Range of EGR in a Heavy-Duty Diesel Engine.
In *SAE Technical Paper*, volume 2007-01-4017. SAE International, 2007. (cited in p. 43)

Idicheria C. A. and Pickett L. M.
Ignition, soot formation, and end-of-combustion transients in diesel combustion under high-EGR conditions.
International Journal of Engine Research, Vol. 12 n^o 4, pp. 376–392, 2011.
(cited in p. 29)

Idicheria Cherian A. and Pickett Lyle M.
Formaldehyde Visualization Near Lift-off Location in a Diesel Jet.
In *SAE Technical Paper*, volume 2006-01-3434. SAE International, 2006.
(cited en pp. 27, 29, 30, 32)

Iijima Akira, Watanabe Takashi, Yoshida Koji and Shoji Hideo.
A Study of HCCI Combustion Using a Two-Stroke Gasoline Engine with a High Compression Ratio.
In *SAE Technical Paper*, volume 2006-32-0043, 2006. (cited en pp. 12, 295)

Iijima Akira, Yoshida Koji and Shoji Hideo.
A Comparative Study of HCCI and ATAC Combustion Characteristics Based on Experimentation and Simulations Influence of the Fuel Octane Number and Internal EGR on Combustion.
In *SAE Technical Paper*, volume 2005-01-3732. SAE International, 2005. (cited in p. 209)

Iwabuchi Yoshinori, Kawai Kenji, Shoji Takeshi and Takeda Yoshinaka.
Trial of New Concept Diesel Combustion System - Premixed Compression-Ignited Combustion.
In *SAE Technical Paper*, volume 1999-01-0185, 1999. (cited in p. 45)

Jante Alfred.
Scavenging and Other Problems of Two-Stroke Cycle Spark-Ignition Engines.
In *SAE Technical Paper*, volume 680468, 1968. (cited in p. 11)

Johnson Timothy V.
Vehicular Emissions in Review.
SAE International Journal of Engines, Vol. 5 n^o 2, pp. 216–234, 2012. (cited en pp. 8, 9)

Kaiadi Mehrzad, Johansson Bengt, Lundgren Marcus and Gaynor John A.
Experimental Investigation on different Injection Strategies for Ethanol Partially Premixed Combustion.
In *SAE Technical Paper*, volume 2013-01-0281, 2013. (cited en pp. 68, 231)

Kalghatgi G. T.
The outlook for fuels for internal combustion engines.
International Journal of Engine Research, Vol. 15 n^o 4, pp. 383–398, 2014. (cited in p. 66)

Kalghatgi G. T., Kumara Gurubaran R., Davenport A., Harrison A. J., Hardalupas Y. and Taylor A. M. K. P.
Some advantages and challenges of running a Euro IV, V6 diesel engine on a gasoline fuel.
Fuel, Vol. 108 n^o 0, pp. 197–207, 2013. (cited in p. 68)

Kalghatgi Gautam, Hildingsson Leif and Johansson Bengt.
Low NOx and Low Smoke Operation of a Diesel Engine Using Gasolinelike Fuels.
Journal of Engineering for Gas Turbines and Power, Vol. 132 n^o 9, pp. 092803–092803, 2010. (cited in p. 65)

Kalghatgi Gautam, Risberg Per and Angstrom Hans.
Partially Pre-Mixed Auto-Ignition of Gasoline to Attain Low Smoke and Low NOx at High Load in a Compression Ignition Engine and Comparison with a Diesel Fuel.
In *SAE Technical Paper*, volume 2007-01-0006, 2007. (cited en pp. 65, 68)

Kamimoto Takeyuki and Bae Myurng Hoan.
High Combustion Temperature for the Reduction of Particulate in Diesel Engines.
In *SAE Technical Paper*, volume 880423, 1988. (cited in p. 40)

Kanda Tomohiro, Hakozaki Takazo, Uchimoto Tatsuya, Hatano Jyunichi, Kitayama Naoto and Sono Hiroshi.
PCCI Operation with Early Injection of Conventional Diesel Fuel.
In *SAE Technical Paper*, volume 2005-01-0378. SAE International, 2005. (cited in p. 50)

Kim T. and Ghandhi J.
Quantitative 2-D Fuel Vapor Concentration Measurements in an Evaporating Diesel Spray using the Exciplex Fluorescence Method.
In *SAE Technical Paper*, volume 2001-01-3495, 2001. (cited in p. 34)

Kim T. and Ghandhi J. B.
Characterization of evaporating diesel sprays using exciplex laser-induced fluorescence.
Atomization and Sprays, Vol. 13 n^o 5-6, pp. 535–559, 2003. (cited in p. 125)

Kimura S, Ogawa H, Matsui Y and Enomoto Y.
An experimental analysis of low-temperature and premixed combustion for simultaneous reduction of NOx and particulate emissions in direct injection diesel engines.
International Journal of Engine Research, Vol. 3 n^o 4, pp. 249–259, 2002. (cited in p. 51)

Kimura Shuji, Aoki Osamu, Kitahara Yasuhisa and Aiyoshizawa Eiji.
Ultra-Clean Combustion Technology Combining a Low-Temperature and Premixed Combustion Concept for Meeting Future Emission Standards.
In *SAE Technical Paper*, volume 2001-01-0200, 2001. (cited in p. 51)

Kimura Shuji, Aoki Osamu, Ogawa Hiroshi, Muranaka Shigeo and Enomoto Yoshiteru.

New Combustion Concept for Ultra-Clean and High-Efficiency Small DI Diesel Engines.
In *SAE Technical Paper*, volume 1999-01-3681, 1999. (cited in p. 51)

Kitamura Yasutaka, Mohammadi Ali, Ishiyama Takuji and Shioji Masahiro.
Fundamental Investigation of NOx Formation in Diesel Combustion Under Supercharged and EGR Conditions.
In *SAE Technical Paper*, volume 2005-01-0364, 2005. (cited in p. 165)

Kitano Koji, Nishiumi Ryoji, Tsukasaki Yukihiro, Tanaka Toshiaki and Morinaga Masataka.
Effects of Fuel Properties on Premixed Charge Compression Ignition Combustion in a Direct Injection Diesel Engine.
In *SAE Technical Paper*, volume 2003-01-1815, 2003. (cited en pp. 50, 64)

Knecht Walter.
Diesel engine development in view of reduced emission standards.
Energy, Vol. 33 n^o 2, pp. 264–271, 2008. (cited in p. 7)

Knoll R.
The two-stroke List diesel -a new approach to motorize small comfort cars.
In *In proceedings of the FISITA Congress, June 1996, Prague, Czech Republic.*, 1996. (cited in p. 11)

Knoll R and Gutmann P.
The two-stroke engine professional List diesel engine for future small comfort cars.
In *In proceedings of the SIA International Congress, April 1996, Paris, France.*, 1996. (cited in p. 11)

Knoll Reinhard.
AVL Two-Stroke Diesel Engine.
In *SAE Technical Paper*, volume 981038, 1998. (cited in p. 11)

Knox Benjamin W, Genzale Caroline L., Pickett L., Garcia-Oliver Jose M. and Vera-Tudela Walter.
Combustion Recession after End of Injection in Diesel Sprays.
In *SAE Technical Paper*, volume 2015-01-0797, 2015. (cited en pp. 39, 40)

Kokjohn S. L., Hanson R. M., Splitter D. A. and Reitz R. D.
Fuel reactivity controlled compression ignition (RCCI): a pathway to controlled high-efficiency clean combustion.
International Journal of Engine Research, Vol. 12 n^o 3, pp. 209–226, 2011.
(cited in p. 46)

Kolmel A., Spicher U., Dusterwald R. and Wytrykus F. M.
Analysis of Mixture Conditions Close to Spark Plug Location using a Time Resolved Gas Sampling Valve.
In *SAE Technical Paper*, volume 982473. SAE International, 1998. (cited in p. 115)

Kolodziej C.
Particulate matter emissions from Premixed Diesel Low Temperature Combustion.
PhD thesis. Universitat Politecnica de Valencia, Departamento de Maquinas y Motores Termicos, 2012. (cited in p. 166)

Kolodziej Christopher P., Ciatti Stephen, Vuilleumier David, Das Adhikary Bishwadipa and Reitz Rolf.
Extension of the Lower Load Limit of Gasoline Compression Ignition with 87 AKI Gasoline by Injection Timing and Pressure.
In *SAE Technical Paper*, volume 2014-01-1302. SAE International, 2014.
(cited en pp. 68, 231)

Kook Sanghoon, Bae Choongsik, Miles Paul C., Choi Dae and Pickett Lyle M.
The Influence of Charge Dilution and Injection Timing on Low-Temperature Diesel Combustion and Emissions.
In *SAE Technical Paper*, volume 2005-01-3837. SAE International, 2005.
(cited en pp. 50, 64)

Kook Sanghoon, Pickett Lyle M. and Musculus Mark P. B.
Influence of Diesel Injection Parameters on End-of-Injection Liquid Length Recession.
SAE Int. J. Engines, Vol. 2 n^o 1, pp. 1194–1210, 2009. (cited en pp. 54, 55)

Kosaka H, Aizawa T and Kamimoto T.
Two-dimensional imaging of ignition and soot formation processes in a diesel flame.
International Journal of Engine Research, Vol. 6 n^o 1, pp. 21–42, 2005.
(cited en pp. 27, 29)

Kosaka Hidenori, Nishigaki Takahiro, Kamimoto Takeyuki, Sano Takashi, Matsutani Akira and Harada Shinichi.
Simultaneous 2-D Imaging of OH Radicals and Soot in a Diesel Flame by Laser Sheet Techniques.
In *SAE Technical Paper*, volume 960834. SAE International, 1996. (cited in p. 33)

Kubota Masaru, Yoshida Koji, Shoji Hideo and Tanaka Hidenori.
A Study of the Influence of Fuel Temperature on Emission Characteristics and Engine Performance of Compression Ignition Engine.
In *SAE Technical Paper*, volume 2002-32-1777. SAE International, 2002. (cited in p. 99)

Lachaux Thierry and Musculus Mark P. B.
In-cylinder unburned hydrocarbon visualization during low-temperature compression-ignition engine combustion using formaldehyde PLIF.
Proceedings of the Combustion Institute, Vol. 31 n^o 2, pp. 2921–2929, 2007.
(cited in p. 35)

Laget O, Ternel C, Thiriot J, Charmasson S, Tribotte P and Vidal F.
Preliminary Design of a Two-Stroke Uniflow Diesel Engine for Passenger Car.
In *SAE Technical Paper*, volume 2013-01-1719, 2013. (cited en pp. 12, 307)

Lapuerta M.
Un modelo de combustion fenomenologico para un motor Diesel de inyeccion directa rapido.
PhD thesis. Universitat Politecnica de Valencia, Departamento de Maquinas y Motores Termicos, 1988. (cited in p. 119)

Lapuerta M., Armas O. and Hernandez J. J.
Diagnosis of DI Diesel combustion from in-cylinder pressure signal by estimation of mean thermodynamic properties of the gas.
Applied Thermal Engineering, Vol. 19 n^o 5, pp. 513–529, 1999. (cited en pp. 119, 120)

Lewis Samuel A., Storey John M. E., Bunting Bruce and Szybist James P.
Partial Oxidation Products and other Hydrocarbon Species in Diesel HCCI Exhaust.
In *SAE Technical Paper*, volume 2005-01-3737, 2005. (cited in p. 214)

Li Zhihua, He Bang-quan and Zhao Hua.
The Influence of Intake Port and Pent-Roof Structures on Reversed Tumble Generation of a Poppet-Valved Two-Stroke Gasoline Engine.
In *SAE Technical Paper*, volume 2014-01-1130, 2014. (cited in p. 144)

Linstrom P.J. and Mallard W.G.
NIST Chemistry WebBook, NIST Standard Reference Database Number 69.
National Institute of Standards and Technology, Gaithersburg MD, 20899. http://webbook.nist.gov., 2011. (cited in p. 126)

Liu Haifeng, Ma Shuaiying, Zhang Zhong, Zheng Zunqing and Yao Mingfa.
Study of the control strategies on soot reduction under early-injection conditions on a diesel engine.
Fuel, Vol. 139 n^o 0, pp. 472–481, 2015. (cited en pp. 53, 54)

Lopez J.J.
Estudio Teorico-Experimental del chorro libre diesel no evaporativo y de su interaccion con el movimiento del aire.
PhD thesis. Universitat Politecnica de Valencia, Departamento de Maquinas y Motores Termicos, 2003. (cited in p. 26)

Magno Agnese, Mancaruso Ezio and Vaglieco Bianca Maria.
Combustion Analysis of Dual Fuel Operation in Single Cylinder Research Engine Fuelled with Methane and Diesel.
In *SAE Technical Paper*, volume 2015-24-2461, 2015. (cited in p. 46)

Mancaruso Ezio and Vaglieco Bianca Maria.
UV-Visible Spectroscopic Measurements of Dual-Fuel PCCI Engine.
SAE International Journal of Fuels and Lubricants, Vol. 4 n^o 2, pp. 271–281, 2011.
(cited in p. 46)

Mancaruso Ezio and Vaglieco Bianca Maria.
UV-Visible Imaging of PCCI Engine Running with Ethanol/Diesel Fuel.
In *SAE Technnical Paper*, volume 2012-01-1238, 2012. (cited in p. 46)

Mancaruso Ezio and Vaglieco Bianca Maria.
Characterization of PCCI Combustion in a Single Cylinder CI Engine Fuelled with RME and Bio-Ethanol.
In *SAE Technical Paper*, volume 2013-01-1672, 2013. (cited in p. 46)

Manente V., Johansson B. and Cannella W.
Gasoline partially premixed combustion, the future of internal combustion engines?
International Journal of Engine Research, Vol. 12 n^o 3, pp. 194–208, 2011.
(cited en pp. 66, 67, 68)

Manente Vittorio, Johansson Bengt and Tunestal Per.
Partially Premixed Combustion at High Load using Gasoline and Ethanol, a Comparison with Diesel.
In *SAE Technical Paper*, volume 2009-01-0944. SAE International, 2009.
(cited en pp. 50, 66)

Manente Vittorio, Johansson Bengt, Tunestal Per and Cannella William.
Effects of Different Type of Gasoline Fuels on Heavy Duty Partially Premixed Combustion.
SAE International Journal of Engines, Vol. 2 n^o 2, pp. 71–88, 2010.
(cited en pp. 50, 66, 67)

Manente Vittorio, Tunestal Per and Johansson Bengt.
Effects of Ethanol and Different Type of Gasoline Fuels on Partially Premixed Combustion from Low to High Load.
In *SAE Technical Paper*, volume 2010-01-0871, 2010. (cited en pp. 50, 66)

Martyr A.J. and Plint M. A.
Engine Testing, 3rd Edition Theory and Practice.
Butterworth-Heinemann, 2007. (cited in p. 101)

Masuda Tatsuyuki, Itoh Hideaki and Ichihara Yasusi.
Research on the Practical Application of 1 liter, Semi-DI, 2-Stroke Diesel Engine to Compact Cars.
In *SAE Technical Paper*, volume 1999-01-1249, 1999. (cited in p. 11)

Mead R., Gilmour S.G. and Mead A.
Statistical Principles for the Design of Experiments: Applications to Real Experiments.
Cambridge University Press, 2012. (cited in p. 143)

Molenkamp H.
Zur Genavigkeit der Brenngesetzrechnung eines Dieselmotors mit Nichtunterteiltem Brennraum.
MTZ Motortechnische Zeitschift, Vol. 37 n^o 7-8, pp. 285–291, 1976. (cited in p. 120)

Molina Santiago.
Influencia de los parametros de inyeccion y la recirculacion de gases de escape sobre el proceso de combustion en un motor Diesel.
PhD thesis. Universitat Politecnica de Valencia, Departamento de Maquinas y Motores Termicos, 2003. (cited in p. 108)

Muniz L. and Mungal M. G.
Effects of heat release and buoyancy on flow structure and entrainment in turbulent nonpremixed flames.
Combustion and Flame, Vol. 126 n^o 1-2, pp. 1402–1420, 2001. (cited in p. 125)

Murata Y., Kusaka J., Odaka M., Daisho Y., Kawano Daisuke, Suzuki Hisakazu, Ishii Hajime and Goto Yuichi.
Achievement of Medium Engine Speed and Load Premixed Diesel Combustion with Variable Valve Timing.
In *SAE Technical Paper*, volume 2006-04-03, 2006. (cited in p. 64)

Musculus M. P. B.
Entrainment waves in decelerating transient turbulent jets.
Journal of Fluid Mechanics, Vol. 638, pp. 117–140, 2009. (cited in p. 27)

Musculus Mark P. B.
Multiple Simultaneous Optical Diagnostic Imaging of Early-Injection Low-Temperature Combustion in a Heavy-Duty Diesel Engine.
In *SAE Technical Paper*. SAE International, 2006. (cited in p. 35)

Musculus Mark P. B. and Kattke Kyle.
Entrainment Waves in Diesel Jets.
In *SAE Technical Paper*, volume 2009-01-1355, 2009. (cited en pp. 27, 35, 37)

Musculus Mark P. B., Lachaux Thierry, Pickett Lyle M. and Idicheria Cherian A.

End-of-Injection Over-Mixing and Unburned Hydrocarbon Emissions in Low-Temperature-Combustion Diesel Engines.
In *SAE Technical Paper*, volume 2007-01-0907. SAE International, 2007.
(cited en pp. 35, 36, 37, 38, 40, 237)

Musculus Mark P. B., Miles Paul C. and Pickett Lyle M.
Conceptual models for partially premixed low-temperature diesel combustion.
Progress in Energy and Combustion Science, Vol. 39 n^o 2-3, pp. 246–283, 2013.
(cited en pp. 55, 56, 58, 61, 62, 224, 227, 237, 251)

Naber Jeffrey D. and Siebers Dennis L.
Effects of Gas Density and Vaporization on Penetration and Dispersion of Diesel Sprays.
In *SAE Technical Paper*, volume 960034, 1996. (cited en pp. 26, 27, 126)

Nagle J and Strickland-Constable RF.
Oxidation of carbon between 1000 - 2000 C.
In *Proceedings of the Fifth Carbon Conference*, volume Proceedings of the Fifth Carbon Conference, pp. 154–164, 1962. (cited in p. 129)

Nevin Ryan M., Sun Yong, Gonzalez Manuel A. and Reitz Rolf D.
PCCI Investigation Using Variable Intake Valve Closing in a Heavy Duty Diesel Engine.
In *SAE Technical Paper*, volume 2007-01-0903, 2007. (cited en pp. 50, 64)

Noehre Christof, Andersson Magnus, Johansson Bengt and Hultqvist Anders.
Characterization of Partially Premixed Combustion.
In *SAE Technical Paper*, volume 2006-01-3412, 2006. (cited en pp. 43, 64)

Nomura K and Nakamura N.
Development of a New Two-Stroke Engine with Poppet-Valves: Toyota S-2 Engine.
A New Generation of Two-Stroke Engines for the Future? Proceedings of the International Seminar, Rueil-Malmaison, France, Editions Technip, Pairs, 1993. (cited in p. 11)

Novella R.
Estudio de la influencia de los ciclos Atkinson y Miller sobre el proceso de combustion y las emisiones contaminantes en un motor diesel.
PhD thesis. Universitat Politecnica de Valencia, Departamento de Maquinas y Motores Termicos, 2009. (cited in p. 166)

Obernesser Philippe, Quechon Nicolas and Servant Cedrid.
Two-stroke engine e.g. two-stroke diesel engine, has air deflector located downstream of part of seat in intake valve of intake duct, and directing air flow from intake duct towards lower part of combustion chamber.
France Patent FR20080053623, 2009. (cited in p. 86)

Ogawa Hideyuki, Miyamoto Noboru, Shimizu Hajime and Kido Shingo.
Characteristics of Diesel Combustion in Low Oxygen Mixtures with Ultra-High EGR.
In *SAE Technical Paper*, volume 2006-01-1147. SAE International, 2006. (cited in p. 43)

Okude Keiichi, Mori Kazutoshi, Shiino Shiroh and Moriya Takeshi.
Premixed Compression Ignition (PCI) Combustion for Simultaneous Reduction of NOx and soot in Diesel Engine.
In *SAE Technical Paper*, volume 2004-01-1907, 2004. (cited en pp. 52, 53)

Olsen D, Hutcherson G, Wilson B and Mitchell C.
Development of the Tracer Gas Method for Large Bore Natural Gas Engines: Part 1 Method Validation.
Journal of Engineering for Gas Turbines and Power, Vol. 124 n^o 3, pp. 678–685, 2002. (cited in p. 102)

Olsen D, Hutcherson G, Wilson B and Mitchell C.
Development of the Tracer Gas Method for Large Bore Natural Gas Engines: Part 2 Measurement of Scavenging Parameters.
Journal of Engineering for Gas Turbines and Power, Vol. 124 n^o 3, pp. 686–694, 2002. (cited in p. 102)

Onishi Shigeru, Jo Souk Hong, Shoda Katsuji, Jo Pan Do and Kato Satoshi.
Active Thermo-Atmosphere Combustion (ATAC) - A New Combustion Process for Internal Combustion Engines.
In *SAE Technical Paper*, volume 790501. SAE International, 1979. (cited in p. 12)

Osborne R. J., Stokes J., Lake T. H., Carden P. J., Mullineux J. D., Helle-Lorentzen R., Evans J. C., Heikal M. R., Zhu Y., Zhao Hua and Ma T.
Development of a Two-Stroke/Four-Stroke Switching Gasoline Engine - The 2/4SIGHT Concept.
In *SAE Technical Paper*, volume 2005-01-1137, 2005. (cited en pp. 12, 295)

Pastor Jose V., Javier Lopez J., Garcia Jose M. and Pastor Jose M.
A 1D model for the description of mixing-controlled inert diesel sprays.
Fuel, Vol. 87 n^o 13-14, pp. 2871–2885, 2008. (cited en pp. 27, 124, 125, 217, 226)

Payri F., Margot X., Gil A. and Martin J.
Computational Study of Heat Transfer to the Walls of a DI Diesel Engine.
In *SAE Technical Paper*, volume 2005-01-0210. SAE International, 2005. (cited in p. 120)

Payri F., Molina S., Martin J. and Armas O.
Influence of measurement errors and estimated parameters on combustion diagnosis.
Applied Thermal Engineering, Vol. 26 n^o 23, pp. 226–236, 2006. (cited in p. 120)

Payri Francisco, Benajes Jesus, Novella Ricardo and Kolodziej Christopher.
Effect of Intake Oxygen Concentration on Particle Size Distribution Measurements from Diesel Low Temperature Combustion.
In *SAE Technical Paper*, volume 2011-01-1355, 2011. (cited in p. 166)

Payri R., Garcia J.M., Salvador F. and Gimeno J.
Using spray momentum flux measurements to understand the influence of diesel nozzle geometry on spray characteristics.
Fuel, Vol. 84 n^o 5, pp. 551–561, 2005. (cited en pp. 26, 90)

Payri R., Salvador F. J., Gimeno J. and Bracho G.
A new methodology for correcting the signal cumulative phenomenon on injection rate measurements.
Experimental Techniques, Vol. 32 n^o 1, pp. 46–49, 2008. (cited in p. 90)

Payri R., Salvador F. J., Gimeno J. and Novella R.
Flow regime effects on non-cavitating injection nozzles over spray behavior.
International Journal of Heat and Fluid Flow, Vol. 32 n^o 1, pp. 273–284, 2011.
(cited in p. 126)

Payri Raul, Garcia Antonio, Domenech Vicent, Durrett Russell and Plazas Alejandro H.
An experimental study of gasoline effects on injection rate, momentum flux and spray characteristics using a common rail diesel injection system.
Fuel, Vol. 97 n^o 0, pp. 390–399, 2012. (cited in p. 92)

Payri Gonzalez Francisco and Desantes Jose Maria.
Motores de combustion interna alternativos.
Editorial Reverte, 2011. (cited en pp. 144, 190)

Petersen Benjamin, Miles Paul C. and Sahoo Dipankar.
Equivalence Ratio Distributions in a Light-Duty Diesel Engine Operating under Partially Premixed Conditions.
SAE Int. J. Engines, Vol. 5 n^o 2, pp. 526–537, 2012. (cited en pp. 50, 57, 237)

Pickett L. M. and Siebers D. L.
Orifice diameter effects on diesel fuel jet flame structure.
In *Proceedings of the Fall Technical Conference of the ASME Internat Combustion Engine Division*, pp. ICE 37–41, 2001. (cited in p. 32)

Pickett Lyle M., Manin Julien, Genzale Caroline L., Siebers Dennis L., Musculus Mark P. B. and Idicheria Cherian A.
Relationship Between Diesel Fuel Spray Vapor Penetration/Dispersion and Local Fuel Mixture Fraction.
SAE Int. J. Engines, Vol. 4 n^o 1, pp. 764–799, 2011. (cited en pp. 26, 32)

Pinchon P., Walter B., Reveille B. and Miche M.
New concepts for diesel combustion.
In *THIESEL Conference Proceedings*, 2004. (cited in p. 46)

Pohorelsky Ludek, Brynych Pavel, Macek Jan, Vallaude Pierre-Yves, Ricaud Jean-Charles, Obernesser Philippe and Tribotte Pascal.
Air System Conception for a Downsized Two-Stroke Diesel Engine.
In *SAE Technical Paper*, volume 2012-01-0831, 2012. (cited en pp. 12, 150)

Pope Stephen B.
Turbulent flows.
Cambridge university press, 2000. (cited in p. 26)

Potter Mike and Durrett Russ.
High-Efficiency Clean Combustion Design for Compression Ignition Engines.
In *2006 Diesel Engine-Efficiency and Emissions Research (DEER) Conference Presentations.*, Detroit, Michigan, 2006. (cited en pp. 40, 42)

Regitz S. and Collings N.
Study of Cycle-By-Cycle Air-to-Fuel Ratio Determined from the Exhaust Gas Composition and a Novel Fast Response Device Based on a Wide Band Lambda Sensor.
In *SAE Technical Paper*, volume 2008-01-2439, 2008. (cited in p. 115)

Reitz Rolf D. and Duraisamy Ganesh.
Review of high efficiency and clean reactivity controlled compression ignition (RCCI) combustion in internal combustion engines.
Progress in Energy and Combustion Science, Vol. 46 n^o 0, pp. 12–71, 2015.
(cited en pp. 8, 46)

Rekab K. and Shaikh M.
Statistical Design of Experiments with Engineering Applications.
Taylor & Francis, 2005. (cited in p. 143)

Ribaucour M., Minetti R., Sochet L. R., Curran H. J., Pitz W. J. and Westbrook C. K.
Ignition of isomers of pentane: An experimental and kinetic modeling study.
Proceedings of the Combustion Institute, Vol. 28 n^o 2, pp. 1671–1678, 2000.
(cited in p. 50)

Ricou F. P. and Spalding D. B.
Measurements of entrainment by axisymmetrical turbulent jets.
Journal of Fluid Mechanics, Vol. 11 n^o 01, pp. 21–32, 1961. (cited in p. 26)

Ruiz S.
Estudio Teorico-Experimental de los procesos de atomizacion y de mezcla en los chorros diesel D.I.
PhD thesis. Universitat Politecnica de Valencia, Departamento de Maquinas y Motores Termicos, 2003. (cited in p. 26)

Ryan, T. W. III and Matheaus A. C.
Fuel Requirements for HCCI Engine Operation.
In *SAE Technical Paper*, volume 2003-01-1813. Society of Automotive Engineers, 2003.
(cited in p. 46)

Ryan Thomas W. and Callahan Timothy J.
Homogeneous Charge Compression Ignition of Diesel Fuel.
In *SAE Technical Paper*, volume 961160, 1996. (cited en pp. 45, 46)

Salvador F.J.
Estudio teorico experimental de la influencia de la geometria de la tobera de inyeccion sobre las caracteristicas del flujo interno y del chorro.
PhD thesis. Universitat Politecnica de Valencia, Departamento de Maquinas y Motores Termicos, 2003. (cited in p. 26)

Saxena Samveg and Bedoya Ivan D.
Fundamental phenomena affecting low temperature combustion and HCCI engines, high load limits and strategies for extending these limits.
Progress in Energy and Combustion Science, Vol. 39 n^o 5, pp. 457–488, 2013.
(cited en pp. 8, 47, 224)

Schwarz F. and Spicher U.
Determination of Residual Gas Fraction in IC Engines.
In *SAE Technical Paper*, volume 2003-01-3148, 2003. (cited in p. 115)

Sellnau Mark, Foster Matthew, Hoyer Kevin, Moore Wayne, Sinnamon James and Husted Harry.
Development of a Gasoline Direct Injection Compression Ignition (GDCI) Engine.
SAE International Journal of Engines, Vol. 7 n^o 2, pp. 835–851, 2014.
(cited en pp. 68, 231)

Sellnau Mark, Moore Wayne, Sinnamon James, Hoyer Kevin, Foster Matthew and Husted Harry.
GDCI Multi-Cylinder Engine for High Fuel Efficiency and Low Emissions.
SAE Int. J. Engines, Vol. 8 n^o 2, pp. 775–790, 2015. (cited in p. 229)

Sellnau Mark, Sinnamon James, Hoyer Kevin and Husted Harry.
Gasoline Direct Injection Compression Ignition (GDCI) - Diesel-like Efficiency with Low CO2 Emissions.
In *SAE Technical Paper*, volume 2011-01-1386, 2011. (cited en pp. 68, 231)

Sellnau Mark C., Sinnamon James, Hoyer Kevin and Husted Harry.
Full-Time Gasoline Direct-Injection Compression Ignition (GDCI) for High Efficiency and Low NOx and PM.
SAE International Journal of Engines, Vol. 5 n^o 2, pp. 300–314, 2012.
(cited en pp. 68, 231, 252, 273)

Sellnau Mark C., Sinnamon James, Hoyer Kevin, Kim Junghwan, Cavotta Marilou and Husted Harry.
Part-Load Operation of Gasoline Direct-Injection Compression Ignition (GDCI) Engine.
In *SAE Technical Paper*, volume 2013-01-0272, 2013. (cited en pp. 68, 252, 273)

Senecal P. K., Richards K. J., Pomraning E., Yang T., Dai M. Z., McDavid R. M., Patterson M. A., Hou S. and Shethaji T.
A New Parallel Cut-Cell Cartesian CFD Code for Rapid Grid Generation Applied to In-Cylinder Diesel Engine Simulations.
In *SAE Technical Paper*, volume 2007-01-0159. SAE International, 2007.
(cited in p. 127)

Shen Mengqin, Tuner Martin, Johansson Bengt and Cannella William.
Effects of EGR and Intake Pressure on PPC of Conventional Diesel, Gasoline and Ethanol in a Heavy Duty Diesel Engine.
In *SAE Technical Paper*, volume 2013-01-2702. SAE International, 2013. (cited in p. 68)

Siebers Dennis L.
Scaling Liquid-Phase Fuel Penetration in Diesel Sprays Based on Mixing-Limited Vaporization.
In *SAE Technical Paper*, volume 1999-01-0528. SAE International, 1999. (cited in p. 27)

Siebers Dennis L. and Higgins B.
Flame Lift-Off on Direct-Injection Diesel Sprays Under Quiescent Conditions.
In *SAE Technical Paper*, volume 2001-01-0530, 2001. (cited in p. 32)

Singh S, Reitz R D, Musculus M P B and Lachaux T.
Validation of engine combustion models against detailed in-cylinder optical diagnostics data for a heavy-duty compression-ignition engine.
International Journal of Engine Research, Vol. 8 n^o 1, pp. 97–126, 2007. (cited in p. 35)

Singh Satbir and Musculus Mark P. B.
Numerical Modeling and Analysis of Entrainment in Turbulent Jets After the End of Injection.
Journal of Fluids Engineering, Vol. 132 n^o 8, pp. 081203–081203, 2010. (cited in p. 37)

Sjoberg Magnus and Dec John E.
Effects of Engine Speed, Fueling Rate, and Combustion Phasing on the Thermal Stratification Required to Limit HCCI Knocking Intensity.
In *SAE Technical Paper*, volume 2005-01-2125. SAE International, 2005. (cited in p. 47)

Sjoberg Magnus and Dec John E.
Smoothing HCCI Heat-Release Rates Using Partial Fuel Stratification with Two-Stage Ignition Fuels.
In *SAE Technical Paper*, volume 2006-01-0629. SAE International, 2006. (cited in p. 47)

Sjoberg Magnus, Dec John E. and Cernansky Nicholas P.
Potential of Thermal Stratification and Combustion Retard for Reducing Pressure-Rise Rates in HCCI Engines, Based on Multi-Zone Modeling and Experiments.
In *SAE Technical Paper*, volume 2005-01-0113. SAE International, 2005. (cited in p. 47)

Solaka Hadeel, Aronsson Ulf, Tuner Martin and Johansson Bengt.
Investigation of Partially Premixed Combustion Characteristics in Low Load Range with Regards to Fuel Octane Number in a Light-Duty Diesel Engine.
In *SAE Technical Paper*, volume 2012-01-0684, 2012. (cited en pp. 67, 227, 273)

Solsjo Rickard, Jangi Mehdi, Tuner Martin and Bai Xue-Song.
Large Eddy Simulation of Partially Premixed Combustion in an Internal Combustion Engine.
In *SAE Technical Paper*, volume 2012-01-0139. SAE International, 2012. (cited in p. 68)

Splitter Derek, Hanson Reed, Kokjohn Sage, Wissink Martin and Reitz Rolf.
Injection Effects in Low Load RCCI Dual-Fuel Combustion.
In *SAE Technical Paper*, volume 2011-24-0047, 2011. (cited in p. 46)

Splitter Derek, Wissink Martin, DelVescovo Dan and Reitz Rolf.
RCCI Engine Operation Towards 60
In *SAE Technical Paper*, volume 2013-01-0279, 2013. (cited in p. 46)

Splitter Derek A. and Reitz Rolf D.
Fuel reactivity effects on the efficiency and operational window of dual-fuel compression ignition engines.
Fuel, Vol. 118 n^o 0, pp. 163–175, 2014. (cited in p. 46)

Su Wanhua, Lin Tiejian and Pei Yiqiang.
A Compound Technology for HCCI Combustion in a DI Diesel Engine Based on the Multi-Pulse Injection and the BUMP Combustion Chamber.
In *SAE Technical Paper*, volume 2003-01-0741. SAE International, 2003. (cited in p. 46)

Su Wanhua, Wang Hui and Liu Bin.
Injection Mode Modulation for HCCI Diesel Combustion.
In *SAE Technical Paper*, volume 2005-01-0117. SAE International, 2005. (cited in p. 46)

Suzuki Hisakazu, Koike Noriyuki, Ishii Hajime and Odaka Matuo.
Exhaust Purification of Diesel Engines by Homogeneous Charge with Compression Ignition Part 1: Experimental Investigation of Combustion and Exhaust Emission Behavior Under Pre-Mixed Homogeneous Charge Compression Ignition Method.
In *SAE Technical Paper*, volume 970313, 1997. (cited in p. 45)

Takeda Yoshinaka, Keiichi Nakagome and Keiichi Niimura.
Emission Characteristics of Premixed Lean Diesel Combustion with Extremely Early Staged Fuel Injection.
In *SAE Technical Paper*, volume 961163, 1996. (cited en pp. 45, 46)

Tanaka Shigeyuki, Ayala Ferran, Keck James C. and Heywood John B.
Two-stage ignition in HCCI combustion and HCCI control by fuels and additives.
Combustion and Flame, Vol. 132 n^o 1-2, pp. 219–239, 2003. (cited in p. 49)

Teakle B Philip Robert.
A numerical investigation of a two-stroke poppet-valved diesel engine concept.
Tribology and Materials Technology Group. PhD Thesis. Queensland University of Technology, 2004. (cited in p. 146)

Torregrosa A., Olmeda P., Degraeuwe B. and Reyes M.
A concise wall temperature model for DI Diesel engines.
Applied Thermal Engineering, Vol. 26 n^o 11-12, pp. 1320–1327, 2006. (cited in p. 120)

Tree Dale R. and Svensson Kenth I.
Soot processes in compression ignition engines.
Progress in Energy and Combustion Science, Vol. 33 n^o 3, pp. 272–309, 2007. (cited in p. 166)

Tribotte Pascal, Ravet Frederic, Dugue Vincent, Obernesser Philippe, Quechon Nicolas, Benajes Jesus, Novella Ricardo and De Lima Daniela.
Two Strokes Diesel Engine - Promising Solution to Reduce CO2 Emissions.
Procedia - Social and Behavioral Sciences, Vol. 48, pp. 2295–2314, 2012. (cited en pp. 12, 86, 87, 150, 159)

Tuner Martin, Johansson Thomas, Aulin Hans, Tunestal Per, Johansson Bengt and Cannella William.
Multi Cylinder Partially Premixed Combustion Performance Using Commercial Light-Duty Engine Hardware.
In *SAE Technical Paper*, volume 2014-01-2680. SAE International, 2014. (cited in p. 68)

Turner J. W. G., Blundell D. W., Pearson R. J., Patel R., Larkman D. B., Burke P., Richardson S., Green N. M., Brewster S., Kenny R. G. and Kee R. J.
Project Omnivore: A Variable Compression Ratio ATAC 2-Stroke Engine for Ultra-Wide-Range HCCI Operation on a Variety of Fuels.
SAE Int. J. Engines, Vol. 3 n^o 1, pp. 938–955, 2010. (cited in p. 12)

Tutuianu Monica, Marotta Alessandro, Steven Heinz, Eva Ericsson, Haniu Takahiro, Ichikawa Noriyuki and Ishii Hajime.
Development of a World-wide Worldwide harmonized Light duty driving Test Cycle (WLTC). Technical Report.
UNECE DHC subgroup, 2013. (cited in p. 6)

Vashishtha Ashish, Rathinam Balamurugan, Delahaye Laurent, Ravet Frederic and Justet Frederic.
Study of Intake Ports Design for Ultra Low Cost (ULC) Gasoline Engine Using STAR-CD.
In *SAE Technical Paper*, volume 2012-01-0407, 2012. (cited in p. 12)

Walter Bruno and Gatellier Bertrand.
Development of the High Power NADITM Concept Using Dual Mode Diesel Combustion to Achieve Zero NOx and Particulate Emissions.
In *SAE Technical Paper*, volume 2002-01-1744, 2002. (cited en pp. 45, 46)

Warey Alok, Hardy Jean-Paul, Hennequin Manuela, Tatur Marek, Tomazic Dean and Cannella William.
Fuel Effects on Low Temperature Combustion in a Light-Duty Diesel Engine.
In *SAE Technical Paper*, volume 2010-01-1122, 2010. (cited in p. 64)

Way R.
Methods for determination of composition and thermodynamic properties of combustion products for internal combustion engine calculations.
Proceedings of the Institution of Mechanical Engineers, Vol. 190, pp. 686–97, 1976. (cited in p. 124)

Weall Adam and Collings Nick.
Investigation into Partially Premixed Combustion in a Light-Duty Multi-Cylinder Diesel Engine Fuelled with a Mixture of Gasoline and Diesel.
In *SAE Technical Paper*, volume 2007-01-4058, 2007. (cited in p. 51)

Weall Adam and Collings Nick.
Gasoline Fuelled Partially Premixed Compression Ignition in a Light Duty Multi Cylinder Engine: A Study of Low Load and Low Speed Operation.
In *SAE Technical Paper*, volume 2009-01-1791, 2009. (cited in p. 68)

Welling Orian and Collings Nick.
UEGO Based Measurement of EGR Rate and Residual Gas Fraction.
In *SAE Technical Paper*, volume 2011-01-1289, 2011. (cited in p. 115)

Westbrook C. K., Curran H. J., Pitz W. J., Griffiths J. F., Mohamed C. and Wo S. K.
The effects of pressure, temperature, and concentration on the reactivity of alkanes: Experiments and modeling in a rapid compression machine.
Symposium (International) on Combustion, Vol. 27 n^o 1, pp. 371–378, 1998. (cited en pp. 49, 50)

Westbrook Charles K.
Chemical kinetics of hydrocarbon ignition in practical combustion systems.
Proceedings of the Combustion Institute, Vol. 28 n^o 2, pp. 1563–1577, 2000. (cited en pp. 49, 50)

Woschni G.
A Universally Applicable Equation for the Instantaneous Heat Transfer Coefficient in the Internal Combustion Engine.
In *SAE Technical Paper*, volume 670931. SAE International, 1967. (cited in p. 120)

Woschni G.
Die Berechnung der Wandverluste und der thermischen Belastung der Bauteile von Dieselmotoren.
MTZ Motortechnische Zeitschift, Vol. 31 n^o 12, pp. 491–499, 1970. (cited in p. 120)

Yanagihara H., Sato Y. and Minuta J.
A simultaneous reduction in NOx and soot in diesel engines under a new combustion system (Uniform Bulky Combustion System -UNIBUS).
In *17th International Vienna Motor Symposium*, pp. 303–314, 1996.
(cited en pp. 45, 46)

Yao M., Zheng Z., Zhang B. and Chen Z.
The Effect of PRF Fuel Octane Number on HCCI Operation.
In *SAE Technical Paper*, volume 2001-01-2992, 2004. (cited in p. 46)

Yao Mingfa, Zheng Zhaolei and Liu Haifeng.
Progress and recent trends in homogeneous charge compression ignition (HCCI) engines.
Progress in Energy and Combustion Science, Vol. 35 n^o 5, pp. 398–437, 2009.
(cited in p. 8)

Zhang Y. and Zhao H.
Investigation of combustion, performance and emission characteristics of 2-stroke and 4-stroke spark ignition and CAI/HCCI operations in a DI gasoline.
Applied Energy, Vol. 130 n^o 0, pp. 244–255, 2014. (cited en pp. 12, 209, 295)

Zhang Yan, Ojapah Mohammed, Cairns Alasdair and Zhao Hua.
2-Stroke CAI Combustion Operation in a GDI Engine with Poppet Valves.
In *SAE Technical Paper*, volume 2012-01-1118, 2012. (cited en pp. 12, 209, 295)

Zhang Yan, Zhao Hua, Ojapah Mohammed and Cairns Alasdair.
CAI combustion of gasoline and its mixture with ethanol in a 2-stroke poppet valve DI gasoline engine.
Fuel, Vol. 109 n^o 0, pp. 661–668, 2013. (cited en pp. 12, 209, 295)

Zhao H.
HCCI and CAI engines for the automotive industry.
Woodhead Publishing in mechanical engineering. Woodhead Pub., 2007.
(cited en pp. 12, 295)